ACCSCIENCE PUBLISHING

Explora: Environment and Resource

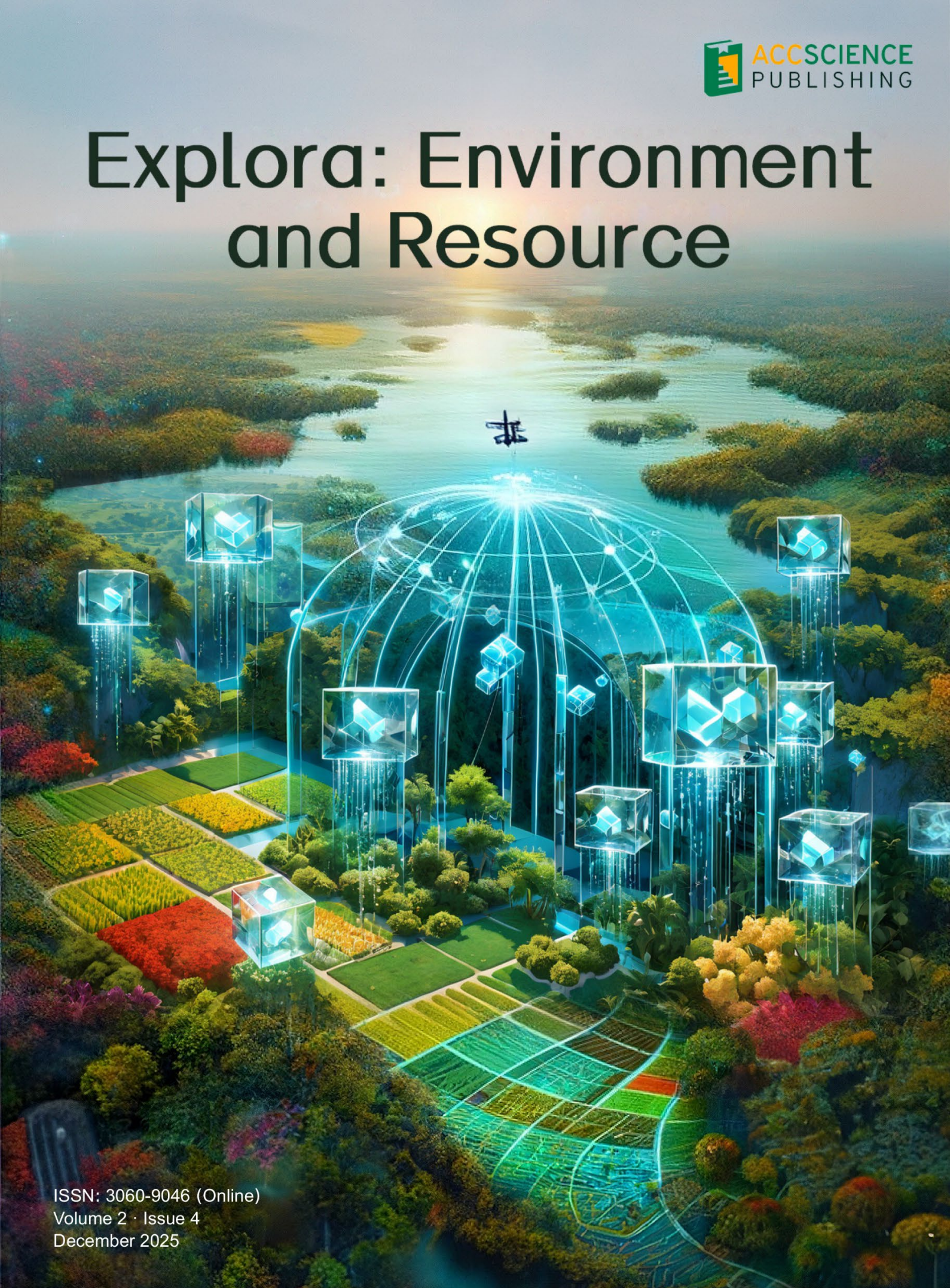

ISSN: 3060-9046 (Online)
Volume 2 · Issue 4
December 2025

Explora: Environment and Resource

Online ISSN: 3060-9046

Explora: Environment and Resource is an international and multidisciplinary journal covering all aspects of the environmental impacts of socio-economic development. It is concerned with the complex interactions among society, development, and the environment, aiming to explore ways and means of achieving sustainability in all human activities related to development. The journal welcomes scientific research papers, review papers, and discussion papers addressing environmental sustainability issues from various fields, including the biological sciences, agriculture, geology, meteorology, energy, food sciences, soil and water sciences, geography, nutrition, physical sciences, politics, economics, and law.

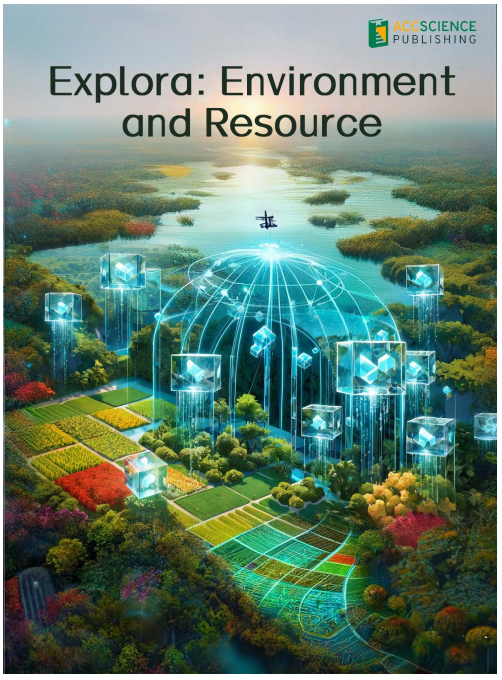

About the Publisher

AccScience Publishing is a publishing company based in Singapore. We publish a range of high-quality, open-access, peer-reviewed journals and books from a broad spectrum of disciplines.

Contact Us

Managing Editor
eer.office@accscience.sg

AccScience Publishing
9 Raffles Place, Republic Plaza 1 #06-00 Singapore 048619.

Volume 2 • Issue 4 • December 2025
ISSN 3060-9046 (online)

EXPLORA: ENVIRONMENT AND RESOURCE

ACCSCIENCE PUBLISHING

Access Science Without Barriers

EXPLORA: ENVIRONMENT AND RESOURCE

ISSN: 3060-9046 (online)

Editorial and Production Credits

Publisher: AccScience Publishing
Managing Editor: Dora Zhang
Production Editor: Sharmila Velapasamy
Article Layout and Typeset: Sinjore Technologies (India)

For all advertising queries, contact eer.office@accscience.sg.

Supplementary file

Supplementary files of articles can be obtained at https://accscience.com/journal/EER/2/4.

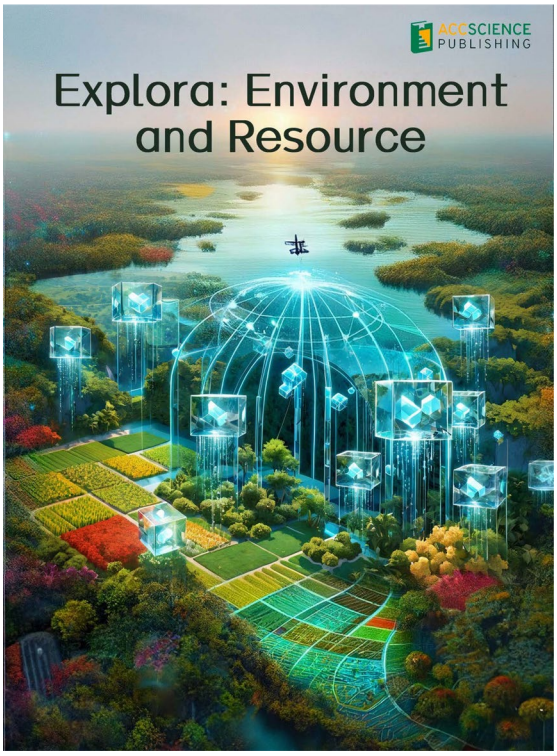

Explora: Environment and Resource

Editorial Board

*Editorial Board Members as of December 30, 2025

ACCSCIENCE PUBLISHING

Volume 2 | Issue 4 | December 2025 |

Explora: Environment and Resource

https://accscience.com/journal/EER

CONTENTS

ACCSCIENCE PUBLISHING

Explora: Environment and Resource

REVIEW ARTICLE

Development of corrosion inhibitors and nanocontainers for self-healing epoxy coatings: A review

Joghee Manivannan[1] and Kalaiselvan Shanmugam[2]*

[1]Department of Chemistry, V.S.B. College of Engineering Technical Campus, Coimbatore, Tamil Nadu, India

[2]Department of Chemistry, Rathinam Technical Campus, Coimbatore, Tamil Nadu, India

Abstract

Self-healing coatings are composed of anti-corrosive polymers that can recover from any damage caused to the coating film and regain their original performance. One of the methods for preparing self-healing coatings is by incorporating a healing agent stored in nanocontainers. When there is damage to the coating film, the nanocontainer ruptures due to the mechanical impact. It releases the healing agents, which form a protective film via polymerization over the damaged part, thereby protecting against corrosion. The second method for preparing self-healing coatings involves the embedment of corrosion inhibitors (healing agent) into a nanocontainer. Upon damage, the inhibitor is released into the exposed part of the film and retards corrosion reactions occurring at the defective part of the metal surface. The two components responsible for the self-healing functions are the nanocontainers and the corrosion inhibitors (polymerizable material). This article provides a detailed report on the development of several types of corrosion inhibitors and nanocontainers, their properties, and applications as self-healing coating materials, including their advantages and limitations.

Keywords: Epoxy resin; Corrosion inhibitors; Nano materials; Polymerization; Biomaterials

***Corresponding author:**
Kalaiselvan Shanmugam
(kalaiselvan.sh@rathinam.in)

Citation: Manivannan J, Shanmugam K. Development of corrosion inhibitors and nanocontainers for self-healing epoxy coatings: A review. *Explora Environ Resour*. 2025;2(4):025220043. doi: 10.36922/EER025220043

Received: May 29, 2025

Revised: July 20, 2025

Accepted: August 25, 2025

Published online: September 10, 2025

1. Introduction

Paints and organic coatings have become a key method for protecting against corrosion in equipment, machinery, and large metal structures across various fields. The binder is the major ingredient of paint, and there is a wide range of synthetic resins available for the coating industry. Modern synthetic resins comprise polymers with a wide range of molecular weights, including alkyd, amino, vinyl, acrylics, epoxies, polyurethanes, silicones, nitrocellulose, and chlorinated rubbers. Epoxy resins are one of the important classes of synthetic resins that provide high chemical and corrosion resistance. The epoxy resin is widely used as a coating material due to its easy conversion into high molecular weight products upon reacting with a curing agent through its terminal epoxy or hydroxyl groups (or both). There is a wide variety of curing agents available, and the choice of curing agent depends on the end-application requirement. The coating protects metal structures against corrosion, but the coating surface can be damaged externally, making them susceptible to corrosion due to the easy permeation of water, oxygen, and

other ions through these damaged sites. Recently, coating systems with the capability to repair damage internally and recover their coating properties have been developed.[1] These self-healing coating systems utilize self-healing materials that respond to external damage and retard corrosion.[2-4]

There are types of self-healing coatings commonly reported. The first type of self-healing coating involves microcapsules (loaded with polymerizable components) dispersed in the coating film. The polymerizable components are released when the coating film is damaged, and this disrupted region is healed through polymerization reactions.[5-7] The second type of self-healing coatings involves loading micro/nanocontainers with corrosion inhibitors, which are released to the damaged region in a controlled manner, protecting the surface.[8-10] This self-healing action of coatings with nanocapsules occurs through various methods, for example, controlled release of inhibitor by desorption, pH-controlled release, ion exchange, and mechanical rupture.[11] The mechanism of self-repair in coatings by external stimuli is displayed in Figure 1.

This review covers some of the important classes of corrosion inhibitors and nanocontainers used to carry the inhibitors. The important factors considered for choosing the inhibitors are based on the compatibility of the material with the coating matrix, its ability to be encapsulated, and its inhibitor efficiency. In contrast, the factors considered for nanocontainers are the type of inhibitor used, the healing mechanism, and the ability to release the inhibitor in a controlled manner when triggered by specific stimuli. The investigations on these inhibitors and nanocontainers presented in this review were selected based on the intrinsic advantages these self-healing materials have over similar functional materials. The inhibition mechanism and effectiveness of each type of corrosion inhibitors and nanocontainers to function as self-healing coatings for repairing damaged coating films are also discussed.

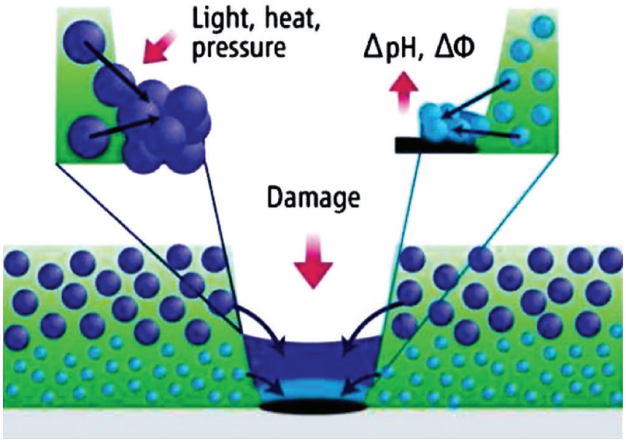

Figure 1. Self-healing mechanism. Reproduced with permission from ref.[1]

2. Nanocontainers

2.1. Inorganic nanocontainers

Nanocontainers are used to encapsulate inhibitors, protecting them and enabling controlled release into the damaged part of the coating. Inorganic nanocontainers are preferred due to their environmental friendliness; in contrast, polymeric nanoparticles generally possess lower mechanical stability. Hence, research focus has shifted to the use of inorganic nanoparticles. Various inorganic nanoparticles have been used as nanocontainers for self-healing coatings, including nanoparticles, nanotubes, and nanomaterials with porous nanostructures.

2.1.1. Mesoporous silica

The commonly used mesoporous inorganic materials for nanocontainers include mesoporous TiO_2, ZrO_2, and silica. Among these materials, mesoporous silica particles are not reactive with the corrosion inhibitors, stable under ultraviolet light, and have a large pore volume and surface area to incorporate a higher quantity of inhibitor.[12] It is reported that the inhibitor-loaded silica nanoparticle could be modified with octyl group functionalization to enhance its dispersibility in oil-based coatings.[13] However, corrosion inhibitor encapsulated in mesoporous silica nanocontainers could be released prematurely, necessitating the development of novel nanocontainers with controlled pore opening/closing at a molecular level. This could be achieved by functionalizing silica nanoparticles with organic substances (e.g., en-triacetate, ethylenediamine).[14] Mesoporous silica nanocontainers functionalized with organic groups have been reported to be excellent anti-corrosive containers for encapsulating inhibitors.

2.1.2. Halloysite nanotubes

Halloysite nanotubes are potential inorganic nanocontainers that are natural and inexpensive. These are 2:1 layered aluminosilicates with hollow tubular structures. The inner halloysite lumen has an inhibitor loading capacity of up to 20 wt%, depending on the origin of halloysite. The loading capacity can be increased by 2–3 times when the alumina within halloysite lumen is etched with sulfuric acid.[15] The dispersion of inhibitor-loaded halloysite nanotubes requires intensive mixing to avoid aggregating the nanocontainers. Shchukin and Mohwald[16] reported that halloysite nanotubes containing inhibitors were covered by a layer-by-layer assembly of

polyelectrolyte cell, which facilitates precise controlled release of inhibitors.

Several other inorganic nano clay containers have been studied, such as Kaolin, montmorillonite, bentonite, and graphene oxide.[17] The key characteristics assessed are eco-friendliness and safety concerns, and these are primarily dependent on particle size and chemical composition. The biosafety of several nanocontainers is presented in Table 1. The presented order suggests that halloysite nanotubes are the safest among all inorganic nano clay nanocontainers.

2.2. Nanocontainers with layer-by-layer assembled shell

The layer-by-layer assembly method is a new approach where oppositely charged molecules are adsorbed on a flat surface. The technique allows for proper control over the film thickness of the multilayer and composition. The technique has been applied first to silica nanoparticles by coating with layers of polyethylene imine and polystyrene sulfonate, and the corrosion inhibitor is entrapped within the polyelectrolyte multilayer; pH changes during corrosion initiate the release of the entrapped inhibitor.[18]

The layer-by-layer assembly technique for self-healing assembly has been further modified with the formation of core-shell-type containers with core oil and polyelectrolyte shell. It has been observed that the layer-by-layer coated emulsion improved stability toward droplet aggression, and the interfacial layer improved its resistance to rupture.[19,20] The prospect of customizing the functionality of the shell is the major advantage of the layer-by-layer assembly approach. However, the approach is challenged by the poor mechanical strength of the shell, making it difficult to maintain the integrity of the dried coating films.

Table 1. Biosafety ranking of nanocontainers

Safety number	Nanocontainers	Origin/type	Biocompatibility
1	Halloysite	Aluminosilicate nanotube	Generally good and safest
2	Kaolin	Aluminosilicate (Kaolinite)	Moderate to good
3	Montmorillonite	Smectite clay (layered)	Good biocompatibility
4	Silica (amorphous)	Non-crystalline silicon oxide	Generally good (amorphous)
5	Bentonite	Mostly montmorillonite-based	Similar to Montmorillonite
6	Graphene oxide (GO)	Carbon-based 2D nanomaterial	Variable (dependent on oxidation and size)

Note: Safety numbers are presented as follows: 1 represents the highest safety; 6 represents the lowest safety.

2.3. Nanocontainers with polymer shell

Nanocontainers with an organic shell (polymer shell) are prepared by oil-water emulsion polymerization. Though these shell structures are not as controlled as the layer-by-layer assembled shells, they have better mechanical strength. These nanocontainers are responsive to local pH changes. A research study revealed that a polymer shell nanocontainer made from urea formaldehyde and encapsulated with linseed oil effectively healed a damaged site on an epoxy coating.[21] Linseed oil from the organic shell was released and formed a protective film on the damaged part of the film.

A bilayer nanocapsule made with a hydrophilic inner shell and a hydrophobic outer shell could load amine-type corrosion inhibitors.[22] The amine released from the nanocapsules as a self-healing coating enhanced the corrosion resistance of the coating film.

The organic polymer shell nanocontainer forms an effective self-healing material for water-borne coatings to protect steel and aluminum alloys. However, it has limited applications to oil-based coatings due to the dissolution of these shells in organic solvents. Thus, both organic and inorganic nanocontainers are developed for the encapsulation of various corrosion inhibitors for self-healing anticorrosion coatings.

3. Inhibitors

Metal corrosion develops due to a disruption in the protective coating layer and propagates faster from the damaged part. Considerable investigations have been carried out to arrest corrosion at the damage site through self-healing with corrosion inhibitors (organic or inorganic) encapsulated in micro/nanocontainers. These inhibitors retard the reaction between metals and the environment by either adsorption of the molecules onto the metal surface or by altering the anodic or cathodic reaction. The performance of several common organic inhibitors in different corrosive media is described below.

3.1. Organic corrosion inhibitors

Organic compounds contain oxygen, nitrogen, and sulfur atoms and act as corrosion inhibitors due to their higher basicity and electron density. These atoms become the active centres for adsorption on the defective surface, and their efficiency follows the order: Oxygen < nitrogen < sulfur < phosphorus atoms. The lone pair electrons and p-electrons in inhibitors are involved in electron transfer to the metal surface, forming coordinate covalent bonds.

Heterocyclic compounds with sulfur and nitrogen having various substituents form effective corrosion inhibitors. The physicochemical properties and chemical structure of the inhibitor compound (e.g., electron density at the donor atom, p-orbital character, the functional group) and electron structure of the molecule determine the efficiency of the inhibitor. Replacing a hydrogen atom in the carbon in the ring with a functional group (-NO_2, -CHO, or -COO) would enhance its inhibition.[23] The nature of the binding between metal and organic inhibitor molecules determines the corrosion inhibition performance of the protective layer formed. Therefore, more active sites in the heterocyclic parts provide a stronger inhibitor-adsorption shield through chelation on the metal surface.[24] At the point of attachment, the electron density increases, consequently decelerating anodic or cathodic reactions. The electrons are absorbed by the cathode, regulating the anodic oxidation or corrosion.

The derivatives of thiophene, hydrazine, and pyrrole effectively inhibit metal corrosion in acidic solutions. However, these inhibitors are relatively toxic, thereby limiting their application as anticorrosive coatings and primers. Organic compounds containing heteroatoms in the conjugated system are an alternative to the above inhibitors (Table 2).

Synthetic organic inhibitors are widely studied for their inhibition efficiency, including 8-hydroxyquinoline, benzotriazole, 2-mercaptobenzothiazole (MBT), mercaptobenzoimidazole, and polyaniline. MBT and mercaptobenzoimidazole have reportedly improved corrosion resistance when incorporated into montmorillonite nanoparticles.[22,25] MBT and mercaptobenzoimidazole form a thin protective layer on the damaged metal surface during the self-healing process. Benzotriazole, as a corrosion inhibitor, is adsorbed on the metal surface and provides anodic inhibition.[26] 8-Hydroxyquinoline, a chelating agent, acts as a cathodic inhibitor for aluminum in neutral chloride solution by forming poorly soluble chelate complexes.[27]

Table 2. Types of organic corrosion inhibitors

Type of inhibitors	Examples
Nitrogen-containing compounds	Amines, pyridine derivatives, quaternary ammonium salts, triazole derivatives, Schiff base, amino acids, and indazole
Nitrogen- and sulfur-containing compounds	Imidazole derivatives, thiadiazole derivatives, and thiazole derivatives
Nitrogen- and oxygen-containing compounds	Oxazole derivatives, phthalimides, and plant extracts/natural
Sulfur-containing compounds	Thiourea derivatives and sulfonates

3.2. Important organic corrosion inhibitors

3.2.1. Indole-3 butyric acid (IBA)

Various corrosion inhibitors provide improved corrosion resistance, as they are more ductile with less stress tension. These inhibitors are classified according to their inhibition mechanism and composition.[28] The inhibitive and healing efficiency are determined using the scanning vibrating electrode technique and electrochemical impedance spectroscopy (EIS). Hang *et al.*[29] studied clay modified with IBA and observed enhanced corrosion resistance due to increased inhibitive action of IBA at the carbon steel surface by the enhanced barrier properties. Therefore, the self-healing property of the IBA-modified clay improves protection against corrosion. This has been confirmed by polarization curves, whereby IBA acts as an anodic inhibitor for carbon steel; local electrochemical impedance measurements on a scratched sample were in agreement with the findings.

3.2.2. Polyaniline

In general, larger molecules with a bulky structure cover more area on the electrode surface. In addition, they possess chemisorptive properties, as they contain nitrogen atoms in the polymer chain. These nitrogen atoms provide a reactive site for chemisorption, which further enhances the inhibition. Due to their stability and lower cost, these conducting polymers are widely investigated. The presence of large pi-electron clouds and quaternary nitrogen atoms confers inhibitive properties.[30,31] In its conductive state, polyaniline displaces the electroactive interface from its usual location and retards corrosion. The mechanism of corrosion inhibition of polyaniline begins with iron being oxidized, along with simultaneous electron release. Metal dissolution due to the initiation of corrosion causes a cathodic shift of the potential, which induces the reduction of polyaniline and transfer of the stored positive charge in its oxidized form to the defect site. This action forms a passive layer of metal oxide, which retards the propagation of corrosion.[32]

Han *et al.*[33] investigated the self-healing anti-corrosion properties of polyaniline/epoxy copolymer-urea-formaldehyde microcapsule coatings on rusty steel sheets. The polyaniline/epoxy copolymer, as a core material, at the ratio of 0.05:1 (wt.%), exhibited the highest electrochemical resistance to corrosion. The microcapsule (15 wt.%) within the coating provided excellent corrosion resistance due to the self-healing action. It was inferred that the polyaniline/epoxy copolymer-containing microcapsule system acts as

an effective anticorrosion coating and could be applied directly onto rusty steel surfaces.

3.2.3. 8-Hydroxyquinoline

Various studies have been conducted on the application of quinoline derivatives as corrosion inhibitors in acidic media.[34] Among these, 8-hydroxyquinoline has been reported as an outstanding complexing agent.[35,36] 8-Hydroxyquinoline is a good bidentate-complexing agent, which can form four and six covalent complexes with many metal ions**.** Based on this, 8-hydroxyquinoline has been used specifically for metal corrosion protection. Recent studies have revealed that 8-hydroxyquinoline is a mixed-type inhibitor of aluminum corrosion and forms complexes with copper and aluminum.[37] The inhibition process is formed by this complex formation with dissolved metals, enabling barrier film formation to retard further corrosion.

8-Hydroxyquinoline functions as an effective corrosion inhibitor for high-strength pipeline steel in 15% HCl solution.[36] It forms a protective surface film through adsorption by acting as a mixed-type inhibitor. The inhibitive efficiency increases with increasing concentrations of 8-hydroxyquinoline and is further enhanced upon the addition of potassium iodide (KI). The heteroatoms present in hydroquinone complexes with iron ions, forming a protective film.

3.2.4. Benzotriazole

Benzotriazole is a renowned corrosion inhibitor that forms a protective layer on metal surfaces through covalent and coordinate bonds. It is also used in combination with other corrosion inhibitors to enhance inhibition efficiency.

The corrosion inhibition efficiency of benzotriazole on carbon steel used as reinforcement in concrete has been studied.[38] To imitate marine environments, the effect of benzotriazole (1.5 wt.%) on the corrosion resistance of carbon steel of a matured concrete, along with the addition of 3.5 wt.% NaCl solution was studied. The investigation was carried out using potentiodynamic polarization tests and EIS. Compared to the nitrites used for inhibiting corrosion of reinforcement steel in concrete, benzotriazole addition displayed better inhibitor efficiency; hence, benzotriazole can be a desirable and attractive alternative to nitrites.

In one study, 1,2,3-benzotriazole was incorporated into an acrylic coating that was applied onto cold-rolled mild steel in an acidic medium (H_2SO_4 solution); further testing of the organic corrosion inhibitor revealed that there was no corrosion progression on the coated film even after 30 days of exposure of the coated substrate.[39] The study was conducted with different concentrations of benzotriazole, and 0.1 wt.% benzotriazole in acrylic coating reported the best corrosion protection.

3.2.5. Mercaptobenzothiazol

Several studies have been conducted to investigate the efficiency of corrosion inhibition of 2-MBT on various metals, including copper, aluminum alloy, and carbon steel. The studies have indicated that the heterocyclic compound 2-MBT is a good corrosion inhibitor on these metals.[40,41]

Copper-based alloys (primarily Cu-Ni) find extensive use across various fields of applications in industries. The performance of 2-MBT and its inhibition efficiency on Cu-Ni alloys in a corrosive environment (with 3 wt.% NaCl solution) was evaluated using weight loss methods, potentiodynamic polarization, and EIS. It was observed that MBT enhances the corrosion resistance of copper-based alloys; at 80 ppm, the maximum inhibition was approximately 92%. Furthermore, 2-MBT functioned as a mixed-type inhibitor. The nitrogen and exocyclic sulfur atoms of 2-MBT are adsorbed on the metal surface, forming a thin film that inhibits corrosion.[42]

Another study evaluated the inhibitive efficiency of 2-MBT in 5% HCl solution on aluminum and aluminum–titanium alloys.[43] EIS and Tafel polarization were employed to assess varying concentrations of 2-MBT and temperatures. It was found that 2-MBT exhibited good anticorrosive properties on aluminum and aluminum–titanium alloys. As the concentration of 2-MBT increased, inhibition efficiency enhanced as well. Conversely, inhibition efficiency decreased with increasing temperature.

3.2.6. Mercaptobenzimidazole

Benzimidazole, a heterocyclic compound, and its derivatives are regarded as good corrosion inhibitors for many metals and their corresponding alloys, even in highly corrosive environments (both acidic and basic media) and salt solutions.[44] Benzimidazole and its derivatives behaved as mixed-type inhibitors, with the inhibitive effect more evident towards cathodic reactions over anodic reactions.

The inhibition efficiency of imidazolium-based inhibitors on mild steel in H_2SO_4 was studied recently.[45] The corrosion inhibition performance indicated that the molecular modification of benzimidazole led to enhanced corrosion inhibition. Theoretical molecular modelling methods have helped develop potential corrosion inhibitors. The mechanism for the corrosion protection of benzimidazole and its derivatives is attributed to the presence of pi-electrons on the planar-fused moiety and non-bonding lone pair electrons on the heteroatoms.

Obot *et al.*[46] studied the corrosion inhibition performance of 2-mercaptobenzimidazole on iron, copper, and aluminum surfaces. The study revealed higher inhibitor efficiency of 2-mercaptobenzimidazole (MBI) on steel compared to aluminum and copper. EIS measurements indicated that benzimidazoles are readily adsorbed, and the thin layer formed on the metal surface provides a physical barrier, which inhibits charge transfer reactions at the metal-solution interface. Benzimidazole derivatives are regarded as mixed-type inhibitors, exhibiting better inhibitive effect on cathodic reactions over anodic reactions. Furthermore, adsorption of the inhibitors on the metal surface to protect the metals was also confirmed by scanning electron microscopy images. The study also reported that benzimidazoles exhibit high inhibition efficiencies of up to 99% in concentrated HCl or H_2SO_4 solutions at different temperatures.[47] The inhibiting properties observed at different temperatures presented a marginal decrease in inhibition efficiency with increasing temperature.

However, the disadvantages of using synthetic organic inhibitors have limited their scope of application, necessitating the development of cost-effective, non-toxic products or natural green inhibitors.

3.3. Green inhibitors

Due to changes in environmental laws and the awareness of environmental issues, the research focus has shifted from conventional corrosion inhibitors towards environmentally friendly green inhibitors. These natural products contain a range of active substances that can bind to organic compounds, subsequently adhering to metal surfaces and forming a film layer to protect against corrosive elements. As natural extracts contain abundant active elements, a wide range of corrosion inhibitors can be produced from these extracts. For instance, natural extracts containing a mix of phytochemicals and functional groups have an affinity to adsorb onto metal surfaces. These natural extracts are non-toxic and biodegradable, making them the preferred option as corrosion inhibitors in organic coatings.[48]

A handful of studies have investigated the inhibition effect of naturally occurring materials in both acidic and alkaline conditions. The extract of *Delonix regia* was found to inhibit metal corrosion in HCl solutions. In addition, higher concentrations of the inhibitor are associated with enhanced inhibition efficiency. However, inhibition efficiency decreases with longer exposure time when tested on aluminum in HCl solutions.[49] Rosemary leaves (*Rosmarinus officinalis*) have been studied as corrosion inhibitors on aluminum-magnesium alloys in a 3% NaCl solution; the presence of flavonoids in the extract enhanced the passivating film properties of the steel.[50]

El-Etre[51] studied the corrosion inhibition property of natural honey on carbon steel and reported that natural honey exhibited a remarkable corrosion inhibition in high saline water. Although the inhibition efficiency increased with increasing natural honey concentration, the inhibition efficiency decreased over time due to fungal growth in the medium**.** He investigated the corrosion inhibition efficiency of *Opuntia* extract on aluminum; the efficiency of inhibition increased with increasing concentration of the extract.[52] A separate study assessed the corrosion inhibition efficiency of khillah seed extract on SX 316 steel in HCl solution; the inhibition mechanism is attributed to the formation of insoluble complexes from the interaction of iron cations with khellin.[53]

Ebenso *et al.*[54,55] investigated the corrosion inhibition of aluminum and mild steel using ethanolic extracts of African bush pepper, *Carica papaya* leaves, and neem leaves (*Azadirachta indica*). The concentration and temperature of the extracts have a direct correlation with inhibitor efficiency; *C. papaya* exhibited maximum inhibition at 30°C, whereas *A. indica*'s performance peaked at 40°C.[56] Zucchi and Omar[57] observed reduced corrosion in steel using various plant extracts, with an efficiency of 88–96% in 1 N HCl and a marginally lower efficiency in 2 N HCl. It was reported that the protein content of these plants is hydrolyzed into products with inhibitory properties. Another study investigated the corrosion inhibition capacity of honey and *R. officinalis*[58]; the inhibitive effect of these compounds increased when zinc was polarized by the addition of salts, such as NaCl and Na_2SO_4. Likewise, the electronegativity of halide ions enhances inhibition efficiency, suggesting a significant role in the surface adsorption process.[59] In another study, guar gum, a polysaccharide compound, has been used as a corrosion inhibitor for carbon steel,[60] reportedly enhancing the efficiency of corrosion inhibition. The inhibitive property of guar gum is attributed to its horizontal adsorption on the steel surface, and it follows the Langmuir adsorption isotherm. Okafor *et al.*[61,62] studied the extracts of onion (*Allium sativum*), *C. papaya*, *Garcinia kola*, and *Phyllanthus amarus* for their corrosion inhibition efficiency; the results suggest that these extracts served as good corrosion inhibitors through chemical adsorption on the metal surface.

A large number of studies have been carried out using the extracts of natural honey, jojoba oil, Artemisia oil, *Telfaria occidentalis*, *Ocimum viridis*, *A. indica*, *Sanseviera trifasciata*, and rosemary for their anti-corrosion properties.[63-69] The results indicate that these extracts inhibit the corrosion process in both acidic and basic

solutions; inhibition efficiency increased with increasing concentrations of these extracts. Similarly, the inhibition efficiency of *Musa* peel and *Punica granatum* extract was evaluated.[70,71]; the inhibition efficiency of *P. granatum* extract increased with increasing concentration but decreased with increasing temperature and time. Nonetheless, most of these studies are limited to steel, and only a few studies have used aluminum and copper.

The corrosion inhibition efficiency of natural plant extracts has been tested mostly in mildly acidic or basic solutions at varying concentrations. Hence, natural plant products have great potential to serve as a corrosion-inhibiting material, effective in preventing metal corrosion and comparable to organic inhibitors. Although natural plant extracts are environmentally safe, inexpensive, and derived primarily from renewable sources, further research is warranted to study the inhibition efficiency of plant extracts under varying conditions, their compatibility with different coating systems, and their effectiveness in different substrates.

3.4. Drugs as green corrosion inhibitors

In the virtual screening method, results from corrosion studies of drugs have indicated that the substructures of drugs share many similarities with general corrosion inhibitors.[72] Five- and six-membered rings of heterocyclic and carbocyclic systems are commonly found in drug structures, and most of these compounds are aromatic. Hence, heterocycles and substituted benzene rings, such as furans, thiophenes, pyridines, isoxazoles, and imidazole, commonly occur in drug structures. The effectiveness of a corrosion inhibitor depends on its molecular structure, chemical composition, and binding affinity to the metal surface. Owing to their high molecular weight, compounds containing heteroatoms (O, S, or N) with lone-pair electrons and aromatic rings can enhance adsorption onto the metal surface, particularly at damaged sites to prevent corrosion.[73]

There is great potential for further exploration, as these compounds are environmentally friendly. Over the past two decades, several research investigations have been carried out on the use of a wide range of drugs as corrosion inhibitors. The drugs investigated so far are predominantly hydrophilic and biodegradable. However, since the transformation products of some drugs may be highly hazardous to the environment, more studies are required before any drug can be considered truly eco-friendly when evaluating its suitability as a green corrosion inhibitor.

4. Conclusion

In this review, we discussed some of the most important classes of organic corrosion inhibitors and highlighted their observed improvements in corrosion resistance. Most organic inhibitors investigated have been found to adsorb onto metal surfaces, forming a protective barrier coating. The availability of non-bonding electrons and pi-electrons in the inhibitor molecules facilitates electron transfer from the inhibitor to the metal, and the efficiency of inhibition depends on the stability of the chelate formed. Among these compounds, triazoles and benzotriazoles are particularly known for their strong adsorption and protective film formation on metal surfaces.

The importance of green inhibitors of plant origin has been reviewed, as they are derived from renewable resources and are biodegradable. The inhibition efficiency of plant-based green inhibitors, along with their effectiveness under increasing extract concentration, elevated temperature, and different environments (acidic and alkaline conditions), has been reported. Green inhibitors containing compounds such as tannins, flavonoids, and alkaloids adsorb onto the metal surface and form a protective layer.

This review also focused on studies of some of the most essential classes of nanocontainers, their effectiveness as smart containers, and the advantages and limitations associated with their practical applications. Mesoporous silica and halloysite clays are among the most widely studied inorganic nanocontainers, owing to their superior performance in self-healing coatings and their biosafety.

The self-healing coatings developed to date are capable of repairing only minor damages, such as abrasion or puncture, on the substrate. Future research could look into developing intelligent healing mechanisms capable of repairing more complex damage. In addition to self-healing, future research should also focus on incorporating antimicrobial functions in nanocontainers to broaden their industrial applications. Currently, most nanocontainers are based on single-stimulus-responsive materials; however, multi-stimulus-responsive nanocontainers may be developed to further enhance self-healing performance.

Acknowledgments

The authors sincerely acknowledge their respective institutions, V.S.B. College of Engineering Technical Campus and Rathinam Technical Campus, for providing the necessary facilities, research support, and access to scientific resources to prepare this review article.

Funding

None.

Conflict of interest

The authors declare they have no competing interests.

Author contributions

Conceptualization: Joghee Manivannan
Writing–original draft: Joghee Manivannan
Writing–review & editing: Kalaiselvan Shanmugam

Ethics approval and consent to participate

Not applicable.

Consent for publication

Not applicable.

Availability of data

Not applicable.

References

1. Zhang F, Ju P, Pan M, *et al*. Self-healing mechanisms in smart protective coatings: A review. *Corros Sci*. 2018;144:74-88.

   doi: 10.1016/j.corsci.2018.08.005

2. Hughes AE, Cole IS, Muster TH, Varley RJ. Designing green, self-healing coatings for metal protection. *NPG Asia Mater*. 2010;2:143-151.

   doi: 10.1038/asiamat.2010.136

3. Yabuki A, Okumura K. Self-healing coatings using superabsorbent polymers for corrosion inhibition in carbon steel. *Corros Sci.* 2012;59:258.

   doi: 10.1016/j.corsci.2012.03.007

4. Wei H, Wang Y, Guo J, *et al*. Advanced micro/nano capsules for self-healing smart anticorrosion coatings. *J Mater Chem* A. 2015;3:469.

   doi: 10.1039/c4ta04791E

5. Cho SH, White SR, Braun PV. Self-healing polymer coatings. *Adv Mater.* 2009;21:645.

   doi: 10.1002/adma.200802008

6. Hasanzadeh M, Shahidi M, Kazemipour M. Application of EIS and EN techniques to investigate the self-healing ability of coatings based on microcapsules filled with linseed oil and CEO2 nanoparticles. *Prog Org Coat*. 2015;80:106.

   doi: 10.1016/j.porgcoat.2014.12.002

7. Siva T, Sathiyanarayanan S. Self-healing coatings containing dual active agent loaded urea formaldehyde (UF) microcapsules. *Prog Org Coat*. 2015;82:57.

   doi: 10.1016/j.porgcoat.2015.01.010

8. Zheludkevich ML, Tedim J, Freire CS, *et al*. Self-healing protective coatings with "green" chitosan-based pre-layer reservoir of corrosion inhibitor. *J Mater Chem*. 2011;21:4805.

   doi: 10.1039/c1jm10304k

9. Sonawane SH, Bhanvase BA, Jamali AA, *et al*. Improved active anticorrosion coatings using layer-by-layer assembled ZnO nanocontainers with benzotriazol. *Chem Eng J*. 2012;189-190:464-472.

   doi: 10.1016/j.cej.2012.02.076

10. Kopec M, Szczepanowicz K, Mordarski G, *et al*. Self-healing epoxy coatings loaded with inhibitor- containing polyelectrolyte nanocapsules. *Prog Org Coat*. 2015;84:97.

    doi: 10.1016/j.porgcoat.2015.02.011

11. Zheludkerich ML, Tedim J, Ferriera MGS. Smart coatings for active corrosion protection based on multi-functional micro and nanocontainers. *Electrochim Acta*. 2012;82:314.

    doi: 10.1016/j.electacta.2012.04.095

12. Borisova D, Mohwald H, Shchukin DG. Mesoporous silica nanoparticles for active corrosion protection. *ACS Nano.* 2011;5:1939.

    doi: 10.1021/nn102871v

13. Hollamby MJ, Fix D, Donch I, Borisova D, Mohwald H, Shchukin DG. Hybrid polyester coating incorporating functionalized mesoporous carriers for the holistic protection of steel surfaces. *Adv Mater.* 2011;23:1361.

    doi: 10.1002/adma.201003035

14. Zheng Z, Schenderlein M, Huang X, Brownball NJ, Blanc F, Shchukin DG. Influence of functionalization of nanocontainers on self-healing anticorrosive coatings. *ACS Appl Mater Interfaces*. 2015;7:22756.

    doi: 10.1021/acsami.5b08028

15. Abdullayev E, Joshi A, Wei EB, Zhao YF, Lvov Y. Enlargement of halloysite clay nanotube lumen by selective etching of aluminium oxide. *ACS Nano.* 2012;6:7216.

    doi: 10.1021/nn302328x

16. Shchukin DG, Mohwald H. Surface-engineered nanocontainers for entrapment of corrosion inhibitors. *Adv Funct Mater.* 2007;17:1451.

    doi: 10.1002/adfm.200601226

17. Kryuchkova M, Danilushkina A, Lvov Y, Fakhrullin R. Evaluation of toxicity of nanoclays and graphene oxide *in vivo*: A *Paramecium caudatum* study. *Environ Sci Nano.* 2016;3:442.

    doi: 10.1039/c5en00201j

18. Shchukin DG, Zheludkevich M, Yasakau K, Lamaka S, Ferreira MGS, Mohwald H. Layer-by-layer assembled nanocontainers for self-healing corrosion protection. *Adv Mater.* 2006;18:1672.

    doi: 10.1002/adma.200502053

19. Grigoriev D, Shchukina E, Shchukin DG. Nanocontainers for self-healing coatings. *Adv Mater Interfaces*. 2017;4(1):1600318.

    doi: 10.1002/admi.201600318

20. Grigoriev DO, Bukreeva T, Mohwald H, Shchukin DG. New method for fabrication of loaded micro- and nanocontainers: Emulsion encapsulation by polyelectrolyte layer-by-layer deposition on the liquid core. *Langmuir*. 2008;24:999-1004.

doi: 10.1021/la702873f

21. Suryanarayana C, Rao KC, Kumar D. Preparation and characterization of microcapsules containing linseed oil and its use in self-healing coatings. *Prog Org Coat*. 2008;63:72-78.

doi: 10.1016/j.porgcoat.2008.04.008

22. Choi H, Kim KY, Park JM. Encapsulation of aliphatic amines into nanoparticles for self-healing corrosion protection of steel sheets. *Prog Org Coat*. 2013;76:1316-1324.

doi: 10.1016/j.porgcoat.2013.04.005

23. Evans UR. *The Corrosion and Oxidation of Metals*. London: Edward Arnold (Publishers) Ltd.; 1976.

24. Al-Amiery AA, Mohamad AB, Kadhum AAH, Shaker LM. Experimental and theoretical study on the corrosion inhibition of mild steel by nonanedioic acid derivative in hydrochloric acid solution. Sci Rep. 2022;12:4705.

doi: 10.1038/s41598-022-081466-8

25. Pilbath A, Szabo T, Telegdi LNJ. SECM study of steel corrosion under scratched microencapsulated epoxy resin. *Prog Org Coat*. 2012;75:480-485.

doi: 10.1016/j.porgcoat.2012.06.006

26. Choi H, Song YK, Kim KY, Park JM. Encapsulation of triethanolamine as organic corrosion inhibitor into nanoparticles and its active corrosion protection for steel sheets. *Surf Coat Technol.* 2012;206:2354.

doi: 10.1016/j.surfcoat.2011.10.030

27. Huang M, Yang J. Facile microencapsulation of HDI for self-healing anticorrosive coatings. *J Mater Chem*. 2011;21:11123.

doi: 10.1039/c1jm10794a

28. Latnikova A, Grigoriev DO, Hartmann J, Mohwald H, Shchukin DG. Polyfunctional microencapsulation of HDI damage -triggered water-repelling effect. *Soft Matter*. 2011;7:369.

doi: 10.1039/c0sm00842g

29. Hang TT, Truc TA, Oliver MG, Vandermiers C. Corrosion protection mechanisms of carbon steel by an epoxy resin containing indole-3 butyric acid modified clay. *J Porg Coat*. 2010;69:410-416.

doi: 10.1016/j.porgcoat.2010.08.004

30. Li XG, Huang MR, editors. *Milestones in Powerful Adsorbents of Heavy Metal Ion*s. Cambridge: Cambridge Scholars Publishing; 2024.

31. Morsi RE, Khamis EA, Al-Sabagh AM. Polyaniline nanotubes: Facile synthesis, electrochemical, quantum chemical characteristics and corrosion inhibition efficiency. *J Taiwan Inst Chem Eng.* 2016;60:573-581.

doi: 10.1016/j.jtice.2015.10.028

32. Abu-Thabit NY, Makhlouf ASH. *Recent Advances in Polyaniline (PANI)-Based Organic Coatings for Corrosion Protection*. New Delhi: Woodhead Publishing Limited; 2014. p. 459-486.

doi: 10.1533/9780857096883.2.459

33. Han R, He H, Liu X, *et al*. Anti-corrosion and self-healing coatings with polyaniline/epoxy copolymer-urea-formaldehyde microcapsules for rusty steel sheets. *J Colloid Interface Sci*. 2022;616:605-617.

doi: 10.1016/j.jcis.2022.02.088

34. Obot IB, Ankah NK, Sorour AA, Gasem ZM, Haruna K. 8-Hydroxyquinoline as an alternative green and sustainable acidizing oilfield corrosion inhibitor. *Sustain Mater Technol.* 2017;14:1-10.

doi: 10.1016/j.susmat.2017.09.001

35. Bardez E, Devol I, Larrey B, Valeur B. Excited-state processes in 8-hydroxyquinoline: Photoinduced tautomerization and solvation effects. *J Phys Chem.* 1997;101:7786-7793.

doi: 10.1021/jp971293u

36. Filip E, Humelnicu I, Ghirvu C. Some aspects of 8-hydroxyquinoline in solvents. *Acta Chem Iasi*. 2009;96: 85-96.

37. Liu W, Singh A, Lin Y, Ebenso EE, Zhou L, Huang B. 8-Hydroxyquinoline as an effective corrosion inhibitor for 7075 aluminium alloy in 3.5% NaCl solution. *Int J Electrochem Sci.* 2014;9:5574-5584.

doi: 10.1016/S1452-3981(23)08190-7

38. Mennucci MM, Banczek EP, Rodrigues PRP, Costa I. Evaluation of benzotriazole as corrosion inhibitor for carbon steel in simulated pore solution. *Cement Concr Compos.* 2009;31(6):418-424.

doi: 10.1016/j.cemconcomp.2009.04.005

39. Ammar S, Ma IAW, Muhammad FMS, Bashir S. Electrochemical studies of 1,2,3-benzotriazole inhibitor for acrylic-based coating in different acidic media systems. *J Polym Res.* 2020;27:142.

doi: 10.1007/s10965-020-02130-4

40. Wu X, Wiame F, Maurice V, Marcus P. Adsorption and thermal stability of 2-mercaptobenzothiazole corrosion inhibitor on metallic and pre-oxidized Cu (1 1 1) model surfaces. *Appl Surf Sci.* 2020;508:145132.

doi: 10.1016/j.apsusc.2019.145132

41. Jafari H, Akbarzade K, Danaee I. Corrosion inhibition of carbon steel immersed in a 1M HCl solution using benzothiazole derivatives. *Arab J Chem.* 2013;12:1387-1394.

doi: 10.1016/j.arabjc.2014.11.018

42. Zarebidaki A, Mofidi SHH, Bahri FI. Effect of 2-mercaptobenzothiazole on the corrosion inhibition of Cu-10Ni alloy in 3 wt% NaCl solution. *J Appl Electrochem.* 2022;52:1773-1788.

doi: 10.1007/s10800-022-01750-6

43. l-Sayed AR, El-Hendawy MM, El-Mahdy MS, Hassan FSM, Mohamed AE. The inhibitive action of 2-mercaptobenzothiazole on the porosity of corrosion film formed on aluminum and aluminum-titanium alloys in hydrochloric acid solution. *Sci Rep.* 2023;13:4812.

doi: 10.1038/s41598-023-31795-2

44. Marinescu M. Recent advances in the use of benzimidazoles as corrosion inhibitors. *BMC Chem.* 2019;13:136.

doi: 10.1186/s13065-019-0655-y

45. Zhou Y, Guo L, Zhang S. Corrosion control of mild steel in 0.1 M H_2SO_4 solution by benzimidazole and its derivatives: An experimental and theoretical study. *RSC Adv.* 2017;7:23961-23969.

doi: 10.1039/c7ra02192e

46. Obot IB, Gasem ZM, Umoren SA. Understanding the mechanism of 2-mercaptobenzimidazole adsorption on Fe (110), Cu (111) and Al (111) surfaces: DFT and molecular dynamics simulations approaches. *Int J Electrochem Sci.* 2014;9:2367-2378.

doi: 10.1016/S1452-3981(23)07933-6

47. Popova A, Sokolova E, Raicheva S, Christov M. AC and DC study of the temperature effect on mild steel corrosion in acid media in the presence of benzimidazole derivatives. *Corros Sci*. 2003;45(1):33-58.

doi: 10.1016/S0010-938X(02)00072-0

48. Abdel-Karim AM, El-Shamy AM. A review on green corrosion inhibitors for protection of archaeological metal artifacts. *J Bio Tribo Corros*. 2022;8(2):35.

doi: 10.1007/s40735-022-00636-6

49. Abiola OK, Oforka NC, Ebenso EE, Nwinuka NM. Eco-friendly corrosion inhibitors: The inhibitive action of *Delonix regia* extract for the corrosion of aluminium in acidic media. *Anti Corros Methods Mater.* 2007;54:219-224.

doi: 10.1108/00035590710762357

50. Kliskic M, Radoservic J, Gudic S, Katalinic V. Aqueous extract of *Rosmarinus officinalis* L. as inhibitor of Al-Mg alloy corrosion in chloride solution. *J Appl Electrochem.* 2000;30(7):823-830.

doi: 10.1023/A:1004041530105

51. El-Etre AY. Natural honey as corrosion inhibitor for metals and alloys. I. Copper in neutral aqueous solution. *Corros Sci.* 1998;40(11):1845-1850.

doi: 10.1016/S0010-938X(98)00082-1

52. El-Etre AY. Inhibition of aluminium corrosion using *Opuntia* extract. *Corros Sci.* 2003;45(11):2485-2495.

doi: 10.1016/S0010-938X(03)00066-0

53. El-Etre AY. Khillah extract as inhibitor for acid corrosion of SX 316 steel. *Appl Surf Sci.* 2006;252(24):8521-8525.

doi: 10.1016/j.apsusc.2005.11.066

54. Ebenso EE, Ibok UJ, Ekpe UJ, *et al*. Corrosion inhibition studies of some plant extracts on aluminium in acidic medium. *Trans SAEST*. 2004;39(4):117-123.

doi: 10.1016/S0254-0584(02)00446-7

55. Ebenso EE, Ekpe UJ. Kinetic study of corrosion and corrosion inhibition of mild steel in H2SO4 using *Parica papaya* leaves extract. *West Afr J Biol Appl Chem.* 1996;41:21-27.

56. Ekpe UJ, Ebenso EE, Ibok UJ. Inhibitory action of *Azadirachta indica* leaves extract on the corrosion of mild steel in H_2SO_4. *J West Afr Sci Assoc.* 1994;37:13-30.

doi: 10.1016/S1452-3981(23)15337-5

57. Zucchi F, Omar IH. Plant extracts as corrosion inhibitors of mild steel in HCl solutions. *Surf Technol.* 1985;24(4): 391-399.

doi: 10.5897/ijps11.923

58. Yee YJ. *Green Inhibitors for Corrosion Control: A Study on the Inhibitive Effects of Extracts of Honey and Rosmarinus officinalis* L. (*Rosemary*) [M.S. thesis], University of Manchester, Institute of Science and Technology; 2004.

59. Umoren SA, Obot IB, Ebenso EE. Corrosion inhibition of aluminium using exudate gum from *Pachylobus edulis* in the presence of halide ions in HCl. *Eur J Chem.* 2008;5(2): 355-364.

doi: 10.1155/2008/138407

60. Abdallah M. Guar gum as corrosion inhibitor for carbon steel in sulphuric acid solutions. *Port Electrochim Acta*. 2004;22:161-175.

doi: 10.4152/pea.200402161

61. Okafor PC, Ekpe UJ, Ebenso EE, Umoren EM, Leizou KE. Inhibition of mild steel corrosion in acidic medium by *Allium sativum* extracts. *Bull Electrochem.* 2005;21(8): 347-352.

62. Okafor PC, Ebenso EE. Inhibitive action of *Carica papaya* extracts on the corrosion of mild steel in acidic media and their adsorption characteristics. *Pigment Resin Technol.* 2007;36(3):134-140.

doi: 10.1108/03699420710748992

63. Okafor PC, Osabor VI, Ebenso EE. Eco-friendly corrosion inhibitors: Inhibitive action of ethanol extracts of *Garcinia kola* for the corrosion of mild steel in H2SO4 solutions. *Pigment Resin Technol.* 2007;36(5):299-305.

doi: 10.1108/03699420710820414

64. Okafor PC, Ikpi ME, Uwah IE, Ebenso EE. Inhibitory action of *Phyllanthus amarus* extracts on the corrosion of mild steel in acidic media. *Corros Sci.* 2008;50(8):2310-2317.

doi: 10.1016/j.corsci.2008.05.009

65. El-Etre AY, Abdallah M. Natural honey as corrosion inhibitor for metals and alloys. II. C-steel in high saline water. *Corros Sci.* 2000;42(4):731-738.

doi: 10.1016/S0010-938X(99)00106-7

66. Chetouani A, Hammouti B, Benkaddour M. Corrosion inhibition of iron in hydrochloric acid solution by jojoba oil. *Pigment Resin Technol.* 2004;33(1):26-31.

doi: 10.1108/03699420410512077

67. Bouyanzer A, Hammouti B. A study of anti-corrosive effects of Artemisia oil on steel. *Pigment Resin Technol.* 2004;33(5):287-292.

doi: 10.1108/03699420410560489

68. Oguzie EE. Inhibition of acid corrosion of mild steel by *Telfairia occidentalis* extract. *Pigment Resin Technol.* 2005;34(6):321-326.

doi: 10.1108/03699420510630336

69. Oguzie EE. Studies on the inhibitive effect of *Occimum viridis* extract on the acid corrosion of mild steel. *Mater Chem Phys.* 2006;99:441-446.

doi: 10.1016/j.matchemphys.2005.11.018

70. Eddy NO, Odoemelam SA, Odiongenyi AO. Ethanol extract of *Musa* species peels as a green corrosion inhibitor for mild steel: Kinetics, adsorption and thermodynamic considerations. *Electron J Environ Agric Food Chem.* 2009;8(4):243-255.

doi: 10.1016/0376-4583(85)90057-3

71. Deepa Rani P, Selvaraj S. Inhibitive and adsorption properties of *Punica granatum* extract on brass in acid media. *J Phytol.* 2010;2(11):58-64.

72. Chambers BD, Taylor SR, Kendig MW. Rapid discovery of corrosion inhibitors and synergistic combinations using high-throughput screening methods. *Corrosion.* 2005;61:480-489.

doi: 10.5006/1.3280648

73. Gece G. Drugs: A review of promising novel corrosion inhibitors. *Corros Sci.* 2011;53(12):3873-3898.

doi: 10.1016/j.corsci.2011.08.006

ACCSCIENCE PUBLISHING

Explora: Environment and Resource

REVIEW ARTICLE

Emergence of Marine Fishery Advisory services and their impact on achieving sustainable fisheries in India: A review

Sudip Kumar Kundu[1,2] and Harini Santhanam[1,3,4]*

[1]Department of Public Policy, Manipal Academy of Higher Education, Manipal, Karnataka, India

[2]India Meteorological Department, Regional Meteorological Centre, Ministry of Earth Sciences, Government of India, Guwahati, Assam, India

[3]Centre for Excellence in Smart Coastal Sustainability, Manipal Academy of Higher Education, Manipal, Karnataka, India

[4]Department of Sciences and Humanities, Manipal Institute of Technology, Manipal Academy of Higher Education, Manipal, Karnataka, India

Abstract

Sustainable fisheries development is increasingly critical amid rising global demand for marine resources. In this context, the Indian Marine Fishery Advisories, particularly Potential Fishing Zone (PFZ) and Ocean State Forecast (OSF) Advisories, have emerged as key tools to enhance fishery practices while reducing uncertainty and risks. The Earth System Science Organization-Indian National Centre for Ocean Information Services, under the Ministry of Earth Sciences, has been providing satellite-based PFZ and OSF Advisories since 1999 and 2009, respectively. PFZ Advisories guide fishers to areas of high fish aggregation, whereas OSF services enhance safety through accurate ocean weather forecasts. These advisories are disseminated daily to the coastal fishing community across India through multiple channels. Despite demonstrable improvements in catch per unit effort and fisher incomes in many regions, significant disparities remain in access and utilization of these services. Public–private partnerships, particularly those involving non-profit organizations, have the potential to bridge these gaps by improving outreach and community capacity-building at the grassroots level. In addition, international experience shows that co-management practices can support long-term sustainability in fisheries. This study reviews the dissemination and utilization of PFZ and OSF Advisories globally, with a focus on India, and evaluates their socioeconomic and environmental impacts. It identifies barriers to access, highlights successful models, and explores future needs for inclusive and sustainable fishery development. The findings aim to inform policy frameworks that align with the Sustainable Development Goals, particularly those related to poverty reduction, food security, and marine resource sustainability.

Keywords: Potential fishing zones; Ocean state forecast; Indian National Centre for Ocean Information Services; Marine Fishery Advisory; Dissemination; Sustainable fisheries; Catch per unit effort; Sustainable Development Goals 14

***Corresponding author:**
Harini Santhanam
(harini.santhanam@manipal.edu)

Citation: Kundu SK, Santhanam H. Emergence of Marine Fishery Advisory services and their impact on achieving sustainable fisheries in India: A review. *Explora Environ Resour.* 2025;2(4):025280054. doi: 10.36922/EER025280054

Received: July 8, 2025

1st revised: July 20, 2025

2nd revised: September 16, 2025

3rd revised: September 29, 2025

Accepted: October 9, 2025

Published online: November 4, 2025

1. Introduction

The fisheries and aquaculture sectors have been treated as the "sunrise sector" in India.[1] The fishery sector in India can be characterized by small-scale farming, employs over 16 million people, and doubles in the value chain.[1,2] During the 11th 5-Year Plan, the output value of growth from the fishery sector was about 3.6% annually, where ₹24.83 billion was allocated for the fishery sector.[3] The fish production in India has since been increased by almost 17-fold, from 0.75 million metric tons (Mt) in 1950–1951 to 13.42 Mt in 2018–2019.[2] In general, India as the second largest fish producer country in the world after China, accounted for 6.56% of global fish production during 2017–2018.[4] Fishery sector has contributed for 5.23% to the Agricultural Gross Value Added (GVA) and 1.07% to the country's GVA during financial year (FY) 2017–2018 (Figure 1A), which is about ₹1755.73 billion.[2] India also earned a significant amount of foreign exchange worth ₹465.89 billion (US$6.73 billion) from fishery export, which is 5% of the overall export and 19.23% of the total agricultural export.[2] Along with the utilization of 8118 km long coastline consisting of 0.53 million km^2 continental shelf area within 2.02 million km^2 of exclusive economic zone (EEZ) in India, the estimated total annual harvestable marine fishery potential was about 5.31 Mt whereas 3.71 Mt (approximately 71%) has been harnessed across its nine maritime states, two union territories, and two island territories (Figure 2) during FY 2018–2019.[2,3,5,6]

According to the Food and Agriculture Organization of the United Nations (FAO), total global marine fish production was about 108 Mt in 2016, where India contributes about 3.65%.[4] Currently, fish provides 16% of the total global protein[7]; however, India only accounts for 28% of the marine fish production (3.71 Mt) of the total production of 13.42 Mt.[2] India stands in sixth position in global marine fish production after China, Indonesia, USA, Russia, and Peru, which contributed about 4.5% to the total global production.[4] According to the report prepared by the Marine Products Export Development Authority, the marine fish production in India has increased from 0.53 Mt in 1950 to 3.71 Mt in 2018 (Figure 1B). However, marine fish capture from the Indian mainland declined by 9% in 2018 compared to 2017.[8] The maritime state of Gujarat, located in the north-west of the Indian coast, remained the largest producer of marine fish (approximately 0.72 Mt) in the country. At the same time, maximum species diversity (735 species) was contributed by Tamil Nadu and Kerala.[8] India exported 1.38 Mt of seafood (worth US$7.08 billion) during 2017–2018 compared to 1.13 Mt (worth US$5.78 billion) during 2016–2017, with an annual growth rate of 21.35% in terms of quantity, where Frozen Shrimp (41.10% of overall export) was the major exported item.[6] Countries, such as the USA, along with Southeast Asia and Europe, are the major importers of these seafoods. According to the decade report prepared by the Department of Agricultural Research and Education–Indian Council of Agricultural Research,[8] the composition of commercially important fish species in India has decreased dramatically in recent years due to the changes in environmental parameters, such as water quality and salinity.

Monitoring of fishing activities in the deep ocean is required for better fisheries management as well as to conserve marine biodiversity.[9] Although fish productivity is limitless and it is a renewable resource, overexploitation due to high demand, along with global warming and climate change, renders this sector critical, which becomes a major threat to the livelihoods of the coastal community.[10] The continuous exposure to salt water, sand, and frequent natural calamities, such as cyclones and storm surges, increases the vulnerability of their livelihoods in India.[11,12] Bottom trawling, overcapacity of the fishing boat, and continuation of the government subsidies for the mechanized fishing crafts are the main

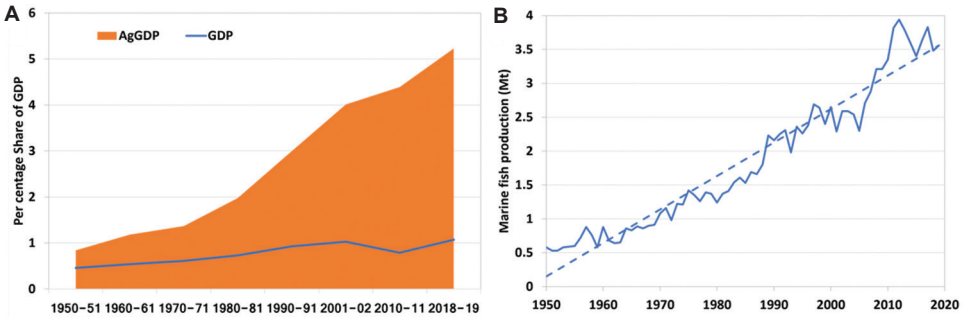

Figure 1. Trends in marine fish landings and economic contributions over the past decades. (A) The change in marine fish landings over the past decades. (B) Contribution to the total GDP and agricultural GDP from the fisheries sector in India over the past decades. Image created by the author.
Abbreviations: AgGDP: Agricultural gross domestic product; GDP: Gross domestic product.

Figure 2. The location of nine maritime states, two union territories, and two island territories contributed to the marine fish production in India. Image created by the author.

reasons behind the overexploitation of the marine fish, resulting in severe damage to some species, requiring preservation.[13] Adequate resource management (Figure 3) for sustainable utilization of marine resources needs to be strategized under current scenarios.[14] Empirically, fishing populations used traditional indicators of ocean features, such as temperature and color "breaks," feeding birds, foam, and accumulation of floating objects, to locate fish aggregation zones in the open sea.[15] However, the locating and catching of the marine fish became challenging due to the decline in the fish stocks in the usually available locations, which can be recovered by a reliable and timely forecast on the fish aggregation using remotely sensed data.[16] In this connection, remote sensing technology is being used for sustainable fisheries management by locating fish schools in the open sea more prominently and also for monitoring the ocean environment.[17-19] To avoid tremendous pressure in the traditional fishing zones due to increasing fishing fleets, several fishing effort needs to be diverted to the suitable potential fishing zone (PFZ) of the open sea.[20] Remote sensing technology can identify PFZ based on various satellite-derived products, such as sea surface temperature (SST) and chlorophyll concentrations (CC), where fish are available. Therefore, remote sensing techniques can play a huge role in marine resource exploitation (mainly fish) with the lower effective cost by saving fuel as well as search time, which also reduces the burning of fossil fuels.[15] Due to the sustainable use of marine fishery resources, the regulation related to fisheries must be implemented through scientific Marine Fishery Advisories (MFAs) based on satellite data.[21] To reduce the uncertainty and risk during the fishing operation, remotely sensed MFAs have high potential. Historically, the USA first started fish predicting zone using remotely sensed data in 1971.[22,23] To reduce the unpredictable weather patterns and non-availability of fish in the usually available location, the Indian National Centre for Ocean Information Services (INCOIS) had started to provide PFZ Advisory in the late 1990s on behalf of the Government of India.[24] PFZ, a short-term and reliable forecast on the fish aggregation zone in the open sea, helps fishers to locate large fish shoals through the reduction in search time and saves fuel.[17,25] The increasing demand for marine fishery products was also a major reason behind the adaptation of PFZ Advisory in India.[25] In the case of India, presently, marine fishing practices have been concentrated within the narrow belt of 50 m depth in inshore water.[26] INCOIS has also started the ocean state forecast (OSF) service in 2009, which includes wave heights, wave direction, wind speed and wind direction, tides, and currents to ensure the safety of the fishermen during fishing. OSF is also helpful as a decision-making tool for venturing into the deep ocean, and is also useful for the other coastal communities during extreme events.[27,28]

The current review provides a detailed mechanism of the INCOIS-derived MFAs along with their evolution throughout the periods. Besides, the usefulness and benefits of the MFAs are discussed across various maritime states in India through reviewing various literature. Therefore,

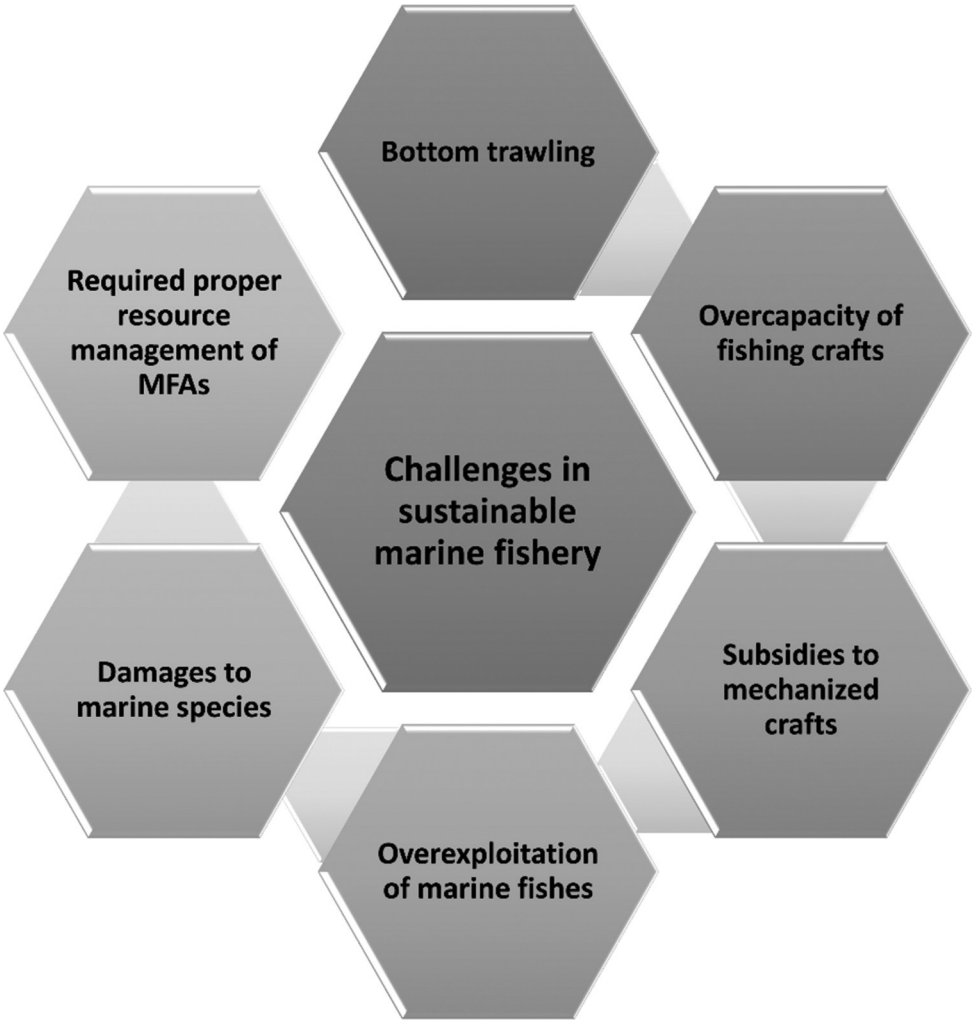

Figure 3. Challenges and managerial problems in the marine fishery sector in India and scope through the use of Marine Fishery Advisories (MFAs), such as the Potential Fishing Zone and Ocean State Forecast. Image created by the author.

the present review is significant for understanding the overall scenario of the development, dissemination, and impacts of advisories in the Indian context. Moreover, a global overview of the MFA has also been discussed. Furthermore, the role of MFAs in achieving various Sustainable Development Goals (SDGs) imposed by the United Nations through sustainable fishery practices was reviewed. These will also be helpful to understand the futuristic scope to improve the same with respect to its development and dissemination, as well as usages to enhance the sustainable fisheries in India.

2. Materials and methods

The literature reviewed in this article was identified through targeted searches in several scientific databases, including Web of Science, Scopus, and Google Scholar, covering publications between 1984 and 2025. Keywords used in various combinations included: "Marine Fishery Advisory," "Ocean State Forecast," "Dissemination," "CPUE," and "SDG 14," depending on the specific focus of each subsection.

Publications were selected based on their relevance to the topic and their contribution to the understanding of various criteria. For example, biological control of invasive alien plant species, physio-biological processes behind fish abundance, development and dissemination of PFZ Advisories, influence on the fish capture, socioeconomic benefits of PFZ and OSF Advisories, and methodological robustness. Preference was given to peer-reviewed journal articles, although relevant books, reports, and gray literature were also considered where appropriate. No strict inclusion/exclusion criteria were applied, as this is a narrative review aiming to provide a broad overview of the current knowledge and emerging trends in the field.

3. Development of MFAs in India

3.1. Physio-biological processes in the ocean and fish abundance

The static nature of the marine ecosystem controls the distribution of fish, whereas the oceanographic conditions, such as SST and CC, that indicate the fish stocks,[17,29] can be traced by utilizing the remotely sensed data.[30] The presence of phytoplankton containing high CC indicates high primary productivity regions where the marine fishes concentrate due to the presence of food.[23] Therefore, the ocean color (high CC) provides the area of rich biological products, which are also related to the oceanic fronts, topographic structure, upwelling, and eddies, known as fish accumulation zones for their feeding and spawning.[31-33] On the other hand, SST can be characterized by a suitable environment in terms of temperature for enhancing biological productivity.[34] For instance, cool water contains the highest nutrient materials, and therefore, SST is inversely correlated with PFZ areas.[32,34] The studies conducted by Solanki *et al.*[35] and Kripa *et al.*[36] also found that the temperature gradient in the ocean attracts fish, whereas the ocean color features coincided with the thermal fronts associated with the high primary productivity. In this context, special oceanic processes (SOPs), such as upwelling zones, the location and evolution of frontal boundaries, and current eddies, are also significant in the case of marine fisheries habitat.[37] For instance, cyclonic eddies found with high CC lead to high fish catch, whereas the anti-cyclonic eddies are associated with low fish catch due to the absence of high CC.[30] Therefore, the presence of chlorophyll (Chl) along with favorable SST is highly favorable for the fish aggregation in the open ocean, as illustrated in Figure 4.[23]

The behavior of fish is influenced by the favorable ocean environment, including seawater temperature, salinity, pH, and dissolved oxygen (DO), as each fish species has their own favored water temperature range, prey availability (near fronts), water clarity (turbidity), and productivity zones (ocean color) for their survival.[14,17,20,27] Marine pelagic fishes usually aggregate with a sharp horizontal temperature gradient up to a depth of 50 m in the ocean.[38,39] Seawater temperature and its seasonal and interannual fluctuation are the most important environmental parameters to find out the relationship between the behavior of fish and their abundance in the ocean environment.[15] It has been recorded that the optimum temperature for cold water fishes ranges between 20°C and 28°C, whereas warm water fishes can survive above 28°C.[22] On the other hand, CC >0.2 mg/m^3 in the sea is favorable for commercial fishery.[40] Furthermore, DO, an important water quality parameter required for acquiring the living organism, is inversely correlated with the water temperature,[41] while sea surface salinity (SSS) determines the density of seawater.[9] It is interesting to note that more fishing spots are found during the winter season; however, fishers need to travel farther offshore and spend more time at sea to reach deeper fishing areas compared to the summer season.[42] For example, organized tuna fishing is conducted at the submarine ridge of the Lakshadweep region, consisting of low seasonal variability in terms of different seawater parameters, such as salinity and turbidity, due to the distance from the mainland.[43] Tuna fish is also highly sensitive to temperature.[31] Due to the wind direction and wind movement, the oceanic features, such as eddies, rings, and fronts, are found to be shifted. This water mass movement due to the wind is also closely associated with the dispersal of fish shoals.[44] To understand the probable shift, Hossain *et al.*[29] incorporated the wind speed and wind direction data in the PFZ map.

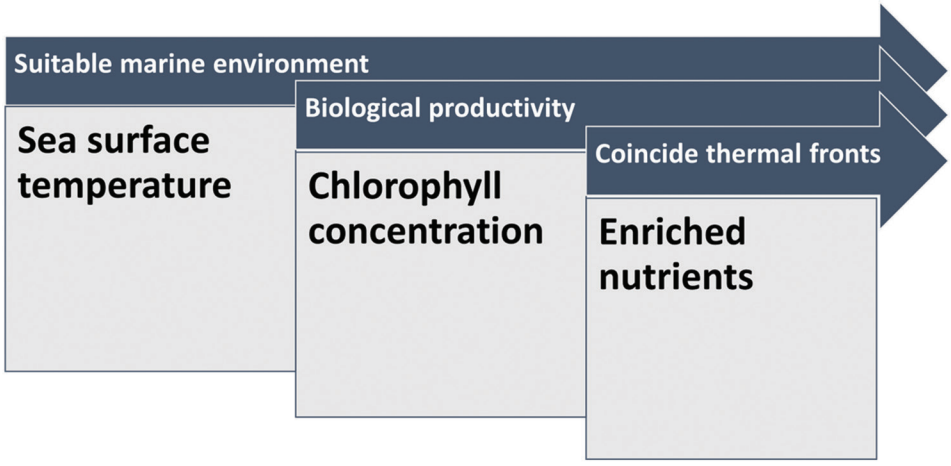

Figure 4. Key physio-biological processes influencing fish abundance in the ocean, forming the scientific basis for Marine Fishery Advisories. Image created by the author.

3.2. Background and evolution of MFAs

Historically, the USA started a fish-prediction zone in 1971 worldwide for the first time using remotely sensed data. To understand the relationship between Chl and SST, Arnone[45] used coastal zone color scanner and National Oceanographic and Atmospheric Administration-Advanced Very High-Resolution Radiometer (NOAA–AVHRR) data, whereas Laurs *et al.*[46] found that tuna fish are distributed in the vicinity of fronts where water is relatively warmer, utilizing these datasets. In the case of India, MFAs in the form of PFZ forecast had been developed during 1989–1990 for the first time using NOAA–AVHRR derived SST at Space Application Centre (SAC), Ahmedabad.[37] Meanwhile, the National Remote Sensing Agency was the institutional body for PFZ Advisory generation and dissemination. By developing "merged SST," incorporating the buoy temperature, wind observations (diurnal variation correction) with the AVHRR-extracted SST, Karthikeyan[47] stated that SST will also be useful to locate cold-blooded fish in the ocean. Tingote and Mane[48] also found that the environmental parameter called SST can easily be correlated with the availability of pelagic fish. However, SST-derived PFZ Advisory was inadequate in tropical and equatorial waters during summer due to strong stratification, preventing the arrival of cool nutrient-rich waters to the sea surface from the deeper layer, and surface wind might also affect the frontal structure.[49] Later, SAC developed an integrated approach using satellite-derived CC and SST to locate PFZ in the Indian seawater, and it was handed over to the Earth System Science Organization (ESSO)-INCOIS in late 2001 after the successful launching of the Indian Remote Sensing Satellite-P4 (IRS-P4) Ocean Colour Monitor (OCM) on May 26, 1999.[50] For the experimental PFZ forecast, an integrated approach had been developed by Solanki *et al.*,[35] where CC was calculated through atmospheric corrected OCM data utilizing Ocean Chlorophyll-2 algorithm and SST was estimated through multichannel SST approach as suggested by McClain *et al.*[51] Solanki *et al.*[52] also did a synergistic analysis of Sea-WiFS derived CC and NOAA–AVHRR derived SST for fishery resources exploration and observed an inter-relationship between CC and SST. Later, Solanki *et al.*[53] had analyzed Chl data from IRS-P4 OCM and SST data from NOAA–AVHRR to generate a composite image (using both Chl and SST) by monitoring common oceanic features, as the thermal features represented by coincident CC and SST contours indicated high bio-physical processes in the ocean. Recently, Mane and Mishra[37] also stated that integrated CC and SST are also able to identify SOPs, namely frontal boundaries, upwelling zones, current eddies, and meander, in the tropical ocean where fish accumulate due to the favorable environmental conditions along the temperature boundary. Therefore, the integration of SST with CC is more effective for PFZ forecast, as fish such as to congregate along the temperature boundary enriched with biological productivity.[26] INCOIS used both the approach where composite images were generated using common frontal structures using SST and Chl data, along with the second approach, the usage of the Chl data alone.[49]

3.3. Identification and visualization of PFZs utilizing remotely sensed data

The fish shoals can be located according to their feeding grounds from the combined SST/Chl image generation through the detection of various oceanic features.[54,55] The Chl features coincide with the temperature boundaries, indicating the maximum physio-biological processes in the open sea, which are useful for the exploration of living marine resources.[31] IRS-P4 OCM-derived CC and NOAA–AVHRR-derived SST data (Table 1) are transferred onto a scaled base map through the ground control points from the SOPs to generate the integrated PFZ map.[14,56,57] Therefore, the matching features from both Chl and SST in the SOPs are crucial to identify the PFZ map. To understand the probable shift of the PFZ area, wind vectors had been overlaid on the color-coded Chl/SST combined images after the geometrical correction. In this connection, wind data derived from Seasat-A Satellite Scatterometer

Table 1. Details of the datasets, along with the respective satellite name and agencies used to generate the PFZ Advisory

Basic input of PFZ Advisory	Details of the satellite		
	Satellite name	Respective agency	Remarks
SST	NOAA–AVHRR	NASA, USA	Retrieved from thermal-infrared channels of the respective satellites
	Met-Op	EUMETSAT, ESA	
Chl	Oceansat-II	ISRO, India	Retrieved from the optical bands of the respective satellites
	MODIS Aqua	NASA, USA	

Abbreviations: Chl: Chlorophyll; ESA: European Space Agency; EUMETSAT: European Organization for the Exploitation of Meteorological Satellites; ISRO: Indian Space Research Organization; Met-Op: Meteorological Operational Satellite; MODIS: Moderate Resolution Imaging Spectroradiometer (onboard Aqua satellite); NASA: National Aeronautics and Space Administration; NOAA–AVHRR: National Oceanic and Atmospheric Administration–Advanced Very High-Resolution Radiometer; PFZ: Potential fishing zone; SST: Sea surface temperature; USA: United States of America.

had also been tested for improved results.[56] Solanki *et al.*[44] developed an algorithm to compute the shifting nature of ocean features and the water mass movement due to the wind circulation, utilizing QuikSCAT from the National Aeronautics and Space Administration (NASA)-derived SeaWinds data. To understand the effect of wind on the PFZ Advisory, Chandran *et al.*[31] had also used wind data obtained from QuikSCAT Scatterometer. Therefore, due to the proven linkage between SST and Chl for the fish aggregation zone, the PFZ line/curves can be delineated by understanding the SOPs due to their high biological productivity.[16,36] Using the superimposed PFZ map from 2003 to 2007, Kripa *et al.*[36] also observed that the 50 m depth in the nearshore region over the southeastern Arabian Sea is more persistent for fish abundance due to high river water discharge containing high nutrients.

In the case of India, the PFZ Advisory began under the MFA services of INCOIS, imposed by the Government of India, and was closely associated with locating pelagic fish. According to the report prepared by Swetha *et al.*[58] on behalf of ESSO-INCOIS, the vector traced from one image was initially superimposed on another image to delineate the PFZ map (Figure 5), which was time-consuming and highly prone to manual error. Thereafter, the method associated with the automated identification of the frontal zone was implemented, reducing the human-induced error and also shortening the operational process chain. For example, single-image edge detection-derived output was considerably modified through polyline vector and cloud masking, where the ArcGIS toolbox, such as "Spatial Analyst" and "Cartography," was utilized to make smooth line curvature. Using this geospatial approach, the detection time of thermal fronts within the EEZ was shortened by 10–15 min. Later in 2011, ESSO-INCOIS initiated the generation of PFZ Advisory using SST and Chl from multiple satellites, which became completely automated in 2013.[50] Over 2008–2017, ESSO-INCOIS also developed the Satellite Coastal and Oceanographic Research program to overcome the difficulties in generating PFZ Advisory during cloudy days, especially during the monsoon, which is the peak fishing period, and also to encourage the fishing personnel to restrict themself only to pelagic fishing practices in the deep ocean.[50] Therefore, INCOIS used both the approach where composite images were made using common frontal structures using SST and Chl data, along with the second approach, the usage

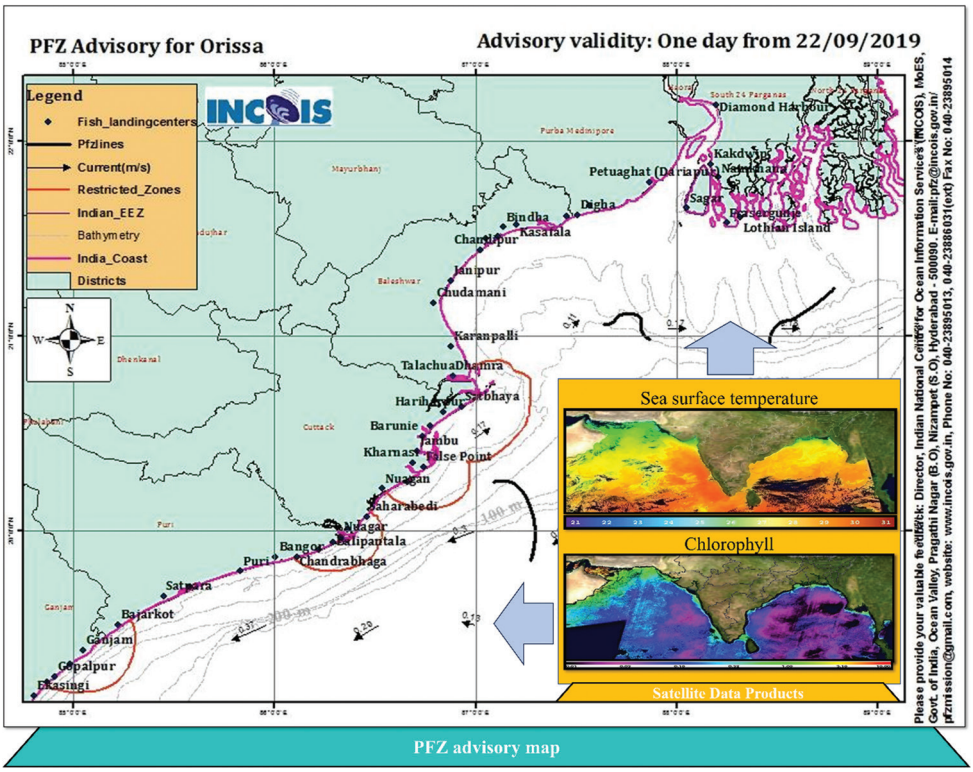

Figure 5. Visualization of basic primary input. The sea surface temperature and chlorophyll of the PFZ Advisory (inset panel) and a sample of the PFZ Advisory for Odisha for September 22, 2019. (Source: INCOIS web portal, weblink: https://incois.gov.in/MarineFisheries/PfzWebGis).
Abbreviations: INCOIS: Indian National Centre for Ocean Information Services; PFZ: Potential fishing zone.

of the Chl data alone.[49] The feedback analysis over the Indian West Coast during 1999–2001 also indicated that the SST-Chl-integrated approach was 70–90% reliable and can increase the catch by up to 200%, whereas the SST-based approach was only 50% reliable.[55] In another study conducted by Solanki *et al.*[33] revealed that the catch per unit effort (CPUE) in the matching features (SST and Chl) was extremely high; 85% of the observations reported higher fish catch compared to other areas.

Though SST and Chl are used in India to develop and deliver PFZ Advisory, Balaguru *et al.*[59] reported that net primary production estimated from the vertically generalized production model using photosynthetically available radiation and Chl can also be treated as a key parameter to assess fish stock in the open sea. This is because the presence of high nutrients in the cool water is a suitable region for higher fish catch. Giri *et al.*[23] have developed a local spatial model to detect PFZ by generating line density using satellite-derived SST and Chl over the West Bengal Coast, and identified several highly probable fish catch zones, which were very close to the INCOIS-derived Advisory. Andrews *et al.*[60] enhanced the precision of PFZ using the support vector machine (SVM) mechanism, which can be predictive in the absence of satellite data, thereby reducing time wastage and making the process cost-effective. However, Natteshana and Kumar[61] found that a statistical model is more efficient in identifying PFZ using the rough clustering techniques compared to an SVM classifier. To improve the existing remote sensing technology for identifying PFZs using satellite-derived SST and Chl data in Ratnagarh District, Maharashtra, Mane and Mishra[37] utilized the R tool, achieving an accuracy level of up to 89% within the predicted area. After calculating the SST (20–25°C) and Chl (0.10–0.22 mg/m^3), the values were combined with the X and Y coordinates to obtain the SST and Chl matrix, which was used to delineate the PFZ region utilizing the R tool. Mudliar *et al.*[9] developed a machine learning model to identify the PFZ in the open sea using water quality parameters, including DO and SSS, through an autoregressive integrated moving average and a random forest model. Furthermore, Chakraborty *et al.*[50] have developed a model to reproduce PFZ with high confidence, transforming PFZ Advisories into PFZ forecasts using model-derived Chl and SST, even on cloudy days, for sustainable and effective marine fisheries. Satellite altimetry data can also be utilized to provide pelagic fish advisories throughout the year by avoiding the unavailability of satellite data on cloudy days.[62] Altimetry-derived sea surface height anomaly (SSHa) and eddy kinetic energy data have been analyzed and compared with optical satellite products to obtain PFZ Advisories even on cloudy days.[59] This study revealed that the usage of optical sensor data along with altimetry (multi-sensor data) is very useful to identify the PFZ, as well as species-specific PFZ. Solanki *et al.*[63] also carried out an integrative analysis of the CC, SST, and Satellite with Argos and Altika-derived SSHa for better fisheries application, where it has been found that satellite-derived low SST and low SSHa designate high CC. Therefore, negative SSHa regions are characterized by rich nutrients, enhanced phytoplankton growth, and increased biological productivity, attracting fish shoals. However, an ocean-color sensor can penetrate into the ocean water up to 10 m, and can represent more frontal structures, which are true biological fronts. Currently, active remote sensing instruments, such as radar and sonar, are utilized in the field of marine fisheries.

4. Dissemination processes and managerial practices of MFAs

Indian INCOIS provides the PFZ and OSF Advisories for the marine fishing community to all the fish landing centers across the country, except during the fish ban period imposed by the Government of India.[24,38,64] Utilizing satellite data on SST, Chl, water clarity, and SSHa, INCOIS provided PFZ service for the 299 days during FY 2018–2019, along with 290 days of Yellowfin Tuna Advisory.[65] The advisories related to the PFZ and OSF are being disseminated to the various fishing villages/fish landing centers along the entire Indian coast through various information and communication (ICT) based tools, *viz.* digital display systems (DDSs), e-mails, phone calls, text messages, audio messages, radios, fisheries helpline numbers, mobile applications, local television networks, newspapers, community networks, and distributions of forecast printouts in person (Figure 6) to the targeted fishermen.[24,62] The PFZ forecast has also been sent via e-mail to various companies and agencies, including the Agromet Field Unit, All India Radio, and local functionaries of the Department of Fisheries (DOF), for radio and newspaper transmission, where it is challenging to obtain feedback on this process. In some states, such as Tamil Nadu, INCOIS collaborated with several non-profit organizations (NGOs), including the M. S. Swaminathan Research Foundation (MSSRF) and Reliance Foundation Information Services (RFIS), for local-level dissemination.[24] In this context, MSSRF acts as a catalyst by raising awareness through village resource centers (VRC) and village knowledge centers (VKC) in Tamil Nadu and Puducherry.[66] MSSRF has also conducted several awareness campaigns across 29 districts of Odisha, Andhra Pradesh, Puducherry, Tamil Nadu, and Kerala, reaching over 90,000 fishing population.[67] According to the market study report conducted by MSSRF[68] in collaboration with INCOIS, it was reported that some fishers in the coastal villages of TN and PND were unable to utilize PFZs

Figure 6. Different information and communication-based dissemination processes of the potential fishing zone and Ocean State Forecast Advisories in India. Image created by the author.
Abbreviations: DDS: Digital display system; EDB: Electronic display board; FFMA: Fisherman-friendly mobile application; SMS: Short message service; VKC: Village knowledge center; VRC: Village resource center.

as the forecasted zones were located far away from their traditional fishing ground, and they came on an irregular basis. There was also a demand for species-specific PFZs for Tuna (already started), Mackerel, Carangids, Oil Sardines, Seer-fish, *etc*. The fisherfolk population also expected additional training for the effective utilization of the PFZ and OSF Advisory. The study conducted by the National Council of Applied Economic Research (NCAER)[66] also concluded that greater emphasis needs to be placed on the dissemination processes of the PFZ and OSF services at the grassroots level. In this context, the INCOIS–MSSRF partnership could be a milestone in this sector for the purpose of smooth dissemination through the "Fisher Friends Programme." Kumar *et al.*[38] also noted that an awareness enhancement program may be helpful for the smooth dissemination of these advisories and increase economic benefits in terms of reduction in search time, fuel saving, and enhancement in CPUE.

The new generation electronic display boards (EDBs), known as DDSs, were inaugurated by INCOIS in January 2018. A total of 66 DDSs were installed along with 72 existing EDBs as of March 31, 2018.[28] The problems of the usage of the electronic board in the PFZ dissemination are the requirement of electricity, maintenance, and the skill to operate.[69] Currently, INCOIS has installed 98 DDSs along India's coastal regions, in addition to 85 existing EDBs. During 2018–2019, the total number of registered users of MFAs at INCOIS reached nearly 9 lakhs (approximately 900,000).[65] *The DDS* also has the capability to reduce the strains of different hazards by disseminating the real-time ocean state, namely wave heights, wind speed, and wind direction, and tsunami warnings along with PFZ Advisory.[62] However, the effective utilization of DDS was hampered due to limited installation, prevalence of poor GPRS, lack of local expertise to address the issues in DDS units, and the issues related to the power supply at the installed sites. ICT-based EDB/DDS consists of two parts: a liquid crystal display and a secure siren system. It also has two components: a table and a map.[25] Along with the possible fish aggregation zones in dark line (known as PFZ), the map also provides the probable shifting location of fish, depending on the wind speed and wind direction. The texts contain details of direction, distance, depth, latitude, and longitude, along with the global positioning system location of fish aggregation zones.[25] For better usage of PFZ, it is advised to catch fish on the same day after receiving it. Fishing in the middle of the PFZ line, inside the curved area, and between two PFZ lines yields maximum catch. The shifting features of the PFZ line indicate the movement of the fish shoal for the next two

days.[25] Therefore, the fishing operation became more useful when it was undertaken on or closer to the dates when the related SST/Chl data were received from the satellite.[38]

The information and forecast on different oceanographic parameters, namely waves, tides, currents, SST, and mixed layer depth (MLD), are being provided on a daily basis under the OSF Advisory; the frequency of dissemination generally increases during extreme weather conditions for the people who venture into the sea, and also for the near-seashore people.[28] According to the study of Chrispin *et al.*[70], a positive correlation was found between awareness/usage of PFZ and OSF Advisories and the level of education, where the utilization of the PFZ Advisory is negatively correlated with the usage types of crafts, namely mechanized and motorized crafts, in the state of Tamil Nadu. Furthermore, the study revealed that government organizations, such as the DOF, are less effective but more sustainable, while NGOs are more effective but less sustainable in the case of INCOIS-derived advisory dissemination at the grassroots level. It was concluded that effective public–private participation (PPP) is necessary for community participation and the utilization of ICT-based tools to further strengthen the dissemination processes at the grassroots level.[70]

5. Impacts of MFAs

According to various studies conducted by different agencies,[66-68,71,72] it has been noted that the CPUE increased due to the use of PFZ and OSF Advisories (Figure 7). In addition to enhancing fish catch, PFZ Advisory is useful in reducing search time, thereby decreasing fuel consumption, making marine fishing more environmentally friendly by emitting less carbon dioxide. On the other hand, OSF Advisory is very helpful in making the decision to venture into the sea and can save the lives and livelihoods of fishers, as well as those of coastal communities. Regarding the usage of advisories, various socio-technical constraints were identified among marine fishers, along with their socioeconomic factors, which influenced the dissemination and utilization of MFAs in Odisha. It is also noted that fishers agreed about the fruitfulness of the advisories if these could be used regularly.[73,74]

5.1. Influence on the fish catch

To investigate the effectiveness of PFZ Advisory in India, most studies have focused on two widely used methods: CPUE and benefit–cost ratio (BCR). The formula used for the CPUE is shown in Equation (1).

$$\text{CPUE} = \frac{\text{Total weight of fish catch}}{\text{Fishing effort}} \quad (1)$$

Typically, CPUE is expressed in kg/h, where the total weight of fish caught is measured in kg and the fishing effort is expressed in hours. High CPUE represents the most favorable oceanographic conditions for fishing operations.[20] Chrispin *et al.*[70] studied the CPUE within the PFZ notified area, which is significantly higher than that in the non-notified area, saving 50% of fuel and reducing search time along the Maharashtra coast. The study conducted by Solanki *et al.*[33] concluded that species-wise CPUE and seasonal CPUE were also found to be higher in the PFZ-notified area compared to the non-notified area along the Gujarat coast from 1999 to 2002.

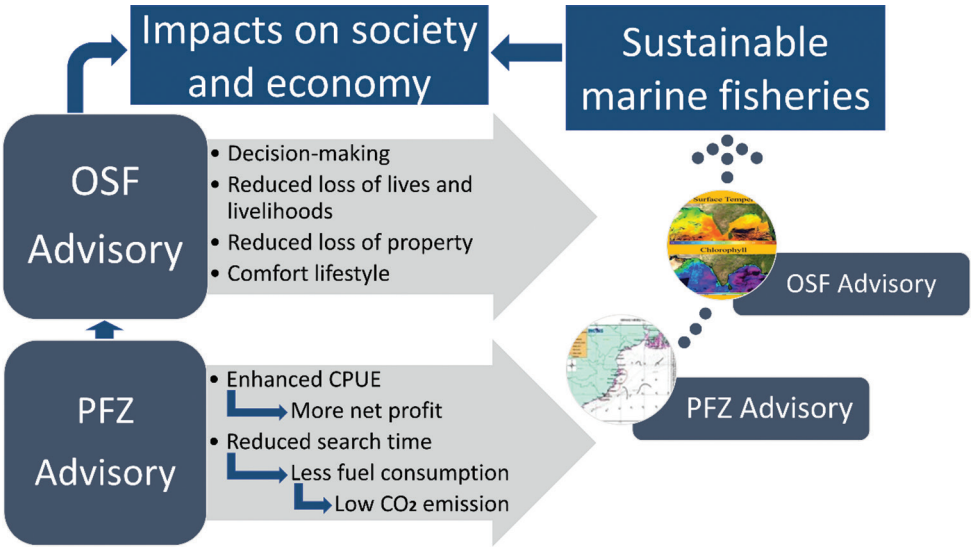

Figure 7. Impacts of PFZ and OSF on marine fisheries for the sustainable fishery to achieve socioeconomic improvement in India. Image created by the author. Abbreviations: CPUE: Catch per unit effort; OSF: Ocean State Forecast; PFZ: Potential fishing zone.

On the other hand, BCR compares the total expenditure of each trip against the total benefit of each trip, also known as cost-benefit analysis.[75] To compute the BCR, Nayak *et al.*[54] considered the cost toward the forecast generation, expenditure toward fishing, and profits from the increased catch, summarizing BCR by the total returns against total cost (Equation [2]).

$$BCR = \frac{\text{Total returns}}{\text{Total cost}} \quad (2)$$

The feedback received from various studies conducted in different regions of India since 2001 to validate the PFZ Advisory is presented in Table 2.

To locate pelagic fish in the open sea, the PFZ Advisory generated from satellite-derived SST and CC can reduce the overall operating costs of fishing.[80] This remote sensing technique is more suitable for pelagic fish compared to demersal fish, as light cannot penetrate deeper water.[33,79] Furthermore, Tummala *et al.*[14] also concluded that the success rate of the PFZ Advisory is about 85% for the bottom trawling and 95% for the gillnetting, which can be improved by incorporating parameters such as MLD and wind. In

Table 2. Economic improvement in marine fisheries through the use of the Potential Fishing Zone Advisory compared to non-potential fishing zone areas at various spatio-temporal scales in India

No.	Location on the Indian coast	Year	Crafts and gears used	Total catch or yield	Status of CPUE	Status of net profit	Status of BCR	References
1	Gujarat	2001			Two- to three-fold increased			Solanki *et al.*[35]
2	Lakshadweep	2002		55 kg increased	Three-fold increased			Pillai *et al.*[43]
3	Western coast	2003 and 2005	Trawler and gillnet			₹26,887 (trawler) and ₹1299 (gillnet) increased	0.85 (trawler) and 0.84 (gillnet) increased	Nayak *et al.*[54] Dwivedi *et al.*[55]
4	East coast	2002–2004	Trawler, gillnet, and longliner	Increased by 36.50±1.97 kg/h, 33.82±2.42 kg/h, and 30.41±3.58 kg/h for gillnetters, trawlers, and long liners				Choudhury *et al.*[57]
5	Kerala	2006–2008		2671 kg increased	4.3-fold increased	₹54,423 increased		Tummala *et al.*[14]
6	Gujarat	2010		0.99 tonnes increased	1.3-fold increased	₹99,202 increased		Das *et al.*[76]
7	Kerala	2003–2011						Nair and Pillai[27]
8	West Bengal	2008–2011		Increased by 51.47±4.30 kg/h	Two-fold increased		4.5 increased	Maity *et al.*[75]
9	West Bengal	2008–2011		Increased by 17.48 kg/h	Two-fold increased			Dutta *et al.*[21]
10	East coast	2010–2012		Increased by 4.64 kg/h	2.32-fold increased			Dutta *et al.*[21]
11	Tamil Nadu	2007–2011		Increased by 45 to 1070 kg	8.64-fold increased	₹4300 to ₹36,000 increased		Nammalwar *et al.*[26]
12	Andaman and Nicobar Islands	2009–2012	Gillnet, trawler, and longliner	Percentage increased by 36.50±1.97, 33.82±2.42, and 30.41±3.58, respectively				George *et al.*[77]
13	Goa			Increased by 1.06 tonnes/h		Six times increased		Sreekanth *et al.*[78]
14	Mumbai	2014		Increased by 12 kg/h				Kamei *et al.*[22]
15	Goa			Increased by 2405.1 kg/h	2.35-fold increased	1.86 lakhs increased	1.69 increased	Sreekanth *et al.*[79]
16	Gujarat						0.08 increased	Nayak *et al.*[16]

Abbreviations: BCR: Benefit–cost ratio; CPUE: Catch per unit effort.

most cases, the trawl operation of PFZ Advisory is more beneficial at 50 m depth.[70] According to different studies, it can be said that the net profit obtained by the fisherfolk population, as well as the species diversity, was higher in the PFZ region compared to the non-PFZ region.[61] Dutta *et al.*[21] also found that the differences in total catch and profit were statistically significant at a 5% level of significance on the West Bengal coast. According to the validation of the satellite-based PFZ Advisory along the Kerala coast during 2003–2011, Nair and Pillai[27] exhibited that the CPUE and net profit earned by the fishing community were higher within the PFZ notified area compared to outside the PFZ. There was also a positive correlation between PFZ and the occurrence of commercially important pelagic fishes. However, the abundance of fish decreased when the forecast gap increased.

The validation of PFZ Advisory reveals that motorized and small mechanized crafts are the primary beneficiaries, with a forecast reliability of up to 80%.[16] Hossain *et al.*[29] also concluded that catch is higher in the PFZ area compared to other areas, beneficial for the artisanal, motorized, and small mechanized crafts engaged in pelagic fishing. In another study conducted by Dutta *et al.*,[21] the total CPUE in West Bengal has declined due to the increase in mechanized boats and over-exploitation of fish. The INCOIS technical report prepared by Kumar *et al.*[38] concluded that PFZ Advisory is beneficial for fishing by reducing search time and, consequently, reducing fuel consumption. They also studied that commercially important fish species are abundant in the PFZ area compared to the non-PFZ area. Sreekanth *et al.*[78] utilized 304 feedbacks based on 136 PFZ Advisories to compute CPUE and net profit along the Goa Coast, where the searching time was also reduced by 50% due to the usage of PFZ Advisory. The study conducted by Nammalwar *et al.*[26] also concluded that the PFZ forecast by INCOIS using remotely sensed data was highly useful for fishing, as it can enhance the CPUE by minimizing search time and thereby saving fuel and human effort, resulting in an overall profit for the fisherfolk population.[39] It not only saves fuel by reducing search time but also makes their livelihood more reliable by increasing income and preventing them from venturing into the sea in adverse weather conditions as a result of the OSF Advisory.[24] Masuluri *et al.*[81] found that PFZ Advisory is useful and effective to reduce the environmental stress by decreasing the carbon dioxide (CO_2) emission in the open sea; the average CO_2 emission reduced by 0.8 tonnes in the PFZ region (0.161 tonnes) compared to the non-PFZ region (0.959 tonnes) along the Kerala Coast from 2008 to 2011. Therefore, the comparative study of CPUE drastically varied between PFZ and non-PFZ locations. High yielding (CPUE) can also boost the economic status of small-scale fishing communities. It is crucial to note that the emergence of COVID-19 and its associated lockdowns in various phases significantly impacted the marine fishery sector in India.[82]

5.2. Socioeconomic benefits of PFZ and OSF Advisories

The socioeconomic status of the fishing population depends on assets, such as fishing craft and gear. Traditional catamarans (dinghies) represent the poor fishers, whereas motorized or mechanized craft holders are comparatively rich.[83] The fishing gears, including types of nets and lines, influence the socioeconomic status of the fishing population. The majority of the Indian population (65%) relies on the agricultural sector to pursue their livelihoods, where the fishery sector is also an important component.[84] The renewable nature of marine fish in the fishery sector plays an important role in the socioeconomic development in India for the following factors: increasing food security, sharing a significant amount of foreign exchange, and generating employment.[71] Therefore, the Union Government of India focused on the high fish productivity to ensure the socioeconomic security of the artisanal fishermen by means of the sustainability of the marine fisheries. In general, fisheries come under the state subject as per Article 246. However, fishing beyond the territorial waters is a subject of the central government.[10]

The National Council of Applied Economic Research was appointed by the Ministry of Earth Sciences (MoES) in 2010 to conduct a comprehensive study to estimate the economic and social benefits due to the weather and marine services, such as agro-meteorological advisory services, fishery services, tsunami warning services, severe weather warning services, and public weather forecast services. According to the study of NCAER,[66] where a total of 400 respondents were selected for impact assessment of the marine fishery services from five villages across four districts (Kalyani, Guntur, Nagapattanam, and Puducherry) of corresponding four states (West Bengal, Andhra Pradesh, Tamil Nadu, and Puducherry), PFZ and OSF, provided by INCOIS were found quite useful among the fishing community. Identification of PFZ improves the catch size by increasing fish productivity. It also reduces fuel consumption by minimizing search times. On the other hand, information regarding ocean state (OSF) is useful for the fishing population/general public in timing departures and arranging shore activities by avoiding extreme weather events in coastal zones.[66] This study also claimed that the adaptation of PFZ Advisory for all mechanized, motorized, and traditional crafts can contribute up to 2.04% of the national gross domestic product (GDP). The total annual net economic benefits due to the satellite-based PFZ Advisory were estimated within the range of ₹34,000 to ₹50,000 crore based on the export

of approximately 21% additional catch due to the usage of PFZ Advisory. NCAER[66] reported that 90% of fishers in the southern coastal region and 64% in the eastern region are aware of the usefulness of the ocean state services. In 2015, another study was conducted by RFIS–NCAER to assess the economic benefits, along with the environmental and ecological benefits, of INCOIS-derived PFZ and OSF Advisories in the coastal villages of seven maritime states in India. According to NCAER,[71] marine fisheries GDP can increase up to 7.8% from the current 3.9% after the uniform operationalization of PFZ and OSF Advisories across all the coastal regions of the country. Due to the usage of PFZ and OSF forecasts, fishers can also obtain an additional profit of ₹3000 crore per annum. Identification of PFZ also minimizes search time, resulting in a reduction in diesel consumption. Saving one liter of diesel can reduce 2.63 kg of CO_2 emissions and ₹36,200 crores per annum over a 25-year life. Due to the greater accuracy of PFZ and OSF, the fishers can improve their health and spend quality time with their family members, as their manual work in the crafts will decrease significantly; accuracy in the PFZ may also reform a new ecosystem, which can be treated as its ecological benefit.[71] Furthermore, the study conducted by Kundu and Santhanam[85] reported that 2.20 lakh tonnes of CO_2 emission can be reduced due to the usage of PFZ Advisories in Odisha.

Apart from NCAER studies, INCOIS also conducted several market studies from 2012 to 2013 to assess the impacts of PFZ and OSF Advisories on improving the lives and livelihoods of the marine fishing communities in different parts of the country, especially across the coastal villages of Andhra Pradesh, Tamil Nadu, and Puducherry. The MSSRF collaboration with INCOIS since 2009 bridges the gap between scientific know-how and ground-level do-how in the coastal districts of Tamil Nadu and Puducherry, disseminating the PFZ and OSF Advisories through VKC and VRC.[68] The market study conducted by MSSRF[68] among 300 individuals from the fisherfolk population across six coastal districts of Tamil Nadu and Puducherry revealed that 94% of the total fisherfolk utilize either PFZ or OSF Advisories through the text messages of their mobile phones. The total net income for all the fisherfolk has increased by at least ₹1000 to ₹50,000, along with the reduction of several issues regarding overfishing due to the usage of PFZ Advisory, while oil sardines were the most dominant species caught. OSF includes wind speed and direction, and wave heights are closely related to the effective decision-making of fisherfolk for fishing; a timely forecast can prevent economic loss by avoiding natural hazards at the ocean. The majority (35%) of the fisherfolk agreed that due to the usage of OSF, they can attain net economic savings of ₹5000 to ₹20,000.[68] According to another market study conducted by MSSRF[67] among 32 fishers, including a woman boat owner in the Gilakaladindi Village of Krishna District (Andhra Pradesh), reveals that the usage of PFZ improved the quality and quantity of catch. For instance, the yield of tuna fishing has increased from 200–300 kg to 400–500 kg per haul. The number of days spent in the ocean was also reduced from 10-15 days to 4-5 days, thereby reducing diesel consumption, a major economic gain of nearly ₹25,000 per trip. Therefore, the income of the boat owners and crew members (drivers and laborers) has increased significantly. The study conducted by Tummala *et al.*[14] along the Kerala Coast over 2006–2008 revealed that the search time was reduced by 50% within the PFZ region, indicating an annual saving on the diesel consumption (6 lakhs for mechanized crafts and 1.80 lakhs for motorized crafts). To locate pelagic fishes in the open sea, the PFZ Advisory generated from satellite-derived SST and CC reduced the overall operating costs of the fishing.[80] Therefore, it can be concluded that the benefits of PFZ-OSF Advisories are useful for time saving (reducing the time of the trip), fuel saving (decreasing CO_2 emission and pollution), as well as increasing catch (more income) and producing safety among the fishing population. The doctoral research conducted by Kundu[86] investigated the development and dissemination processes of MFAs in detail for Odisha. It was found that the assimilation of the MFAs usage was hampered in this state due to various socio-technical constraints, as only 30% of the total fishers utilized this advisory during the study. However, significant environmental and economic benefits were achieved through MFAs. It was reported that the emission of 2.20 lakh tonnes of CO_2 could be reduced per year using MFAs, while 45% of daily expenditure for fishing can be reduced through its regular utilization, which enables climate-resilient fishing in Odisha. A recent study by Santhanam *et al.*[87] also revealed that MFAs are crucial for reducing emissions to achieve the optimal social cost of carbon in India.

It is well-documented that climate change poses significant threats to marine fisheries by altering ocean temperatures, currents, productivity, and species distribution, which in turn undermine the sustainability of fish stocks and the livelihoods of coastal communities that rely on them. Singh[69] reported that SST can be increased over the Indian coast by 2.0 to 3.5°C by 2099 from the current level of 0.2 to 0.3°C (1960 to 2005). Two major concerns of the marine fisheries in India are the decline in fish catch and the increase in fuel prices.[69] Therefore, better fisheries management is needed in the near future to maximize the utilization of living marine resources, such as fish, through a deep understanding of marine ecology. Apart from fishery management, such as monitoring the environment

and locating fish populations, ocean color is also used to monitor harmful algal blooms, as well as to locate coastal populations.[49] It is evident from the present analysis that the utilization of MFAs not only benefits fishers economically by increasing their catch but also reduces search time, thereby decreasing fuel consumption and resulting in lower CO_2 emissions to the marine environment. Therefore, this adaptive strategy not only enhances economic efficiency but also promotes ecosystem-based sustainable fishing practices, thereby strengthening the resilience of fisheries and fishing communities to climate variability and long-term climate change.

6. Global overview of the Marine Fishery Advisory

The nature of MoES's advisories related to PFZ and OSF is a public good in the Indian context. The PFZ and OSF Advisories are disseminated to all the coastal fishing community freely (non-excludable), and the utilization of these advisories by a fisherman cannot affect the others (non-rival), as anybody can venture into the sea to fish in the PFZ areas.[88] On the other hand, the marine fishery resources are treated as a common public property, which is non-excludable but not non-rival.[88] The common property problems caused by a lack of property rights in the fisheries resources create problems such as economic inefficiency. In this context, the individual transferable quotas (ITQs) can be adopted to establish property rights in the fishery sector, thereby minimizing the economic inefficiencies. Despite the dynamic nature of the fishery, ITQ can bring sustainable economic benefits, leading to an increase in economic efficiency. This is implemented in Iceland along with the Netherlands, New Zealand, and Australia.[89] Community-based coastal resource management systems can also be treated as an active social process by involving resource users—the local fishers and communities—as partnership management in the resource management.[90] According to the international experience, fisheries co-management, a decentralized system of marine resource management where user participation is involved, needs momentum to get its solid motion; however, decentralization does not necessarily mean participatory management or co-management always.[91] The community participation and ownership collaboration with the municipal government play a creative role in the usage of a financial mechanism for a long-term, self-supporting marine protected area in the Philippines.[92] For instance, in the San Salvador Island, Philippines, the community and local government contrasted with the National Marine Park based on the Marine Protected Area to pursue better management under the National Integrated Protected Areas. Pinkerton[93] examined the potential of the community-based self-management and government-community co-management to clarify the biological, economic, and political problems regarding the salmon fishery in British Columbia and Canada. According to Pomeroy,[94] three key elements were identified to understand the achievements of locally based regimes: logistical, cost-sharing, and power-sharing elements. Logistical arrangements included clear boundaries, membership criteria, interception agreements, and management-unit sizes appropriate to the abundance of the natural and human resources; cost-sharing arrangements include local cost recovery and local volunteerism; and power-sharing arrangements include checks and balances between local multiparty boards, a provincial board, and the Department of Fisheries and Oceans. The primary goal of the co-management program is to mobilize and strengthen public participation in government, as well as to ensure the equal distribution of resources and powers among local-level people and communities.[94] In fishery practices, cooperation and participation of fishers are needed to develop laws and regulations for the fishing population.[90] To minimize the resource management problems related to resource deterioration (Philippines and the Tanzanian marine), conflicts between stakeholders (e.g., Norway's Lofoten cod fishery and Philippines coastal fisheries), conflicts between management agencies and local fishers (e.g., Canada's Atlantic coast fishery), and governance problems in general (e.g., Philippines, United States Fishery), the fisheries co-management had been adopted globally.[94]

After World War II, world fisheries had been increasing steadily. In developing countries, fish have been treated as the primary source of animal protein, as they consume 70% of the total fish landings. Despite the Third United Nations Conference on the Law of the Sea, the fishing pattern has not changed significantly. However, the developing countries produced the largest catch, accounting for nearly 80% of the total world catch.[95] The estimations of several hydrological factors, such as the upwelling zone, along with high primary productivities that attract fish shoals for their food, are needed to assess marine fish.[17,96] Mansor *et al.*[97] realized that it is urgent to develop a model suitable for the PFZ determination in tropical water to meet the sustainable harvest of the fisheries resources. Based on the satellite-derived SST and CC, a fishery forecasting model, the Tropical Fish Forecasting System, was developed to provide PFZ Advisory to end-users in the South China Sea. Klemas[17] reported that SST (NOAA–AVHRR), CC (SeaWiFS/SeaStar), along with SSHa (Ocean Topography Experiment/Poseidon) and wind velocity (Scatterometer/European Remote Sensing Satellite-1 and -2) were helpful to trace out the abundance of yellowfin tuna in the tropical Atlantic region. Apart from this, commonly used acoustic sensing methods, such as echo-sounders (used for deep fishing) and

side-scan sonars (used for near-surface fishing), can provide high-resolution data on fish distribution and abundance from the trawler itself. The Ocean Acoustic Waveguide Remote Sensing method is also a useful technique for continuously monitoring fish population behaviors, dynamics, and abundance on the continental shelf. In the case of airborne remote sensing, the spatial resolution/coverage, along with a cloud-free environment, low altitude (tidal) conditions can be chosen easily. Therefore, airborne Lidar can overcome the limitations of passive remote sensing, while side-looking airborne radar can track fish shoals by accumulating small-scale waves (2–20 cm) resulting from fish swimming activity. Active microwave devices, such as radar altimeters, scatterometers, and synthetic aperture radar, are being used to detect physical ocean features. Despite limited spatial resolution (effective only for open seas) and inability to penetrate cloud cover (due to its polar orbit), the Moderate Resolution Imaging Spectroradiometer is attractive as it can produce both CC and SST.[17] Pillai and Nair[39] also mentioned that satellite-derived SST and CC are ideal for providing high receptivity and large spatial coverage for monitoring the ocean. Dimech *et al.*[98] reported a negative correlation between the perception of fishers over the Malta fishing zone and the fishing activity. The fishing zone was not beneficial for commercial fishers, whereas recreational fishers were the main beneficiaries. They also found that the differences in individual incomes among the fishing population lead to attitudinal differences, which enhance the resources, as well as the conflicts among user groups.

In the case of India, the fisheries sector needs a proper management system for food security, similar to the White Revolution, in the near future.[99] Currently, the annual average fish production by Indian fish farmers is 2 tonnes per person, whereas it is 172 tonnes per person in Norway. To increase the standard of living of the Indian fishing community, it is necessary to increase productivity and export marine fish at a higher intensity. In this context, the transfer of knowledge from the developed country is also very important for sustainable fishing.[80] It is also needed to raise awareness among the fishing community to stop illegal fishing, for example, through the use of double-fold nets.[47] The Central Marine Fisheries Research Institute had proposed to ban fishing during the breeding season, prohibit gears with a 30 mm mesh size, and restrict the export grade to 1400 Nos./kg and above by the fishers in the context of overexploitation.[13]

7. MFAs and sustainable fisheries

Hinds[95] projected that fisheries may be a major contributor to food security in the future by improving management strategies. There is an urgent need for collaboration among fisheries, industry, and remote sensing scientists to improve forecasting models and develop suitable management strategies.[17] In this context, SDG 14 provides the development targets with respect to marine resources management, which can be enhanced using PFZ and OSF Advisories, specifically in relation to regulating pelagic overfishing, conservation of marine fisheries, implementation of subsidies, and regulating the socio-economics.[100] It is noted that fishing utilizing the scientific MFAs is economically beneficial and environmentally sustainable due to higher fish catch in a shorter duration. The adopted 17 SDGs with 169 targets and 230 indicators under the "Agenda 2030" by the United Nations, SDG 14—Conserve and sustainably use the oceans, seas and marine resources for sustainable development—is one of these goals where FAO is the custodian agency. Apart from SDG 14 (Life Below Water), small-scale fisheries (SSF) can be related to SDG 1 (No Poverty), SDG 2 (Zero Hunger), SDG 5 (Gender Equality), SDG 12 (Responsible Consumption and Production), SDG 13 (Climate Action), and SDG 16 (Peace, Justice and Strong Institutions). According to the workshop proceedings, edited by Franz, FAO,[101] SSFs (including fishery resources, land, and market) are facing a wide number of challenges regarding lack of infrastructure, overfishing by big trawlers, pollution, habitat degradation, insufficient market information, post-harvest losses, weak organizations, and lack of access to financial services. Therefore, it is crucial to develop a reasonable, legal, and regulatory framework to achieve SDG 14, especially SDG14.b (Life Below Water). To serve this purpose, three variables: existing regulators, ongoing guidelines, and the existence mechanism in the field of SSFs have been prepared based on the FAO Code of Conduct for Responsible Fisheries. To serve this purpose, questionnaires can be prepared against these variables utilizing reliable methods at the national level to collect the information, which should include a multi-stakeholder, multi-disciplinary, and participatory approach based on a bottom-up approach. In this connection, a capacity-building program among the fisherfolk population may contribute to ensuring a robust reporting process. Based on the discussion made in this workshop, it is necessary to develop ICTs for disseminating the required methods through workshops, media campaigns, training, and social media to the target groups. It is also urgent to develop a database to evaluate the status of SSFs in developing nations, such as India, where exchanges of thoughts can take place at various levels among countries. Finally, participation of SSF organizations in various decision-making processes by following the SSF Guidelines may be useful in achieving the SDG 14 goal.[101] Therefore, fish production may become a useful tool against malnutrition to improve the socio-economics of the fishing community by playing an effective role in the co-management of fisheries.[10]

The major problem with remotely sensed data in the PFZ forecast is the time lag between SST and Chl observations.[22] Microwave radiometers are a better choice for measuring temperature than IR, as they can penetrate clouds.[15,80] Due to the limitation in temporal resolution of polar-orbiting satellites, INCOIS explored the possibility of utilizing SST data from Indian geostationary satellites INSAT-3D and INSAT-3DR.[28] INCOIS also tried to incorporate PPP in the process of PFZ identification for the ecosystem-based fishery advisory. For the continuation of Hilsa Shad Advisory, INCOIS initiated the establishment of a coastal laboratory facility at Digha in association with the West Bengal Fisheries Department.[65] INCOIS also planned for wind monitoring (from QuikSCAT), species-specific advisory, and location-based advisory.[16] Future development in the fishing operation will rely on the combined usage of visible, infrared, and microwave sensors, as well as the availability of satellite technology to everyone connected to this activity, including fishing personnel, fish-allied industrialists, and fishery scientists.[15] In this way, it is possible to overcome the limitations in the field of fishery advisories, including the lack of support for demersal fishing and the unavailability of satellite data during cloudy seasons. To reduce drawbacks, such as the lack of sufficient knowledge to understand and recognize the PFZ area and the lack of interest in upgrading mechanized crafts, the fishing communities need to follow a cooperative approach within their society.[48] In this context, INCOIS is also involved in conducting various awareness programs among the fish farmers across the country with the help of different NGOs, such as MSSRF. The species-specific advisories related to tuna are already operationalized by the INCOIS.

Therefore, it is understood that MFAs are useful for sustainable fishing practices in India. However, the assimilation of the advisories was hampered, which can be mitigated by improving the dissemination networks, as well as adopting an active remote sensing technique to provide MFAs seamlessly even in cases of adverse weather conditions. In short, MFAs increase resource dependability by improving catch efficiency, ensuring safety, reducing costs, and supporting sustainable resource use, collectively making marine fisheries a more reliable source of livelihood and food security.

8. Conclusion

The MFAs, developed and disseminated by ESSO-INCOIS under the MoES, the Government of India, play a vital role in the country's socioeconomic development related to the marine fishery sector through promoting sustainable fishing practices. Based on cloud-free satellite data, SST and CC are used to extract PFZ lines as fish shoals are found in suitable marine environments, such as those with relatively low SST and high CC. Several studies provided quantitative analysis regarding the benefits of fish catch from the usage of advisories, which is almost two to three times higher than fishing in non-PFZ areas in India. Advisories were also useful in decreasing carbon emissions due to reduced search time. Climate-resilient, sustainable fishing in attaining several targets of SDGs is achievable through the MFAs, as their use is economically beneficial for fishers and environmentally sustainable for the marine ecosystem. However, fishers reported that the PFZ Advisories they received were located far away from their traditional grounds, and the requirement for species-specific advisories was also noted. In addition, awareness programs associated with the reception and utilization of the advisories were identified as crucial for the fishers to use them. This would also help fishers to comply with regulatory guidelines related to illegal fishing or the use of inappropriate mesh sizes. On the other hand, PFZ Advisories are still not feasible during adverse weather conditions, which affect the continuity of receiving the same. In addition, the time lag between the dissemination of the advisory to the end-user and the fishing activity needs to be reduced for the effective use of MFAs. Advanced remote sensing techniques and fisheries co-management can play a vital role in reducing these drawbacks in the field of marine fisheries. This detailed review of the emergence of MFAs and their significance in sustainable fishing practices in the context of India may be useful for the marine research community in providing seamless next-generation advisories.

Under these circumstances, specific recommendations can be delivered as follows:

- Improving the transformational spaces for MFA deliveries by fostering participatory co-design, multichannel communication, localized content, and continuous feedback loops that enhance trust, accessibility, and adaptive use among fishing communities.
- Improving the focus or emphasis on transitioning to sustainable use of technologies for ensuring sustainable fishery development.
- Contextualization of specific SDG14 goals to specific tasks in MFA creation and delivery.

Furthermore, it is advisable to use the MFAs wherever feasible regularly, especially for mechanized crafts, as they can venture into the deep sea, unlike small motorized or non-motorized crafts for fishing, where PFZ Advisories are demarcated. Hence, this review is crucial to formulate required developmental plans for the marine fishing community so that fishers can receive and utilize PFZ and OSF Advisories seamlessly.

Acknowledgments

The authors are grateful to Dr. Srinivasa Kumar Tummala and Dr. Nagaraja Kumar Masuluri, ESSO-INCOIS, for providing valuable insights into the dissemination processes of MFAs in the state of Odisha. The authors are also grateful to the Manipal Academy of Higher Education, Manipal and Bengaluru Campus, for the encouragement to conduct the research activities.

Funding

None.

Conflict of interest

The authors declare that they have no competing interests.

Author contributions

Conceptualization: All authors
Visualization: Sudip Kumar Kundu
Writing–original draft: Sudip Kumar Kundu
Writing–review & editing: All authors

Ethics approval and consent to participate

Not applicable.

Consent for publication

Not applicable.

Availability of data

All data are available upon request from the corresponding author.

References

1. NABARD. *Sectoral Paper on Fisheries and Aquaculture*. Mumbai; 2018. Available from: https://www.nabard.org/auth/writereaddata/file/fisheries and aquaculture.pdf [Last accessed on 2021 Apr 24].
2. NFDB. *National Fisheries Policy*, *2020. Sixth Draft for Consideration*. Hyderabad; 2020. Available from: https://nfdb.gov.in/pdf/policy/english.pdf [Last accessed on 2021 Apr 24].
3. DADF. *DADF Annual Report 2017-18*; 2018. Available from: https://dadf.gov.in/sites/default/filess/annual_report_17-18.pdf [Last accessed on 2021 Apr 24].
4. Department of Fisheries. *Handbook on Fisheries Statistics 2018*. New Delhi; 2019. Available from: https://dof.gov.in/sites/default/filess/handbook on fs 2018.pdf [Last accessed on 2021 Apr 24].
5. Sathianandan TV. *Marine Fish Production in India - Present Status*; 2017. Available from: https://eprints.cmfri.org.in/12164/1/2-marine fish production in india.pdf [Last accessed on 2021 Apr 24].
6. MPEDA. *MPEDA Annual Report*. Kochi; 2018. Available from: https://www.mpeda.gov.in/mpeda/admin/app/webroot/files/annualreport/1550120514mpedaar201718.pdf [Last accessed on 2021 Apr 24].
7. Ministry of Statistics and Programme Implementation. *Manual on Fishery Statistics 2011*. New Delhi; 2011. Available from: https://www.mospi.gov.in/sites/default/files/publication_reports/manual_fishery_statistics_2dec11_0.pdf [Last accessed on 2021 Apr 24].
8. DARE-ICAR. *DARE-ICAR Annual Report 2016-17*. New Delhi; 2018. Available from: https://icar.org.in/files/dare-icarannualreport 2016-17english.pdf [Last accessed on 2021 Apr 24].
9. Mudliar SL, Shashank S, Chandak M. Machine learning model to predict potential fishing zone. *J Indian Assoc Environ Manag*. 2019;39(1-4):18-20.
10. Singh TK, Patnaik S. Marine fisheries; Its current status, sustainable management and socio-economic status of the marine fishers of Odisha, through Indian marine policy: A case study. *Res J Anim Vet Fish Sci Int Sci*. 2014;2(7):10-19.
11. Mishra SK. Beach livelihoods of Odisha. *Econ Polit Wkly*. 2020;55(10):69-70.
12. Kundu SK, Santhanam H. A report on the impacts of cyclone Yaas over a fish landing centre vulnerable to cyclonic storms and natural hazards - Talsari, Northern Odisha. *Local Environ*. 2021;26(9):1043-1050.

    doi: 10.1080/13549839.2021.1964457
13. Filipe JA, Coelho M, Ferreira MAM, Mutharasu SA. Fisheries, chaos and ethics. A note on India status. *Int J Latest Trends Financ Econ Sci*. 2013;3(1):365-371.
14. Tummala SK, Masuluri NK, Nayak S. Benefits derived by the fisherman using potential fishing zone (PFZ) advisories. In: Frouin RJ, Andrefouet S, Kawamura H, Lynch MJ, Pan D, Platt T, editors. *Remote Sensing of Inland, Coastal, and Oceanic Waters*. Vol 7150. Qatar: SPIE; 2008.

    doi: 10.1117/12.804766
15. Miguel A, Santos P. Fisheries oceanography using satellite and airborne remote sensing methods: A review. *Fish Res*. 2000;49(1):1-20.

    doi: 10.1016/S0165-7836(00)00201-0
16. Nayak S, Srinivaskumar T, Nagarajakumar M. Satellite-based fishery service in India. In: GEO Secretariat, editor. *The Full Picture*. Geneva, Switzerland: Tudor Rose; 2007. p. 256-257. Available from: https://www.researchgate.net/publication/233996104/satellite/based_fishery_service_in_india [Last accessed on 2021 Apr 24].
17. Klemas V. Remote sensing of environmental indicators of potential fish aggregation: An overview. *Baltica*. 2012;25(2):99-112.

    doi: 10.5200/baltica.2012.25.10

18. Kundu SK, Santhanam H, Srikanth R. A Technical Assessment of the Use of Current Geospatial Technologies to Derive Marine Fishery Advisories in India and the Way Forward. In: *Asian Conference on Remote Sensing (ACRS2020)*. Deqing, China: ACRS 2020 - 41st Asian Conference on Remote Sensing; 2020. p. 10. Available from: https://acrs-aars.org/proceeding/ACRS2020/ifomqo.pdf [Last accessed on 2025 Nov 03].

19. Kundu SK, Santhanam H, Srikanth R. Use of geospatial technology for sustainable development of small scale fisheries in India: Challenges and way forward. In: *AGU Fall Meeting 2020. Online Everywhere*. United States: AGU; 2020.

    doi: 10.1002/essoar.10505256.1

20. Bhaware BG, Kurhe AR, Mane UH. The catch per unit efforts (CPUE) through validations of potential fishing zone advisories along Sindhudurg District coast of Maharashtra State. *Int J Pharm Biol Sci Fundam*. 2013;3(1):20-29.

21. Dutta S, Maity S, Hazra S. Catch per unit effort comparison between potential fishing zone and non- potential fishing zone from 2008 to 2011 of West Bengal coast, India. *Indian J Geo Marine Sci*. 2016;45(6):763-768.

22. Kamei G, Felix JF, Shenoy L, Shukla SP, Devi HM. Application of remote sensing in fisheries: Role of potential fishing zone advisories. In: Sundaresan J, Santosh KM, Déri A, Roggema R, Singh R, editors. *Geospatial Technologies and Climate Change*. Cham: Springer International Publishing; 2014. p. 175-186.

    doi: 10.1007/978-3-319-01689-4

23. Giri S, Manna S, Chanda A, *et al*. Implementing a spatial model to derive potential fishing zones in the Northern bay of bengal lying adjacent to West Bengal Coast, India. *J Indian Soc Remote Sens*. 2016;44(1):59-66.

    doi: 10.1007/s12524-015-0472-2

24. Balasubramanian S. Satellite data aid India's fishermen for better livelihood. *Rural Int J Rural Dev*. 2015;49(3):22-23.

25. Subramanian S, Manjulekshmi N, Narendra Pratap S, Janhavi K, Tejaswini P, Pastta MF. *A Manual on the use of Potential Fishing Zone (PFZ)*. Goa: ICAR Research Complex For Goa; 2014.

    doi: 10.13140/2.1.5169.0565

26. Nammalwar P, Satheesh S, Ramesh R. Applications of remote sensing in the validations of potential fishing zones (PFZ) along the coast of North Tamil Nadu, India. *Indian J Mar Sci*. 2013;42(3):283-292.

27. Nair PG, Pillai VN. Satellite based potential fishing zone (PFZ) advisories - acceptance levels and benefits derived by the user community along the Kerala coast. *Indian J Fish*. 2012;59(2):69-74.

28. ESSO-INCOIS. *ESSO-INCOIS Annual Report 2017-18*. Hyderabad: ESSO-INCOIS; 2018. Available from: https://incois.gov.in/documents/annual_reports/2017-2018_english.p [Last accessed on 2021 Apr 24].

29. Hossain S, Rahaman T, Parvin M, Khan MS. Advance use of GIS and RS in the Validation of Potential Fishing Zones (Pfz) Forecasting along the Bay of. In: *Marine Conservation and Blue Economy Symposium*. Dhaka, Bangladesh, 2015. p. 1-7.

30. Solanki HU, Mankodi PC, Dwivedi RM, Nayak SR. Satellite observations of main oceanographic processes to identify ecological associations in the Northern Arabian Sea for fishery resources exploration. *Hydrobiologia*. 2008;612(1):269-279.

    doi: 10.1007/s10750-008-9496-8

31. Chandran RV, Solanki HU, Dwivedi RM, Nayak S, Jeyaram A, Adiga S. Studies on the drift of ocean colour features using satellite-derived sea surface wind for updating potential fishing zone. *Indian J Mar Sci*. 2004;33(2):122-128.

32. Solanki HU, Dwivedi RM, Nayak SR. Seasonal and spatial variability in satellite derived thermal and chlorophyll features: A synergistic application for exploring fishery resources. In: *Large Marine Ecosystems: Exploration and Exploitation for Sustainable Development and Conservation on Fish Stocks*. Mumbai: Fishery Survey of India; 2004. p. 166-182. Available from: https://login.proxy.lib.duke.edu/login?url=https://search.proquest.com/docview/17851482?accountid=10598%0ahttp://pm6mt7vg3j.search.serialssolutions.com?ctx_ver=z39.88/2004&ctx_enc=info:ofi/enc:utf/8&rfr_id=info: sid/aquatic+science+%2526+fisheries+abstract [Last accessed on 2021 Apr 24].

33. Solanki HU, Mankodi PC, Nayak SR, Somvanshi VS. Evaluation of remote-sensing-based potential fishing zones (PFZs) forecast methodology. *Cont Shelf Res*. 2005;25(18):2163-2173.

    doi: 10.1016/j.csr.2005.08.025

34. Solanki HU, Dwivedi RM, Nayak S, Gulati DK, John ME, Somvanshi VS. Potential fishing zones (PFZ) forecast using satellite data derived biological and physical processes. *J Indian Soc Remote Sens*. 2003;31(2):67-69.

    doi: 10.1007/BF03030773

35. Solanki HU, Dwivedi RM, Nayak SR, *et al*. Application of Ocean colour monitor chlorophyll and AVHRR SST for fishery forecast: Preliminary validation results of Gujarat coast, northwest coast of India. *Indian J Mar Sci*. 2001;30:132-138.

36. Kripa V, Mohamed KS, Prema D, Mohan A, Abhilash KS. On the persistent occurrence of potential fishing zones in the southeastern Arabian Sea. *Indian J Geo Marine Sci*. 2014;43(5):737-745.

37. Mane SU, Mishra AD. Application of remote sensing with R Tool in validation of PFZ along coast of Ratnagiri: A survey. *IOSR J Electron Commun Eng*. 2017;12(3):104-109.

    doi: 10.9790/2834-120302104109

38. Tummala SK, Kumar N, Padmaja, Swetha N, Nayak S.

Validation of Potential Fishing Zone (PFZ) Advisories (2006-2007) [Report No: INCOIS-ASG-PFZ-TR-08-2007]. Hyderabad; 2007.

39. Pillai VN, Nair PG. Potential fishing zone (PFZ) advisories-are they beneficial to the coastal fisherfolk ? A case study along Kerala coast, South India. *Biol Forum Int J*. 2010;2(2):46-55.

40. Klemas V. Fisheries applications of remote sensing: An overview. *Fish Res*. 2013;148:124-136.

    doi: 10.1016/j.fishres.2012.02.027

41. Dutta S, Chanda A, Akhand A, Hazra S. Correlation of phytoplankton biomass (chlorophyll-a) and nutrients with the catch per unit effort in the PFZ forecast areas of Northern bay of bengal during simultaneous validation of winter fishing season. *Turkish J Fish Aquat Sci*. 2016;16(4):767-777.

    doi: 10.4194/1303-2712-v16_4_03

42. Jagannathan S, Samraj A, Rajavel M. Potential fishing zone estimation by rough cluster predictions. In: *Proceedings of International Conference on Computational Intelligence, Modelling and Simulation*; 2012. p. 82-87.

    doi: 10.1109/CIMSim.2012.34

43. Pillai VN, Sivadas M, Santosh KM. Validation of potential fishing zone advisories in Minicoy region of Lakshadweep with special reference to skipjack tuna. In: Pillai NGK, Menon N., Pillai PP, Ganga U, editors. *Management of Scombroid Fisheries*. Kochi: Central Marine Fisheries Research Institute; 2002. p. 1-13. Available from: https://www.com/eprints.cmfri.org.in/4136 [Last accessed on 2021 Apr 24].

44. Solanki HU, Pradhan Y, Dwivedi RM, Nayak S, Gulati DK, Somvamshi VS. Application of QuikSCAT SeaWinds data to improve remotely sensed potential fishing zones (PFZs) forecast methodology: Preliminary validation results. *Indian J Mar Sci*. 2005;34(4):441-448.

45. Arnone RA. Satellite-derived color-temperature relationship in the Alboran Sea. *Remote Sens Environ*. 1987;23(3):417-437.

    doi: 10.1016/0034-4257(87)90099-X

46. Laurs RM, Fiedler PC, Montgomery DR. Albacore tuna catch distributions relative to environmental features observed from satellites. *Deep Sea Res Part A Oceanogr Res Pap*. 1984;31(9):1085-1099.

    doi: 10.1016/0198-0149(84)90014-1

47. Karthikeyan K. *Finding of Potential Fishing Zones Using Remote Sensing Techniques*. Chennai; 2012. Available from: https://www.academia.edu/7216835/finding_of_potential_fishing_zones_using_remote_sensing_techniques [Last accessed on 2021 Apr 24].

48. Tingote R, Mane U. Miscellaneous marine fishes caught under PFZ and Non-PFZ realm off Ratnagiri Coast, Maharashtra State, India. *Int J Aquac Fish Sci*. 2017;3(2):30-34.

    doi: 10.17352/2455-8400.000025

49. Wilson C, Morales J, Nayak S, Asanuma I. Ocean-colour radiometry and fisheries. In: *Why Ocean Colour? The Societal Benefits of Ocean-Colour Technology*. United States: IOCCG; 2008. p. 47-58.

50. Chakraborty K, Maity S, Lotliker AA, Samanta A, Ghosh J, Masuluri NK. Modelling of marine ecosystem in regional scale for short term prediction of satellite-aided operational fishery advisories. *J Oper Oceanogr*. 2019;12(Suppl 2):S157-S175.

    doi: 10.1080/1755876X.2019.1574951

51. McClain EP, Pichel WG, Walton CC. Comparative performance of AVHRR-based multichannel sea surface temperatures. *J Geophys Res*. 1985;90(C6):587-511, 601.

    doi: 10.1029/JC090iC06p11587

52. Solanki HU, Dwivedi RM, Nayak SR. Synergistic analysis of SeaWiFS chlorophyll concentration and NOAA-AVHRR SST features for exploring marine living resources. *Int J Remote Sens*. 2001;22(18):3877-3882.

    doi: 10.1080/01431160110069845

53. Solanki HU, Dwivedi RM, Nayak SR, Somvanshi VS, Gulati DK, Pattnayak SK. Fishery forecast using OCM chlorophyll concentration and AVHRR SST: Validation results off Gujarat coast, India. *Int J Remote Sens*. 2003;24(18):3691-3699.

    doi: 10.1080/0143116031000117029

54. Nayak S, Solanki HU, Dwivedi RM. Utilization of IRS P4 ocean colour data for potential fishing zone - A cost benefit analysis. *Indian J Mar Sci*. 2003;32(3):244-248.

55. Dwivedi RM, Solanki HU, Nayak1 SR, Gulati D, Somvanshi VS. Exploration of fishery resources through integration of ocean colour with sea surface temperature: Indian experience. *Indian J Mar Sci*. 2005;34(4):430-440.

56. Sreedhar U. Remote sensing and fisheries. In: *Handbook of Fishing Technology*. 2002. p. 11. Available from: https://krishi.icar.gov.in/jspui/bitstream/123456789/47245/1/remote/sensing/and fisheries.pdf [Last accessed on 2021 Apr 24].

57. Choudhury SB, Jena B, Rao MV, *et al*. Validation of integrated potential fishing zone (IPFZ) forecast using satellite based chlorophyll and sea surface temperature along the east coast of India. *Int J Remote Sens*. 2007;28(12):2683-2693.

    doi: 10.1080/01431160600987878

58. Swetha N, Kumar N, MNK, *et al*. *Automated Identification of Oceanic Fronts for Operational Generation of Potential Fishing Zone (PFZ) Advisories*. Hyderabad; 2017. Available from: https://www.com/moeseprints.incois.gov.in/4506 [Last accessed on 2021 Apr 24].

59. Balaguru B, Ramakrishnan SS, Vidhya R, Thanabalan P. A comparative study on utilization of multi-sensor

satellite data to detect potential fishing zone (PFZ). *Int Arch Photogramm Remote Sens Spat Inf Sci ISPRS Arch*. 2014;40(8):1017-1026.

doi: 10.5194/isprsarchives-XL-8-1017-2014

60. Andrews S, Varunbabu BS, Subash P, Swaminathan MR. Finding the high probabilistic potential fishing zone by accelerated SVM classification. *Int J Inf Commun Technol*. 2017;11(4):576.

doi: 10.1504/IJICT.2017.087460

61. Natteshana NVS, Kumar NSA. Survey of various methods of potential fishing zone identification. *Int J Control Theory Appl*. 2016;9(40):697-703.

62. George G, Sarma K, Bharathi G, Kaliyamoorthy M, Krishnan P, Kirubasankar R. Efficacy of different modes in disseminating potential fishing zone (PFZ) forecasts - a case study from Andaman and Nicobar Islands reference points in Nicobar. *Indian J Fish*. 2014;61(1):84-87.

63. Solanki HU, Bhatpuria D, Chauhan P. Integrative analysis of AltiKa-SSHa, MODIS-SST, and OCM-Chlorophyll signatures for fisheries applications. *Mar Geod*. 2015;38(Supp1):672-683.

doi: 10.1080/01490419.2015.1010757

64. MPEDA. *Ban Period*. Available from: https://www.mpeda.gov.in/mpeda/cms.php?id=ymfulxblcmlvza [Last accessed on 2020 May 20].

65. ESSO-INCOIS. *ESSO-INCOIS Annual Report 2018-19*. Hyderabad; 2019. Available from: https://incois.gov.in/documents/annual_reports/2018-2019_english.pdf [Last accessed on 2021 Apr 24].

66. NCAER. *Impact Assessment and Economic Benefits of Weather and Marine Services*. New Delhi; 2010. Available from: https://moes.gov.in/writereaddata/files/impactassessment-moes.pdf [Last accessed on 2021 Apr 24].

67. MSSRF. *Potential Fishing Zone Advisories and Conversion from Partnership in Gilakaladindi Village in Krishna District, Andhra Pradesh-a Preliminary Study*. Chennai; 2014. Available from: https://incois.gov.in/documents/gilakaladindi_study.pdf [Last accessed on 2021 Apr 24].

68. MSSRF. *Impact of INCOIS Scientific Forecast Services Towards Improving the Lives and Livelihoods of Fishing Communities Across Tamilnadu and Puducherry*. Chennai; 2014. Available from: https://incois.gov.in/documents/scientificforecastservices.pdf [Last accessed on 2021 Apr 24].

69. Singh D. *NAIP Component – 3: Strategies to Enhance Adaptive Capacity to Climate Change in Vulnerable Regions (Blue Ocean Innovation: MKRISHI® - Fisheries Service)*. Mumbai; 2012. Available from: https://incois.gov.in/documents/mkrishiblue_ocean_innovation_story.pdf [Last accessed on 2021 Apr 24].

70. Chrispin CL, Ananthan PS, Krishnan M, Mahalakshmi P. Effectiveness of institutional arrangements for delivery of Potential Fishing Zone and Ocean State Forecast advisory services to fishers in Tamil Nadu. *Agric Econ Res Rev*. 2012;25:485-493.

71. NCAER. *Economic Benefits of Dynamic Weather and Ocean Information and Advisory Services in India And Cost and Pricing of Customized Products and Services of ESSO NCMRWF & ESSO-INCOIS*. New Delhi; 2015. Available from: https://incois.gov.in/documents/impactassessment-ncaer2015.pdf [Last accessed on 2021 Apr 24].

72. NCAER. *Estimating the Economic Benefits of Investment in Monsoon Mission and High Performance Computing Facilities*. New Delhi; 2020. Available from: https://www.ncaer.org/wp/content/uploads/2020/07/1604990035report_moes2020.pdf [Last accessed on 2021 Apr 24].

73. Santhanam H, Kundu SK. Assessment of socio-technical constraints of marine fishers in the utilisation of marine fishery advisories in Southern Odisha, India. *Anthr Sci*. 2022;1:109-120.

doi: 10.1007/s44177-022-00014-4

74. Kundu SK, Santhanam H. Transitional contexts and transformational pathways through the utilisation of marine fishery advisories in Odisha, India: Challenges and way forward. *Anthr Sci*. 2024;3(1-2):35-49.

doi: 10.1007/s44177-024-00069-5

75. Maity S, Kumar TS, Dutta S, Akhand A, Hazra S. Satellite based integrated potential fishing zone advisories: A feasibility analysis in the coastal water of West Bengal. *Proc Zool Soc*. 2015;68(1):14-19.

doi: 10.1007/s12595-013-0088-x

76. Das S, Madhu VR, Sreejith PT, Jethva JK, Meenakumari B. Validation of Potential Fishing Zones along Saurashtra Coast, Gujarat Validation of Potential Fishing Zones along Saurashtra Coast, Gujarat. In: *Coastal Fishery Resources of India Conservation and Sustainable Utilisation*. Kochi; 2010. p. 138-144. Available from: https://www.researchgate.net/publication/258505375%0avalidation [Last accessed on 2021 Apr 24].

77. George G, Krishnan P, Roy SD, *et al*. Validation of potential fishing zone (PFZ) forecasts from Andaman and Nicobar Islands. *Fish Technol*. 2013;50:1-5.

78. Sreekanth GB, Subramanian S, Lekshmi NM, Fernandes PM, Singh NP. *Potential Fishing Zone Advisories - A Promising Tool for Precision Fishing*. Goa; 2014. Available from: https://ccari.res.in/extension%20folder%20no.%2070.pdf [Last accessed on 2021 Apr 24].

79. Sreekanth GB, Subramanian S, Lekshmi NM, Madhu VR, Fernandes PM, Singh NP. Validations on satellite based potential fishing zone advisories along Goa, South-West coast of India. *Indian J Fish*. 2016;63(1):8-15.

doi: 10.21077/ijf.2016.63.1.44455-02

80. Devi GK, Ganasri BP, Dwarakish GS. Applications of

Remote Sensing in Satellite Oceanography: A Review. *Aquat Procedia*. 2015;4(Icwrcoe):579-584. doi:10.1016/j.aqpro.2015.02.075

81. Masuluri NK, Nair P, Pillai VN, Kumar TS. Environmental benefits due to adoption of satellite-based fishery advisories. *Fish Technol*. 2018;55:100-103.

82. Kundu SK, Santhanam H. All pain and no gain: Factors impacting local and regional sustainability due to COVID-19 pandemic with respect to the Indian marine fisheries. *Curr Res Environ Sustain*. 2021;3:100086.

doi: 10.1016/j.crsust.2021.100086

83. Naskar P. A study of changing livelihoods of Odisha's coastal fishing communities : Reasons and effects. *Int J Humanit Soc Sci Invent*. 2018;7(6):14-17.

84. DeviNongmaithem B, Ngangbam AK. Socioeconomic conditions and cultural profile of the fishers in India- a review. *IOSR J Agric Vet Sci*. 2014;7(9):42-48.

doi: 10.9790/2380-07914248

85. Kundu SK, Santhanam H. Modelling the influence of marine fishery advisories on the reduction of carbon dioxide emissions for Odisha under varying climate change scenarios using CMIP models: An evidence-based approach for policymaking. In: Dhyani S, Adhikari D, Dasgupta R, Kadaverugu R, editors. *Ecosystem and Species Habitat Modeling for Conservation and Restoration*. Singapore: Springer Nature Singapore; 2023. p. 341-353.

doi: 10.1007/978-981-99-0131-9_18

86. Kundu SK. *Evidence Based Assessment of the Utilisation of Geospatial Technology Products for Marine Fishing in Odisha India*; 2023. Available from: https://shodhganga.inflibnet.ac.in/handle/10603/525516 [Last accessed on 2021 Apr 24].

87. Santhanam H, Kundu SK, Ghosh A. A new transitions policy index to assess the co-benefits of infrastructural enhancement and technological development for Sustainable Marine Fisheries Management in India. *Sustain Futur*. 2025;9:100812.

doi: 10.1016/j.sftr.2025.100812

88. Freebairn JW, Zillman JW. Economic benefits of meteorological services. *Meteorol Appl*. 2002;9(1):33-44.

doi: 10.1017/S1350482702001044

89. Arnason R. Property rights in fisheries: Iceland's experience with ITQs. *Rev Fish Biol Fish*. 2005;15(3):243-264.

doi: 10.1007/s11160-005-5139-6

90. Pomeroy RS, Berkes F. Two to tango: The role of government in fisheries co-management. *Mar Policy*. 1997;21(5):465-480.

doi: 10.1016/S0308-597X(97)00017-1

91. McCky BJ, Jentoft S. From the bottom up: Participatory issues in fisheries management. *Soc Nat Resour*. 1996;9:237-250.

doi: 10.1080/08941929609380969

92. White AT, Courtney CA, Salamanca A. Experience with marine protected area planning and management in the Philippines experience with marine protected area planning and management in the Philippines. *Coast Manag*. 2002;30(1):1-26.

doi: 10.1080/08920750252692599

93. Pinkerton EW. Local fisheries co-management: A review of international experiences and their implications for salmon management in British Columbia. *Can J Fish Aquat Sci*. 1994;51(10):2363-2378.

doi: 10.1139/f94-238

94. Pomeroy RS. Devolution and fisheries co-management. In: *Collective Action, Property Rights and Devolution of Natural Resource Management: Exchange of Knowledge and Implications for Policy*. The International Aquatic Resources Management (ICLARM); 2001. p. 108-145. Available from: https://citeseerx.ist.psu.edu/viewdoc/download;jsessionid=3d3adce14f7026147749adadf98888da?doi=10.1.1.298.4927&rep=rep1&type=pdf [Last accessed on 2021 Apr 24].

95. Hinds L. World marine fisheries: Management and development problems. *Mar Policy*. 1992;16(5):394-403.

doi: 10.1016/0308-597X(92)90007-C

96. Shixing H. Reomte sensing in Chinese fisheries. In: Fritz LW, Lucas JR, editors. *XVIIth ISPRS Congress, Technical Commission VII: Interpretation of Photographic and Remote Sensing Data*. Washington, DC; 1992. p. 66-68. Available from: https://www.isprs.org/proceedings/xxix/congress/part7/66_xxix-part7.pdf [Last accessed on 2021 Apr 24].

97. Mansor S, Tan CK, Ibrahim HM, Shariff R. *Satellite Fish Forecasting in South China Sea. 22nd Asian Conference on Remote Sensing*. Vol. 2. 2001. p. 5-9. Available from: https://www.crisp.nus.edu.sg/~acrs2001/pdf/015venka.pdf [Last accessed on 2021 Apr 24].

98. Dimech M, Darmanin M, Philip Smith I, Kaiser MJ, Schembri PJ. Fishers' perception of a 35-year old exclusive fisheries management zone. *Biol Conserv*. 2009;142(11):2691-2702.

doi: 10.1016/j.biocon.2009.06.019

99. Karunakaran D, Mohanty BP. Information technology - potential application in fisheries. *Environ Ecol*. 2014;24(2):359-365.

100. ECOSOC. *Special Edition: Progress towards the Sustainable Development Goals*. United Nations Economic and Social Council; 2019. Available from: https://www.com/undocs.org/e/2019/68 [Last accessed on 2021 Apr 24].

101. FAO. Exploring SDG 14.b and its proposed indicator 14.b.1. In: Franz N, editor. *FAO Fisheries and Aquaculture Proceedings*. Vol 59. Rome: Food and Agriculture Organization of the United Nations; 2018. p. 1-39. Available from: https://www.fao.org/3/ca0140en/ca0140en.pdf [Last accessed on 2021 Apr 24].

ACCSCIENCE PUBLISHING

Explora: Environment and Resource

REVIEW ARTICLE

Artificial intelligence and Tourism 4.0 for sustainable transformation: A systematic review of environmental and governance impacts

Maryam Kalhoro[1,2]*, Hui-Nee AuYong[1], and Abdelhak Senadjki[1]

[1]Department of Economics, Faculty of Business and Finance, Universiti Tunku Abdul Rahman, Kampar, Perak, Malaysia

[2]Department of Business Administration, Institute of Business Administration, University of Sindh, Jamshoro, Sindh, Pakistan

Abstract

Artificial intelligence (AI) and the concept of Tourism 4.0 have transformative potential in advancing sustainable tourism, particularly in addressing environmental and governance challenges. This systematic literature review, conducted in accordance with the Preferred Reporting Items for Systematic Reviews and Meta-analyses 2020 guidelines, compiles peer-reviewed studies from 2015 to 2023 to evaluate AI's role within Tourism 4.0 in promoting sustainability. The analysis focuses on two domains: Environmental impacts, such as energy efficiency, resource conservation, and low-carbon tourism strategies, and governance impacts, including transparent certification, accountable digital platforms, and data-driven policy innovation. While AI and related smart systems demonstrate positive outcomes, critical issues, such as cost barriers, data privacy concerns, and limited long-term evaluation, remain underexplored. The review also highlights research gaps, including the scarcity of integrated frameworks and longitudinal studies. Building on these findings, recommendations for Malaysia emphasize strengthening smart infrastructure, piloting blockchain-based transparency systems, enhancing institutional coordination, and embedding energy-efficient AI solutions into governance frameworks. By situating Malaysia at a mid-evolution stage of digital tourism, the study offers practical insights into how AI and Tourism 4.0 can support environmentally sustainable and ethically governed tourism futures.

Keywords: Tourism 4.0; Sustainable tourism; Artificial intelligence; Digital transformation; Environmental governance; Industry 4.0 technologies

***Corresponding author:**
Maryam Kalhoro
(maryamkalhoro@1utar.my)

Citation: Kalhoro M, AuYong H, Senadjki A. Artificial intelligence and Tourism 4.0 for sustainable transformation: A systematic review of environmental and governance impacts. *Explora Environ Resour.* 2025;2(4):025320058. doi: 10.36922/EER025320058

Received: August 9, 2025

Revised: September 24, 2025

Accepted: October 10, 2025

Published online: November 26, 2025

1. Introduction

During the Fourth Industrial Revolution, the tourism industry has experienced a significant transformation with the advent of Tourism 4.0. Characterized by the integration of the latest digital technologies, such as artificial intelligence (AI), the Internet of Things (IoT), big data analytics, virtual reality (VR), and blockchain, Industry 4.0 is revolutionizing traditional paradigms in most sectors, including tourism.[1] This development has given rise to the concept of Tourism 4.0, which seeks to utilize these innovations to enhance tourist experiences, optimize operational efficiencies, and advance sustainable practices in the tourism sector.[2]

Tourism 4.0 is not merely the adoption of technology but a holistic concept that integrates stakeholders from tourists and service providers to governments and local communities into a collaborative system.[3,4] With the utilization of real-time data and smart systems, destinations can offer personalized experiences, manage their resources more effectively, and mitigate the adverse impacts of mass tourism. For instance, IoT devices can monitor tourist flows to prevent overcrowding, and AI-driven platforms can provide personalized recommendations, both of which can enhance visitor satisfaction and promote equitable distribution of tourism benefits.[4]

Sustainable development, as framed by the United Nations' Sustainable Development Goals, provides a wider context for understanding the role of digital technologies in tourism.[5] New Industry 4.0 technologies, such as AI, IoT, blockchain, and augmented reality (AR)/VR, affect the functioning of tourism enterprises by reshaping energy management, transparency, and customer engagement in ways that align with sustainability principles. For example, AI and IoT enable resource efficiency and lower emissions; blockchain provides transparent supply chains and certification systems; and AR/VR offer low-impact tourism alternatives.[6] These technologies demonstrate how Industry 4.0 is not only a driver of competitiveness but also a key facilitator of sustainable development. Tourism enterprises increasingly embed these tools into their operations by linking digital transformation with ecological conservation, community empowerment, and responsible governance practices.[6]

Sustainability has become a central principle in contemporary tourism development, especially against the backdrop of phenomena such as climate change, resource depletion, and sociocultural disruption. Tourism 4.0 offers promising solutions to these challenges by facilitating data-driven decision-making, promoting sustainable consumption, and enhancing community engagement.[7] Recent reviews also highlight that AI is increasingly integrated into sustainability reporting frameworks across industries, supporting transparency, accountability, and responsible governance. This broader trend underscores the relevance of AI applications in tourism governance.[7,8] However, the application of Industry 4.0 technologies to tourism practices also creates challenges such as data privacy issues, digital divides, and the need for significant infrastructural investments.

This review is relevant because it clarifies how Industry 4.0 technologies contribute to sustainability in tourism at a time when destinations face urgent pressures to recover from the pandemic without reverting to unsustainable mass-tourism models. It contributes to the research area by providing one of the first systematic reviews that explicitly frames AI within the Tourism 4.0 paradigm, linking environmental and governance outcomes to the broader discourse on sustainable development.

While growing attention has been given to Tourism 4.0, in-depth studies examining the intersection of Industry 4.0 technologies and sustainable tourism development in a systematic manner remain limited. Literature is often focused on either specific technological applications or individual case studies without offering an integrating framework that outlines the grand implications of this digital revolution.[9] This lack undermines the need for a systematic literature review that consolidates current knowledge, explains prevailing trends, and identifies areas warranting further research and governance.

This systematic review aims to:

(i) Present a systematic literature review of the application of Industry 4.0 technologies in the tourism sector.
(ii) Analyze the potential of these technologies to enable sustainable tourism.
(iii) Identify challenges and opportunities for the implementation of Tourism 4.0 initiatives.
(iv) Propose an agenda for future research in this multidisciplinary field.

By achieving these objectives, this study can provide a general overview of how Industry 4.0 technologies are revolutionizing the tourism industry, particularly in relation to sustainability. The results may benefit researchers, practitioners, and policymakers seeking to address digital transformation challenges in tourism.

2. Methodology

This systematic literature review was conducted in accordance with the Preferred Reporting Items for Systematic Reviews and Meta-analyses (PRISMA) 2020 guidelines by Page *et al.*[10] that were built on the original PRISMA principles proposed by Moher *et al.*[11] A prespecified review protocol outlined the search strategy, inclusion and exclusion criteria, data-extraction procedures, and synthesis steps.

2.1. Data sources

Systematic searches were performed in electronic databases (i.e., Scopus, Web of Science, ScienceDirect) and Google Scholar for articles published between 2015 and 2023 (including early 2024 where available). Reference lists identified during the review process were also screened to supplement the database search. The search strings combined terms related to sustainable tourism and Industry 4.0 technologies (e.g., "sustainable tourism" AND "Industry 4.0" OR "AI" OR "IoT" OR "blockchain" OR "big data" OR "virtual reality").

Google Scholar was used only to capture additional references and gray literature. To reduce bias, only the first 10 pages of Google Scholar results were reviewed, whereas Scopus, Web of Science, and ScienceDirect served as the primary indexed sources.

2.2. Inclusion and exclusion criteria

This research considered conference papers and peer-reviewed journal articles that explicitly mentioned the use of one or more Industry 4.0 technologies to improve or investigate sustainable tourism outcomes. The research could be empirical or conceptual, but needed to address tourism sustainability (environmental, social/cultural, or economic). Only studies written in the English language were considered. We excluded studies that did not focus on tourism or sustainability (e.g., pure tech development papers without a tourism context), did not address the said technologies, and were unavailable in full text. To ensure recency and relevance, preference was given to research in the recent decade with a global scope.

2.2.1. Screening and selection

After database searches, all records were merged and duplicates removed. Titles and abstracts of unique records were screened for inclusion criteria, and full-text screening was performed for eligible papers. Two independent reviewers conducted screening, with disagreements resolved through consensus. Figure 1 shows the PRISMA flow diagram of study selection.

The search identified 520 records from database searches and additional sources. After duplicate removal (n = 100), 420 unique records were screened, of which 350 were excluded for irrelevance. Full-text articles (n = 70) were assessed for eligibility, and 20 studies met all inclusion criteria.

2.2.2. Data extraction and synthesis

Study information, such as author/year, target technology, study context/methods, and key findings relating to sustainable tourism, was mapped using a data extraction form. We then performed qualitative thematic synthesis. Initial coding of findings within each study was performed to identify emerging themes or outcome domains. Codes were iteratively refined and grouped into more encompassing thematic categories that reflect how Industry 4.0 technologies enable sustainable tourism. Coding and theme development were checked for consistency by a second reviewer. Study characteristics (Table 1) and thematic findings (Table 2) were tabulated. Finally, we considered overall trends, key findings, research gaps, and future research directions. Evidence strength was considered when making recommendations, with the Malaysian tourism context taken into account for applicability.

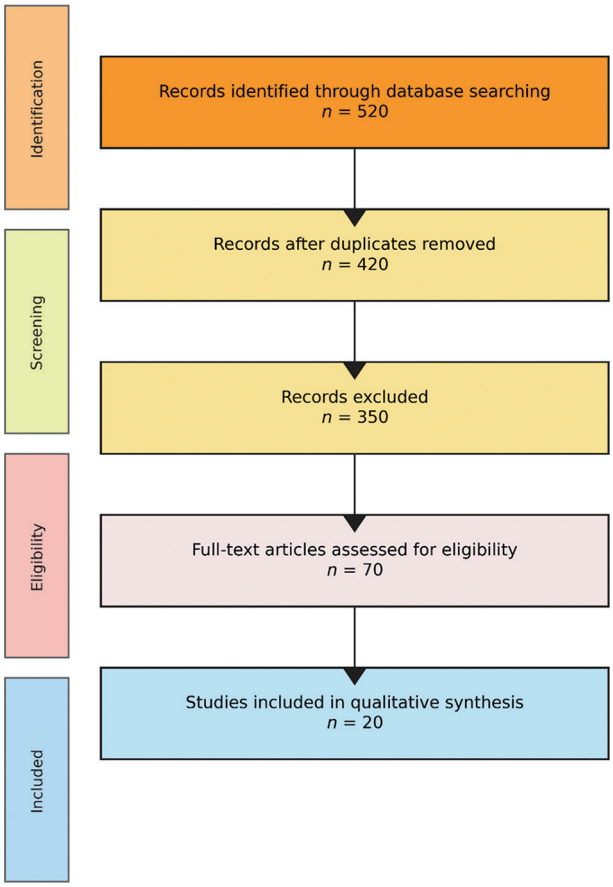

Figure 1. Preferred Reporting Items for Systematic Reviews and Meta-analyses (PRISMA) 2020 flow diagram
Source: Created by Authors through PRISMA Synthesis.

3. Results and discussion

Data extraction and study details are summarized in Table 2, which presents the 20 reviewed studies by author, year, leading Industry 4.0 innovation, study approach, and principal findings pertinent to sustainable tourism.

3.1. Contextual thematic synthesis of findings

The selected studies demonstrate a global coverage, with studies being undertaken in China, Malaysia, Europe, the Middle East, and multi-country settings. Empirical research and conceptual studies were represented, from small-scale case studies in hotels and heritage areas to large-scale systematic reviews. Although various technologies were represented, such as IoT, blockchain-based technologies, and AR/VR (for VR experiences), AI

Table 1. Systematic literature review method used

Step	Description
Design	Systematic literature review following PRISMA 2020 with predefined protocol
Data sources	Scopus, Web of Science, ScienceDirect, Google Scholar (2015–2023), plus manual search
Search strategy	Search terms: "sustainable tourism" AND ("Industry 4.0," "AI," "IoT," "blockchain," "big data," "VR")
Inclusion criteria	Peer-reviewed articles in English focusing on Industry 4.0 and sustainability in tourism
Exclusion criteria	Excluded: Non-tourism, non-sustainability, non-English, or tech-only without tourism context
Screening process	Title/abstract screening, followed by full-text review; two independent reviewers with consensus

Abbreviations: AI: Artificial intelligence; IoT: Internet of Things; PRISMA: Preferred Reporting Items for Systematic Reviews and Meta-analyses; VR: Virtual reality.

Table 2. Summary of key outcomes for sustainable tourism

Study (author, year)	Tech focus	Type of study	Key outcomes for sustainable tourism
Majid *et al.* (2023)[12]	AI (intelligent automation)	Systematic review (213 papers)	Identified five major application themes of AI for sustainability: enhancing tourist experience, preserving heritage, improving quality of life, measuring experiences, and conserving the environment. Found more focus on economic and sociocultural aspects than environmental, indicating a gap in AI addressing environmental sustainability. Proposed an "AI4GoodTourism" framework to guide future AI innovations for sustainability.
Rahmadian *et al.* (2022)[13]	Big data analytics	Systematic review (131 papers)	Big data applications in sustainable tourism have emerged since 2016. Big data are used for behavior prediction (e.g., tourist flows) and to support decision-making and policymaking for sustainability. Demonstrated how integrating big data with AI and IoT enables smart tourism services in smart cities. Highlighted challenges: Data quality, privacy, cost, and need for cross-sector data sharing.
Kannan (2024)[14]	AI	Comprehensive review	Reviewed AI integration in tourism operations and customer experience. Concluded that AI-driven personalization and automation improve tourist satisfaction and operational efficiency, while also offering future opportunities for smarter, more sustainable tourism services.
Rane *et al.* (2023)[15]	AI, blockchain, IoT, AR/VR	Conceptual review (multitech)	Explored all five techs as solutions to tourism's sustainability challenges (environmental degradation, cultural disruption, and socioeconomic imbalances). Found that: AI enables optimized resource allocation, personalized experiences, and data-driven sustainability strategies; Blockchain creates transparent, traceable supply chains for equitable economic benefits and lower environmental impact; IoT supports real-time environmental monitoring and adaptive conservation measures; AR enriches cultural heritage interpretation, deepening tourist understanding; VR provides virtual experiences that reduce the need for physical travel, cutting carbon footprints. Overall, a technology-driven approach can significantly enhance environmental, social, and economic sustainability in tourism.
Kontogianni *et al.* (2024)[16]	AI and blockchain	Book chapter (Springer)	Discussed smart tourism through AI and blockchain integration. Emphasized AI's role in customer-facing smart tourism (chatbots, personalization) and blockchain's role in secure data management and trust in tourism transactions. Suggested that combining these technologies can improve tourist experience and accountability (e.g., verifying sustainable practices), though empirical validation was noted as a future need.
Treiblmaier (2022)[17]	Blockchain	Handbook chapter (review)	Provided an overview of blockchain applications in tourism (payments, inventory, and loyalty). Highlighted how blockchain can disintermediate travel services and reduce costs and fraud. Emphasized improved transparency and efficiency in tourism operations via smart contracts and decentralized ledgers.
Rashideh (2020)[18]	Blockchain	Conceptual framework	Developed a blockchain framework for tourism. Identified potential benefits: Enhanced security for transactions, reduced operational and commission costs, and greater transparency across stakeholders. Envisioned blockchain for secure identity management (e.g., digital passports, seamless check-ins) and use of cryptocurrency for peer-to-peer payments to build trust in platforms.

(Cont'd...)

Table 2. ***(Continued)***

Study (author, year)	Tech focus	Type of study	Key outcomes for sustainable tourism
Li and Jiang (2023)[19]	AR	Empirical study (China, survey)	Investigated tourist acceptance of AR for creating memorable experiences. Using the Technology Acceptance Model, found that the perceived usefulness of AR enhancements at attractions leads to higher acceptance. Implies AR can increase tourist engagement and satisfaction, potentially encouraging sustainable behaviors if AR content emphasizes conservation.
Polukhina *et al.* (2025)[20]	VR, digital platforms	Case studies (Russia, transition economy)	Examined digital solutions for sustainable tourism development. Found that VR experiences can substitute physical travel, reducing travel-related emissions and pollution. Also noted that VR and digital platforms raise environmental awareness among tourists by showcasing conservation content. It is concluded that smart tourism tools contribute to sustainability in emerging destinations but require supportive infrastructure.
Zhuang *et al.* (2022)[21]	Mobile apps, VR	Quantitative analysis (China, FDI, and tourism)	Analyzed the impact of technology innovation on tourism and the environment. Reported that digital platforms (mobile apps) can foster tourist engagement in sustainable practices (e.g., apps informing tourists about responsible behaviors). In addition, noted that VR can mitigate environmental pressure by offering virtual visits, thereby lowering carbon emissions from tourism.
Farid and Rashid (2024)[22]	IoT	Conceptual paper (smart destinations)	Discussed IoT-enabled "smart destinations." illustrated how IoT devices in hotels and tourist sites lead to personalized services (smart rooms, automated check-in) and efficient operations. Highlighted IoT-driven energy management and predictive maintenance in hotels (e.g., sensor-based energy savings at Crowne Plaza) to reduce resource waste. It is concluded that IoT improves visitor satisfaction and reduces the environmental footprint of hospitality operations.
Eskerod *et al.* (2019)[23]	IoT (smart hotels)	Multicase study (five high-end hotels)	Explored drivers for IoT adoption to enhance sustainability in luxury hotels. Found that pressure to reduce hotels' significant carbon footprint and to cut energy costs were key motivators. IoT-based smart management systems (integrating HVAC, lighting, etc.) enabled guests to control room settings via one interface while optimizing energy use. Identified management support and brand image (green reputation) as additional drivers for implementing IoT innovations.
Yang *et al.* (2021)[24]	Blockchain	Case analysis (heritage tourism)	Demonstrated blockchain's utility in cultural heritage preservation. By recording and tracking community heritage assets on a tamper-proof ledger, blockchain enhances transparency in managing these resources. This transparency helps ensure that tourism activities around heritage sites remain accountable and sustainable. Authors suggest that such blockchain-based tracking can support community trust and long-term cultural sustainability in tourism.
Rodrigues *et al.* (2024)[25]	Multitech (Industry 4.0)	Systematic review (Heliyon)	Assessed digital transformation in tourism via Industry 4.0. Noted that although many studies examine individual technologies, there is a lack of integrated perspectives on their collective impact on transformative sustainable tourism. This indicates a research gap in understanding synergies among AI, IoT, blockchain, etc., Authors call for holistic approaches and more empirical cases of multiple tech adoption.
Capucho *et al.* (2025)[26]	Bibliometrix software for bibliometric mapping	Systematic review and bibliometric analysis of 223 selected papers	It identified three thematic clusters: (i) Sustainable tourism, (ii) tourism, (iii) well-being, and proposed a new taxonomy for sustainable tourism that integrates well-being and sustainable development, enhancing conceptual clarity and supporting balanced tourism planning.
Luu *et al.* (2025)[27]	Digitalization in tourism supply chains under Industry 4.0	Bibliometric review of literature on digitalization in tourism supply chains	Identified research clusters showing a shift from supply chain efficiency to innovation-driven sustainability; highlighted how Industry 4.0 tools can optimize resource use and improve environmental performance in tourism logistics.
Bekele and Raj (2025)[28]	Digital transformation in the tourism industry	Bibliometric review and research agenda setting	Mapped four primary research clusters linking digital transformation to tourism growth; stressed the need for sustainable integration of digital tools to enhance resilience and competitiveness of the tourism sector.
Astanakulov *et al.* (2025)[29]	IoT for smart tourism	Thematic analysis of IoT innovations in tourism	Found that IoT can significantly improve tourist experience, resource management, and sustainability monitoring; proposed frameworks for integrating IoT into Tourism 4.0 strategies.

(Cont'd...)

Table 2. ***(Continued)***

Study (author, year)	Tech focus	Type of study	Key outcomes for sustainable tourism
Duarte Alonso *et al.* (2025)[30]	Industry 4.0 adoption in hospitality	Case study of Vietnamese hospitality organizations	It identified 11 dimensions of Industry 4.0 application in hospitality, with benefits including improved energy efficiency, reduced waste, and enhanced service customization to support sustainable tourism models.
Sjukriana *et al.* (2025)[31]	Event technology in hospitality and tourism	Systematic review	Found that technology adoption in events is driven by perceived ease of use and usefulness; emphasized the potential to reduce environmental impact through virtual and hybrid event formats, contributing to sustainability goals.

Abbreviations: AI: Artificial intelligence; AR: Augmented reality; HVAC: Heating, ventilation, and air conditioning; IoT: Internet of Things; VR: Virtual reality.

and data analytics were the most frequently highlighted tools.[32]

Scientific interest in this area has increased significantly over the past 5–6 years due to the intersection between digitalization and sustainability agendas. In a qualitative review, several recurring themes emerged regarding how Industry 4.0 technologies facilitate sustainable tourism. These are shown in Table 3 with representative examples from the literature.

3.1.1. Thematic insights

Industry 4.0 technologies are contributing to the three pillars of sustainable tourism. Environmentally, AI, IoT, and VR technologies reduce energy and resource consumption, lower emissions, and facilitate the preservation of natural and cultural heritage sites. AI-based energy management platforms minimize hotel electricity usage, IoT products offer real-time environmental monitoring, and VR enables low-impact exploration of sensitive locations, thereby reducing ecological pressure.[33]

In sociocultural terms, AR/VR has been effective in tourism education and awareness, facilitating deeper cultural appreciation and learning for sustainability. Blockchain-based transparency systems help empower stakeholders by revealing how tourism benefits are distributed, thereby enhancing perceptions of fairness.

Economically, AI and automation increase efficiency and reduce costs, presenting a sound business case for investment. Technologies, such as VR-based tourist products and intelligent tourism apps, create new sources of revenue and attract niche markets. Blockchain removes intermediaries, raising returns for suppliers and reducing costs for consumers. As reported in Malaysia, AR/VR tourism pilots demonstrate how new products can simultaneously increase competitiveness and instill sustainability, as shown in Figure 2.

Synthesizing these findings indicates that Industry 4.0 technologies are not an end in themselves; rather, they serve as facilitators of sustainable tourism outcomes. AI and big data enable predictive outcomes to maximize resources and minimize risks of overcrowding. IoT enables intelligent destinations for achieving energy and water efficiency. Blockchain enables accountability and eco-certification. AR/VR optimizes experience while providing alternatives to physical travel.[33] All these technologies, together, balance economic recovery with sustainability in post-pandemic tourism environments.

3.2. Environmental impacts of AI in tourism 4.0

Environmental consequences are the most well-documented in the literature examined. AI-powered hotel energy systems are said to minimize electricity usage by up to 20%, whereas IoT-powered conservation initiatives enable real-time monitoring of ecosystems. Digital tourism and virtual tours reduce travel intensity, resulting in quantifiable carbon savings.

However, the evidence is not entirely positive. Several studies[32,33] reported that small- and medium-sized enterprises (SMEs) incurred significant upfront costs that limited adoption. Others were alert to rebound effects, whereby efficiency savings lead to greater demand, thereby counteracting environmental gains. Rodrigues *et al.*[25] provided a comprehensive review of Industry 4.0 implications for tourism, noting that while technological adoption is widespread, integrated frameworks linking multiple technologies to sustainability outcomes remain underdeveloped.[34]

In addition, most evaluations rely on short-term pilot studies; there is insufficient longitudinal data to determine if environmental gains are sustained at scale. This implies that AI is an enabler of environmental sustainability but is contingent upon governance structures, affordability, and regular monitoring.

3.3. Governance impacts of AI in Tourism 4.0

AI also assists in enhancing tourism governance. Research indicates that AI-based dashboards and data platforms increase transparency through real-time monitoring of visitor movement, energy consumption, and emissions.

Table 3. Thematic synthesis of findings

Thematic category	Role of Industry 4.0 tech in sustainable tourism	Illustrative evidence
1. Resource efficiency and environmental conservation	Technologies drive more efficient use of resources and the reduction of tourism's environmental footprint. AI and big data enable data-driven resource management (e.g., optimizing energy and water use in hotels, predicting tourist flows to prevent overcrowding). IoT sensors monitor environmental conditions in real time, enabling adaptive conservation measures (e.g., adjusting facilities usage based on wildlife activity). AR and VR can substitute or complement physical travel, helping lower carbon emissions by offering virtual experiences. Overall, Industry 4.0 innovations support greener operations and informed environmental stewardship in tourism.	AI-driven smart systems in destinations reduce energy waste (smart grids, HVAC). Big data analysis helps managers plan visitor distribution to avoid overuse of natural sites. IoT deployments in parks track soil, air, and wildlife data to inform carrying capacity decisions. VR "virtual tourism" experiences have demonstrably cut down actual visits in some cases, curbing emissions and pollution.
2. Enhanced tourist experience and education	Industry 4.0 tech enables more immersive, personalized, and educational tourism experiences that align with sustainability. AI-powered personalization (recommendation engines, chatbots) helps tourists with eco-friendly options and tailors experiences without extra resource strain. IoT creates "smart" service environments (e.g., smart hotels, attractions) that improve convenience (e.g., keyless entry, automated transit info) and encourage responsible behavior (e.g., apps that nudge energy-saving). AR enriches on-site experiences by overlaying interpretive content about heritage or ecology, educating tourists on sustainability and cultural significance. VR provides enjoyment and pre-trip learning about destinations, raising awareness, and reducing impulsive travel. By making sustainable choices attractive through a tech-enhanced experience, tourists' satisfaction and willingness to support conservation increase.	Airbnb's AI algorithms personalize travel plans, including suggesting less crowded, eco-friendly attractions, enhancing the experience while avoiding overtourism. Smart destination apps (mobile platforms) engage tourists with real-time guidance and sustainability tips (e.g., water-saving reminders). An AR application in a Malaysian heritage site guides tourists with cultural stories, making the visit more engaging and meaningful (local example). Studies show AR can significantly improve the "memorable tourism experience" for visitors, which destinations leverage to promote environmental education.
3. Transparency, trust, and governance	Blockchain and data analytics improve transparency in tourism supply chains and governance, leading to more sustainable practices. Blockchain's immutable ledgers enable tracing of tourism products and services—for instance, tracking if a hotel's operations meet sustainability certifications or if community tourism funds are distributed. This builds trust among consumers and stakeholders that sustainability claims are genuine (preventing "greenwashing"). Smart contracts can ensure fair payments (e.g., automatic carbon offset contributions). Open data platforms and big data dashboards (often government-led) enable monitoring of tourism impacts and evidence-based policy interventions. Collectively, these technologies encourage accountability: tourism businesses are incentivized to adopt sustainable operations, knowing that data are transparent. Governments and communities gain tools to enforce regulations and share benefits equitably.	Blockchain pilots in tourism (e.g., in Hungary) have improved transaction security and transparency between tourists and service providers. Tourism authorities using big data dashboards can publicly share indicators, such as footfall in protected areas or waste generated, pressuring operators to reduce impacts. Studies reported that blockchain could verify the authenticity of heritage crafts and ensure revenue goes to local artisans. Such transparency mechanisms help tourists make informed choices and foster trust in sustainability certifications (e.g., a blockchain-based ecolabel for hotels that travelers can verify).
4. Cultural heritage preservation and social inclusiveness	Several technologies help protect cultural and natural heritage and promote inclusive community development. AR and VR offer new ways to experience cultural heritage sites without causing wear and tear on artifacts or disturbance to communities. Virtual tours can reduce the need for large numbers of tourists at fragile sites while still generating interest and educational value. AI and big data tools aid in managing visitor impact on heritage (e.g., predictive models for site erosion based on visitor numbers). Blockchain can empower local communities by recording their cultural assets and ensuring benefits from tourism are returned to them transparently. IoT can be used in heritage sites for surveillance to prevent vandalism or to control microclimates in sensitive museums. Overall, Industry 4.0 can mitigate the negative impacts of tourism on heritage and ensure communities remain central beneficiaries.	Augmented reality apps allow tourists to visualize historical scenes or artifacts in situ, enriching appreciation without physical touching or damaging them. VR heritage tours (e.g., virtual walk-throughs of UNESCO sites) gained popularity during COVID-19, showing they can provide access while reducing congestion at sites. Community-based tourism projects are testing blockchain for the transparent sharing of profits and funding of local conservation, addressing trust issues with external tour operators. In addition, AI translation and digital platforms provide residents with a greater voice and involvement in tourism experiences than the traditional approach, supporting sociocultural sustainability.
5. Data-driven planning and policy	Widespread adoption of analytics (big data, AI) and IoT feeds is enabling smarter tourism planning and policy geared toward sustainability. Destination managers and policymakers use predictive models to anticipate	Big data analyses have shown their usefulness in tourism strategy—for instance, analyzing geotagged social media to identify overvisited hotspots and then implementing

(Cont'd...)

Table 3. *(Continued)*

Thematic category	Role of Industry 4.0 tech in sustainable tourism	Illustrative evidence
	anticipate tourism demand and environmental impacts, allowing proactive measures such as visitor caps or dynamic pricing to prevent overtourism. Scenario simulations (e.g., using AI or digital twins) help evaluate sustainability strategies (like the impact of diverting tourists to alternative sites). Real-time data from sensors and social media provide early warnings of issues (wildfires, coral reef stress, crowding) such that authorities can respond quickly. These approaches support evidence-based decision-making and align tourism development with sustainability targets (e.g., SDGs). Importantly, data-driven insights help balance economic benefits with ecological limits and community well-being, guiding policies on destination growth, transportation, and resource management.	measures to redistribute visitor flows. Several cities (such as Amsterdam and Barcelona) employ AI to predict peak tourist congestion and adjust city services or issue travel advisories, thereby reducing strain on infrastructure. In national parks, IoT-based visitor counting and environmental monitoring inform adaptive management plans each season. Such data-driven initiatives result in more adaptive, resilient tourism systems that can maintain sustainability even as tourism volumes change.

Abbreviations: AI: Artificial intelligence; AR: Augmented reality; HVAC: Heating, ventilation, and air conditioning; IoT: Internet of Things; SDGs: Sustainable Development Goals; UNESCO: United Nations Educational, Scientific, and Cultural Organization; VR: Virtual reality.

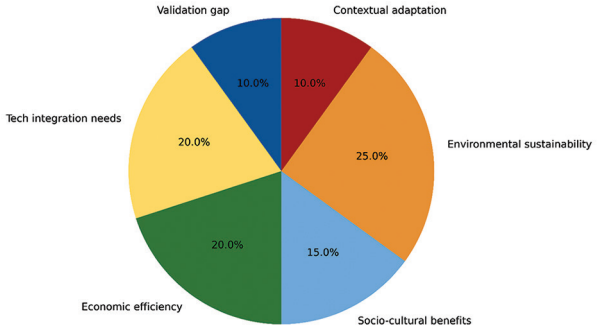

Figure 2. Distribution of research emphasis in Industry 4.0 and sustainable tourism. Environmental sustainability represents the largest share of research focus, followed by economic efficiency and technology integration needs.
Source: Created by the authors based on synthesized review data.

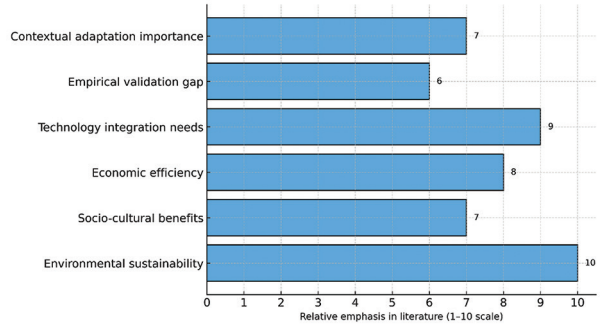

Figure 3. Relative emphasis of key research themes in Industry 4.0 and sustainable tourism (1–10 scale). Environmental sustainability shows the highest emphasis (score = 10), followed by technology integration (score = 9) and economic efficiency (score = 8).
Source: Created by the authors based on synthesized review data.

Blockchain technologies, though less studied, hold potential for transparent eco-certification and reducing fraud in tourism supply chains. They can enhance regulatory control and accountability among stakeholders.[34] As emphasized by recent reviews, integrating Industry 4.0 into sustainability agendas requires not only technological innovation but also supportive governance, cross-sectoral alignment, and inclusive stakeholder engagement.

However, governance-based constraints are evident. Ethical issues regarding data privacy are rarely addressed, although travelers are likely to oppose surveillance-based monitoring.[35] Smaller companies and rural operators are likely to be left out of digital governance structures, resulting in disparities. Furthermore, policymaking mechanisms to help control responsible AI use in tourism are also lacking. Consequently, governance impacts become conditional and vulnerable: AI can enhance transparency only if it is embedded within broader institutional support frameworks that ensure fairness and inclusion.

3.4. Critical problems and paradoxes

While most of the literature is positive, a critical synthesis shows contradictions. AI forecasting models are praised for helping predict and manage overtourism, but few studies show that these forecasts have led to long-term policy change or quantifiable visitor redistribution. Blockchain is commonly referred to as a transparency tool, but in practice, its implementation is rare due to its technical sophistication and the uncertainty in returns on investment.[34] AI-based personalization is cherished to enhance tourist experiences, but also denounced for violating privacy and eroding confidence. Figure 3 depicts how the reviewed literature reconciles beneficial consequences with critical issues.

Most benefits reported are from pilot studies or conceptual models, often across limited time perspectives. There is a lack of longitudinal studies examining sustained influences on emissions, conservation, or reforms of governance. These inconsistencies highlight that AI and

Tourism 4.0 must be treated as possible facilitators, rather than certainties.

3.5. Research gaps identified

The review also exposes important research gaps, shown in Figure 4. There are limited studies that combine multiple technologies into integrated frameworks; most compartmentalize AI, IoT, or blockchain separately. Strong empirical case studies remain rare, especially in the developing world, and longitudinal data are sparse. Measurement issues continue, although promises of carbon savings or transparency gains are routine; there are few studies with hard, measurable numbers. Ethical and privacy aspects are not yet well explored, as are the threats of digital exclusion. Geographically, the research is skewed toward Europe and China, whereas Southeast Asia, Africa, and Latin America remain somewhat underrepresented.

The small dataset of 20 included studies further limits generalizability. Although the studies provide valuable information, conclusions must be viewed as indicative, rather than definitive. More comprehensive studies are needed to synthesize evidence across contexts and technologies. This aligns with recent evidence that highlights the need for longitudinal, integrated approaches to Industry 4.0 and sustainability.[36]

3.6. Synthesis and implications

In general, AI in Tourism 4.0 shows great potential to drive sustainability. Environmentally, AI and linked technologies support efficiency gains, resource savings, and emissions reductions. At the governance level, AI and blockchain help support transparency and accountability. Contradictions exist, though: adoption is expensive, benefits are unequal, privacy issues are unresolved, and evidence over the long term is lacking.

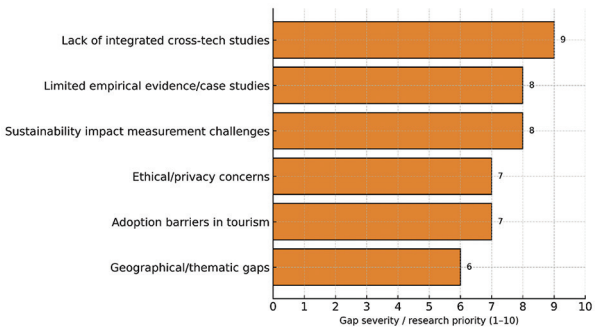

Figure 4. Identified gaps in Industry 4.0 and sustainable tourism. The figure highlights limited longitudinal evidence, fragmented multi-technology integration, under-representation of developing regions, and insufficient attention to ethics, privacy, and inclusiveness.
Source: Created by the authors based on synthesized review data.

For Malaysia, these results indicate that while there are early pilots and policies, system integration has yet to be achieved. The nation is at a mid-evolutionary point: beyond disconnected projects but not yet a fully entrenched Tourism 4.0 system. Scaling AI-enabled solutions, therefore, needs to be supported not just by technical infrastructure but also by inclusive governance frameworks, ethical safeguards, and longitudinal monitoring systems. The following section presents in-depth recommendations for Malaysia directly linked to the environmental and governance findings of the review.

While the literature generally highlights positive contributions of Industry 4.0 technologies to sustainable tourism, it also reveals critical tensions. Adoption remains uneven, especially for SMEs with limited resources, and sustainability claims are often based on short-term pilot projects rather than longitudinal evidence. Moreover, the risks of privacy intrusion, digital exclusion, and cost inefficiencies are underexplored in numerous studies. This limits the ability to fully understand both the theoretical implications of digital transformation for sustainable development and the practical challenges faced by tourism enterprises. A deeper critical reflection indicates that Industry 4.0 cannot be assumed to guarantee sustainability; rather, its benefits depend on careful design, supportive governance, and alignment with local contexts.

4. Future research directions

Based on the identified gaps, the review proposes several future research directions (Figure 5):

(i) Longitudinal case studies and experiments: Destinations must work with researchers to deploy technologies and monitor outcomes. For example, a city or resort may be a "living lab" where IoT, AI, and AR projects are implemented to increase sustainability,

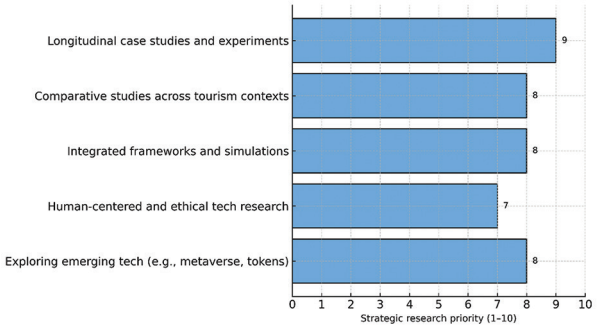

Figure 5. Strategic future research agendas for sustainable Tourism 4.0. This framework outlines key directions, including longitudinal case studies, cross-context comparative analyses, integrated multitechnology simulations, participatory human-centered design, and ethical artificial intelligence adoption.
Source: Created by the authors based on synthesized review data.

and researchers monitor the effect pre- and post-deployment on energy usage, tourist satisfaction, community livelihoods, etc. Long-term monitoring will determine the efficacy of tech solutions and whether rebound effects occur (e.g., does refining something make it more efficient or lead to increased demand?).

(ii) Cross-context comparative analysis: Future studies can compare how Industry 4.0 affects sustainable tourism across different contexts, for example, a tech-savvy city vs. a remote ecotourism community. This can determine contextual factors and best practices. Malaysia, with its mix of urban (Kuala Lumpur) and natural (Borneo, islands) destinations, is an excellent country for cross-context comparative analyses on how technology adoption strategies would differ.

(iii) Integrated frameworks and simulations: Research must strive to design integrated frameworks that combine multiple technologies to achieve maximum gains in sustainability. Simulation packages, such as system dynamics or agent-based models, can be employed to simulate a destination with various tech interventions (like simulating a 10% reduction in tourists through the adoption of VR or a 20% increase in IoT efficiency and examining how the system responds).[35] This would be useful in forecasting the impacts of collaborative interventions and guiding real-life trials.

(iv) Human science and ethical research: Since this topic is sociotechnical, human science research is also required. These are research on the acceptance of tech-mediated tourism experiences (will tourists accept virtual experiences as alternatives or just complements?), employee adaptation to the automation of tourism services, and regulatory research on data privacy and ethics. For example, exploring tourist satisfaction and learning gains from AR/VR experiences specifically designed with sustainability can help create improved content. In addition, co-designing technology solutions for tourism with local communities may be a research area (participatory design approach) in which solutions are well accepted and culturally appropriate.

(v) Technological innovations and new opportunities: The pace of technology is rapid. Further studies should monitor emerging technological trends, such as AI-powered predictive analytics (even more sophisticated), blockchain tokens or rewards for green behavior (e.g., earn tokens for being off-beat sites), IoT convergence with renewable energy (hotels leveraging IoT to use solar/wind maximally), and the Metaverse or enhanced VR for travel. Evaluating the potential benefits and drawbacks of such revolutionary trends prior to their full adoption within the mainstream tourism market can position the industry to leverage them ethically.[37]

In essence, an interdisciplinary approach will be crucial—involving tourism scholars, data scientists, engineers, and social scientists to collaboratively address these research agendas. This will ensure that the next wave of tourism technology research is holistic, impact-oriented, and in alignment with sustainability imperatives.

The findings verify the initial research propositions that Industry 4.0 technologies, especially AI, have significant but uneven impacts on sustainability outcomes. Evidence confirms their contribution to environmental efficiency and governance transparency, but also reveals challenges, such as costs, privacy, and limited scalability. Based on these insights, further studies should expand longitudinal evaluations, explore cross-technology integration, and examine adoption in developing-country contexts, including Malaysia.

5. Recommendations for Malaysia's tourism industry

Although this review synthesizes global literature, Malaysia is chosen for contextual recommendations because it represents a developing economy at a transitional stage of Tourism 4.0 adoption. The country has launched initiatives, such as MyDIGITAL and Smart Tourism 4.0, yet integration of AI into governance and sustainability remains fragmented. This makes Malaysia an appropriate case for illustrating how global lessons can be localized to strengthen both environmental outcomes and institutional governance in tourism.

Worldwide, discussions on Tourism 4.0 highlight that AI, IoT, blockchain, big data, and AR/VR can bring sustainability benefits, but are implemented piecemeal and without integration. Malaysia is not beginning from zero. There are national policies, including MyDIGITAL, the National Tourism Policy 2020–2030,[37] and the Malaysia Smart Tourism 4.0, that have already introduced the significance of tourism digitalization. Pilot AR/VR heritage experiences, fintech sandboxes for regulation, and IoT-enabled monitoring initiatives in ecotourism destinations are also early indicators. Most initiatives, however, are still fragmented or small in scale. The following recommendations are thus adjusted for mid-evolution: Malaysia has progressed beyond standalone pilots but is not yet at a fully institutionalized, interconnected smart tourism ecosystem.

5.1. Invest in smart tourism infrastructure

Malaysia's digital economy agenda already encompasses infrastructure expansion, but has uneven tourism-specific

deployment.[38] As a next step for MyDIGITAL and Smart Tourism 4.0, investment needs to focus on broadband availability, 5G deployment, and IoT-sensor networks in key destinations. For instance, IoT monitoring in Taman Negara or Sabah's marine parks would facilitate data-driven visitor management, while growing "smart city" infrastructure in Kuala Lumpur or Penang would streamline transport flows and ease congestion. These infrastructures are the bedrock for AI-powered analytics, driving both environmental protection and enhanced tourist experiences. In contrast to previous disjointed pilots, this proposition locates infrastructure as an integrated national priority for tourism sustainability.

5.2. Facilitate tech-enabled sustainable experiences

Malaysia has experimented with AR heritage trails and isolated VR ecotourism activities, yet these continue as standalone initiatives. A synergistic program, such as national AR trails in George Town and Malacca, or VR tourism packages highlighting marine biodiversity in Sabah, would turn these small-scale experiments into mass market tourism products. These programs not only appeal to digitally connected tourists but also mitigate pressure on vulnerable ecosystems by providing immersive, low-impact options. Public-private partnerships, digital hackathons, and seed-funding programs might be used to produce locally centered content that fosters both heritage appreciation and conservation awareness. This extends existing pilots but converges them into a more cohesive national digital tourism system.[39]

5.3. Use blockchain to ensure transparency and certification

Malaysia has already run sustainability certification programs, yet transparency and verification remain issues. By utilizing its fintech regulatory sandbox, Malaysia can test blockchain-based platforms in holding and authenticating eco-certifications, carbon accounting, and community benefit-sharing schemes. A national "Green Tourism Blockchain" would allow tourists to immediately check green claims while encouraging companies to take sustainable actions. Token-based systems could further incentivize environmentally friendly behavior (e.g., booking low-carbon tours) through redeemable rewards. This suggestion thus capitalizes on Malaysia's fintech preparedness to put the nation at the vanguard of open and accountable sustainable tourism management.[39]

5.4. Inclusive innovation and capacity building

Previous initiatives, such as the Malaysia Tourism Transformation Plan, focused on training, but SMEs and rural operators do not always have the resources to adopt digital tools. To bridge this gap, Malaysia needs to create targeted accelerators and incubators that integrate digital capabilities to SMEs and community-based businesses, ranging from IoT system maintenance to AR/VR content development. Inclusive innovation ensures that rural guides, indigenous entrepreneurs, and small operators are not left behind in the digital economy. For example, upskilling locals to operate drone-based monitoring or to co-create AR heritage stories would create employment while retaining cultural authenticity. By integrating inclusivity, Malaysia reduces excessive reliance on external providers and promotes culturally appropriate solutions.[40]

5.5. Policy integration and multistakeholder collaboration

Malaysia's tourism administration now mentions digitalization within strategic papers, but it remains fragmented across ministries. In line with the National Tourism Policy 2020–2030,[41] there needs to be a multistakeholder platform comprising the Ministries of Tourism, Environment, and Communications, as well as academia, SMEs, and tech companies to harmonize standards, ensure the ethical use of data, and establish measurable sustainability parameters. Pilot work with universities, for example, testing AI-controlled tourist dispersion systems in Langkawi or Penang, can provide evidence-based benefits, informing policy formulation. A larger co-creation platform, in support of the Malaysia Tourism Transformation program, would guarantee solutions are not only technologically innovative but also ethically founded, socially inclusive, and environmentally sustainable.[42]

Malaysia stands at a crossroads: It has set the stage for Tourism 4.0 with strategic policies and pilot projects, yet systematic integration remains unfinished.[35,37] By advancing infrastructure, expanding sustainable digital experiences, embracing blockchain transparency, developing inclusive capacity, and harmonizing multistakeholder policies, Malaysia can turn its disjointed efforts into a streamlined, sustainable tourism system. These recommendations thus sit at the midpoint of system development, building on what is there while laying the foundation for an entirely institutionalized, people-first, and sustainable smart tourism future.[25,43,44]

This review is based on a relatively small but highly targeted set of 20 studies. While sufficient for capturing key themes, the limited studies require cautious interpretation, particularly regarding emerging technologies, such as blockchain. Future reviews with expanded datasets and longitudinal evidence will further consolidate these findings.

6. Conclusion

This review demonstrates that Industry 4.0 technologies, particularly AI within the Tourism 4.0 framework, contribute to sustainable development by promoting environmental efficiency, transparent governance, and resilience in the tourism sector. Environmentally, AI and IoT enable measurable reductions in energy and resource consumption, while VR and AR lower ecological pressure by providing low-impact visitor experiences. From a governance perspective, blockchain and AI-based monitoring systems enhance accountability, certification, and decision-making. Together, these technologies help tourism enterprises integrate sustainability into their operations, balancing growth with conservation.

The findings suggest that smart tourism infrastructure, interactive and educational digital experiences, blockchain-enabled transparency, inclusive capacity-building programs, and multistakeholder policy integration are key enablers of sustainable tourism. Effective adoption, however, requires a balanced approach that combines technological innovation with community engagement, environmental sustainability, and cultural authenticity.

The review's main achievement lies in synthesizing how AI-centered Industry 4.0 innovations interact with environmental and governance dimensions of sustainability. However, the study has limitations: the dataset comprises 20 studies, and the evidence is heavily skewed toward short-term pilots and emerging technologies, such as blockchain, which remain under-researched. These limitations imply that conclusions must be treated as indicative rather than definitive, and further longitudinal and context-specific studies are required.

Acknowledgments

The authors would like to acknowledge the Universiti Tunku Abdul Rahman, Malaysia, for providing institutional and research support throughout the completion of this study.

Funding

None.

Conflict of interest

The authors declare they have no competing interests.

Author contributions

Conceptualization: Maryam Kalhoro
Visualization: All authors
Writing–original draft: Maryam Kalhoro
Writing–review & editing: Hui Nee Au Yong, Abdelhak Senadjki

Ethics approval and consent to participate

Not applicable.

Consent for publication

Not applicable.

Availability of data

Not applicable.

References

1. Rane N, Choudhary S, Rane J. Sustainable tourism development using leading-edge artificial intelligence (AI), blockchain, Internet of Things (IoT), augmented reality (AR), and virtual reality (VR) technologies. *SSRN Electron J.* 2023:1-22.

   doi: 10.2139/ssrn.4642605

2. Gomes S, Lopes JM, Ferreira L. Looking at the tourism industry through the lenses of Industry 4.0: A bibliometric review of concerns and challenges. *J Hosp Tour Insights.* 2024;7(1):436-457.

   doi: 10.1108/JHTI-01-2023-0028

3. Stankov U, Gretzel U. Tourism 4.0 technologies and tourist experiences: A human-centered design perspective. *Inf Technol Tour.* 2020;22(3):477-488.

   doi:10.1007/s40558-020-00172-y

4. Buhalis D, Efthymiou L, Uzunboylu N, Thrassou A. Charting the progress of technology adoption in tourism and hospitality in the era of Industry 4.0. *Eur Med J Bus.* 2024;19(1):1-20.

   doi: 10.1108/EMJB-01-2023-0025

5. Boluk KA, Cavaliere CT, Higgins-Desbiolles F. A critical framework for interrogating the United Nations Sustainable Development Goals 2030 Agenda in tourism. *J Sustain Tour.* 2019;27(7):865-880.

   doi: 10.1080/09669582.2018.1479037

6. Dixit P. *Tourism and Technology: The Future.* New Delhi, India: Educohack Press; 2025.

7. Basu M, editor. Tech-driven horizons: Pioneering sustainable tourism for environmental resilience and SDGs triumph. In: *The Need for Sustainable Tourism in an Era of Global Climate Change: Pathway to a Greener Future.* Bingley, UK: Emerald Publishing; 2024. p. 215-247.

   doi: 10.1108/978-1-80455-178-020241011

8. Topsakal Y. Artificial intelligence-based sustainable tourism planning: a conceptual model proposal. In: Çetinkaya MY, Özdemir M, editors. *Advancing Smart Tourism Through Analytics.* Hershey, PA: IGI Global; 2025. p. 65-94.

   doi: 10.4018/978-1-6684-9452-8.ch004

9. Pencarelli T. The digital revolution in the travel and tourism industry. *Inf Technol Tour.* 2020;22(3):455-476.

doi: 10.1007/s40558-019-00160-3

10. Page MJ, McKenzie JE, Bossuyt PM, *et al.* The PRISMA 2020 statement: An updated guideline for reporting systematic reviews. *BMJ.* 2021;372:n71.

doi: 10.1136/bmj.n71

11. Moher D, Liberati A, Tetzlaff J, Altman DG, The PRISMA Group. Preferred reporting items for systematic reviews and meta-analyses: The PRISMA statement. *PLoS Med.* 2009;6(7):e1000097.

doi: 10.1371/journal.pmed.1000097

12. Majid GM, Tussyadiah I, Kim YR, Pal A. Intelligent automation for sustainable tourism: A systematic review. *J Sustain Tour.* 2023;31(11):2421-2440.

doi: 10.1080/09669582.2022.2155904

13. Rahmadian E, Feitosa D, Zwitter A. A systematic literature review on the use of big data for sustainable tourism. *Curr Issues Tour.* 2022;25(11):1711-1730.

doi: 10.1080/13683500.2021.1910217

14. Kannan V, Zhang T, Li H. A review of the intelligent condition monitoring of rolling element bearings. *Machines.* 2024;12(7):484.

doi: 10.3390/machines12070484

15. Rane N, Choudhary S, Rane J. Enhanced product design and development using artificial intelligence (AI), virtual reality (VR), augmented reality (AR), 4D/5D/6D printing, Internet of Things (IoT), and blockchain: Review. *Virtual Real Augment Real Digit Des.* 2023;4:1-12.

doi: 10.2139/ssrn.4680072

16. Kontogianni A, Alepis E, Virvou M, Patsakis C. *Smart Tourism-the Impact of Artificial Intelligence and Blockchain.* Berlin/Heidelberg, Germany: Springer; 2024.

doi: 10.1007/978-3-031-42076-2

17. Treiblmaier H. Blockchain and tourism: Paradoxes, misconceptions, and a research roadmap. *Tour Econ.* 2022;28(7):1956-1960.

doi: 10.1177/1354816620957621

18. Rashideh W. Blockchain technology framework: Current and future perspectives for the tourism industry. *Tour Manag.* 2020;80:104125.

doi: 10.1016/j.tourman.2020.104125

19. Li S, Jiang S. The technology acceptance on AR memorable tourism experience-The empirical evidence from China. *Sustainability.* 2023;15(18):13349.

doi: 10.3390/su151813349

20. Polukhina A, Sheresheva M, Napolskikh D, Lezhnin V. Digital solutions in tourism as a way to boost sustainable development: Evidence from a transition economy. *Sustainability.* 2025;17(3):877.

doi: 10.3390/su17030877

21. Zhuang Y, Yang S, Razzaq A, Khan Z. Environmental impact of infrastructure-led Chinese outward FDI, tourism development and technology innovation: A regional country analysis. *J Environ Plann Manag.* 2023;66(2):367-399.

doi: 10.1080/09640568.2022.2048502

22. Farid MT, Rashid M. Unleashing the potential of Industry 4.0: Analyzing Pakistan's tourism in the global arena. *J Excellence Soc Sci.* 2024;3(2):157-187.

23. Eskerod P, Hollensen S, Morales-Contreras MF, Arteaga-Ortiz J. Drivers for pursuing sustainability through IoT technology within high-end hotels-an exploratory study. *Sustainability.* 2019;11(19):5372.

doi: 10.3390/su11195372

24. Yang Y, Zhang CX, Rickly JM. A review of early COVID-19 research in tourism: Launching the Annals of Tourism Research's curated collection on coronavirus and tourism. *Ann Tour Res.* 2021;91:103313.

doi: 10.1016/j.annals.2021.103313

25. Rodrigues V, Breda Z, Rodrigues C. The implications of Industry 4.0 for the tourism sector: A systematic literature review. *Heliyon.* 2024;10(11):e27621.

doi: 10.1016/j.heliyon.2024.e27621

26. Capucho J, Leitão J, Alves H. Mapping and linking well-being, tourism economics, sustainable tourism and sustainable development: An integrative systematisation of the literature and bibliometric analysis. *Discov Sustain.* 2025;6(1):291.

doi: 10.1007/s43621-025-00367-5

27. Astanakulov O, Balba ME, Khushvakt K. IoT innovations for transforming the future of the tourism industry: Towards smart tourism systems. *J Intell Syst.* 2025;34(2):145-162.

doi: 10.1515/jisys-2024-0019

28. Bekele H, Raj S. Digitalization and digital transformation in the tourism industry: A bibliometric review and research agenda. *Tour Rev.* 2025;80(4):894–913.

doi: 10.1108/TR-07-2023-0509

29. Duarte Alonso A, Kim OVT, Tran TD. Exploring the relationships between Industry 4.0 adoption and business model: The case of Vietnamese hospitality organisations. *Int J Hosp Tour Manag.* 2025;15(1):50-68.

30. Luu NTM, Pham TH, Siriwardana A. Bibliometric review of digitalization in tourism supply chains in the context of Industry 4.0. *Strateg Change.* 2025;34(2):123-140.

doi: 10.1002/jsc.2807

31. Sjukriana J, Hanafiah MH, Asyraff MA, Kusumah G. Unveiling the landscape of event technology adoption in the hospitality and tourism industry: Insights from a systematic literature review. *Int J Event Fest Manag.* 2025;16(2):207-228.

doi: 10.1108/IJEFM-06-2024-0077

32. Gonzaga S. The role of prototyping in participatory design projects. In: Dias P, Santos R, editors. *International Conference on Design and Digital Communication.* Cham, Switzerland: Springer Nature; 2024. p. 687-700.

doi: 10.1007/978-3-031-68017-3_52

33. Au Yong HN, Kalhoro M, Morrison C, Hanna D, Rehman HM. Community-driven sustainability practices in cultural heritage tourism: A qualitative study. *Qual Quant.* 2025;59:1–21.

doi: 10.1007/s11135-025-02444-9

34. MyDIGITAL. *Malaysia Digital Economy Blueprint.* Putrajaya, Malaysia: Government of Malaysia, Ministry of Economy; 2021.

35. AlAfnan MA, Mohdzuki SF. Malaysia's National Blockchain Roadmap 2021–2025: A critical discourse analysis of focus, goals, and challenges. *World J Engl Lang.* 2024;14(5):482-492.

doi: 10.5430/wjel.v14n5p482

36. MyDIGITAL. *Support Pours In for the MyDIGITAL Initiative and National 4IR Policy.* Putrajaya, Malaysia: Government of Malaysia, MyDIGITAL; 2022.

37. AlAfnan MA, Mohdzuki SF. Malaysia's National Blockchain Roadmap 2021–2025: A critical discourse analysis of focus, goals, and challenges. *World J Engl Lang.* 2024;14(5):482-492.

doi: 10.5430/wjel.v14n5p482

38. Government of Malaysia. *National 4IR Policy.* Putrajaya, Malaysia: MyDIGITAL, Ministry of Science, Technology and Innovation; 2023.

39. Tourism Malaysia, Ministry of Tourism, Arts and Culture. *National Tourism Policy 2020-2030-Executive Summary.* Putrajaya, Malaysia: Tourism Malaysia; 2020.

40. Malaysian Investment Development Authority (MIDA). *Smart Tourism: Future of Tourism in Malaysia.* Kuala Lumpur, Malaysia: MIDA; 2021.

41. Tourism Malaysia. *Smart Tourism 4.0 to be Tourism Game-Changer for Malaysia.* Kuala Lumpur, Malaysia: Tourism Malaysia; 2018.

42. Amir S, Nur'Hidayah Dura N, Yusof,MA. Nakamura H, Nong RA. Challenges of smart tourism in Malaysia eco-tourism destinations. Planning Malaysia. *J Malaysian Inst Plan* 2020;18(4):442–451.

doi: 10.21837/pm.v18i14.844

43. Al-Qudah AA, Alzoubi HM, Al-Debei MM, Al-Dmour AM, Masa'deh R, Abualoush SH. The convergence of artificial intelligence and sustainability reporting: A systematic review of applications, challenges and future directions. *Bus Strateg Environ.* 2024;33(1):70090.

doi: 10.1002/bse.70090

44. Kumar RR, Sharma GD, Singh SK. Integrating Industry 4.0 for enhanced sustainability: Pathways and prospects. *J Clean Prod.* 2024;437:140355.

doi: 10.1016/j.jclepro.2024.140355

ACCSCIENCE PUBLISHING

Explora: Environment and Resource

REVIEW ARTICLE

Environmentally benign conducting polymers: A sustainable approach to biomedical devices

Imene Bekri-Abbes* and **Nour Guetif**

Laboratory of Composite Material and Clay Minerals, National Center of Material Science, Technopole of Borj Cedria, Soliman, Tunisia

Abstract

The rising issue of biomedical discharges underscores the need for sustainable alternatives, leading to emerging applications of biodegradable conducting polymers (CPs). This review aims to emphasize current progress in this research area, focusing on applications for "green" biomedical uses. Novel biomaterials are distinct from others by virtue of their electrical conductivity, while being biocompatible and biodegradable such as conventional biomaterials, making them very suitable for biomedical applications that require safe, controlled degradation within the human body. In addition, the paper draws on current progress in the synthesis of conducting and novel biomaterials, as well as in the processes for controlled degradation, and also addresses their utilization in biomedical applications within biodegradable systems. Essential details on CPs synthesis, with a focus on their emerging applications ranging from temporary biomedical implants to tissue engineering and bioresorbable biosensors, are also discussed. Finally, this review aims to address essential issues and future research for prompt clinical applications and continuous innovations in emerging applications of conducting, biodegradable biomaterials.

Keywords: Medical waste; Biodegradable conducting polymers; Biomedical applications; Sustainable materials

***Corresponding author:**
Imene Bekri-Abbes
(bekrimene@gmail.com)

Citation: Abbes I, Guetif N. Environmentally benign conducting polymers: A sustainable approach to biomedical devices. *Explora Environ Resour.* 2025;2(4):025350063. doi: 10.36922/EER025350063

Received: August 30, 2025

Revised: November 28, 2025

Accepted: December 5, 2025

Published online: December 23, 2025

1. Introduction

Since the groundbreaking discovery of conducting polymers (CPs), this fascinating class of organic materials has received considerable attention because of their unique combination of metallic conductivity and processability comparable to conventional polymers.[1] Their characteristic properties, such as light-weight, flexibility, and adjustability, have already found numerous applications in electronic displays, ranging from sensors and transistors to flexible electronics. The capability to control their properties perfectly while in thin-film format is cementing their position in the emerging biomedical applications domain. Despite this, the lack of biodegradability is still a significant disadvantage in the case of conventional CPs, posing numerous issues in the long run, particularly in the context of biomedical applications.[1] Owing to the increasing demand within the biomedical sector for sustainable alternatives, the emergence of CP materials with biodegradable properties represents one of the most significant requirements within this research field.[2] The presence of biodegradable properties within CP biomaterials not only addresses the issue of biomedical waste but also helps in the development of biomedical devices

with transient properties engineered to degrade within the body.[2] The process of making CP biomaterials begins with the development of composites through the addition of other biomaterials, such as poly (lactic acid) (PLA) and poly(ε-caprolactone) (PCL), or other natural biomaterials.[3] Although this approach significantly enhances the sustainability of CP biomaterials, there is often a decline in electrical properties, mainly owing to issues with electrical interfaces.[3] Recent innovations within this research field have been based on more advanced approaches. These are based on the synthesis of CP biomaterials through modified biomaterials, the addition of degradable links within the polymer, and the development of oligomers based on controlled degradation properties.[3]

This review examines the latest advances in the development of the biodegradable CP for use in biomedical applications, emphasizing the approaches used in designing and making CP. The prospects of this material in shaping the development of sustainable biomedical technology, as well as outlooks and research opportunities in this field, are also discussed.

2. Fundamentals of conducting biodegradable polymer

2.1. Structure and conductivity

The development of CPs emerged in the 1970s with the breakthrough discovery of polyacetylene-enhanced conductivity upon doping. This finding sparked widespread interest, leading to the exploration of diverse polymers such as polypyrrole (PPy), polyaniline (PANi), and poly(3,4-ethylenedioxythiophene) (PEDOT). These materials derive their unique electrical properties from a molecular structure featuring alternating single and double bonds, forming a conjugated system that enables efficient charge mobility through electron delocalization. CPs serve as a vital link between flexible organic materials and highly conductive metals.[4-6] Their molecular architecture, as depicted in Figure 1, includes a range of structures such as polyacetylene derivatives, heterocyclic polymers such as PPy and PEDOT, and aromatic systems like PANi, each tailored for specific electronic applications. The hallmark of CPs is their π-conjugated backbone, where alternating σ- and π-bonds create pathways for electron movement.[7] In their undoped state, these polymers show low conductivity, usually around 10^{-10} S/cm, which makes them insulators. Doping, through either oxidation (p-doping) or reduction (n-doping), introduces charge carriers such as polarons or bipolarons. This boosts conductivity to levels similar to that of metals, within the range between 10^2 and 10^3 S/cm. Doping is a crucial process that turns CPs into highly conductive materials. For instance, p-doping involves removing electrons from the polymer chain, creating mobile positive charge carriers that help with electrical conduction.[8] This ability to adjust, along with the natural flexibility and processability of CPs, makes them great for uses in flexible electronics, sensors, and biomedical devices. However, the strong conjugated systems that give them conductivity also make traditional CPs resistant to natural breakdown. This creates environmental issues, especially for short-term applications such as biodegradable implants or disposable sensors. The long lifespan of conventional

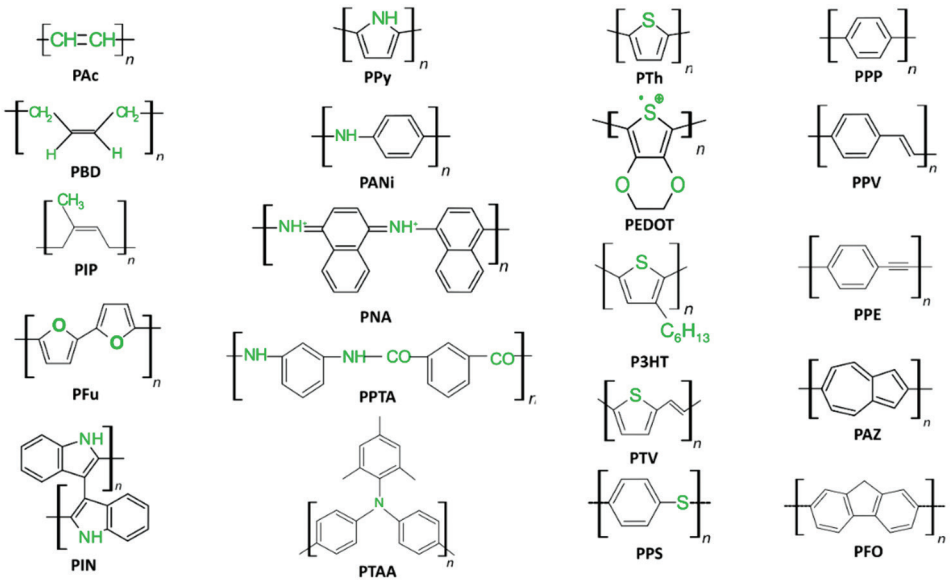

Figure 1. Inventory of conducting polymers along with their abbreviations[7]

CPs clashes with the growing demand for sustainable materials. To tackle this, researchers are looking into new ways to combine the electrical properties of CPs with the ability to break down of eco-friendly polymers. The goal is to create materials that perform well and decompose harmlessly after use. These efforts are vital for promoting sustainable biomedical technologies and cutting down on electronic waste.

2.2. Synthesis and fabrication techniques

The advancement of CPs with specific properties depends on the careful selection of synthesis and processing methods. These approaches provide precise control over material structure, conductivity, and morphology, thereby facilitating their application in transient biomedical devices. Figure 2 summarizes the three primary synthesis methods for CPs: solution-based chemical synthesis, solid-solid reaction synthesis, and electrosynthesis.

2.2.1. Solution-based chemical synthesis

Solution-based chemical synthesis is a cornerstone method for producing CPs such as PPy and PANi, widely valued for its scalability and versatility in biomedical applications. This technique employs a redox reaction where monomers with electron-donating groups are oxidized by chemical agents, generating reactive intermediates that polymerize through chain propagation or step-growth mechanisms.[9] Common oxidants, such as ammonium persulfate or ferric chloride, are cost-effective and facilitate large-scale production.[9] The method's flexibility supports integration with advanced fabrication techniques like inkjet printing, spin coating, or dip coating, enabling the creation of structured materials for biosensors, electrodes, and drug delivery systems.[10,11] Precise control over reaction conditions, particularly the oxidant-to-monomer ratio, is critical to avoid over-oxidation, which can reduce electrical conductivity.[11] Recent studies have explored innovative approaches, such as the spontaneous polymerization of pyrrole within Fe^{3+}-exchanged montmorillonite (MMT) to form intercalated PPy-MMT nanocomposites.[12] By varying the molar proportion of pyrrole to interlayer Fe^{3+}, researchers achieved tailored DC conductivity and dielectric properties, with AC conductivity following a power-law behaviour governed by correlated barrier hopping.[12] This enhances the suitability of solution-based CPs for transient biomedical devices, where controlled morphology and electrical performance are essential.

2.2.2. Electrosynthesis

Electrosynthesis offers a highly controlled approach to CP fabrication, ideal for producing thin, uniform films with customized properties. This method employs an electrochemical cell with a working electrode, counter electrode, and reference electrode immersed in a monomer-electrolyte solution. By applying a specific voltage or current, monomers undergo oxidation or reduction at the electrode surface, initiating polymerization and depositing the CP directly as a film.[13] This technique ensures high purity and allows fine-tuning of film characteristics, such as thickness, crystallinity, and conductivity, by adjusting parameters like voltage, electrolyte composition, or pH. Its single-step process eliminates the need for extensive post-processing, making it suitable for creating multilayered or patterned structures for bioelectronic interfaces.

2.2.3. Solid-solid reaction synthesis

Solid-solid reaction synthesis is a solvent-free method for fabricating CPs such as PANi and PPy, offering significant potential for biodegradable biomedical applications. This technique involves blending solid monomer powders, like

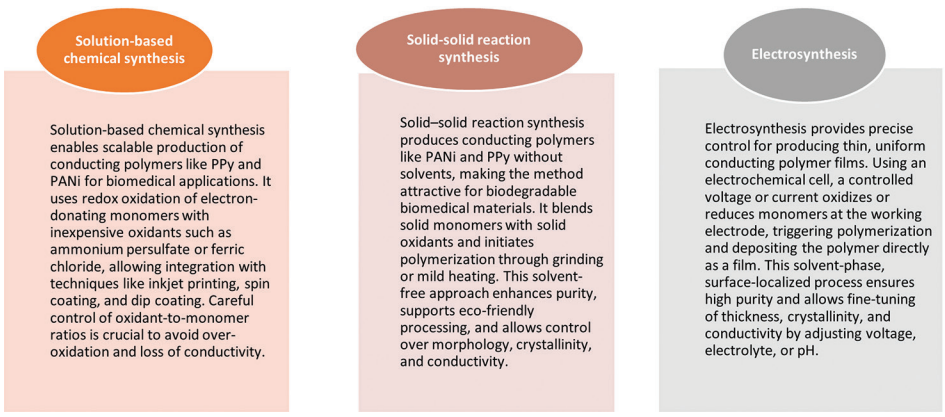

Figure 2. Different synthesis methods of conducting polymers
Abbreviations: PANi: Polyaniline; PPy: Polypyrrole.

an ilinium chloride, with solid oxidants, such as ammonium peroxydisulfate, and initiating polymerization through mechanical grinding or mild heating.[14-18] Unlike solution-based or vapor-phase methods, solid–solid synthesis relies on solid-state diffusion and surface interactions, producing high-purity polymers without solvent-related impurities, thus supporting eco-friendly manufacturing principles.[18] The method enables precise control over polymer morphology, crystallinity, and electrical conductivity by adjusting parameters such as the oxidant-to-monomer ratio and grinding duration.[17,16] For instance, PANi-MMT nanocomposites synthesized through this route exhibit a branched fibrous morphology and enhanced thermal stability compared to free PANi, attributed to the stabilizing effect of MMT's interlayer structure.[14,18] Ground MMT serves dual roles as an oxidant and reinforcement, leveraging Fe^{3+} cations in its octahedral layers and atmospheric oxygen to drive an ilinium polymerization.[5] AC conductivity studies reveal a frequency-dependent regime with low-frequency DC conductivity transitioning to a power-law behavior at higher frequencies, indicating robust electrical performance suitable for biomedical devices.[14,16,18] The solvent-free nature of this method reduces environmental impact, aligning with the demand for sustainable biomedical materials. By integrating CPs with biodegradable polymers like PLA, composites can maintain electrical functionality while degrading harmlessly in physiological environments.[1]

3. Biodegradability and transiency

3.1. Biodegradable CPs

Environmentally benign CPs are defined as polymeric materials capable of undergoing substantial degradation within a specified timeframe, ensuring that no adverse environmental impacts occur.[19,20] The term "environmentally benign" extends beyond simple mass loss or fragmentation of the CPs. A rigorous definition requires that the material and its degradation products undergo complete assimilation into natural biogeochemical cycles without leaving persistent, bioaccumulative, or toxic residues. The fate within the human body is generally favorable for the matrix components. Polyesters such as PLA and PCL undergo hydrolysis to yield metabolites such as lactic acid and caproic acid. These degradation products are efficiently cleared by the renal or metabolized through the Krebs cycle, resulting in low cytotoxicity. Similarly, natural polymers, such as chitosan and cellulose derivatives, can mineralize into carbon dioxide (CO_2) and water (H_2O), thereby minimizing environmental impact. In biomedical applications, it is crucial that the degradation products are biocompatible and can be metabolized or excreted easily by the body. When developing biodegradable CPs, it is essential to balance biodegradability with the preservation of electrical conductivity and mechanical properties inherent to CPs such as PPy and PEDOT. However, the conjugated backbone of the CP components (PPy, PEDOT, aniline oligomers) poses a greater challenge. Their degradation yields aromatic fragments, such as aniline oligomers or thiophene derivatives, could present significantly higher cytotoxicity, compared to the aliphatic acid metabolites. While these may remain below acute toxicity thresholds in controlled implants, their long-term biological impact requires careful evaluation. There are several methods for addressing the balance between biodegradability and conductivity in conducting biodegradable polymers. One of the more common methods is dispersing a conductive filler made from CP materials (e.g., PPy nanoparticles, or PEDOT nanoparticles) within a biodegradable polymer matrix (e.g., PLA and PCL). However, the presence of the conductive filler generally provides only moderate conductivity values (10^{-} to 10^{-1} S/cm) and can lead to phase separation between the filler and matrix, which can generate inconsistent electrical conductance as the PLA matrix degrades. Alternatively, there are newer potentially more precise methods which can incorporate degradable links at the molecular level. Degradable linkages, such as ester or imine groups, may be incorporated into the CP backbone to maintain π-conjugation for charge transport while also providing for controlled degradation.[21] Alternatively, hydrolyzable side groups, for example, oligoesters, can be added to CPs to maintain conductivity of the backbone while allowing for breakdown.[22] There has also been recent innovative work on more complex architectures, such as star-shaped CPs or hyperbranched CPs with degradable cores, that enhance charge transport while allowing for a more favorable disintegration profile.[23] The choice of dopants is very important for the biodegradability. Typical small-molecule dopants demonstrate little compatibility with the environment, causing researchers to transition to bio-derived dopants such as polyglutamic acid, or heparin which can serve both charge compensation and degradation pathways.[24] For instance, PEDOT doped with a modified poly (styrenesulfonate) including polyethylene glycol grafts was found to show improved biodegradability while maintaining good conductivity.[24] Characterization assesses various aspects including measurement of conductivity (e.g., via four-point probe or impedance spectroscopy), degradation kinetics through *in vitro* testing that imitates physiological or environmental conditions, and examination of mechanical properties such as tensile strength in cases of wearables or implants.[25]

4. Biomedical applications

The field of biomedical utilization and applications has rapidly progressed with CPs by incorporating conductivity, flexibility, and biocompatibility, contributing to technological advancements in healthcare.[26-41] Bio-conjugated polymers, PPy, PANi, and PEDOT, have been studied widely on their capacity to interface with biological systems, parse out electric stimuli, and detect biological signals, as well as the role in controlled degradation. New development that made strides to improve these CPs through biodegradability, developing transient devices that degrade once their purpose is served, which removes the need for surgical removal.[26,27] This section will elaborate on the various biomedical applications of biodegradable CPs, such as biosensors, tissue engineering, neural interfaces, drug delivery, and antimicrobial systems.

4.1. Biosensors for health monitoring

In biosensing applications, CPs are essential materials thanks to their high electrical conductivity, high surface area, and ability to modify the surface chemistry of CPs to achieve the right properties to isolate/deploy the biological analyte of interest.[26] As shown in Figure 3, the role of CPs is significant as they are responsible for changing a certain type of input stimulus into an electrical signal in monitoring health. The illustration in Figure 3 breaks the process into three pathways based on the type of signal: Chemical, electrochemical, or mechanical. The first pathway is activated by a biochemical signal, such as a protein or DNA, and illustrates how CPs can stimulate this signal. A biological receptor which is functionalized with a "bio-factor" will bind to the analyte (signal), and the CP will emit a signal, transmitting the signal to the processing unit. For electrochemical-type signals, such as heat or pH, CPs can either directly record the signal, or the CPs can be modified to enhance the reception of the signal. CPs could also be modified to act as a transducer for electrochemical signals. Finally, for mechanical signals, such as pressure or vibration, CPs will transduce the physical force into electrical signal. In all examples, the CP-based device will be connected to a signal unit for independent signal processing or for use as a part of a data set. The figure visually summarizes how CPs act as an active and flexible constituent in the biosensor designs.[26]

The aforementioned quality makes CPs (e.g., PPy and PEDOT) favorable for developing sensors for continuous glucose monitoring, lactate detection, and cardiac biomarker analysis (human troponin) classifiers for diabetes management, sports performance monitoring, and heart health assessment.[26] For instance, PPy-based biosensors have been incorporated into a wearable sensor for real-time glucose monitoring with high sensitivity and flexibility.[26] Similarly, both PEDOT-based DNA sensors and biochips have taken advantage of PPy's capacity to functionalize surfaces with biomolecules to achieve highly specific detection of genetic material or pathogens.[26] Recent studies have advanced CP-based biosensors through the addition of components that lead to biodegradability. For example, PPy-dextrin (*in situ*) nanocomposites have antibacterial and antioxidant properties, and can also be useful in infection monitoring sensors.[30] These composites demonstrate conductivity (up to 10^{-3} S/cm) and biodegradability.[30] Furthermore, researchers have experienced highly sensitive CP-based biosensors through the addition of components, such as carbon nanotubes or silver nanoparticles.[26,33] For example, PPy combined with multi-walled carbon nanotubes (MWCNTs) in biodegradable poly(L-lactide)/poly(3-hydroxybutyrate-co-4-hydroxybutyrate) blends

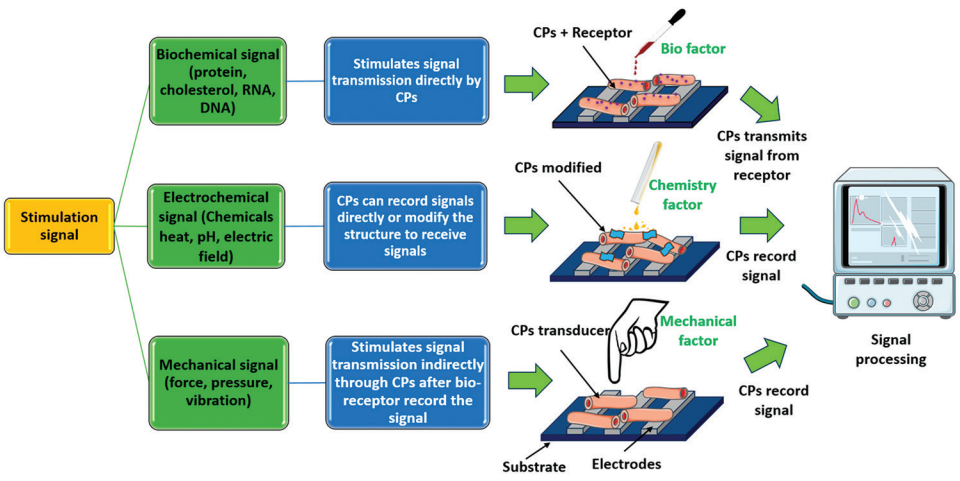

Figure 3. The role of conducting polymers in receiving and processing stimulation signals[7]

achieved a very low percolation threshold (0.58 wt%),which is crucial for conductivity improvements.[36]

4.2. Tissue engineering and regeneration

CPs are widely used in tissue engineering, especially for neural, cardiac, and bladder tissue regrowth, to apply electrical stimulation to facilitate cell growth, cell adhesion and cell differentiation.[26,27] For example, a biodegradable PEDOT-poly(octamethylene-citrate-co-octanol) scaffold was developed for bladder tissue regeneration in athymic rats.[27] This electroactive scaffold reinstated bladder function, and anatomical structure, without the use of exogenous cell seeding, comparable to scaffolds seeded with mesenchymal stromal cell, demonstrating the ability of biodegradable scaffolds without cells.[27] The scaffold conductivity with ~10^{-5} S/cm and degradability allows temporary mechanical property support for non-conductive tissue scaffolds, then degrades into innocuous products once bladder regeneration is complete.[27] In the same context, PPy-chitosan composites increase Schwann cell proliferation, and secretion of neurotrophins, such as nerve growth factor (NGF) and the brain-derived neurotrophic factor (BDNF), upon the application of electrical stimulation.[31] *In vitro* experimentation demonstrated that electrical stimulation through PPy-chitosan scaffolds greatly increased expression of NGF and BDNF, and improved peripheral nerve regeneration in animal models.[31] Synthesized with aniline trimer and doped with camphor sulfonic acid, biodegradable conductive polyurethanes have an elasticity of 30% strain and a conductivity of up to 7.3×10^{-5} S/cm in wet state, and promote fibroblast proliferation, which is important for tissue repair.[29] All of these materials biodegrade into non-toxic byproducts to minimize inflammatory responses and offer advantages for implantation, such as liquidation after degradation. Furthermore, PCL-based scaffolds with conductive fillers such as MWCNTs provide mechanical strength and biocompatibility to promote both bone and cartilage regeneration.[32] The micropatterned surface of these scaffolds drives stem cell differentiation and improves the integration of engineered tissues.[32] In another study, Subramanian *et al.*[42] produced aligned nanofibers of poly(lactic-co-glycolic acid)/poly(3-hexylthiophene)to promote Schwann cell alignment and myelin formation and to aid peripheral nerve repair in rodent models. Xu *et al.*[43] created PEDOT/carboxymethyl chitosan hydrogels to address cranial injury. Huang *et al.*,[44] studied the use of PLA-b-aniline pentamer-b-PLA (PAP) (5×10^{-6} S/cm) to synchronize cardiomyocyte beating for increasing junction formation and contractile force in damaged hearts. Baheiraei *et al.*[45] described electroactive polyurethane scaffolds that restored conduction velocity in disrupted myocardium (but risked arrhythmia). Xie *et al.*,[46] elucidated star polylactide-aniline trimer networks to improve osteoblast mineralization and collagen deposition, leading to 80% defect closure in femoral models.

4.3. Neural interfaces and stimulation

CPs play a key role in neural interfaces due to their unique ability to interface with neural tissue and provide an ability to deliver controlled electrical stimulation to live tissue, allowing neural recording and stimulation. Biodegradable magnesium-based microelectrodes decorated with PEDOT have also been developed specifically for *in vivo* neural recording in the auditory cortex of mice, recording multi-unit stimulus-evoked activity from the brain.[34] These microelectrodes utilize biodegradable polymers for insulation, which will degrade within a safe amount of time after implantation, avoiding the downsides to chronic implantation.[34] In addition, PEDOT has a conductivity of ~10^{-4} S/cm, enabling reliable signal acquisition, making PEDOT suitable for transient neural interfaces.[34] Furthermore, in peripheral nerve repair, a conductive hydrogel integrating polydopamine-modified silicon phosphorus (SiP@PDA) nanosheets in a gelatin methacryloyl matrix promoted differentiation of neural stem cells into Schwann cell-like cells.[28] This hydrogel has a conductivity of ~4.34 mS/cm and has properties comparable to those of neural tissue, causing resident macrophages to polarize toward a pro-healing phenotype, enhancing tissue angiogenesis.[28] In a rat model of Parkinson's disease, this hydrogel combined with acupuncture induced a more than 80% increase in the regeneration of dopaminergic neurons and improved motor function with the electrophysiological spike rates returning to levels comparable to those of healthy rats.[28] Since the scaffolds are biodegradable, complications related to their long-term use owing to non-degradation can be prevented.[28] In addition, polyphosphazene polymers with aniline pentamer side chains also provide a combination of conductivity (~2×10^{-5} S/cm) and biodegradability, which are the characteristics required in neuronal tissue engineering.

4.4. Biomedical implants

For long-lasting implants, materials must exhibit mechanical strength, electrical functionality, and the ability to controllably resorb to prevent secondary surgical interventions. Boutry *et al.*[47] created PPy and PCL-PPy RLC resonators through emulsion polymerization to allow for wireless bioelectronic implants. Both poly(L-lactic acid) (PLLA) and PCL degrade through hydrolytic chain scission into lactic and caproic acid, respectively, which are metabolites capable of elimination by the body through the

Krebs cycle. Lu *et al.*[48] developed PPy/hybrid electrodes for neural probes, where PPy provided the conductivity, and carbon nanotubes aided in mechanical stability; however, full evaluation of the long-term degradation was not provided. For orthopedic application, Wan *et al.*[49] incorporated magnesium into the PLLA forming PLLA/Mg/MgF_2 composites. The released magnesium ions supported osteogenic pathways while PLLA degraded through hydrolysis over the period of 6–12 months. In a separate study, Ghaziof and Mehdikhani-Nahrkhalaji[50] fabricated1 wt% MWCNT/PCL scaffolds using solvent casting and vacuum drying methods, which significantly improved electrical conductivity and compressive strength for myocardial patches; however, the degradation of the PCL matrix was relatively slow and appropriate for load-bearing cardiac repair. Similarly, Wang *et al.*[51] developed nano-Fe_3O_4/PLLA bone screws, which introduced magnetic guidance and were biodegradable. The degradation of the PLLA was accelerated by acidic byproducts, where Fe_3O_4 was included to promote radiopacity. Jiang *et al.*[52] electro spun PCL/gelatin/carbon nanotubes vascular grafts that mimic native vessel mechanics. The gelatin component rapidly degraded via enzymatic action, while PCL provided long-term structural support through gradual hydrolysis.

4.5. Drug delivery and antimicrobial applications

CPs enable precise drug delivery through electrical or environmental stimuli, thereby enhancing therapeutic outcomes. A biodegradable, electroconductive self-healing hydrogel based on polydopamine-coated polyurethane nanoparticles supports neural stem cell proliferation and differentiation, with strong antioxidative and anti-inflammatory effects.[28] This hydrogel, used in a Parkinson's disease model, elevated serum levels transforming growth factor-β1 and stromal cell-derived factor-1, promoting neuroprotection and reducing inflammation.[28] Its conductivity (~4.34 mS/cm) and shear modulus (~280 Pa) mimic brain tissue, making it ideal for injectable drug delivery systems.[28] CPs also exhibit antimicrobial properties, critical for infection-resistant biomedical devices. PPy-dextrin nanocomposites demonstrate antibacterial activity against Gram-positive (e.g., *Staphylococcus aureus*) and Gram-negative (e.g., *Pseudomonas aeruginosa*) bacteria, suitable for wound dressings or implants.[30] Ultrathin electro spun mats combining PCL, silver nitrate, and carboxymethyl chitosan offer high antibacterial efficacy, breathability, and biodegradability, making them effective face mask filters for airborne disease prevention.[33] These mats, with a total thickness of ~300 μm, provide mechanical stability and degrade naturally, reducing environmental impact.[33] Similarly, electrostatically flocked PCL microfibers filled with silver nanoparticles exhibit antimicrobial activity against methicillin-resistant *S. aureus*, supporting tissue formation and vascularization *in vivo*.[37] Sumitha *et al.*[53] electro spun PCL/silver nanofibrous scaffolds, showing a clear zone of inhibition against *S. aureus* proportional to Ag content. PCL degraded through hydrolysis, enabling sustained Ag^+ release.

4.6. Biodegradable electroactive scaffolds

The integration of biodegradability into CP-based systems has opened new avenues for transient biomedical devices. For example, PPy grafted with oligo-3-hydroxybutyrate pendants combines conductivity with biodegradability, suitable for temporary scaffolds in tissue engineering.[38] Electrostatic flocking of silver nanoparticle-filled PCL microfibers creates biphasic scaffolds that degrade naturally while promoting new tissue formation and angiogenesis.[37] Cataractous eye protein isolate -based solid polymer electrolytes achieve high ionic conductivity (~8×10^{-a} S/cm) and biodegradability, offering potential for flexible bioelectronics.[39] These materials leverage natural proteins, enhancing sustainability and biocompatibility.[39] CPs blended with biodegradable polymers, such as PLA or polybutylene succinate, form conductive foams for neural recording or energy storage.[40] Polybutylene succinate-based foams with carbon nanofibers and expanded graphite achieve tailored cellular structures, supporting biomedical applications.[40] In addition, novel CPs with degradable ester linkages, such as quarter thiophene-ester polymers, exhibit electroactivity and cytocompatibility, which are ideal for tissue-engineering scaffolds.[41] These advancements underscore the potential of biodegradable CPs in creating sustainable, high-performance biomedical devices.

5. Synthesis strategy

Chemical precision, structural control, and biocompatibility are critical aspects to consider in the synthesis of biodegradable, electroactive CP-based composites. Condensation polymerization is the cornerstone for block copolymers with controlled degradation. Huang *et al.*[44] synthesized polylactide-block-aniline pentamer-block-polylactide by condensing polylactide diols with aniline pentamer through carbodiimide coupling, yielding a triblock structure with microphase separation and conductivity of 5×10^{-6} siemens per centimeter. Similarly, Rivers *et al.*[54] employed a multi-step condensation sequence—trichloro acetylation, Vilsmeier-Haack formylation, Stetter reaction, Lawesson's thionation, hydrolysis, and adipoyl chloride linkage—to construct a pyrrole-thiophene-pyrrole trimer with ester-linked aliphatic chains, enabling enzymatic surface erosion. Electro spinning dominates nanofibrous scaffold fabrication. Subramanian *et al.*[42] dissolved

poly(lactic-co-glycolic acid) and poly(3-hexylthiophene) in chloroform/dimethylformamide, electrospinning aligned nanofibers under 15 kV to promote Schwann cell orientation. Jiang *et al.*[52] co-electro spun PCL/gelatin/carbon nanotube blends, achieving vascular grafts with native-like mechanics. High-voltage fields induce fiber alignment, enhancing conductivity pathways and cell guidance. Oxidative polymerization enables *in situ* growth of CPs on biodegradable templates. Da Silva *et al.*[55] polymerized PEDOT-copolymer-poly(D,L-lactide) using ammonium persulfate in aqueous media, forming a biodegradable, electroactive copolymer. Boutry *et al.*[47] used emulsion polymerization to coat PLLA/PCL with PPy, forming resistor–inductor–capacitor resonators. Ghaziof *et al.*[50] applied solvent casting with vacuum drying to integrate 1 wt% MWCNTs into PCL, improving conductivity for myocardial patches. These methods—condensation, electrospinning, oxidative/electrochemical polymerization, and emulsion/solvent processing—allow tunable conductivity, porosity, and degradation kinetics, making biodegradable CP-based composites versatile for tissue engineering, implants, and antibacterial therapy.

6. Mechanism of degradation

Degradation of biodegradable CP-based composites is a multistage process governed by chemical structure, environmental conditions, and biological activity. As shown in Figure 4, there are three primary mechanisms of degradation—namely hydrolytic degradation, enzymatic degradation, and surface erosion—each tailored to ensure controlled resorption, non-toxic byproducts, and preserved electroactivity during tissue integration. Hydrolytic degradation dominates polyester-based systems (PLLA, PCL, poly(lactic-co-glycolic acid), poly(D,L-lactide)).

Ester bonds in the polymer backbone undergo nucleophilic attack by water, leading to chain scission and formation of carboxylic acid and alcohol end groups. Huang *et al.*[44] reported polylactide-block-aniline pentamer-block-polylactide degrading through bulk hydrolysis of polylactide blocks, releasing lactic acid over 6–12 months. Subramanian *et al.*[42] observed poly(lactic-co-glycolic acid)/poly(3-hexylthiophene) nanofibers losing 50% mass in 30 days under phosphate-buffered saline immersion, with autocatalysis accelerating degradation as acidic byproducts accumulate. PCL-based implants exhibit slower hydrolysis (lasting 1–2 years), making them ideal for long-term vascular or myocardial support.[50,52] Hydrolysis is pH-, temperature-, and molecular weight-dependent, enabling tunable resorption rates. Enzymatic degradation is critical in polysaccharide-containing composites (chitosan, chitin, carboxymethyl chitosan), comprising 25% of entries. Lysozyme, chitinase, and chitosanase—abundant in human serum and wound exudate—cleave beta-1,4-glycosidic bonds, generating oligosaccharides. Xu *et al.*[43] demonstrated PEDOT/carboxymethyl chitosan hydrogels degrading faster in lysozyme-rich media than phosphate-buffered saline, with surface-limited erosion preserving

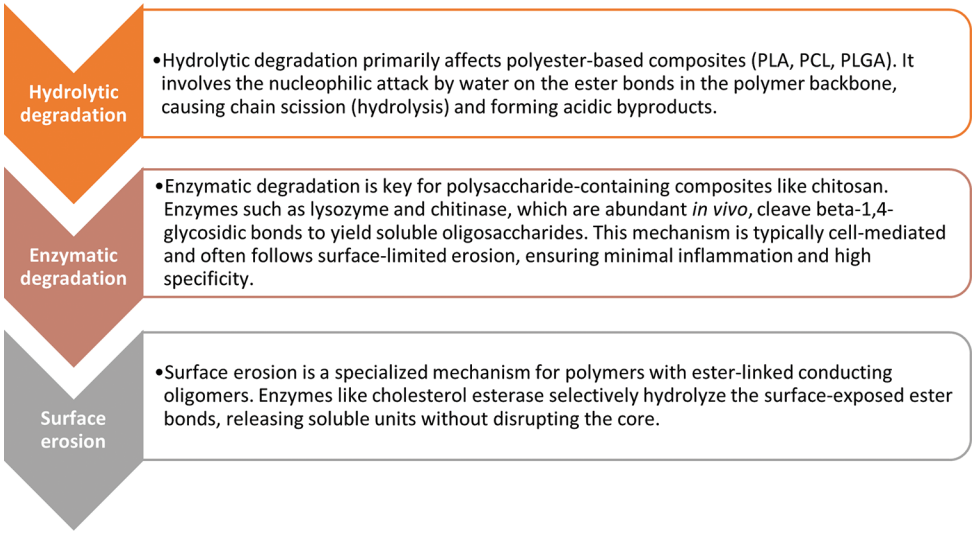

Figure 4. Principle mechanisms of degradation of conducting polymers

bulk conductivity. Enzymatic pathways are cell-mediated, ensuring *in vivo* specificity and minimal inflammation. Surface erosion, unique to CP oligomers, occurs in ester-linked systems like biodegradable electrically CP.[54] Cholesterol esterase selectively hydrolyzes surface-exposed ester linkages, releasing soluble monomers while maintaining core integrity. This mechanism yields zero-order kinetics, ideal for drug delivery or transient neural scaffolds, with conductivity retained until late-stage erosion. These mechanisms—hydrolytic (bulk/surface), enzymatic, and erosive—enable predictable, safe degradation, transforming biodegradable CP-based composites into transient, bioactive platforms for regenerative medicine. It is important to note that for biodegradable CPs, degradability is engineered through strategically placed hydrolyzable (e.g., ester, imine) or enzymatically cleavable (e.g., peptide, glycosidic) segments that preserve π-conjugation and charge mobility during the functional phase, enabling controlled fragmentation only on physiological or environmental triggers.[21,38,44] A fundamental challenge in designing functional biodegradable CPs is managing the inherent conflict between electrical performance and material biodegradability. Conductivity relies on a stable, continuous network of π-conjugated segments to facilitate charge transport. Biodegradability, however, requires controlled, bulk breakdown of the polymer backbone through hydrolyzable linkages. The universal observation is that conductivity is negatively impacted by biodegradation, though the performance can be sustained for a functional period. This makes biodegradable CPs inherently transient materials, whose electrical function must be strategically designed to outlast the duration of the biological application (e.g., nerve regeneration or cardiac repair) before the material fully dissolves. For instance, PAP triblock copolymer is achieved by ingeniously linking distinct functional segments, while their degradation capability stems from separate, chemically labile units.[44] The material's semiconducting performance (5×10^{-6} S/cm) is conferred by the π-conjugated backbone of the aniline pentamer oligomer, which, upon doping, forms mobile charge carriers, polarons and bipolarons, that facilitate electron hopping or tunneling for charge transport. Conversely, biodegradability is engineered through the polylactide segments containing hydrolyzable ester linkages. This morphology permits the polylactide to degrade via hydrolysis without immediately disrupting the conductive pathways, sustaining function during the necessary biological window. However, this is an inherently transient solution, as the inevitable progression of degradation—involving polymer swelling, dopant expulsion, and eventual chain fragmentation—ultimately severs the conjugation. This failure mechanism leads to a significant, unavoidable drop in conductivity (>50%).[44]

7. Comparative analysis of synthesis, degradation, and applications

To provide a comprehensive overview of the diverse biodegradable CP-based composites discussed in this review, Table 1 summarizes key attributes from some selected studies across tissue engineering, biomedical implants, and antibacterial applications. This table compiles essential parameters, including polymer/composite type, conducting component, dopant, synthesis method, degradation mechanism, conductivity, and primary application. Our tabulated data reveal that condensation polymerization and electrospinning are primary methods for synthesizing scaffolds requiring precise molecular control and nanofibrous alignment, respectively, while oxidative and emulsion techniques are predominantly employed in generating implant-focused hybrids for enhanced mechanical integration. Degradation profiles, primarily hydrolytic or enzymatic, ensure controlled release of non-toxic byproducts, aligning with clinical needs for transient devices.

8. Challenges and future directions

Despite their promise, CP-based biomedical devices face challenges in balancing conductivity with degradation rates. Rapid degradation can compromise functionality, while high conductivity often requires stable, non-degradable structures.[26,28] Scalability is another hurdle, as complex synthesis routes, such as those involving organic solvents, limit large-scale production.[27,30] The lack of standardized protocols for assessing biodegradability and biocompatibility across physiological and environmental conditions necessitates universal benchmarks.[26] In addition, achieving consistent mechanical properties, such as flexibility and tensile strength, remains critical for wearable and implantable devices.[32] Future research will focus on developing novel synthesis methods, such as solid-state polymerization, to enhance eco-friendliness and scalability.[30] Incorporating stimuli-responsive triggers (e.g., pH, light, or enzymes) will enable smarter, more precise devices.[28,33] Integration with advanced nanomaterials, like graphene or quantum dots, will further enhance conductivity and functionality.[26] Applications in transient electronics, smart drug delivery, and wearable sensors hold significant potential, particularly for personalized medicine and sustainable healthcare.[26,28] By addressing these challenges, biodegradable CPs will drive the development of next-generation biomedical technologies, combining high performance with environmental responsibility.

Table 1. Composition, synthesis methods, degradation mechanisms, electrical conductivity, and biomedical applications of biodegradable conducting polymers

Polymer or composite	Electricallyconductive component	Dopant	Synthesis method	Degradation mechanism	Electrical conductivity (S/cm)	Application	References
Pyrrole–thiophene–pyrrole trimer	Pyrrole–thiophene–pyrrole trimer	Iodine vapor	Multi-stepchemical condensation process	Enzymatic degradation by cholesterol esterase	10^{-4}	Neural tissue scaffold	54
Polylactide–aniline pentamer–polylactide block copolymer	Aniline pentamer	-	Condensation	Hydrolysis of polylactide chains	5×10^{-6}	Cardiac and brain tissue engineering	44
Poly (lactic-co-glycolic acid) and poly (3-hexylthiophene) nanofibers	Poly (3-hexylthiophene)	-	Electrospinningprocess	Hydrolysis of poly (lactic-co-glycolic acid)	-	Neural tissue regeneration	42
Electroactive polyurethane incorporating aniline pentamer	Aniline pentamer	-	Synthesis of electroactive polyurethane	Hydrolytic and enzymatic degradation	-	Cardiac and bone tissue engineering	45
Star-shaped polylactide network with aniline trimer	Aniline trimer	-	Formation of star-shaped polymer network	Controlled hydrolysis	-	Bone tissue engineering	46
3Dreducedgraphene oxide/PPy/hydroxyapatite composite scaffold	PPy	-	Room-temperature chemical fabrication	-	-	Bone tissue engineering	56
PPyand alginate hybrid hydrogel	PPy	-	Hybridhydrogel fabrication	Hydrolysis of alginate	-	Brain tissue engineering and human mesenchymal stem cell culture	57
PEDOT-co-poly (D, L-lactide) copolymer	PEDOT	Persulfate oxidizing agent	Oxidativepolymerization	Hydrolysis of poly (D, L-lactide)	-	Embryonicstem cell compatibility	55
PEDOT/carboxymethyl chitosan hydrogel	PEDOT	-	Composite hydrogel fabrication	Hydrolytic and enzymatic degradation	-	Neural tissue engineering	43
PANi–chitosanfunctionalizednanocomposite	PANi	-	N-hydroxysuccinimide modification and polymergrafting	Enzymatic degradation	-	Fibroblastapplications	58
PLLA-PPy and PCL-PPycomposites	PPy	-	Emulsion-based composite fabrication	Hydrolysis of PLLA or PCL	-	Bioelectronicresonatordevices	47
PPy/carbon nanotube composite film	PPy	-	Hybridchemical/electrodeposition fabrication	-	-	Neural interface electrodes	48
MWCNT-Reinforced Polycaprolactone Nanocomposite	MWCNTs	-	Solvent casting technique	Hydrolysis of polycaprolactone	Improved compared to pure polycaprolactone	Myocardialtissue engineering	50
PLL Acomposite bone screw with nano-sized iron oxide (magnetite)	Nano iron oxide (Fe_3O_4)	-	Composite bone screw fabrication	Hydrolysis of PLLA	-	Bone screw implant	51
3Dscaffold based on PEDOT: polystyrenesulfonate and MWCNTs	PEDOT: polystyrene sulfonate and MWCNTs	-	3Dcomposite scaffold fabrication	-	-	Biosensingapplications	59

(Cont'd...)

Table 1. ***(Continued)***

Polymer or composite	Electricallyconductive component	Dopant	Synthesis method	Degradation mechanism	Electrical conductivity (S/cm)	Application	References
Poly (3-hydroxybutyrate)/chitosan/ MWCNT electro spun scaffold	MWCNTs	-	Solution blending and electro spinning	Hydrolytic and enzymatic degradation	-	Cartilage tissue engineering	60
PPy/zinc oxide composite coating on biodegradable magnesiumalloy	PPy	-	Composite coating deposition	-	-	Orthopedicimplant coating	61

Abbreviations: MWCNT: Multi-walled carbon nanotubes; PANi: Polyaniline; PCL: Poly(ε-caprolactone); PEDOT: Poly (3,4-ethylenedioxythiophene); PLLA: Poly (L-lactic acid); PPy: Polypyrrole.

9. Conclusion

Biodegradable CPs represent a significant leap forward in the field of biomedical materials, offering a compelling solution to the long-standing challenges of permanent electronic implants and biomedical waste. This review highlights how these innovative materials uniquely combine electrical conductivity, biocompatibility, and controlled degradability to create a new generation of transient medical devices. In addition, the paper discusses the diverse and impactful applications of these materials, from biosensors for real-time health monitoring and electroactive scaffolds that enhance tissue regeneration, to neural interfaces that enable communication with the nervous system and smart systems for targeted drug delivery. The review also examines the synthesis and fabrication methods—including chemical oxidative, electrosynthesis, and solid–solid reactions—that allow for precise control over material properties, a critical factor for clinical success. Despite these remarkable advancements, significant hurdles remain. The key challenge lies in achieving an optimal balance between electrical performance and degradation rate so that the device functions effectively as required and then degrades safely. Issues related to scalability, standardization of testing protocols, and maintaining consistent mechanical properties also require further research. Looking ahead, the future of biodegradable CPs is incredibly promising. Continued innovation in stimuli-responsive degradation, the integration of advanced nanomaterials, and the development of more sustainable fabrication techniques will pave the way for a new era of personalized and eco-friendly medicine. By overcoming these challenges, biodegradable CPs are set to revolutionize healthcare by enabling devices that are not only high-performing but also fully integrated with the body's natural processes.

Acknowledgments

The authors would like to thank the Tunisian Ministry of Higher Education and Scientific Research for funding this research.

Funding

The authors gratefully acknowledge the financial support provided by the Ministry of Higher Education and Scientific Research of Tunisia (MESRS).

Conflict of interest

The authors declare no conflicts of interest.

Author contributions

Conceptualization: All authors
Visualization: Imene Bekri-Abbes

Writing–original draft: All authors
Writing–review & editing: All authors

Ethics approval and consent to participate

Not applicable.

Consent for publication

Not applicable.

Availability of data

Not applicable.

References

1. Scott C. History of conductive polymers. In: *Nanostructured Conductive Polymers*. Chichester: John Wiley and Sons; 2010. p. 1-34.

   doi: 10.1002/9780470661338.ch1

2. Kenry, Liu B. Recent advances in biodegradable conducting polymers and their biomedical applications. *Biomacromolecules*. 2018;19(6):1783-1799.

   doi: 10.1021/acs.biomac.8b00275

3. Khan T, Vadivel G, Ramasamy B, Murugesan G, Sebaey TA. Biodegradable conducting polymer-based composites for biomedical applications-a review. *Polymers (Basel)*. 2024;16(11):1533.

   doi: 10.3390/polym16111533

4. Hasan MB, Parvez MM, Abir AY, Ahmad MF. A review on conducting organic polymers: Concepts, applications, and potential environmental benefits. *Heliyon*. 2025;11(3):e42375.

   doi: 10.1016/j.heliyon.2025.e42375

5. Nezakati T, Seifalian A, Tan A, Seifalian AM. Conductive polymers: Opportunities and challenges in biomedical applications. *Chem Rev*. 2018;118(14):6766-6784.

   doi: 10.1021/acs.chemrev.6b00275

6. Namsheer K, Rout CS. Conducting polymers: A comprehensive review on recent advances in synthesis, properties and applications. *RSC Adv*. 2021;11(10):5659-5691.

   doi: 10.1039/d0ra07800j

7. Le CV, Yoon H. Advances in the use of conducting polymers for healthcare monitoring. *Int J Mol Sci*. 2024;25(3):1564.

   doi: 10.3390/ijms25031564.10.3390/ijms25031564

8. Tadesse MG, Ahmmed AS, Lübben JF. Review on conductive polymer composites for supercapacitor applications. *J Compos Sci*. 2024;8(2):53.

   doi: 10.3390/jcs8020053

9. Bednarczyk K, Matysiak W, Tański T, Janeczek H, Schab-Balcerzak E, Libera M. Effect of polyaniline content and protonating dopants on electroconductive composites. *Sci Rep*. 2021;11(1):7487.

   doi: 10.1038/s41598-021-86950-4

10. Arora EK, Sharma V, Ravi A, *et al*. Polyaniline-based ink for inkjet printing for supercapacitors, sensors, and electrochromic devices. *Energies*. 2023;16(18):6716.

    doi: 10.3390/en16186716

11. Kaushik P, Bharti R, Sharma R, Verma M, Olsson RT, Pandey A. Progress in synthesis and applications of polyaniline-coated nanocomposites: A comprehensive review. *Eur Polym J*. 2024;221:113574.

    doi: 10.1016/j.eurpolymj.2024.113574

12. Zidi R, Bekri-Abbes I, Sdiri N, Vimalanandan A, Rohwerder M, Srasra E. Electrical and dielectric investigation of intercalated polypyrrole-montmorillonite nanocomposite prepared by spontaneous polymerization. *Mater Sci Eng B*. 2016;212:14-23.

    doi: 10.1016/j.mseb.2016.07.006

13. Li C, Bai H, Shi G. Conducting polymer nanomaterials: Electrosynthesis and applications. *Chem Soc Rev*. 2009;38(8):2417-2427.

    doi: 10.1039/b816681c

14. Bekri-Abbes IB, Srasra E. Characterization and AC conductivity of polyaniline-montmorillonite nanocomposites synthesized by mechanical/chemical reaction. *React Funct Polym*. 2010;70(1):11-18.

    doi: 10.1016/j.reactfunctpolym.2009.09.008

15. Bekri-Abbes I, Srasra E. Effect of mechanochemical treatment on structure and electrical properties of montmorillonite. *J Alloys Compd*. 2016;671:34-42.

    doi: 10.1016/j.jallcom.2016.02.048

16. Bekri-Abbes I, Srasra E. Solid-State synthesis and electrical properties of polyaniline/Cu-montmorillonite nanocomposite. *Mater Res Bull*. 2010;45(12):1941-1947.

    doi: 10.1016/j.materresbull.2010.08.012

17. Bekri-Abbes I, Srasra E. Investigation of structure and conductivity properties of polyaniline synthesized by solid-solid reaction. *J Polym Res*. 2011;18(4):659-665.

    doi: 10.1007/s10965-010-9461-x

18. Bekri-Abbes I, Srasra E. Solid phase mechanochemical synthesis of polyaniline-montmorillonite nanocomposite using grinded montmorillonite as oxidant. *Mater Sci Semicond Process*. 2016;56:76-82.

    doi: 10.1016/j.mssp.2016.07.020

19. Gu JD, Wu EK. Biodegradability of synthetic plastics and polymeric materials: An illusion or reality in waste managements? *Appl Environ Biotechnol*. 2020;5(2):9-27.

doi: 10.26789/AEB.2020.02.003

20. ASTM International. *ASTM D6691-24a: Standard Test Method for Determining Aerobic Biodegradation of Plastic Materials in the Marine Environment*. West Conshohocken, PA: ASTM International; 2024.

21. Kuperkar K, Atanase LI, Bahadur A, Crivei IC, Bahadur P. Degradable polymeric bio(nano)materials and their biomedical applications: A comprehensive overview and recent updates. *Polymers (Basel)*. 2024;16(2):206.

doi: 10.3390/polym16020206

22. Jia X, Ma X, Zhao L, *et al*. A biocompatible and fully erodible conducting polymer enables implanted rechargeable Zn batteries. *Chem Sci*. 2023;14(9):2123-2130.

doi: 10.1039/d2sc06342e

23. Guo B, Finne-Wistrand A, Albertsson AC. Enhanced electrical conductivity by macromolecular architecture: Hyperbranched electroactive and degradable block copolymers based on poly(ε-caprolactone) and aniline pentamer. *Macromolecules*. 2010;43(10):4472-4480.

doi: 10.1021/ma100530k

24. Gupta S, Datt R, Mishra A, Tsoi WC, Patra A, Bober P. Poly(3,4-ethylenedioxythiophene):Poly(styrene sulfonate) in antibacterial, tissue engineering and biosensors applications: Progress, challenges and perspectives. *J Appl Polym Sci*. 2022;139(30):e52663.

doi: 10.1002/app.52663

25. Najar Benahmed W, Bekri-Abbes I, Srasra E. Spectroscopic study of polyaniline/AgCl@Ag nanocomposites prepared by a one-step method. *J Spectrosc*. 2017;2017:3514216.

doi: 10.1155/2018/7320654

26. Irimia-Vladu M. "Green" electronics: Biodegradable and biocompatible materials and devices for sustainable future. *Chem Soc Rev*. 2014;43(2):588-610.

doi: 10.1039/C3CS60235D

27. Keate RL, Bury MI, Mendez-Santos M, *et al*. Cell-free biodegradable electroactive scaffold for urinary bladder tissue regeneration. *Nat Commun*. 2025;16(1):11.

doi: 10.1038/s41467-024-55401-9

28. Chen TY, Xu J, Tai CH, Wen TK, Hsu SH. Biodegradable, electroconductive self-healing hydrogel based on polydopamine-coated polyurethane nano-crosslinker for Parkinson's disease therapy. *Biomaterials*. 2025;320:123268.

doi: 10.1016/j.biomaterials.2025.123268

29. Xu C, Yepez G, Wei Z, Bugarin A, Hong Y. Synthesis and characterization of conductive, biodegradable, elastomeric polyurethanes for biomedical applications. *J Biomed Mater Res A*. 2016;104(9):2305-2314.

doi: 10.1002/jbm.a.35765

30. Nazarzadeh Zare E, Mansour Lakouraj M, Mohseni M. Biodegradable polypyrrole/dextrin conductive nanocomposite: Synthesis, characterization, antioxidant and antibacterial activity. *Synth Met*. 2014;187:9-16.

doi: 10.1016/j.synthmet.2013.09.045

31. Huang J, Hu X, Lu L, Zhang Q, Luo Z. Electrical regulation of Schwann cells using conductive polypyrrole/chitosan polymers. *J Biomed Mater Res A*. 2010;93(1):164-174.

doi: 10.1002/jbm.a.32511

32. Golubchikov DO, Petrov AK, Popkov VA, Evdokimov PV, Putlayev VI. Recent advances on 3D-printed PCL-based composite scaffolds for bone tissue engineering. *ACS Biomater Sci Eng*. 2025;11(6):3201-3327.

doi: 10.3389/fbioe.2023.1168504

33. Ganguly K, Randhawa A, Dutta SD, *et al*. Ultrathin, stimuli-responsive, antimicrobial, self-cleaning, reusable, and biodegradable, micro/nanofibrous electrospun mat as an efficient face mask filter for airborne disease prevention. *Nano Lett*. 2025;25(19):7641-7650.

doi: 10.1021/acs.nanolett.4c04525

34. Zhang X, Liu B, Gao J, *et al*. Liquid metal-based electrode array for neural signal recording. *Bioengineering (Basel)*. 2023;10(5):578.

doi: 10.3390/bioengineering10050578

35. Zhang Q, Yan Y, Li S, Feng T. The synthesis and characterization of a novel biodegradable and electroactive polyphosphazene for nerve regeneration. *Mater Sci Eng C Mater Biol Appl*. 2010;30(1):160-166.

doi: 10.1016/j.msec.2009.09.013

36. Hu K, Huang D, Jiang H, *et al*. Toughening biosourced poly(lactic acid) and poly(3-hydroxybutyrate-co-4-hydroxybutyrate) blends by a renewable poly(epichlorohydrin-co-ethylene oxide) elastomer. *ACS Omega*. 2019;4(22):19777-19786.

doi: 10.1021/acsomega.9b02639

37. McCarthy A, John JV, Saldana L, *et al*. Electrostatic flocking of insulative and biodegradable polymer microfibers for biomedical applications. *Adv Healthc Mater*. 2021;10(19):2100766.

doi: 10.1002/adhm.202100766

38. Domagala A, Maksymiak M, Janeczek H, *et al*. Oligo-3-hydroxybutyrate functionalised pyrroles for preparation of biodegradable conductive polymers. *J Mater Sci*. 2014;49(14):5227-5236.

doi: 10.1007/s10853-014-8241-0

39. Chowdhury P, Lincon A, Bhowmik S, *et al*. Biodegradable solid polymer electrolytes from the discarded cataractous eye protein isolate. *ACS Appl Bio Mater*. 2024;7(4):2240-2253.

doi: 10.1021/acsabm.3c01229

40. Cafiero L, Oliviero M, Landi G, *et al*. Preparation and characterization of conductive foams based on PBS, carbon nanofibers and expanded graphite nanocomposites. *AIP Conf Proc*. 2017;1914:060006.

doi: 10.1063/1.5016726

41. Guimard NK, Sessler JL, Schmidt CE. Design of a novel electrically conducting biocompatible polymer with degradable linkages for biomedical applications. *RS Symp Proc*. 2006;950:99-104.

doi: 10.1557/PROC-0950-D09-08

42. Subramanian A, Krishnan UM, Sethuraman S. Axially aligned electrically conducting biodegradable nanofibers for neural regeneration. *J Mater Sci Mater Med*. 2012;23:1797-1809.

doi: 10.1007/s10856-012-4654-y

43. Xu C, Guan S, Wang S, *et al*. Biodegradable and electroconductive poly(3,4-ethylenedioxythiophene)/ carboxymethyl chitosan hydrogels for neural tissue engineering. *Mater Sci Eng C Mater Biol Appl*. 2018;84:32-43.

doi: 10.1016/j.msec.2017.11.032

44. Huang L, Hu J, Lang L, *et al*. Synthesis and characterization of electroactive and biodegradable ABA block copolymer of polylactide and aniline pentamer. *Biomaterials*. 2007;28(9):1741-1751.

doi: 10.1016/j.biomaterials.2006.12.007

45. Baheiraei N, Yeganeh H, Ai J, Gharibi R, Azami M, Faghihi F. Synthesis, characterization and antioxidant activity of a novel electroactive and biodegradable polyurethane for cardiac tissue engineering application. *Mater Sci Eng C Mater Biol Appl*. 2014;44:24-37.

doi: 10.1016/j.msec.2014.07.061

46. Xie M, Wang L, Ge J, Guo B, Ma PX. Strong electroactive biodegradable shape memory polymer networks based on star-shaped polylactide and aniline trimer for bone tissue engineering. *ACS Appl Mater Interfaces*. 2015;7:6772-6781.

doi: 10.1021/acsami.5b00191

47. Boutry CM, Sun W, Strunz T, Chandrahalim H, Hierold C. Development and Characterization of Biodegradable Conductive Polymers for the Next Generation of RF Bio-Resonators. In: *Proceedings of the IEEE International Frequency Control Symposium*; 2010. p. 1-4.

doi: 10.1109/FREQ.2010.5556332

48. Lu Y, Li T, Zhao X, *et al*. Electrodeposited polypyrrole/ carbon nanotubes composite films electrodes for neural interfaces. *Biomaterials*. 2010;31:5169-5181.

doi: 10.1016/j.biomaterials.2010.03.022

49. Wan P, Yuan C, Tan L, Li Q, Yang K. Fabrication and evaluation of bioresorbable PLLA/magnesium and PLLA/magnesium fluoride hybrid composites for orthopedic implants. *Compos Sci Technol*. 2014;98:36-43.

doi: 10.1016/j.compscitech.2014.04.011

50. Ghaziof S, Mehdikhani-Nahrkhalaji M. Preparation, characterization, mechanical properties and electrical conductivity assessment of novel polycaprolactone/multi-wall carbon nanotubes nanocomposites for myocardial tissue engineering. *Acta Phys Pol A*. 2017;131:428-431.

doi: 10.12693/APhysPolA.131.428

51. Wang H, Chiang P, Tzeng J, *et al*. *In vitro* biocompatibility, radiopacity, and physical property tests of nano-Fe3O4 incorporated poly-l-lactide bone screws. *Polymers*. 2017;9:191.

doi: 10.3390/polym9060191

52. Jiang C, Wang K, Liu Y, Zhang C, Wang B. Using wet electrospun PCL/gelatin/CNT yarns to fabricate textile-based scaffolds for vascular tissue engineering. *ACS Biomater Sci Eng*. 2021;7:2627-2637.

doi: 10.1021/acsbiomaterials.1c00097

53. Sumitha MS, Shalumon KT, Sreeja VN, Jayakumar R, Nair SV, Menon D. Biocompatible and antibacterial nanofibrous poly(∈-caprolactone)-nanosilver composite scaffolds for tissue engineering applications. *J Macromol Sci A*. 2012;49:131-138.

doi: 10.1080/10601325.2012.642208

54. Rivers TJ, Hudson TW, Schmidt CE. Synthesis of a novel biodegradable electrically conducting polymer for biomedical applications. *Adv Funct Mater*. 2002;12(1):33-37.

doi: 10.1002/1616-3028(20020101)12:1<33:AID-ADFM33>3.0.CO;2-E

55. Da Silva ACB, Semeano ATS, Dourado AHB, Ulrich H, Cordoba De Torresi SI. Novel conducting and biodegradable copolymers with noncytotoxic properties toward embryonic stem cells. *ACS Omega*. 2018;3:5593-5604.

doi: 10.1021/acsomega.8b00510

56. Song F, Jie W, Zhang T, *et al*. Room-temperature fabrication of a three-dimensional reduced-graphene oxide/ polypyrrole/hydroxyapatite composite scaffold for bone tissue engineering. *RSC Adv*. 2016;6:92804-92812.

doi: 10.1039/C6RA15267H

57. Yang S, Jang L, Kim S, *et al*. Polypyrrole/alginate hybrid hydrogels: Electrically conductive and soft biomaterials for human mesenchymal stem cell culture and potential neural tissue engineering applications. *Macromol Biosci*. 2016;16:1653-1661.

doi: 10.1002/mabi.201600148

58. Borah R, Upadhyay J, Acharjya K. Functionalized polyaniline: chitosan nanocomposites as a potential biomaterial. *Mater Today Proc*. 2020;32:334-343.

doi: 10.1016/j.matpr.2020.01.583

59. Jayaram AK, Pitsalidis C, Tan E, *et al*. 3D hybrid scaffolds based on PEDOT: PSS/MWCNT composites. *Front Chem*. 2019;7:363.

doi: 10.3389/fchem.2019.00363

60. Mohammad Alizadeh Z, Karbasi S, Arasteh S. Physical, mechanical and biological evaluation of poly (3-hydroxybutyrate)-chitosan/MWNTs as a novel electrospun scaffold for cartilage tissue engineering applications. *Polym Plast Technol Mater*. 2020;59:417-429.

doi: 10.1080/25740881.2019.1647244

61. Guo Y, Jia S, Qiao L, *et al*. A multifunctional polypyrrole/zinc oxide composite coating on biodegradable magnesium alloys for orthopedic implants. *Colloids Surf B Biointerfaces*. 2020;194:111186.

doi: 10.1016/j.colsurfb.2020.111186

ACCSCIENCE PUBLISHING

Explora: Environment and Resource

ORIGINAL RESEARCH ARTICLE

Analysis of thermal effects on sediment grain escape velocity under combined cohesive and viscous forces using the truncated pyramid model

Arijit Dutta[1†] and Sanchayan Mukherjee[2†*]

[1]Department of Mechanical Engineering, Faculty of Engineering, Alipurduar Government Engineering and Management College, Alipurduar, West Bengal, India

[2]Department of Mechanical Engineering, Faculty of Engineering, Kalyani Government Engineering College, Kalyani, West Bengal, India

Abstract

A sediment grain on a riverside is surrounded by similar grains and is subjected to both cohesive and viscous forces. The present study considers the orientation of sediment grains based on the established truncated pyramid model and proposes an expression for the grain's escape velocity. The escape velocity depends strongly on the inter-grain separation gap and temperature for a given water volume entrapped between two neighboring grains. This serves as a key measure of the volumetric erosion rate. A thorough comparative study was conducted, linking the escape velocity values reported in published work—where only cohesive forces were considered—with results obtained when both viscous and cohesive forces were accounted for under varying thermal conditions. Both scenarios were evaluated at a fixed liquid bridge volume and at different separation gaps, while all other parameters were kept constant. The findings revealed that the escape velocity increased relative to that reported in earlier research. In this study, the combined effect of viscous and cohesive forces results in a significant increase in the escape velocity required for a grain, indicating enhanced stability of the riverside compared to cases where only cohesive forces are considered at lower separation times. For the 1st time, temperature dependency is incorporated in the truncated pyramid model. In addition, a one-second threshold was identified, after which viscous forces and temperature no longer significantly affect grain binding.

Keywords: Separation gap; Sediment grain; Cohesive force; Escape velocity; Viscous force; Temperature

†*These authors contributed equally to this work.*

***Corresponding author:**
Sanchayan Mukherjee
(sanchayan.mukherjee@kgec.edu.in)

Citation: Dutta A, Mukherjee S. Analysis of thermal effects on sediment grain escape velocity under combined cohesive and viscous forces using the truncated pyramid model. *Explora Environ Resour*. 2025;2(4):025290055. doi: 10.36922/EER025290055

Received: July 17, 2025

1st revised: September 3, 2025

2nd revised: September 22, 2025

Accepted: September 23, 2025

Published online: October 27, 2025

1. Introduction

Riverside erosion rates are considerably lower in stable river systems compared to unstable ones. Each grain on a riverside is surrounded by similar grains, held together by gravitational, viscous, and cohesive forces. Gravitational force is the primary driver of sediment grain deposition along a riverside surface, while viscous and cohesive forces between grains act to counter erosion. When the deposition rate of grains is lower than the entrainment rate, erosion occurs. Analyzing erosion mechanisms at the microscale

is challenging due to inherent variability. However, certain analyses can be conducted to examine sediment grain behavior.

Bank erosion can be quantified by determining the escape velocity of the sediment grains. A smaller escape velocity indicates a higher erosion rate. The escape velocity is directly related to the net force exerted by streamflow along the riverside. To date, the literature does not adequately address changes in both viscous and cohesive forces between sediment grains under distinct microscale conditions. In particular, the variation of viscosity with temperature is often overlooked, despite the fact that the temperature of entrapped water cannot remain constant. In this study, escape velocity is calculated by incorporating both viscous and cohesive forces, with viscosity treated as a function of temperature, across varying inter-grain separation gaps and at a fixed liquid bridge volume.

Darby and Thorne[1] analyzed the stability of riversides for shear-driven cohesive banks that fail under planar failure conditions. Urso *et al.*[2] proposed a model to identify the rupture behavior of liquid bridges in grain systems. In addition, several studies[3-5] investigated liquid bridge systems. Yu *et al.*[6] experimentally determined the relationship between porosity and capillary force for mono-size spheres. Groger *et al.*[7] proposed a simulation model to calculate the tensile strain of sediment grains. Hsiau and Yang[8] employed the discrete element method to analyze motion arising from self-diffusion and mixing of cohesive powders in a two-dimensional vibrating granular bed. Rinaldi *et al.*[9] examined the stability of the Sieve riverside by monitoring pore water pressure. Kohonen *et al.*[10] conducted experiments on dynamically deformed wet grains.

Considering equilibrium conditions, Duan[11] analyzed the forces to determine the escape velocity of grains along a riverside. The principal acting forces on a grain are the lift force, the cohesive force between grains, and the submerged weight of the grain. Kotoky *et al.*[12] investigated Brahmaputra riverside erosion. Soulie *et al.*[13] observed the behavior of wet grains under cohesive forces acting at the macro level. Zhang and Li[14] performed a simulation study to observe the dynamic behavior of cohesive soils. Darby and Thorne[15] estimated the tension crack zone in riverside erosion. Mu and Su[16] derived resultant force expressions for liquid bridges between grains. Achite and Oullion[17] investigated grain transport phenomena in watersheds. Cai and Bhushan[18] performed a detailed numerical analysis of viscous and meniscus forces on hydrophobic and hydrophilic surfaces. During this period, several researchers[19,20] developed mathematical models to forecast soil erosion along riversides.

Mukherjee and Mazumdar[21] developed the truncated pyramid model for the arrangement of sediment grains along riversides. They proposed an extensive equation for sediment grain acceleration and escape velocity, demonstrating that this velocity is strongly linked to inter-grain gap and the amount of interstitial water. Al-Shemmeri[22] established a relationship between the dynamic viscosity of water and environmental temperature, indicating that dynamic viscosity exhibits a non-linear relationship with temperature. Chen *et al.*[23] developed a mathematical framework to analyze the delayed failure of unsaturated soil elements subjected to saturation, where the stability conditions of saturated viscous soils were considered. Similarly, Chen and Buscarnera[24] investigated unsaturated porous media through an analytical approach. Zhanlin and Fengxi[25] examined Bingham slurry and explored its diffusion in porous media using seepage theory, with their findings aligning with the transition to a saturated state.

In addition, several researchers[26-28] examined the viscous behavior of unsaturated soils using both experimental and analytical approaches. Biswas *et al.*[29] developed a model to study the rise and fall of water levels associated with planar failure of riverside blocks. An *et al.*[30] evaluated the effect of temperature on the channel gap of electronic devices and identified the optimal gap between the channel and drain metals for thermal performance. Szabo *et al.*[31] discussed water management in detail in their book, where they clearly explained changes in sediment transport parameters, such as shear stress, with variations in discharge. Yang *et al.*[32] developed a theoretical model to explain the dependence of nanofluid viscosity on different physical parameters, primarily temperature. They demonstrated that this model provides more accurate predictive results than many well-known empirical correlations.

In most published studies, the effects of viscous force, cohesive force, or temperature were considered separately. However, in reality, these effects coexist. Therefore, a microscale analysis that combines all of these effects is essential. In this study, the nature of sediment transport under different conditions is analyzed across multiple parameters, and the resulting escape velocity is used to quantify erosion rate.

The viscous force model proposed by Zhang and Li[14] and the cohesive force model suggested by Soulie *et al.*[13] were applied within the truncated pyramid model developed by Mukherjee and Mazumdar.[21] The expression for the variation of dynamic viscosity with temperature, as given by Al-Shemmeri,[22] was incorporated. The present work provides a comprehensive prediction of sediment grain behavior under the combined influence of cohesive and temperature-dependent viscous forces.

2. Methodology

2.1. Force analysis

A liquid bridge formed between two adjacent sediment grains under conditions of low water content leads to cohesion. Cohesive force analysis is based on the assumed geometry of the water bridge. Soulie *et al.*[13] derived expressions for cohesive force in terms of geometric parameters and physical quantities. For a pair of neighboring grains with radii R_1 and R_2, and an inter-grain gap δ, the cohesive force is calculated according to Equation I:

$$F_s = \pi\sigma\sqrt{R_1R_2}\left[c + \exp\left\{a\left(\delta / R\right) + b\right\}\right] \quad (1)$$

where F_s is the cohesive force joining two neighboring grains (N); σ is the surface tension coefficient (N/m); a, b, and c are coefficients considered to be functions of the volume of entrapped water, V (V in nl); $\emptyset$ is the contact angle (radians), and $R = \max(R_1,R_2)$. The expressions for a, b, and c are given as:

$$a = -1.1(V/R^3)^{-0.53} \quad (2)$$

$$b = (-0.148\ln(V/R^3) - 0.96)\,\emptyset^2 - 0.0082\ln(V/R^3) + 0.48 \quad (3)$$

$$c = 0.0018\ln((V)/R^3) + 0.078 \quad (4)$$

At the liquid bridge zone, the viscosity forces acting between two grains can be decomposed into normal and tangential components. Zhang and Li[14] proposed that the vicious force is a function of both physical and geometric parameters. For a pair of side-by-side sediment grains with radii R_1 and R_2, and an inter-grain separation gap $\delta$the tangential and normal viscous forces are expressed as:

$$F_t = 6\pi\eta R^* v_t\,[(8/15)\{\ln(R^*/\delta)\} + 0.9588] \quad (5)$$

$$F_n = 6\pi\eta R^* v_n\,\{R^*/\delta\} \quad (6)$$

where $F_{n\ and}\ F_t$are the normal and tangential viscous force components between a pair of neighboring grains; η is the dynamic viscosity coefficient; v_t is the relative tangential velocity between neighboring grains; v_n is the relative normal velocity between neighboring grains; and R^* is given by:

$$R^* = (R_1R_2)/(R_1 + R_2) \quad (7)$$

In this study, the viscous force model proposed by Zhang and Li[14] and the cohesive force model proposed by Soulie *et al.*[13] were integrated into the truncated pyramid model developed by Mukherjee and Mazumdar.[21] The grain array in this model, along with an enlarged view of a grain pair connected by a liquid bridge, is shown in Figures 1 and 2, respectively.

Here, the tangential velocity between two adjacent grains, v_t, is defined as:

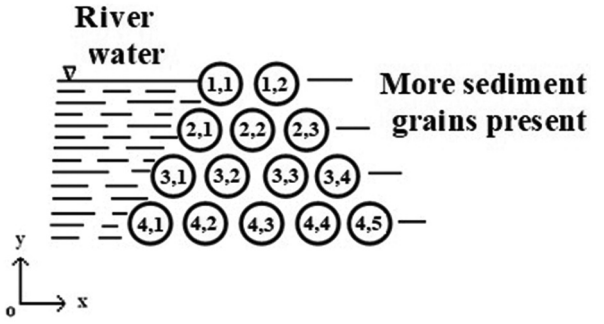

Figure 1. Sediment grain orientation in the truncated pyramid model, showing a trapezium-like arrangement that provides greater stability

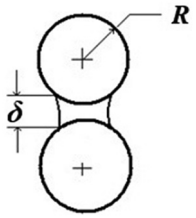

Figure 2. Representation of two neighboring grains connected by a liquid bridge with equal radii (R) and inter-grain separation distance (δ)

$$v_t = \delta/T_s \quad (8)$$

where T_s is the separation time required for a pair of adjacent grains, as proposed by Cai and Bhushan.[18]

The normal velocity between two adjacent grains, v_n, is formulated as:

$$v_n = (R_1 + R_2)/T_s \quad (9)$$

This relation arises from the fact that complete separation occurs when the total distance traversed along the normal direction equals $(R_1 + R_2)$.

Moreover, the dynamic viscosity coefficient, η, is considered to vary with environmental temperature T, as given by Al-Shemmeri:[22]

$$\eta = 2.414x10^{-5}\,x10^{\frac{247.8}{T-140}} \quad (10)$$

When temperature is given in Celsius, Equation 10 is expressed as:

$$\eta = 2.414x10^{-5}\,x10^{\frac{247.8}{T+133}} \quad (11)$$

2.2. Basic framework

Figure 1 depicts the arrangement of grains, while Figure 2 illustrates two neighboring grains. In this arrangement, each grain was placed atop two grains to ensure stability. The riverside configuration depends on grain size, inter-grain gap, and liquid bridge volume. Grains were assumed

to be spherical and materially homogeneous. The surface contact angle was taken as zero, considering pure water in the present analysis. Angles were determined by taking the radii of the three neighboring grains. In the truncated pyramid model, all spherical grains were assumed to have equal grain size (i.e., having equal radii, R). In addition, all grains were considered to be separated by an equal inter-grain distance. The truncated pyramid model exhibits a trapezium-like arrangement for greater stability and was therefore adopted.

2.3. Expression for the escape velocity

Figure 3 illustrates the forces acting on grains e and f. Here, f represents the x-direction coordinate and e represents the y-direction coordinate. F_s, F_t, and F_n indicate cohesive force, viscous tangential force, and viscous normal force between two neighboring grains, respectively. F_G is the weight of the submerged grain. When the equilibrium of a dynamic nature is considered, the minimum acceleration required to detach a grain from the riverside, known as the impending acceleration, can be determined for both the x- and y-components of acceleration. The velocity of the grain corresponding to this minimum acceleration, referred to as the escape velocity, is obtained from the impending acceleration itself. The mass of e, f is given as $4\pi R_{e,f}^3 \rho_s$, assuming each grain is a sphere, where ρ_s is the sediment grain material density.

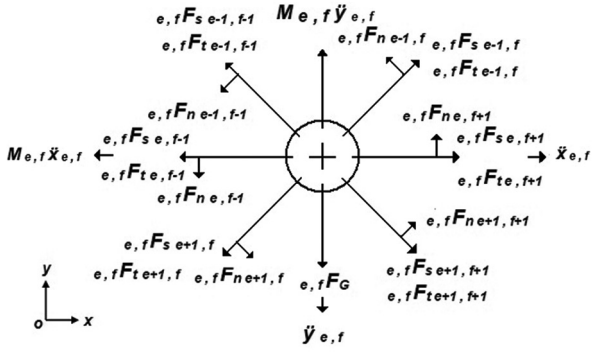

Figure 3. Force diagram of sediment grain (e,f) showing the interactions between the forces and their neighboring grains

The angles between the adjacent grains and the central grain, e, f, expressed in terms of their cosines and based on the radii of the three neighboring grains, are given as (**Equations 12-15** See Page no 6):

The impending acceleration along the x-direction is calculated as (**Equations 16-28** See Page no 6-7):

The impending acceleration along the y-direction is calculated as: (**Equations 29-47** See Page no 7-10):

In addition, g denotes gravitational acceleration and ρ indicates water density.

The resulting impending acceleration of sediment grain e, f is expressed as:

$$f_{e,f} = \left(\ddot{x}_{e,f}^2 + \ddot{y}_{e,f}^2\right)^{0.5} \quad (48)$$

According to Duan,[11] the sediment grain e,f is considered entrained when it is lifted by a gap equal to its diameter. From the law of conservation of linear momentum, the escape velocity of the sediment grain e, f is given by:

$$V_{escape\ e,f} = (2R_{e,f} f_{e,f})^{0.5} \quad (49)$$

The escape velocity is a function of the entrainment rate. For specific cases, volumetric bank erosion may be derived by determining the entrainment rate of grains, the deposition rate of grains, and porosity. According to Duan,[11] from available field data, the entrainment rate of grains, deposition rate of grains, and porosity can be obtained. Considering already established relationships of these parameters with escape velocity, the volumetric erosion rate can be quantified under cohesive and viscous forces.

3. Results and discussion

Mukherjee and Mazumdar[21] derived the escape velocity of grains by considering only cohesive forces at the riverside (f = 1). They assumed all grains had an equal diameter of 0.0008 m. To determine the grain's escape velocity, they considered the following parameters:

(i) Liquid bridge volume, V = 20 nL.
(ii) Surface tension coefficient,σ = 0.073 N/m.
(iii) Contact angle,$\emptyset$ = 0 (assuming pure water for simplicity).
(iv) Water density, ρ = 1,000 kg/m^3.
(v) Grain material density, ρ_s = 2,650 kg/m^3.

Their findings were adopted in the present study to validate the escape velocity using the same input parameters.

Using the above parameters, the dynamic viscosity coefficient η was determined for water at temperatures ranging from 10°C to 40°C, expressed as a function of temperature. In addition, three separation times () were considered: 10^{-7} s, 10^{-4} s, and 1 s.

Tables 1 and 2 summarize the changes in escape velocity with respect to inter-grain separation gap, both for cohesion alone and for the combined effect of viscous and cohesive forces. For the viscous force, the thermal effect on escape velocity at a fixed separation gap was also examined for each separation time and liquid bridge volume.

Figures 4-6 depict the changes in grain escape velocity with varying inter-grain separation gaps, considering either cohesive force alone or the combination of viscous

Table 1. Escape velocity at a separation time of 10^{-7} s for 20 nL liquid bridge volume

Separation gap (m)	Escape velocity due to cohesive force (m/s)	Escape velocity due to cohesive and viscous force (m/s) at different temperatures						
		10°C	15°C	20°C	25°C	30°C	35°C	40°C
0.000145	0.3944	10.2200	9.5539	8.9707	8.4568	8.0012	7.5951	7.2314
0.000150	0.3899	10.0451	9.3905	8.8173	8.3121	7.8643	7.4652	7.1078
0.000155	0.3855	9.8789	9.2351	8.6714	8.1746	7.7342	7.3417	6.9902
0.000160	0.3812	9.7207	9.0872	8.5325	8.0437	7.6103	7.2242	6.8782
0.000165	0.3769	9.5698	8.9462	8.4001	7.9188	7.4923	7.1121	6.7715
0.000170	0.3727	9.4258	8.8116	8.2737	7.7997	7.3796	7.0051	6.6697

Table 2. Escape velocity at a separation time of 10^{-4} s for 20 nL liquid bridge volume

Separation gap (m)	Escape velocity due to cohesive force (m/s)	Escape velocity due to cohesive and viscous force (m/s) for different temperatures						
		10°C	15°C	20°C	25°C	30°C	35°C	40°C
0.000145	0.3944	0.4396	0.4309	0.4242	0.4191	0.4150	0.4118	0.4092
0.000150	0.3899	0.4344	0.4259	0.4194	0.4143	0.4103	0.4072	0.4047
0.000155	0.3855	0.4293	0.4210	0.4146	0.4097	0.4058	0.4027	0.4002
0.000160	0.3812	0.4244	0.4163	0.4100	0.4052	0.4013	0.3983	0.3959
0.000165	0.3769	0.4197	0.4117	0.4056	0.4008	0.3970	0.3940	0.3916
0.000170	0.3727	0.4151	0.4073	0.4012	0.3965	0.3927	0.3898	0.3874

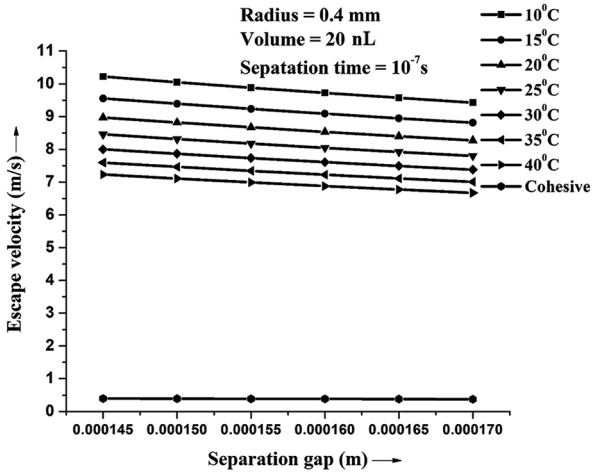

Figure 4. Escape velocity versus inter-grain separation gap at a separation time of 10^{-7} s and 20 nL liquid bridge volume

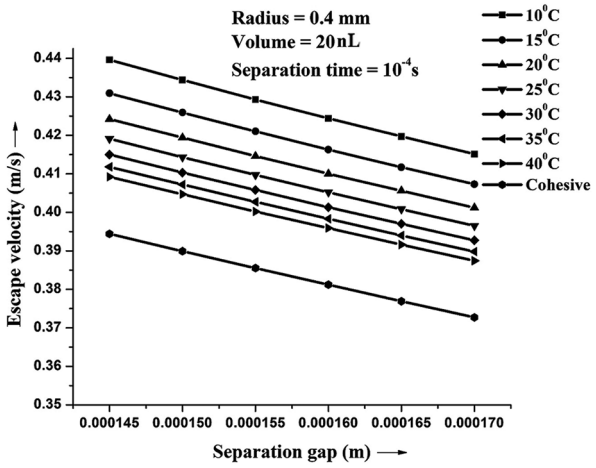

Figure 5. Escape velocity versus inter-grain separation gap at a separation time of 10^{-4} s and 20 nL liquid bridge volume

and cohesive forces, under different temperatures and separation times, for a constant bridge volume of 20 nL.

Figures 4-6 illustrate that the escape velocity requirement decreases as the inter-grain separation gap increases. The results indicate that at larger separation gaps, significantly lower escape velocity is required for the separation of a sediment grain from the bank. In addition, as temperature increases from 10°C to 40°C, the escape velocity decreases at a given separation gap, separation time, and liquid bridge volume. This temperature rise results in a reduction in the dynamic viscosity coefficient and viscous force of the liquid due to the decrease in intermolecular cohesive force.

At a given liquid bridge volume (e.g., 20 nL), the escape velocity requirement considering both viscous and cohesive forces was significantly greater than that considering cohesive force alone at a separation time of 10^{-7} s, as suggested by Cai and Bhushan.[18] The escape velocity decreased with increasing separation time, taken

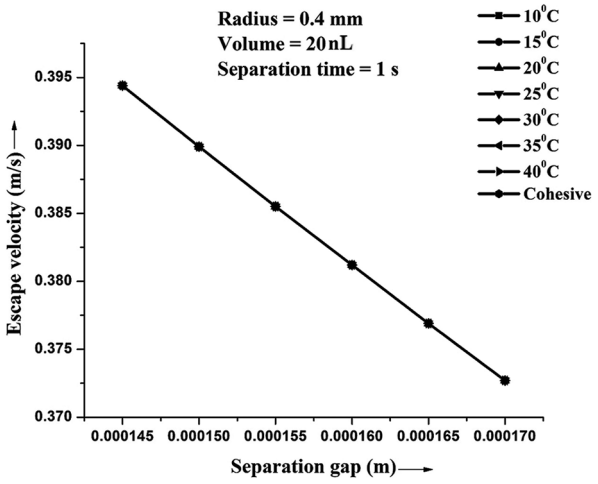

Figure 6. Escape velocity versus inter-grain separation gap at a separation time of 1 s and 20 nL liquid bridge volume

as 10^{-4} s and 1 s, at a fixed separation gap and temperature. Cai and Bhushan[18] demonstrated that the influence of viscosity at a particular liquid bridge persists only for short durations, such as a separation time of 10^{-7} s. Beyond this duration, the impact of viscosity diminishes, and the effect of cohesion increases. It was observed that at a separation time of 1 s, the effect of viscous force vanished, and the escape velocity values were identical to those obtained when considering cohesive force alone, as shown in Figure 6.

With the disappearance of viscous effects at 1 s, the effect of temperature on escape velocity also vanishes. As shown in Figure 6, all temperature-dependent curves overlap with the cohesion-only curve, appearing as a single curve. The escape velocity values were compared with the results reported by Mukherjee and Mazumdar[21] for a 20-nL liquid bridge (Tables 1 and 2). These findings

$$\cos\theta\left(e-1,f:e,f\right)=\left[\left\{\left(R_{e,f}+R_{e-1,f}\right)^2+\left(R_{e,f}+R_{e,f+1}\right)^2-\left(R_{e-1,f}+R_{e,f+1}\right)^2/\left\{2\left(R_{e,f}+R_{e-1,f}\right)\left(R_{e,f}+R_{e,f+1}\right)\right\}\right\}\right] \tag{12}$$

$$\cos\theta\left(e-1,f-1:e,f\right)=\left[\left\{\left(R_{e,f}+R_{e-1,f-1}\right)^2+\left(R_{e,f}+R_{e,f-1}\right)^2-\left(R_{e-1,f-1}+R_{e,f-1}\right)^2/\left\{2\left(R_{e,f}+R_{e-1,f-1}\right)\left(R_{e,f}+R_{e,f-1}\right)\right\}\right\}\right] \tag{13}$$

$$\cos\theta\left(e,f:e+1,f\right)=\left[\left\{\left(R_{e,f}+R_{e,f-1}\right)^2+\left(R_{e,f}+R_{e+1,f}\right)^2-\left(R_{e,f-1}+R_{e+1,f}\right)^2/\left\{2\left(R_{e,f}+R_{e,f-1}\right)\left(R_{e,f}+R_{e+1,f}\right)\right\}\right\}\right] \tag{14}$$

$$\cos\theta\left(e,f:e+1,f+1\right)=\left[\left\{\left(R_{e,f}+R_{e,f+1}\right)^2+\left(R_{e,f}+R_{e+1,f+1}\right)^2-\left(R_{e,f+1}+R_{e+1,f+1}\right)^2/\left\{2\left(R_{e,f}+R_{e,f+1}\right)\left(R_{e,f}+R_{e+1,f+1}\right)\right\}\right\}\right] \tag{15}$$

$$\ddot{x}_{e,f}=\left(3/4\pi R_{e,f}^3\rho_s\right)\left(F_{s1x}+F_{t1x}-F_{n1x}-F_{s2x}-F_{t2x}-F_{n2x}-F_{s3x}-F_{t3x}-F_{s4x}-F_{t4x}+F_{n4x}+F_{s5x}+F_{t5x}+F_{n5x}+F_{s6x}+F_{t6x}\right) \tag{16}$$

$$F_{s1x}=\pi\sigma\sqrt{R_{e,f}R_{e-1,f}}\left[c_{e,f}+\exp\left\{a_{e,f}\left(\delta/R_{e,f}\right)+b_{e,f}\right\}\right]\cos\theta\left(e-1,f:e,f\right) \tag{17}$$

where:

(i) F_{s1x} is the x-direction cohesive force between grains e, f, and $e-1, f$

$$F_{s2x}=\pi\sigma\sqrt{R_{e,f}R_{e-1,f-1}}\left[c_{e,f}+\exp\left\{a_{e,f}\left(\delta/R_{e,f}\right)+b_{e,f}\right\}\right]\cos\theta\left(e-1,f-1:e,f\right) \tag{18}$$

where:

(ii) F_{s2x} is the x-direction cohesive force between grains e, f, and $e-1, f-1$

$$F_{s3x}=\pi\sigma\sqrt{R_{e,f}R_{e,f-1}}\left[c_{e,f}+\exp\left\{a_{e,f}\left(\delta/R_{e,f}\right)+b_{e,f}\right\}\right] \tag{19}$$

where:

(iii) F_{s3x} is the x-direction cohesive force between grains e, f, and $e, f-1$

$$F_{s4x} = \pi\sigma\sqrt{R_{e,f}R_{e+1,f}}\left[c_{e+1,f} + \exp\left\{a_{e+1,f}\left(\delta / R_{e+1,f}\right) + b_{e+1,f}\right\}\right]\cos\theta\left(e,f:e+1,f\right) \quad (20)$$

where:
(iv) F_{s4x} is the x-direction cohesive force between grains $e, f,$ and $e+1, f$

$$F_{s5x} = \pi\sigma\sqrt{R_{e,f}R_{e+1,f+1}}\left[c_{e+1,f+1} + \exp\left\{a_{e+1,f+1}\left(\delta / R_{e+1,f+1}\right) + b_{e+1,f+1}\right\}\right]\cos\theta\left(e,f:e+1,f+1\right) \quad (21)$$

where:
(v) F_{s5x} is the x-direction cohesive force between grains $e, f,$ and $e+1, f+1$

$$F_{s6x} = \pi\sigma\sqrt{R_{e,f}R_{e,f+1}}\left[c_{e,f+1} + \exp\left\{a_{e,f+1}\left(\delta / R_{e,f+1}\right) + b_{e,f+1}\right\}\right] \quad (22)$$

where:
(vi) F_{s6x} is the x-direction cohesive force between grains $e, f,$ and $e, f+1$

$$F_{t1x} = 6\pi\eta\left\{\left(R_{e,f}R_{e-1,f}\right)/\left(R_{e,f} + R_{e-1,f}\right)\right\}\left(\delta / T_s\right)\left[\left(8/15\right)\left\{\ln\left(\left(R_{e,f}R_{e-1,f}\right)/\delta\left(R_{e,f} + R_{e-1,f}\right)\right)\right\} + 0.9588\right]\cos\theta\left(e-1,f:e,f\right) \quad (23)$$

where:
(vii) F_{t1x} is the x-direction tangential viscous force between grains $e, f,$ and $e-1, f$

$$F_{t2x} = 6\pi\eta\left\{\left(R_{e,f}R_{e-1,f-1}\right)/\left(R_{e,f} + R_{e-1,f-1}\right)\right\}\left(\delta / T_s\right)\left[\left(8/15\right)\left\{\ln\left(\left(R_{e,f}R_{e-1,f-1}\right)/\delta\left(R_{e,f} + R_{e-1,f-1}\right)\right)\right\} + 0.9588\right]\cos\theta\left(e-1,f-1:e,f\right) \quad (24)$$

where:
(viii) F_{t2x} is the x-direction tangential viscous force between grains $e, f,$ and $e-1, f-1$

$$F_{t3x} = 6\pi\eta\left\{\left(R_{e,f}R_{e,f-1}\right)/\left(R_{e,f} + R_{e,f-1}\right)\right\}\left(\delta / T_s\right)\left[\left(8/15\right)\left\{\ln\left(\left(R_{e,f}R_{e,f-1}\right)/\delta\left(R_{e,f} + R_{e,f-1}\right)\right)\right\} + 0.9588\right] \quad (25)$$

where:
(ix) F_{t3x} is the x-direction tangential viscous force between grains $e, f,$ and $e, f-1$

$$F_{t4x} = 6\pi\eta\left\{\left(R_{e,f}R_{e+1,f}\right)/\left(R_{e,f} + R_{e+1,f}\right)\right\}\left(\delta / T_s\right)\left[\left(8/15\right)\left\{\ln\left(\left(R_{e,f}R_{e+1,f}\right)/\delta\left(R_{e,f} + R_{e+1,f}\right)\right)\right\} + 0.9588\right]\cos\theta\left(e,f:e+1,f\right) \quad (26)$$

where:
(x) F_{t4x} is the x-direction tangential viscous force between grains $e, f,$ and $e+1, f$

$$F_{t5x} = 6\pi\eta\left\{\left(R_{e,f}R_{e+1,f+1}\right)/\left(R_{e,f} + R_{e+1,f+1}\right)\right\}\left(\delta / T_s\right)\left[\left(8/15\right)\left\{\ln\left(\left(R_{e,f}R_{e+1,f+1}\right)/\delta\left(R_{e,f} + R_{e+1,f+1}\right)\right)\right\} + 0.9588\right]\cos\theta\left(e,f:e+1,f+1\right) \quad (27)$$

where:
(xi) F_{t5x} is the x-direction tangential viscous force between grains $e, f,$ and $e+1, f+1$

$$F_{t6x} = 6\pi\eta\left\{\left(R_{e,f}R_{e,f+1}\right)/\left(R_{e,f} + R_{e,f+1}\right)\right\}\left(\delta / T_s\right)\left[\left(8/15\right)\left\{\ln\left(\left(R_{e,f}R_{e,f+1}\right)/\delta\left(R_{e,f} + R_{e,f+1}\right)\right)\right\} + 0.9588\right] \quad (28)$$

where:
(xii) F_{t6x} is the x-direction tangential viscous force between grains $e, f,$ and $e, f+1$

$$F_{n1x} = 6\pi\eta\left\{\left(R_{e,f}R_{e-1,f}\right)/\left(R_{e,f}+R_{e-1,f}\right)\right\}^2\left\{\left(R_{e,f}+R_{e-1,f}\right)/\left(T_s\delta\right)\right\}\left[1-\cos\theta\left(e-1,f:e,f\right)\right]^{0.5} \tag{29}$$

where:
(xiii)F_{n1x} is the x-direction normal viscous force between grains $e, f,$ and $e-1, f$

$$F_{n2x} = 6\pi\eta\left\{\left(R_{e,f}R_{e-1,f-1}\right)/\left(R_{e,f}+R_{e-1,f-1}\right)\right\}^2\left\{\left(R_{e,f}+R_{e-1,f-1}\right)/\left(T_s\delta\right)\right\}\left[1-\cos\theta\left(e-1,f-1:e,f\right)\right]^{0.5} \tag{30}$$

where:
(xiv)F_{n2x} is the x-direction normal viscous force between grains $e, f,$ and $e-1, f-1$

$$F_{n4x} = 6\pi\eta\left\{\left(R_{e,f}R_{e+1,f}\right)/\left(R_{e,f}+R_{e+1,f}\right)\right\}^2\left\{\left(R_{e,f}+R_{e+1,f}\right)/\left(T_s\delta\right)\right\}\left[1-\cos\theta\left(e,f:e+1,f\right)\right]^{0.5} \tag{31}$$

where:
(xv) F_{n4x} is the x-direction normal viscous force between grains $e, f,$ and $e+1, f$

$$F_{n5x} = 6\pi\eta\left\{\left(R_{e,f}R_{e+1,f+1}\right)/\left(R_{e,f}+R_{e+1,f+1}\right)\right\}^2\left\{\left(R_{e,f}+R_{e+1,f+1}\right)/\left(T_s\delta\right)\right\}\left[1-\cos\theta\left(e,f:e+1,f+1\right)\right]^{0.5} \tag{32}$$

where:
(xvi)F_{n5x} is the x-direction normal viscous force between grains $e, f,$ and $e+1, f+1$

$$\ddot{y}_{e,f} = \left(¾\pi R_{e,f}^3\,\rho_s\right)\left(-F_{s1y}-F_{t1y}-F_{n1y}-F_{s2y}-F_{t2y}+F_{n2y}+F_{n3y}+F_{s4y}+F_{t4y}+F_{n4y}+F_{s5y}+F_{t5y}-F_{n5y}-F_{n6y}\right)+g\left(1-\rho/\rho_s\right) \tag{33}$$

where:
The impending acceleration along the y-direction is calculated as

$$F_{s1y} = \pi\sigma\sqrt{R_{e,f}R_{e-1,f}}\left[c_{e,f}+\exp\left\{a_{e,f}\left(\delta/R_{e,f}\right)+b_{e,f}\right\}\right]\left[1-\cos\theta\left(e-1,f:e,f\right)\right]^{0.5} \tag{34}$$

where:
(i) F_{s1y} is the y-direction cohesive force between grains $e, f,$ and $e-1, f$

$$F_{s2y} = \pi\sigma\sqrt{R_{e,f}R_{e-1,f-1}}\left[c_{e,f}+\exp\left\{a_{e,f}\left(\delta/R_{e,f}\right)+b_{e,f}\right\}\right]\left[1-\cos\theta\left(e-1,f-1:e,f\right)\right]^{0.5} \tag{35}$$

where:
(ii) F_{s2y} is the y-direction cohesive force between grains $e, f,$ and $e-1, f-1$

$$F_{s4y} = \pi\sigma\sqrt{R_{e,f}R_{e+1,f}}\left[c_{e+1,f}+\exp\left\{a_{e+1,f}\left(\delta/R_{e+1,f}\right)+b_{e+1,f}\right\}\right]\left[1-\cos\theta\left(e,f:e+1,f\right)\right]^{0.5} \tag{36}$$

where:
(iii) F_{s4y} is the y-direction cohesive force between grains $e, f,$ and $e+1, f$

$$F_{s5y} = \pi\sigma\sqrt{R_{e,f}R_{e+1,f+1}}\left[c_{e+1,f+1}+\exp\left\{a_{e+1,f+1}\left(\delta/R_{e+1,f+1}\right)+b_{e+1,f+1}\right\}\right]\left[1-\cos\theta\left(e,f:e+1,f+1\right)\right]^{0.5} \tag{37}$$

where:
(iv) F_{s5y} is the y-direction cohesive force between grains $e, f,$ and $e+1, f+1$

$$F_{t1y}=6\pi\eta\left\{\left(R_{e,f}R_{e-1,f}\right)/\left(R_{e,f}+R_{e-1,f}\right)\right\}\left(\delta/T_s\right)\left[\left(8/15\right)\left\{\ln\left(\left(R_{e,f}R_{e-1,f}\right)/\delta\left(R_{e,f}+R_{e-1,f}\right)\right)\right\}+0.9588\right]\left[1-\cos\theta\left(e-1,f:e,f\right)\right]^{0.5} \tag{38}$$

where:
(v) F_{t1y} is the y-direction tangential viscous force between grains $e, f,$ and $e-1, f$

$$F_{t2y}=6\pi\eta\left\{\left(R_{e,f}R_{e-1,f-1}\right)/\left(R_{e,f}+R_{e-1,f-1}\right)\right\}\left(\delta/T_s\right)\left[\left(8/15\right)\left\{\ln\left(\left(R_{e,f}R_{e-1,f-1}\right)/\delta\left(R_{e,f}+R_{e-1,f-1}\right)\right)\right\}+0.9588\right]\left[1-\cos\theta\left(e-1,f-1:e,f\right)\right]^{0.5} \tag{39}$$

where:
(vi) F_{t2y} is the y-direction tangential viscous force between grains $e, f,$ and $e-1, f-1$

$$F_{t4y}=6\pi\eta\left\{\left(R_{e,f}R_{e+1,f}\right)/\left(R_{e,f}+R_{e+1,f}\right)\right\}\left(\delta/T_s\right)\left[\left(8/15\right)\left\{\ln\left(\left(R_{e,f}R_{e+1,f}\right)/\delta\left(R_{e,f}+R_{e+1,f}\right)\right)\right\}+0.9588\right]\left[1-\cos\theta\left(e,f:e+1,f\right)\right]^{0.5} \tag{40}$$

where:
(vii) F_{t4y} is the y-direction tangential viscous force between grains $e, f,$ and $e+1, f$

$$F_{t5y}=6\pi\eta\left\{\left(R_{e,f}R_{e+1,f+1}\right)/\left(R_{e,f}+R_{e+1,f+1}\right)\right\}\left(\delta/T_s\right)\left[\left(8/15\right)\left\{\ln\left(\left(R_{e,f}R_{e+1,f+1}\right)/\delta\left(R_{e,f}+R_{e+1,f+1}\right)\right)\right\}+0.9588\right]\left[1-\cos\theta\left(e,f:e+1,f+1\right)\right]^{0.5} \tag{41}$$

where:
(viii) F_{t5y} is the y-direction tangential viscous force between grains $e, f,$ and $e+1, f+1$

$$F_{n1y}=6\pi\eta\left\{\left(R_{e,f}R_{e-1,f}\right)/\left(R_{e,f}+R_{e-1,f}\right)\right\}^2\left\{\left(R_{e,f}+R_{e-1,f}\right)/\left(T_s\delta\right)\right\}\cos\theta\left(e-1,f:e,f\right) \tag{42}$$

where:
(ix) F_{n1y} is the y-direction normal viscous force between grains $e, f,$ and $e-1, f$

$$F_{n2y}=6\pi\eta\left\{\left(R_{e,f}R_{e-1,f-1}\right)/\left(R_{e,f}+R_{e-1,f-1}\right)\right\}^2\left\{\left(R_{e,f}+R_{e-1,f-1}\right)/\left(T_s\delta\right)\right\}\cos\theta\left(e-1,f-1:e,f\right) \tag{43}$$

where:
(x) F_{n2y} is the y-direction normal viscous force between grains $e, f,$ and $e-1, f-1$

$$F_{n3y}=6\pi\eta\left\{\left(R_{e,f}R_{e,f-1}\right)/\left(R_{e,f}+R_{e,f-1}\right)\right\}^2\left\{\left(R_{e,f}+R_{e,f-1}\right)/\left(T_s\delta\right)\right\} \tag{44}$$

where:
(xi) F_{n3y} is the y-direction normal viscous force between grains $e, f,$ and $e, f-1$

$$F_{n4y}=6\pi\eta\left\{\left(R_{e,f}R_{e+1,f}\right)/\left(R_{e,f}+R_{e+1,f}\right)\right\}^2\left\{\left(R_{e,f}+R_{e+1,f}\right)/\left(T_s\delta\right)\right\}\cos\theta\left(e,f:e+1,f\right) \tag{45}$$

where:
(xii) F_{n4y} is the y-direction normal viscous force between grains $e, f,$ and $e+1, f$

$$F_{n5y}=6\pi\eta\left\{\left(R_{e,f}R_{e+1,f+1}\right)/\left(R_{e,f}+R_{e+1,f+1}\right)\right\}^2\left\{\left(R_{e,f}+R_{e+1,f+1}\right)/\left(T_s\delta\right)\right\}\cos\theta\left(e,f:e+1,f+1\right) \tag{46}$$

where:
(xiii) F_{n5y} is the y-direction normal viscous force between grains $e, f,$ and $e+1, f+1$

$$F_{n6y} = 6\pi\eta\left\{\left(R_{e,f}R_{e,f+1}\right)/\left(R_{e,f}+R_{e,f+1}\right)\right\}^2\left\{\left(R_{e,f}+R_{e,f+1}\right)/\left(T_s\delta\right)\right\} \quad (47)$$

where:
(xiv) F_{n6y} is the y-direction normal viscous force between grains e, f, and e, f+1

All notations used in the text are listed under Appendix.

highlight that a threshold separation time of 1 s exists, beyond which the effect of viscosity becomes negligible and cohesion prevails.

4. Conclusion

Along the riverside, the gap between sediment grains varies depending on local conditions. Thus, a general approach proves highly useful. The inbuilt flexibility of the truncated pyramid model allows for the integration of multiple degrees of freedom, such as sediment grain dimensions, inter-grain separation gaps, geometrical arrays of sediment grains, separation times, and environmental temperatures. Most published studies have focused on either viscous force or cohesive force. In this study, the combined effects of both viscous and cohesive forces, along with thermal variation, were considered and thoroughly investigated. The main findings are as follows:

(i) The grain escape velocity along the riverside decreases, making the bank more vulnerable, as the inter-grain separation gap increases.
(ii) The combined effect of viscous and cohesive forces results in a significant increase in the escape velocity requirement of a grain, indicating greater riverside stability compared to conditions where only cohesion is considered at shorter separation times.
(iii) For a given inter-grain separation gap, separation time, and liquid bridge volume, the escape velocity of a sediment grain decreases with increasing temperature.
(iv) The effect of temperature is valid only up to a threshold separation time of 1 s. Beyond this duration, the effect of viscosity and temperature becomes negligible, and the effect of force of cohesion prevails.

The present study investigated sediment grain behavior in different microscale cases. Predicting the velocity requirement of a sediment grain with temperature for a limiting separation time, considering both viscous and cohesive effects, is essential for practical applications. In addition, the temperature of water in soil varies instead of remaining constant. Based on the analysis, the behavior of sediment grains across varying conditions can be effectively predicted by determining the escape velocity of a grain, which plays a critical role in riverside erosion.

The truncated pyramid model fits well with variations in parameters such as grain size, separation gap between grains, liquid bridge volume, and environmental temperature. However, this model is limited to two-dimensional cases, whereas in reality, all cases are three-dimensional. Therefore, future studies should focus on extending the truncated pyramid model from a two-dimensional to a three-dimensional basis to enable finer data interpretation and more accurate results.

Furthermore, this microscale analysis can be extended to incorporate additional factors such as vegetation effects and the impact of geotextiles, thereby enhancing robustness depending on the data available in real-world situations. Geotextile membranes can function as filters between water and sediment grains, allowing water to pass through while retaining grains, thereby increasing bank stability. Vegetation mitigates erosion through plant root systems that bind soil particles. Thus, integrating geotextile membrane and vegetative root system models into the truncated pyramid model could yield more realistic results.

Acknowledgments

None.

Funding

None.

Conflict of interest

The authors declare that they have no competing interests.

Author contributions

Conceptualization: All authors
Formal analysis: All authors
Investigation: All authors
Methodology: All authors
Visualization: Arijit Dutta
Writing–original draft: All authors
Writing–review & editing: All authors

Ethics approval and consent to participate

Not applicable.

Consent for publication

Not applicable.

Availability of data

All data used here are secondary data taken from published literature, as mentioned in the text.

References

1. Darby SE, Thorne CR. Development and testing of riverbank-stability analysis. *J Hydraul Eng*. 1996;122(8):443-454.

   doi: 10.1061/(ASCE)0733-9429(1996)122:8(443)

2. Urso MED, Lawrence CJ, Adams MJ. A two-dimensional study of the rupture of funicular liquid bridges. *Chem Eng Sci*. 2002;57:677-692.

   doi: 10.1016/S0009-2509(01)00418-3

3. Darby SE, Delbono I. A model of equilibrium bed topography for meander bends with erodible banks. *Earth Surf Process Landf*. 2002;27(10):1057-1085.

   doi: 10.1002/esp.393

4. Rim CS, Gay LW. Estimating soil moisture in small watersheds, using a water balance approach. *Nordic Hydrol*. 2002;33(5):373-390.

   doi: 10.5589/m04-043

5. Simons SJR, Pepin X, Rossetti D. Predicting granule behavior through micro-mechanistic investigations. *Int J Miner Process*. 2003;72:463-475.

   doi: 10.1016/S0301-7516(03)00120-0

6. Yu AB, Feng CL, Zou RP, Yang RY. On the relationship between porosity and inter particle forces. *Powder Technol*. 2003;130:70-76.

   doi: 10.1016/S0032-5910(02)00228-0

7. Groger T, Tuzun U, Heyes DM. Modelling and measuring of cohesion in wet granular materials. *Powder Technol*. 2003;133:203-215.

   doi: 10.1016/S0032-5910(03)00093-7

8. Hsiau SS, Yang SC. Numerical simulation of self-diffusion and mixing in a vibrated granular bed with the cohesive effect of liquid bridges. *Chem Eng Sci*. 2003;58(2):339-351.

   doi: 10.1016/S0009-2509(02)00519-5

9. Rinaldi M, Casagli N, Dapporto S, Gargini A. Monitoring and modelling of pore water pressure changes and riverside stability during flow events. *Earth Surf Process Landf*. 2004;29:237-254.

   doi: 10.1002/esp.1042

10. Kohonen MM, Geromichalos D, Scheel M, Schier C, Herminghaus S. On capillary bridges in wet granular materials. *Physica A Statis Mech Appl*. 2004;339:7-15.

    doi: 10.1016/j.physa.2004.03.047

11. Duan JG. Analytical approach to calculate rate of bank erosion. *J Hydraul Eng*. 2005;131(11):980-989.

    doi: 10.1061/(ASCE)0733-9429(2005)131:11(980)

12. Kotoky P, Bezbaruah D, Baruah J, Sarma JN. Nature of bank erosion along the Brahmaputra River channel, Assam, India. *Curr Sci*. 2005;88(4):634-640.

    doi: 10.1007/BF02989994

13. Soulie F, Youssoufi MSE, Cherblanc F, Saix C. Capillary cohesion and mechanical strength of polydisperse granular materials. *Eur Phys J E Soft Matter*. 2006;21:349-357.

    doi: 10.1140/epje/i2006-10076-2

14. Zhang R, Li J. Simulation on mechanical behavior of cohesive soil by distinct element method. *J Terramech*. 2006;43:303-316.

    doi: 10.1016/j.jterra.2005.05.006

15. Darby SE, Thorne CR. Prediction of tension crack location and riverbank erosion hazards along destabilized channels. *Earth Surf Process Landf*. 2006;19(3):233-245.

    doi: 10.1002/esp.3290190304

16. Mu F, Su X. Analysis of liquid bridge between spherical grains. *China Particuol*. 2007;5:420-424.

    doi: 10.1016/j.cpart.2007.04.006

17. Achite M, Ouillon S. Suspended sediment transport in a semiarid watershed, Wadi Abd, Algeria (1973-1995). *J Hydrol*. 2007;343(3-4):187-202.

    doi: 10.1016/j.jhydrol.2007.06.026

18. Cai S, Bhushan B. Meniscus and viscous forces during separation of hydrophilic and hydrophobic surfaces with liquid-mediated contacts. *Mater Sci Eng*. 2008;61:78-106.

    doi: 10.1016/j.mser.2007.03.003

19. Kisi Ö. River flow forecasting and estimation using different artificial neural network techniques. *Hydrol Res*. 2008;39(1):27-40.

    doi: 10.2166/nh.2008.026

20. Velmurugan A, Swarnam TP, Kumar P. Soil erosion assessment using revised morgan finney model for prioritization of dhanikhari watershed in South Andaman. *Indian J Soil Cons*. 2008;36(3):179-187.

    doi: 10.22541/au.172001663.32097257/v1

21. Mukherjee S, Mazumdar A. Study of effect of the variation of inter-particle distance on the erodibility of a riverbank under cohesion with a new model. *J Hydro Environ Res*. 2010;4:235-242.

    doi: 10.1016/j.jher.2010.01.001

22. Al-Shemmeri T. *Engineering Fluid Mechanics: Fluid Statics*. 1st ed. United States: Ventus Publishing ApS; 2012.

23. Chen Y, Marinelli F, Buscarnera G. Mathematical interpretation of delayed instability in viscous unsaturated soil. *Geotech Lett*. 2020;9(3):165-172.

    doi: 10.1680/jgele.19.00014

24. Chen Y, Buscarnera G. Numerical simulation of unstable suction transients in unsaturated soils: The role of wetting collapse. *Int J Numer Anal Methods Geomech*. 2021;45(11):1569-1587.

doi: 10.1002/nag.3214

25. Zhanlin M, Fengxi Z. Study on diffusion mechanism of viscosity time-varying slurry in unsaturated soil based on displacement effect. *Eur J Environ Civ Eng*. 2023;28(7):1544-1564.

doi: 10.1080/19648189.2023.2263058

26. Cai G, Su Y, Zhou A, Yin F, Shi Y. An elastic-viscoplastic model for time-dependent behavior of unsaturated soils. *Comput Geotech*. 2023;159:105415.

doi: 10.1016/j.compgeo.2023.105415

27. Amarsid L, Awdi A, Fall A, Roux J, Chevoir F. Viscous effects in sheared unsaturated wet granular materials. *J Rheol*. 2024;28(4):523-537.

doi: 10.1122/8.0000824

28. Liangliang W, Zhifei S. Bulk wave manipulation by periodic in-filled barriers in unsaturated soil. *Eng Struct*. 2024;309:118076.

doi: 10.1016/j.engstruct.2024.118076

29. Biswas D, Dutta A, Mukherjee S, Mazumdar A. A new approach to transformation of micro analysis into macro analysis of forces to study the dynamic behaviour of riverbank morphology. *ISH J Hydraul Eng*. 2024;30(3):301-313.

doi: 10.1080/09715010.2024.2317884

30. An DG, Lim UH, Song YS, Kim H, Kim JH. Analysis of thermal effects according to channel and drain contact metal distance. *Case Stud Therm Eng*. 2025;65:105642.

doi: 10.1016/j.csite.2024.105642

31. Szabo J, David L, Loczy D. *Anthropogenic Geomorphology*: *Water management*. 1st ed. Berlin: Springer; 2010.

32. Yang J, Zhao N, Li Z, Sun C. A combined theory model for predicting the viscosity of water-based Newtonian nanofluids containing spherical oxide nanoparticles. *J Therm Anal Calorim*. 2018;135:1311-1321.

doi: 10.1007/s10973-018-7510-6

Appendix

Notations

$a_{e,f}$, $b_{e,f}$, and $c_{e,f}$ coefficients used in the cohesive force equation linking a pair of grains with the bigger grain being e, f

$R_{e,f}$ = Radius of grain e, f, m

δ = Inter-grain separation gap, m

T_S = Separation time, s

T = Temperature, °C

F_{s1x} = x-direction cohesive force linking grains e, f, and $e-1$, f, N

F_{s2x} = x-direction cohesive force linking grains e, f, and $e-1$, $f-1$, N

F_{s3x} = x-direction cohesive force linking grains e, f, and e, $f-1$, N

F_{s4x} = x-direction cohesive force linking grains e, f, and $e+1$, f, N

F_{s5x} = x-direction cohesive force linking grains e,f, and $e+1$,$f+1$, N

F_{s6x} = x-direction cohesive force linking grains e, f, and e, $f+1$, N

F_{s1y} = y-direction cohesive force linking grains e, f, and $e-1$, f, N

F_{s2y} = y-direction cohesive force linking grains e, f, and $e-1$, $f-1$, N

F_{s4y} = y-direction cohesive force linking grains e, f, and $e+1$, f, N

F_{s5y} = y-direction cohesive force linking grains e, f, and $e+1$, $f+1$, N

F_{t1x} = x-direction viscous tangential force linking grains e, f, and $e-1$, f, N

F_{t2x} = x-direction viscous tangential force linking grains e, f, and $e-1$, $f-1$, N

F_{t3x} = x-direction viscous tangential force linking grains e, f, and e, $f-1$, N

F_{t4x} = x-direction viscous tangential force linking grains e, f, and $e+1$, f, N

F_{t5x} = x-direction viscous tangential force linking grains e,f, and $e+1$, $f+1$, N

F_{t6x} = x-direction viscous tangential force linking grains e,f, and e, $f+1$, N

F_{t1y} = y-direction viscous tangential force linking grains e, f, and $e-1$, f, N

F_{t2y} = y-direction viscous tangential force linking grains e, f, and $e-1$, $f-1$, N

F_{t4y} = y-direction viscous tangential force linking grains e, f, and $e+1$, f, N

F_{t5y} = y-direction viscous tangential force linking grains e, f, and $e+1$,$f+1$, N

F_{n1x} = x-direction viscous normal force linking grains e, f, and $e-1$, f, N

F_{n2x} = x-direction viscous normal force linking grains e, f, and $e-1$, $f-1$, N

F_{n4x} = x-direction viscous normal force linking grains e, f, and $e+1$,f, N

F_{n5x} = x-direction viscous normal force linking grains e, f, and $e+1$,$f+1$, N

F_{n1y} = y-direction viscous normal force linking grains e, f, and $e-1$, f, N

F_{n2y} = y-direction viscous normal force linking grains e, f, and $e-1$, $f-1$, N

F_{n3y} = y-direction viscous normal force linking grains e, f, and e, $f-1$, N

F_{n4y} = y-direction viscous normal force linking grains e, f, and $e+1$, f, N

F_{n5y} = y-direction viscous normal force linking grains e, f, and $e+1$, $f+1$, N

F_{n6y} = y-direction viscous normal force linking grains e, f, and e, $f+1$, N

$F_{G\,e,f}$ = Submerged weight of sediment grain e, f, N

$M_{e,f}$ = Mass of sediment grain e, f, kg

$\ddot{x}_{e,f}$ = x-direction impending acceleration of sediment grain e, f, m/s^2

$\ddot{y}_{e,f}$ = y-direction impending acceleration of sediment grain e, f, m/s^2

$f_{e,f}$ = The resulting impending acceleration of sediment grain e, f, m/s^2

$V_{escape\,e,f}$ = Escape velocity of grain e, f from riverside, m/s

g = Gravitational acceleration, m/s^2

ρ = Water density, kg/m^3

ρ_s = Material density of sediment grains, kg/m^3

σ = Coefficient of surface tension, n/m

η = Dynamic viscosity coefficient, pa-s

$\emptyset$ = Contact angle, radians

V = Liquid bridge volume, nL

ACCSCIENCE PUBLISHING

Explora: Environment and Resource

ORIGINAL RESEARCH ARTICLE

Water quality patterns across seasons in major urban lakes of Dhaka Metropolitan City

Ha-mim Ebne Alam[1]*, Kazi Tawkir Ahmed[1], Md. Nizam Uddin[1], Md. Jahidul Hasan[2], and Md. Yeasir Arafat[1]

[1]Department of Oceanography, Faculty of Marine Sciences and Fisheries, University of Chittagong, Chittagong, Bangladesh

[2]Institute of Marine Sciences, Faculty of Marine Sciences and Fisheries, University of Chittagong, Chittagong, Bangladesh

Abstract

Urban lakes in Dhaka are increasingly subjected to environmental degradation due to rapid urbanization and inadequate wastewater management. This study aims to assess and compare the water quality of three major urban lakes—Gulshan, Dhanmondi, and Hatirjheel—across four seasons—winter, pre-monsoon, monsoon, and post-monsoon—by analyzing key physicochemical parameters. In this study, data on various water quality parameters, including pH, dissolved oxygen (DO), biochemical oxygen demand (BOD), chemical oxygen demand (COD), total dissolved solids (TDS), turbidity, suspended solids, electrical conductivity (EC), chloride, and alkalinity, measured using standard methods, were referenced from the Bangladesh government's national report on water quality. The results revealed seasonal and spatial variations in water quality, with monsoon seasons showing dilution effects while pre-monsoon values indicate peak pollution. Among the three lakes, Dhanmondi Lake demonstrated the best water quality, with average BOD and COD levels remaining within environmental quality standards and DO concentrations that support aquatic life. Conversely, Gulshan Lake was found to be the most polluted, with BOD levels reaching up to 48 mg/L, COD up to 202 mg/L, turbidity as high as 208 NTU, and DO dropping to 0.12 mg/L. Hatirjheel Lake exhibited moderate pollution levels, with elevated TDS and EC values, particularly in the post-monsoon season. The study concludes that the urban lake system of Dhaka, particularly Gulshan and Hatirjheel, is subject to immense water quality degradation; therefore, compulsory lake management and pollution prevention actions should be adopted to enhance the ecological and recreational significance of the lakes.

Keywords: Dhaka Metropolitan City; Water quality; Seasonal variation; Gulshan Lake; Dhanmondi Lake; Hatirjheel Lake

***Corresponding author:**
Ha-mim Ebne Alam
(hamim.imsfcu@gmail.com)

Citation: Alam HE, Ahmed KT, Uddin MN, Hasan MJ, Arafat MY. Water quality patterns across seasons in major urban lakes of Dhaka Metropolitan City. *Explora Environ Resour.* 2025;2(4):025310057. doi: 10.36922/EER025310057

Received: August 1, 2025

Revised: September 30, 2025

Accepted: October 9, 2025

Published online: October 29, 2025

1. Introduction

Water is crucial for life and plays a foundational role in ecological sustainability, public health, and economic development.[1] In Bangladesh, although water is naturally abundant, rapid urbanization and inadequate waste management practices have severely impacted the quality of surface water bodies, particularly in metropolitan areas.[2,3] One of the most densely inhabited cities in the world, Dhaka is rapidly transforming into an

urban hotspot,[4] resulting in the degradation of its natural water systems. Gulshan, Dhanmondi, and Hatirjheel Lakes are among them, which traditionally served as significant elements of the urban landscape, offering both drainage and recreational, as well as ecological services.[5,6] As Dhaka continues to expand, the burden on these lakes has intensified. Hatirjheel, covering around 302 acres, currently manages nearly one-third of the city's stormwater, linking various parts of the town and offering both infrastructural and recreational value.[7,8] However, like many urban water bodies, it now suffers from declining water quality due to the inflow of untreated wastewater, industrial discharges, and domestic sewage.[9] Similarly, Dhanmondi Lake, located in a highly residential area, and Gulshan Lake, situated in one of Dhaka's elite neighborhoods, are facing increasing environmental degradation due to human encroachment, solid waste dumping, and poor regulatory enforcement.[6,9,10]

In environmental assessments, physicochemical parameters serve as pivotal indicators of water quality.[11] These comprise pH, dissolved oxygen (DO), biochemical oxygen demand (BOD), chemical oxygen demand (COD), total dissolved solids (TDS), turbidity, chloride, suspended solids (SS), alkalinity, and electrical conductivity (EC). Each of these parameters offers insights into the chemical stability and ecological health of a water body.[12,13] The pH level reflects the water's acidity or alkalinity, which affects aquatic life and the solubility of nutrients and metals.[14] DO is vital for the survival of marine organisms, and levels below 5 mg/L often indicate ecological stress.[15,16] BOD represents the amount of oxygen required for microbial decomposition of organic matter, while COD measures the total oxygen needed to oxidize both organic and inorganic pollutants.[17,18] TDS accounts for the presence of dissolved salts and minerals, with the World Health Organization recommending values below 1000 mg/L for safe use.[19] Turbidity measures water clarity and impacts photosynthesis in aquatic plants.[20] Chloride concentration, often elevated due to domestic waste, can affect the taste and corrosiveness of water.[21] SS contributes to sedimentation and turbidity, degrading aquatic habitats.[22] Alkalinity reflects the water's ability to resist pH changes, maintaining chemical stability.[14] EC is an indicator of the water's ion concentration and is typically used to evaluate its mineral content. The World Health Organization recommends a maximum EC of 1200 μS/cm for drinking water, although lower values are usually found in ecologically healthy lakes.[23-25]

These parameters are essential not only for environmental control but also as indicators in making comparisons that will lead to compliance with international standards. The values are also influenced by seasons. In tropical climates such as Bangladesh, variations across winter, pre-monsoon, monsoon, and post-monsoon seasons can significantly impact water quality by altering temperature, runoff volume, and organic matter concentration.[26-28] Understanding these seasonal dynamics is essential for designing effective water resource management and pollution control strategies.

Although numerous studies have been conducted on the water quality of individual lakes in Dhaka,[15,16,28-30] there remains a lack of comparative research that analyzes seasonal variations in water quality across multiple lakes using a broad spectrum of standard parameters. Most previous assessments do not integrate both interlake and intraseasonal comparisons or consistently evaluate results against international environmental benchmarks. This gap limits the broader understanding of how urban pressures affect water bodies differently over time and space, emphasizing the need for global standards in environmental research.

A comprehensive comparative study involving physicochemical parameters across all major seasons is essential to evaluate the current state of Dhaka's urban lakes. By systematically analyzing and comparing Gulshan, Dhanmondi, and Hatirjheel Lakes with environmental standards, this research seeks to identify which lakes are under critical ecological threat and which seasonal periods show heightened vulnerability. These findings, once implemented, will have a significant impact on urban water management and restoration planning in one of the world's most water-stressed urban environments.

2. Methodology

This research employed a comparative study of water quality parameters of three urban lakes located in Dhaka Metropolitan City: Gulshan Lake, Dhanmondi Lake, and Hatirjheel Lake (Figure 1).

Gulshan Lake is located in the northern part of Dhaka at approximately 23°48′ N and 90°25′ E. It is the northernmost lake in a chain of water bodies that include Hatirjheel and the Balu River. The lake stretches 3.8 km with an average depth of 2.5 m. It is long and narrow, resembling a natural channel. The lake is bordered by Baridhara in the north, Tejgaon-Hatirjheel in the south, Gulshan-Banani in the west, and Badda in the east.[9,16]

Dhanmondi Lake lies at the center of Dhaka, between 23°44′12″ to 23°45′22″ N and 90°22′ to 90°23′ E. It stretches from Jigatola to Road 27 and is surrounded by major residential zones. The lake is 3 km long and varies in width from 35 m to 100 m. It reaches a maximum depth of 4.77 m and spans a total surface area of 37.37 ha. Mohammadpur

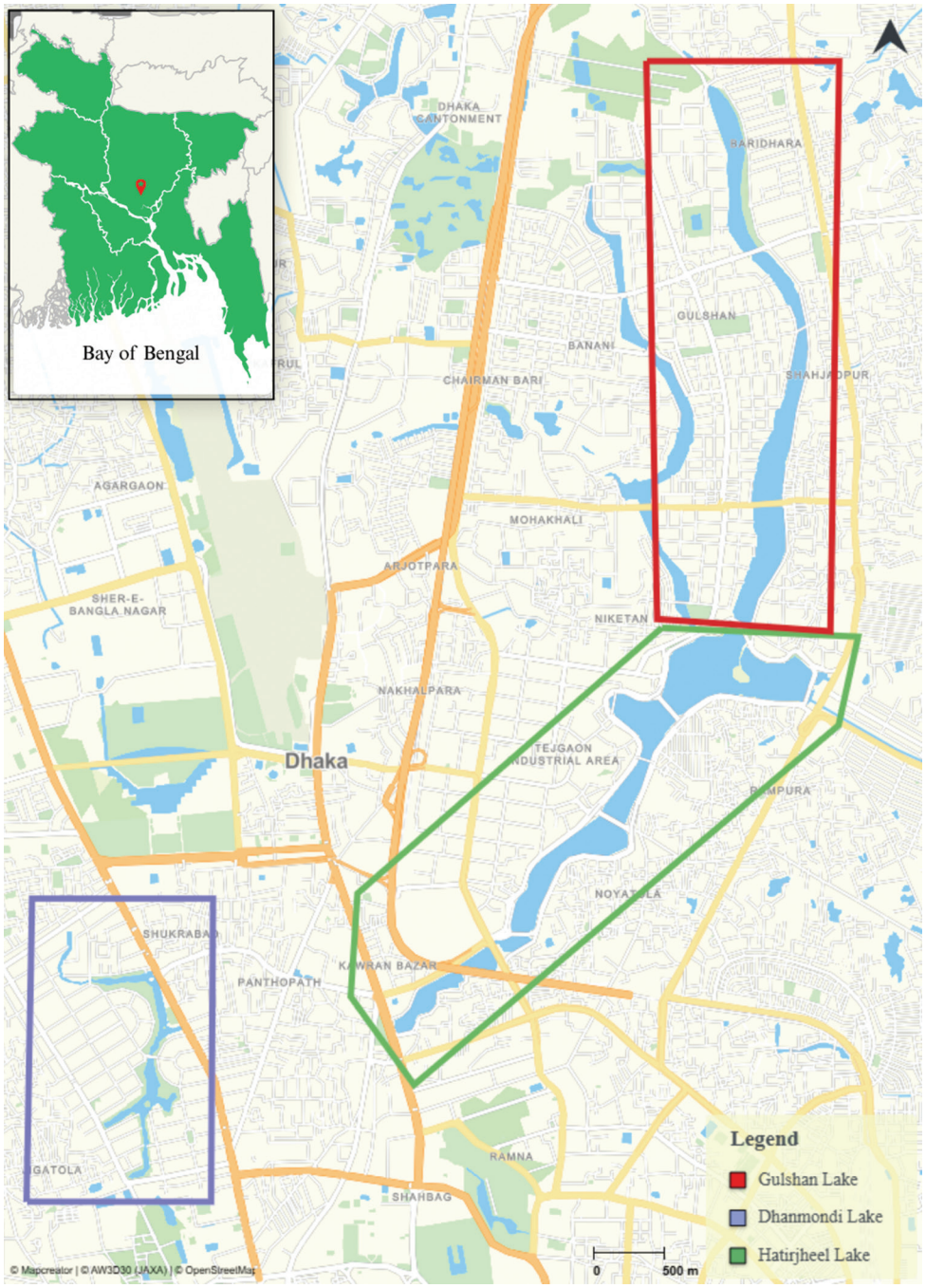

Figure 1. Study area map of Gulshan, Dhanmondi, and Hatirjheel Lake
Source: Open Street Map.

and Lalmatia bound the lake to the north, Satmasjid Road to the west, Border Guard Bangladesh Gate to the south, and Kalabagan to the east.[16,29]

Hatirjheel Lake, situated at 23°44′58.47″ N and 90°23′48.35″ E, is a centrally located urban water body that features recreational and transportation amenities. The lake extends 4.1 km in length with an average depth of 2.6 m and is up to 460 m wide at its broadest section. The surroundings include Gulshan-Banani to the north, Maghbazar and Banglamotor to the west, Rampura-Badda to the east, and Tejgaon industrial area to the south.[16,30-32]

2.1. Data source

The present study was conducted using secondary data sourced from the official publication titled "Surface and Ground Water Quality Report 2022," prepared and

published by the Department of Environment, Ministry of Forest, Environment and Climate Change, Government of the People's Republic of Bangladesh.[10] This report presents credible, methodologically standardized data on surface water quality nationwide, making it suitable for academic and policy-level analyses. According to the original report, the water quality data were collected from the upper surface (within a depth of 1 m). Multiple sub-samples were collected from random places at midday (usually within a 5 m interval) within each sampling station, and the sub-sample data were averaged to form a compact data set for each sampling station. The data used in this study focused on surface water quality parameters of the three lakes. Out of many discrete sampling stations, three distinct locations within each of the selected lakes were chosen for this analysis (Table 1). This deliberate approach in determining specific geographic locations in each lake was strategic and designed to capture the spatial variability in the water quality of the lake systems.

Furthermore, the original data were gathered for four months in 2022 (February, May, August, and November). As these months represent the four climatic seasons in Bangladesh, February was categorized as winter, May as pre-monsoon, August as monsoon, and November as post-monsoon. This classification enabled the analysis of seasonal variation in water quality within each lake and among the three lakes. These data are accessible to the public and are reliable because they were gathered and recorded officially and scientifically.

2.2. Parameters and analytical methods

A total of 10 physicochemical water quality parameters were selected for the assessment. These parameters are widely accepted as indicators of surface water quality in both domestic and international standards.[33,34] The chosen parameters are pH, DO, BOD_5, COD, TDS, turbidity, SS, total alkalinity, and EC. These are critical for characterizing the properties of surface water. Although this research used secondary data, all the parameters listed above were analyzed in the original report using standardized laboratory methods approved by national and international agencies such as the American Public Health Association.[35] pH was estimated using a standard pH electrode, which indicates the degree of acidity or alkalinity of the water. DO was determined by the modified Winkler's method or the titrimetric method. This technique measures the oxygen concentration dissolved in water, which is crucial to the life of aquatic organisms. BOD_5 was measured using the dilution method after a 5-day incubation period at 20°C. This test estimates the oxygen required by microorganisms to decompose organic material in water. COD was determined using the closed reflux colorimetric method, which measures the oxygen equivalent of the organic matter that can be oxidized chemically. TDS was analyzed using the gravimetric method, where a water sample is filtered and the filtrate evaporated to measure the residue weight. Turbidity was measured using the nephelometric method, which uses light scattering to determine the cloudiness or haziness of water caused by SSs. Chloride was determined using the argentometric method, a titrimetric process where silver nitrate is used to quantify chloride ions in the sample. SS was measured using another gravimetric method, where solids retained on a filter are dried and weighed to determine the concentration. Total alkalinity was analyzed using standard titration methods, indicating the buffering capacity of the water against pH changes. EC was estimated with a standard EC meter, which allows detection of the water's conductivity of an electric current as a consequence of the presence of dissolved salts and minerals. These are widely used standard procedures for precise and dependable results and are routinely employed in water quality monitoring programs worldwide.

Table 1. Sampling stations and their surroundings in the selected urban lakes

Study area	Sampling station	Spatial distribution		Surroundings
Gulshan Lake	S_1	23°48′16″N	90°25′00″E	United Hospital Limited
	S_2	23°47′27″N	90°25′19″E	Manarat International School
	S_3	23°46′28″N	90°25′05″E	Shooting complex
Dhanmondi Lake	S_1	23°44′45″N	90°22′39″E	8 no. bridge
	S_2	23°44′19″N	90°22′35″E	Jigatola bus stand
	S_3	23°45′03″N	90°22′33″E	32 no. bridge
Hatirjheel Lake	S_1	23°46′10″N	90°25′16″E	Rampura bridge
	S_2	23°45′41″N	90°24′33″E	Kuni para
	S_3	23°45′16″N	90°24′10″E	FDC Mor Bridge

2.3. Data processing and analysis

The raw data collected from the Surface and Ground Water Quality Report 2022 were systematically structured in Microsoft Excel. Data on each water parameter were tabulated for each lake and by season. In this study, statistical analyses such as Pearson's correlation, type III analysis of variance, coefficient of variance (%), and principal component analysis were applied to the water quality data to understand the correlation among water quality parameters, as well as season-wise and lake-wise variations. These data were then compared across the three lakes to identify lake-seasonal interactions and trends in water quality. The collected data were further evaluated

against national Environmental Quality Standards (EQS) and World Health Organization guidelines to assess their suitability for ecological functions and public health. Using a comparative and seasonal approach, this study aimed to evaluate the degree of pollution, identify the most critical seasons, and determine which types of lakes most urgently require protective measures.

3. Results

The findings on the water quality parameters of three urban lakes in Dhaka—Gulshan Lake, Dhanmondi Lake, and Hatirjheel Lake—focused on the seasonal variations of key water quality parameters within each lake and provided a comparative overview across the three lakes. The average values, along with their minimum, maximum, and standard deviations, are discussed for each parameter across different seasons. Furthermore, the observed water quality parameters were compared with relevant EQS to assess the overall health of these urban aquatic ecosystems.

3.1. Seasonal water quality of Gulshan Lake

The seasonal dynamics of water quality at Gulshan Lake exhibited contrasting patterns of influence, both natural and anthropogenic. As revealed in Table 2, during the winter season, Gulshan Lake had an average pH of 7.46, indicating a slight alkalinity, and a moderate DO value of 5.32 mg/L. The BOD and COD were recorded at 33.33 mg/L and 124 mg/L, respectively, suggesting the presence of organic pollutants. The average TDS stood at 296 mg/L, while turbidity reached 43.6 NTU. EC was relatively high at 498 µmhos/cm. Among all sampling stations, Station S_3 recorded the highest DO value at 6.68 mg/L, reflecting localized variations in water quality.

In the pre-monsoon season, the lake experienced a sharp rise in pollution indicators. BOD increased substantially to an average of 48 mg/L, and COD peaked at 202 mg/L. Turbidity rose drastically to 108.6 NTU, while SS reached its highest average of 214.7 mg/L. Interestingly, DO also peaked during this season, averaging 6.97 mg/L, possibly due to algal growth or increased surface aeration. Station S_3 exhibited high levels of BOD (64 mg/L) and COD (343 mg/L), indicating local contamination (Table 2).

During the monsoon, the variation of water quality was significantly different, implying the dilution impact of precipitation. The DO of the lake decreased drastically, reaching a mean value of 1.41 mg/L, the minimum among all the seasons, thus registering severe oxygen stress. BOD and COD levels declined to 22 mg/L and 82.67 mg/L, respectively. TDS also fell to its lowest seasonal average of 41.33 mg/L, and turbidity was reduced due to water flushing. An extremely low DO value of 0.12 mg/L was recorded at Station S_1, indicating critical conditions for aquatic life (Table 2).

Table 2. Water quality parameters of Gulshan Lake during different seasons

Season	Sampling station	pH	DO (mg/L)	BOD (mg/L)	COD (mg/L)	TDS (mg/L)	Turbidity (NTU)	Chloride (mg/L)	SS (mg/L)	Alkalinity (mg/L)	EC (µmhos/cm)
Winter	S_1	7.34	3.82	40	130	293	43.6	42	136	204	484
	S_2	7.32	5.47	32	122	280	61.4	42	159	189	486
	S_3	7.73	6.68	28	120	315	25.8	42	52	183	524
	Avg.	7.46	5.32	33.33	124	296	43.6	42	115.7	192	498
Pre-monsoon	S_1	7.19	5.7	45	134	204	63.2	39	192	195	388
	S_2	7.41	9.4	35	129	201	54.5	33	199	198	394
	S_3	7.42	5.8	64	343	254	208	48	253	184	440
	Avg.	7.34	6.97	48	202	219.7	108.6	40	214.7	192.3	407.3
Monsoon	S_1	7.01	0.12	22	83	41	47.1	41	92	161	415
	S_2	7.12	2.1	22	75	41	37.1	41	77	162	443
	S_3	7.42	2	22	90	42	38.7	42	81	170	430
	Avg.	7.18	1.41	22	82.67	41.33	40.97	41.33	83.33	164.3	429.3
Post-monsoon	S_1	7.27	5.4	42	76	267	67	40	136	160	360
	S_2	7.32	5	38	78	269	61.4	44	159	158	356
	S_3	7.49	6	32	85	288	50.7	40	52	164	365
	Avg.	7.36	5.47	37.33	79.67	274.7	59.7	41.33	115.7	160.7	360.3

Abbreviations: Avg.: Average; BOD: Biochemical oxygen demand; COD: Chemical oxygen demand; DO: Dissolved oxygen; EC: Electrical conductivity; SS: Suspended solids; TDS: Total dissolved solids.

Table 2 also showed that the post-monsoon measurements reflected some recovery in water quality. DO improved to 5.47 mg/L, and BOD and COD increased moderately to 37.33 mg/L and 79.67 mg/L, respectively. Turbidity remained high at 59.7 NTU, and SS averaged 115.7 mg/L. Despite partial improvements, Gulshan Lake consistently showed higher levels of organic pollution, including BOD, COD, turbidity, and SS, compared to the other lakes in all seasons.

3.2. Seasonal water quality of Dhanmondi Lake

Dhanmondi Lake showed relatively stable and superior water quality across all seasons. In winter, the lake had an average pH of 7.57 and recorded the highest average DO among all lakes at 6.04 mg/L. BOD and COD were low, averaging 6.67 mg/L and 39.67 mg/L, respectively, indicating minimal organic pollution. TDS levels were also low at 144.3 mg/L, and turbidity was measured at 5.6 NTU. SS concentration was only 10 mg/L, confirming the lake's relatively clean status. Station S_3 reported the highest DO value at 7.14 mg/L (Table 3).

According to Table 3, during the pre-monsoon period, DO declined to 4.2 mg/L, yet BOD and COD remained low at 4.67 mg/L and 33 mg/L, respectively. Chloride levels peaked at 51.33 mg/L, while SS increased to 52 mg/L, possibly due to surface runoff. The overall water quality remained within acceptable limits.

In the monsoon season, Dhanmondi Lake showed improved conditions. DO rose to 5.29 mg/L, and turbidity reached its lowest at 1.67 NTU, indicating excellent water clarity. BOD remained low at 6.67 mg/L, although COD increased to 61 mg/L (Table 3), likely due to accumulated organic matter from stormwater discharge.

Table 3 shows that the post-monsoon data reported a decrease in DO to 3.23 mg/L, the lowest for the lake. However, BOD and COD levels declined further to 2.5 mg/L and 27 mg/L, respectively. Turbidity increased to 44.33 NTU, possibly influenced by sediment disturbance. Despite seasonal fluctuations, Dhanmondi Lake consistently exhibited better water quality than Gulshan and Hatirjheel Lakes, with lower values of BOD, COD, turbidity, and TDS throughout the year.

3.3. Seasonal water quality of Hatirjheel Lake

Hatirjheel Lake exhibited a range of conditions from moderately polluted to stressed throughout the seasons. In winter, the lake showed a slightly alkaline average pH of 7.7. DO was relatively low at 3.06 mg/L, and BOD and COD were 29 mg/L and 103 mg/L, respectively, indicating moderate pollution. TDS levels were highest among the three lakes at 313 mg/L, while EC peaked at 556.7 µmhos/cm. Station S_1 recorded the maximum EC value of 597 µmhos/cm (Table 4).

Table 3. Water quality parameters of Dhanmondi Lake during different seasons

Season	Sampling station	pH	DO (mg/L)	BOD (mg/L)	COD (mg/L)	TDS (mg/L)	Turbidity (NTU)	Chloride (mg/L)	SS (mg/L)	Alkalinity (mg/L)	EC (µmhos/cm)
Winter	S_1	7.49	5.27	6	27	138	5.6	29	9	86	251
	S_2	7.54	5.71	8	58	134	4.5	26	8	95	242
	S_3	7.68	7.14	6	34	161	6.7	28	13	89	290
	Avg.	7.57	6.04	6.67	39.67	144.3	5.6	27.67	10	90	261
Pre-monsoon	S_1	7.35	4.5	4	26	142	5.33	51	42	101	277
	S_2	7.19	3.2	6	32	146	18.4	47	67	114	281
	S_3	7.39	4.9	4	41	160	6.22	56	47	102	311
	Avg.	7.31	4.2	4.67	33	149.3	9.98	51.33	52	105.7	289.7
Monsoon	S_1	7.46	5.86	8	34	132	1.6	33	12	89	302
	S_2	7.39	5	6	73	136	1.9	29	14	92	268
	S_3	7.52	5	6	76	150	1.5	35	15	90	294
	Avg.	7.46	5.29	6.67	61	139.3	1.67	32.33	13.67	90.33	288
Post-monsoon	S_1	7.62	4.3	2.8	30	121.7	56	29	48	89	222
	S_2	7.49	2.1	1.4	10	127.2	7	31	5	91	233
	S_3	7.65	3.3	3.3	41	148.9	70	35	62	105	274
	Avg.	7.59	3.23	2.5	27	132.6	44.33	31.67	38.33	95	243

Abbreviations: Avg.: Average; BOD: Biochemical oxygen demand; COD: Chemical oxygen demand; DO: Dissolved oxygen; EC: Electrical conductivity; SS: Suspended solids; TDS: Total dissolved solids.

Table 4. Water quality parameters of Hatirjheel Lake during different seasons

Season	Sampling station	pH	DO (mg/L)	BOD (mg/L)	COD (mg/L)	TDS (mg/L)	Turbidity (NTU)	Chloride (mg/L)	SS (mg/L)	Alkalinity (mg/L)	EC (µmhos/cm)
Winter	S_1	7.53	2.43	32	112	335	40.2	44	103	226	597
	S_2	7.92	4	25	117	315	26.1	47	58	226	559
	S_3	7.65	2.75	30	80	289	8.3	44	11	186	514
	Avg.	7.7	3.06	29	103	313	24.87	45	57.33	212.7	556.7
Pre-monsoon	S_1	7.25	1.8	25	90	272	82.7	51	133	214	521
	S_2	7.34	1.5	23	95	273	67.8	46	121	175	517
	S_3	7.34	3.9	32	80	261	58.5	61	87	151	496
	Avg.	7.31	2.4	26.67	88.33	268.7	69.67	52.67	113.7	180	511.3
Monsoon	S_1	7.49	4.5	24	161	251	40	50	86	151	493
	S_2	7.3	3.65	22	63	162	67.6	44	110	162	497
	S_3	7.4	8	22	58	150	72.2	48	116	150	474
	Avg.	7.4	5.38	22.67	94	187.7	59.93	47.33	104	154.33	488
Post-monsoon	S_1	7.92	4.3	28	96	280	165	63	158	202	508
	S_2	7.92	5.5	21	39	235	35	45	29	189	426
	S_3	7.72	2.1	26	115	284	123	66	116	218	555
	Avg.	7.85	3.97	25	83.33	266.3	107.7	58	101	203	496.3

Abbreviations: Avg.: Average; BOD: Biochemical oxygen demand; COD: Chemical oxygen demand; DO: Dissolved oxygen; EC: Electrical conductivity; SS: Suspended solids; TDS: Total dissolved solids.

Pre-monsoon observations reflected a further decline in water quality. DO dropped to 2.4 mg/L, representing the lowest seasonal value for Hatirjheel. BOD and COD were measured at 26.67 mg/L and 88.33 mg/L, respectively. Turbidity increased to 69.67 NTU, and SS peaked at 113.7 mg/L. Chloride levels also reached a high of 52.67 mg/L (Table 4), pointing to increased domestic and industrial inflow.

Following Table 4, with the onset of the monsoon, Hatirjheel showed signs of improvement in DO. DO increased to a seasonal high of 5.38 mg/L. BOD and COD slightly decreased to 22.67 mg/L and 94 mg/L, respectively. TDS also declined to 187.7 mg/L due to dilution from rainwater inflow.

In the post-monsoon season, Hatirjheel recorded its highest average pH of 7.85. DO slightly improved to 3.97 mg/L, while BOD and COD were measured at 25 mg/L and 83.33 mg/L, respectively. Turbidity reached its highest level for this lake at 107.7 NTU, and chloride peaked at 58 mg/L (Table 4). Overall, Hatirjheel consistently showed higher TDS and EC values compared to Dhanmondi Lake and had lower DO concentrations, reflecting ongoing environmental stress.

3.4. Comparative analysis of water qualities

The correlation between key physicochemical parameters was evaluated using Pearson's correlation analysis and presented as a heatmap in Figure 2. In this analysis, BOD indicated strong positive correlations with COD ($r = 0.8$), SS ($r = 0.81$), alkalinity ($r = 0.77$), and turbidity ($r = 0.65$), signifying that the organic load was closely related to SSs and buffering capacity. COD was also highly correlated with SS ($r = 0.71$) and turbidity ($r = 0.67$). EC exhibited a strong correlation with alkalinity ($r = 0.89$). On the other hand, DO showed a negative correlation with chloride ($r = -0.28$), alkalinity ($r = -0.16$), and EC ($r = -0.24$), emphasizing the lakes' insufficiency under stressed conditions.

3.5. Comparative analysis across lakes and seasons

The seasonal and spatial comparison of key water quality parameters across Gulshan, Dhanmondi, and Hatirjheel Lakes revealed distinct differences in environmental conditions and pollutant loads. These differences are illustrated in Figure 3, which shows trends for each parameter across the four seasons: winter, pre-monsoon, monsoon, and post-monsoon. Table 5 shows the statistical significance (type III analysis of variance) of lake-season effects and the coefficient of variance (%).

pH levels in the lakes remained stable, ranging from 7.18 to 7.85 (Figure 3A) with significant lake effects ($F = 18.32$, $p<0.001$) and moderate seasonal variation ($F = 3.89$, $p=0.023$) (Table 5). Hatirjheel Lake showed the highest average pH (7.85) in the post-monsoon season,

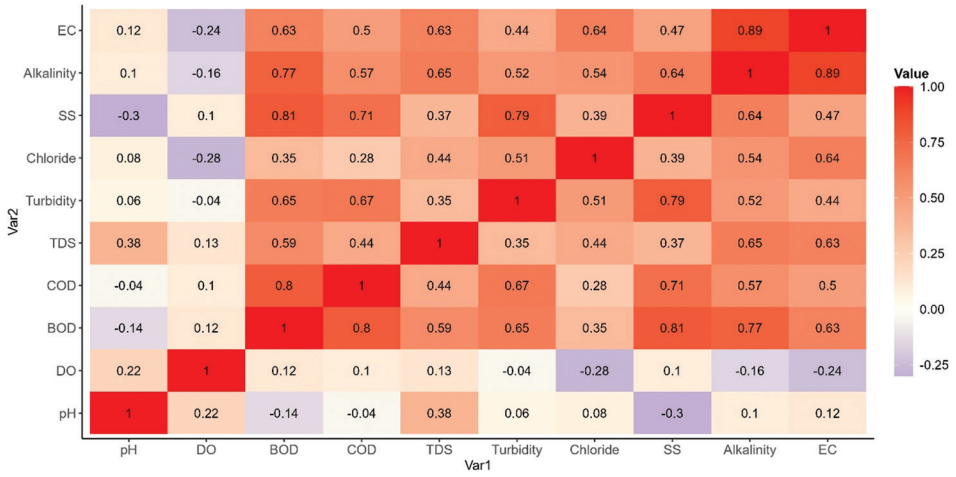

Figure 2. A heatmap showing the correlation among water quality parameters
Abbreviations: BOD: Biochemical oxygen demand; COD: Chemical oxygen demand; DO: Dissolved oxygen; EC: Electrical conductivity; SS: Suspended solids; TDS: Total dissolved solids; Var: Variable.

Table 5. Statistical significance of lake-season effects

Water quality parameter	Lake (*p*-value)	Season (*p*-value)	Lake×Season (*p*-value)
pH	<0.001	0.023	0.215
DO	<0.001	<0.01	0.132
BOD	<0.001	<0.05	0.087
COD	<0.001	0.061	0.243
TDS	<0.001	<0.001	0.054
Turbidity	<0.001	<0.01	<0.01
Chloride	<0.001	<0.05	0.178
SS	<0.001	0.037	<0.05
Alkalinity	<0.001	<0.05	0.096
EC	<0.001	<0.01	0.067

Abbreviations: BOD: Biochemical oxygen demand; COD: Chemical oxygen demand; DO: Dissolved oxygen; EC: Electrical conductivity; SS: Suspended solids; TDS: Total dissolved solids.

Table 6. Coefficient of variation (%) by season

Parameter	Coefficient of variation (%)			
	Winter	Pre-monsoon	Monsoon	Post-monsoon
pH	2.25	1.5	2.59	3.04
DO	33.67	69.97	58.97	35.08
BOD	58.36	79.52	49.02	75.2
COD	50.96	93.24	50.37	43.47
TDS	32.35	24.89	94.47	29.64
Turbidity	77.36	105.1	71.88	64.01
Chloride	18.79	20.34	13.46	27.61
SS	81.65	63.11	56.91	60.3
Alkalinity	29.87	26.82	24.82	28.05
EC	26.63	22.13	23.73	28.88

Abbreviations: BOD: Biochemical oxygen demand; COD: Chemical oxygen demand; DO: Dissolved oxygen; EC: Electrical conductivity; SS: Suspended solids; TDS: Total dissolved solids.

and Gulshan Lake recorded the lowest pH (7.18) value in the monsoon season. The coefficient of variation for pH remained low across all seasons (1.50–3.04%) (Table 6).

DO displayed substantial fluctuation (Figure 3B), with highly significant lake (F = 15.67, p<0.001) and seasonal effects (F = 5.61, p<0.01) (Table 5). Dhanmondi Lake consistently maintained higher DO values, with seasonal averages ranging from 3.23 mg/L in the post-monsoon to 6.04 mg/L in winter. In contrast, Gulshan Lake recorded critically low DO during the monsoon season (1.41 mg/L), with one sampling station recording an extreme value of 0.12 mg/L. Hatirjheel Lake also showed signs of oxygen depletion, particularly during the pre-monsoon season, when the average DO dropped to 2.4 mg/L. The coefficient of variation for DO reached 69.97% during pre-monsoon (Table 6), reflecting high variability in oxygen availability.

BOD and COD levels, which indicate organic pollution, depict the differences with significant lake effects (BOD: F = 142.33, p<0.001; COD: F = 38.45, p<0.001) (Table 5). Dhanmondi Lake showed the lowest BOD (2.5–6.67 mg/L) and COD (27–61 mg/L) across all seasons, signifying minimal organic contamination (Figure 3C and D). In contrast, Gulshan Lake displayed the highest levels, with BOD reaching 48 mg/L and COD peaking at 202 mg/L during the pre-monsoon. A maximum COD value of 343 mg/L was obtained at Gulshan Station S_3, indicating severe localized pollution. Hatirjheel Lake exhibited moderate organic pollution, with BOD ranging from

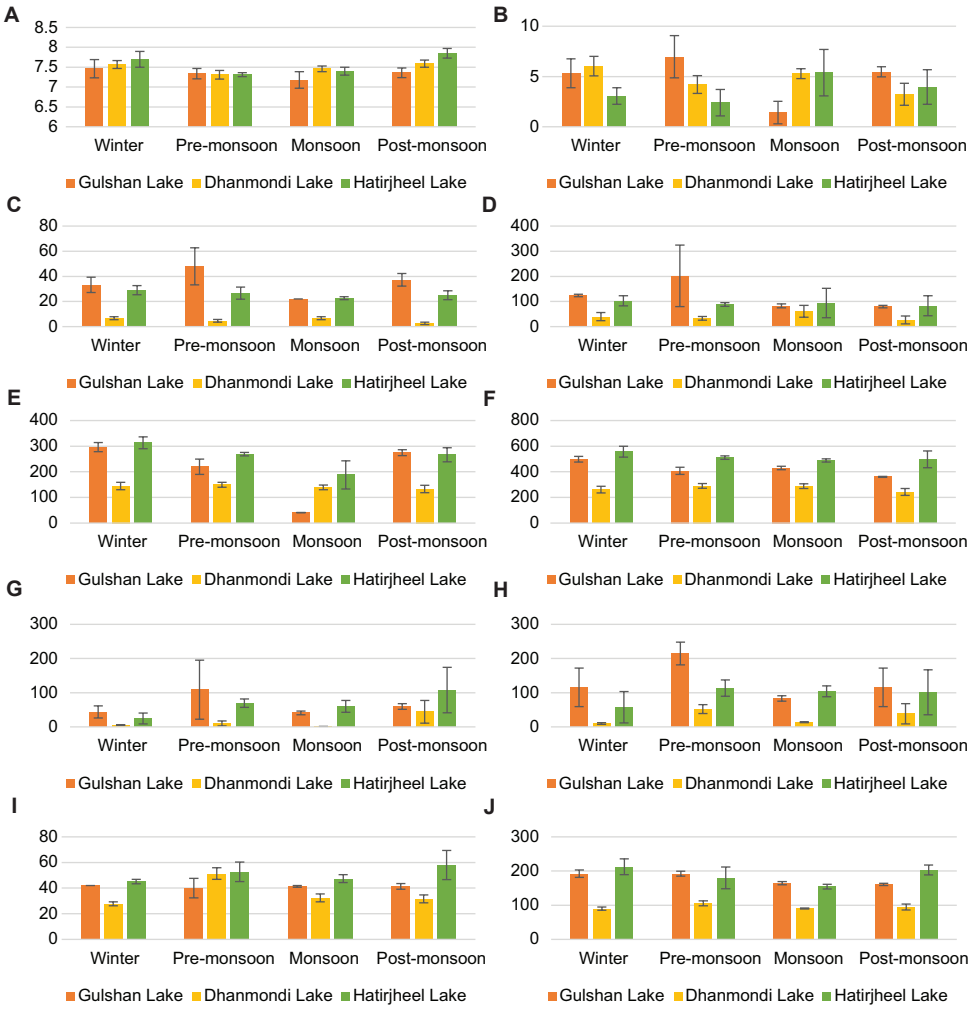

Figure 3. Water quality parameters across seasons in Gulshan, Dhanmondi, and Hatirjheel Lakes. (A) pH, (B) DO, (C) BOD, (D) COD, (E) TDS, (F) EC, (G) Turbidity, (H) SS, (I) chloride, and (J) alkalinity.
Abbreviations: BOD: Biochemical oxygen demand; COD: Chemical oxygen demand; DO: Dissolved oxygen; EC: Electrical conductivity; SS: Suspended solids; TDS: Total dissolved solids.

22.67 to 29 mg/L and COD from 83.33 to 103 mg/L. The coefficients of variation for BOD and COD were significantly high during pre-monsoon (79.52% and 93.24% respectively), as shown in Table 6, reflecting substantial temporal variability in organic loading.

TDSs and EC showed significant lake effects ($F = 27.51$, $p<0.001$ and $F = 64.28$, $p<0.001$, respectively) and seasonal variation ($F = 45.23$, $p<0.001$ and $F = 6.45$, $p<0.01$, respectively) (Table 5). Hatirjheel Lake recorded the highest TDS and EC levels (Figure 3E and F), with TDS peaking at 313 mg/L and EC at 556.7 µmhos/cm during monsoon dilution. Gulshan Lake also exhibited elevated values, particularly during the monsoon season. The coefficient of variation for TDS during monsoon reached 94.47% (Table 6), indicating substantial dilution-driven variability. Dhanmondi Lake consistently reported the lowest TDS (132.6–149.3 mg/L) and EC (243–289.7 µmhos/cm), suggesting less ionic load.

Turbidity and SS demonstrated significant lake-season interactions (turbidity: $F = 3.42$, $p<0.01$; SS: $F = 2.76$, $p<0.05$) (Table 5), indicating that seasonal patterns varied among lakes. Dhanmondi Lake maintained relatively clear water, with turbidity ranging from 1.67 to 44.33 NTU and SS between 10 and 52 mg/L. In comparison, Gulshan and Hatirjheel Lakes showed higher and more variable values. Gulshan's turbidity peaked at 108.6 NTU in the pre-monsoon season, while Hatirjheel's highest turbidity (107.7 NTU) was recorded in the post-monsoon season. Extreme values were observed at Gulshan Station S_3, where turbidity reached 208 NTU, and SS hit 253 mg/L

during the pre-monsoon period (Figure 3G and H). The coefficient of variation for turbidity reached 105.1% during pre-monsoon (Table 6), the highest variability observed among all parameters.

Chloride and alkalinity levels further showed significant lake effects (F = 19.87, p<0.001 and F = 87.34, p<0.001, respectively) with moderate seasonal variations (Table 5). Hatirjheel recorded the highest average chloride concentration at 58 mg/L during the post-monsoon, followed by Gulshan, which maintained average values between 40 and 42 mg/L. Dhanmondi Lake exhibited lower chloride levels, ranging from 27.67 to 51.33 mg/L. In terms of alkalinity, both Gulshan and Hatirjheel Lakes displayed higher values (160.7–212.7 mg/L), while Dhanmondi ranged from 90 to 105.7 mg/L (Figure 3I and J), indicating different buffering capacities among the lakes. The coefficients of variation for chloride and alkalinity remained moderate (13.46–27.61% and 24.82–29.87%, respectively) as shown in Table 6, suggesting relatively stable chemical characteristics across seasons.

Principal component analysis explained 65.8% of total variance, with Dimension 1 (50.6%) primarily loaded by BOD (0.87), COD (0.91), and SS (0.78), representing organic matter dynamics. In comparison, Dimension 2 (15.2%) showed strong loadings from TDS (0.92), EC (0.94), and chloride (0.76), indicating ionic composition variations (Figure 4A). The clear separation of lakes along Dimension 1 positioned Gulshan and Hatirjheel Lakes with positive scores (high organic matter indicators), while Dhanmondi Lake clustered with negative scores, indicating better water quality conditions (Figure 4B).

4. Discussion

This study reveals essential seasonal and spatial variations in water quality across Gulshan, Dhanmondi, and Hatirjheel Lakes. A comprehensive comparison of the observed parameters with EQS (Table 7) and findings from previous studies clarifies the current pollution status and potential causes of degradation in these vital urban water bodies.

The pH values across all three lakes consistently ranged between 6.6 and 7.7 (Tables 2-4), falling well within the EQS for fisheries (6.0–9.0) and industrial standards (6.5–8.5) (Table 7). This pH is stable to an extent, as observed in previous studies,[10,17,28,36] which suggests that despite changes in other parameters, the acid-base status of these lakes has remained stable, probably due to their natural buffering capacity.

DO concentrations, however, showed significant seasonal and spatial variations, highlighting critical differences in lake health (Figure 3B). Dhanmondi Lake maintained consistently healthy DO levels, averaging above 5 mg/L in all seasons except post-monsoon (3.23 mg/L) (Table 3), thereby generally meeting the EQS for fisheries (Table 7). In contrast, the Gulshan and Hatirjheel Lakes frequently recorded critically low DO values, particularly during the monsoon and winter seasons. For instance, Gulshan Lake's average monsoon DO plummeted to 1.41 mg/L, with an alarming low of 0.12 mg/L at station S_1 (Table 2), far below the 5 mg/L fisheries standards (Table 7). Similarly, Hatirjheel Lake's DO averaged only 3.06 mg/L in winter and 2.4 mg/L in pre-monsoon (Table 4), indicating

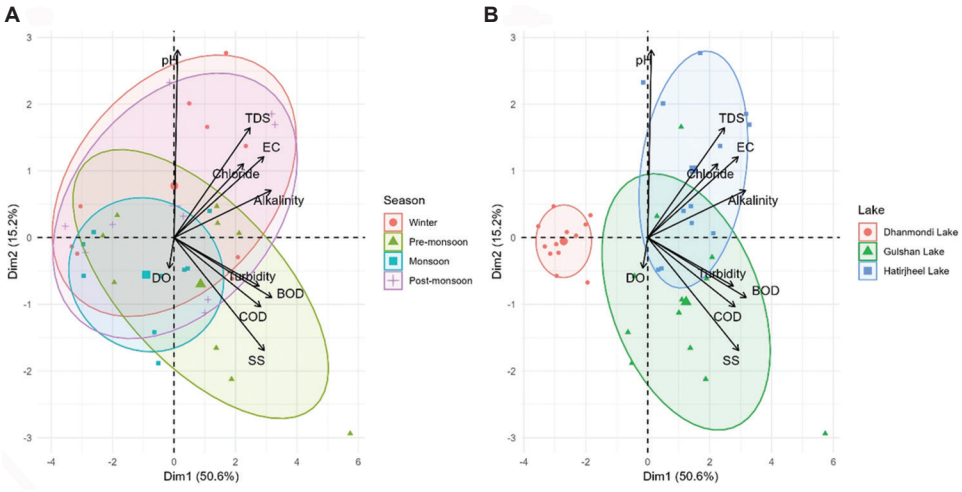

Figure 4. Principal component analysis of water quality parameters. (A) Variable loadings showing parameter contributions and (B) sample scores showing lake separation.
Abbreviations: BOD: Biochemical oxygen demand; COD: Chemical oxygen demand; DO: Dissolved oxygen; EC: Electrical conductivity; SS: Suspended solids; TDS: Total dissolved solids.

Table 7. Environmental Quality Standard for water quality parameters

Parameter	Fisheries	Industrial use	Treated wastewater
pH	6.0–9.0	6.5–8.5	-
Dissolved oxygen	≥5 mg/L	-	-
Biochemical oxygen demand	≤6 mg/L	≤30 mg/L	-
Chemical oxygen demand	≤50 mg/L	≤200 mg/L	-
Total dissolved solids	≤1000 mg/L	-	-
Turbidity	-	-	≤10 NTU
Chloride	-	-	150–600 mg/L
Suspended solids	-	-	≤100 mg/L
Alkalinity	-	-	≤150 mg/L
Electrical conductivity	-	-	≤1200 µmhos/cm

Source: Surface and Ground Water Quality Report 2022.[10]

severe oxygen depletion. These findings align with Uddin *et al.*,[37] who reported severe DO depletion in Gulshan Lake due to untreated sewage discharge. Previous studies[9,38] observed DO levels below 2 mg/L in Hatirjheel during dry seasons. Such low DO values are primarily attributed to high organic loading, limited aeration, and potential stratification effects during specific seasons.

The BOD values further underscore the varying pollution loads. Gulshan Lake consistently exhibited excessive BOD, with averages ranging from 33.33 mg/L in winter to 48 mg/L in pre-monsoon (Table 2), significantly exceeding both the EQS for fisheries (≤6 mg/L) and industrial effluent standards (≤30 mg/L) (Table 7). Hatirjheel Lake also showed elevated BOD, averaging between 22.67 mg/L and 29 mg/L, thus exceeding the fisheries standard but generally remaining below the industrial threshold (Table 7). In sharp contrast, Dhanmondi Lake's BOD was consistently low, averaging between 2.5 mg/L and 6.67 mg/L, consistently meeting the fisheries standard across all seasons. This clear distinction suggests more effective management and fewer direct pollution sources in Dhanmondi Lake.[6] Uddin *et al.*[37] reported similar high BOD trends in Gulshan, while Peeters and Shannon[31] noted that Hatirjheel's proximity to stormwater drains increased organic matter accumulation, explaining its moderate pollution.

COD values mirrored the BOD trends, indicating the extent of chemical contamination (Figure 3C and D). Gulshan Lake's COD values were alarmingly high, peaking at an average of 202 mg/L in pre-monsoon (Table 6), with an individual reading of 343 mg/L at station S_3 (Table 2), far exceeding both the EQS for fisheries (≤50 mg/L) and industrial discharge (≤200 mg/L). Hatirjheel Lake's COD ranged from 82.67 mg/L to 103 mg/L, crossing the fisheries threshold but generally remaining within industrial limits (Table 7). Dhanmondi Lake consistently showed the lowest COD levels, averaging between 27 mg/L and 61 mg/L, thereby meeting both standards across all seasons. These findings align with previous studies[9,38,39] that identified industrial effluents and residential wastewater as primary contributors to COD in Gulshan and Hatirjheel. Dhanmondi's lower values likely result from fewer direct inflow sources and better containment measures.

Regarding TDS and EC, levels across all lakes were generally below the EQS for fisheries (≤1000 mg/L for TDS and ≤1200 µmhos/cm for EC) (Table 7). However, Hatirjheel and Gulshan Lakes occasionally showed elevated TDS values, exceeding 300 mg/L (Hatirjheel's average was 313 mg/L in winter, and Gulshan's average was 296 mg/L in winter), suggesting moderate pollution from urban runoff. EC values, while within acceptable limits, were highest in Hatirjheel (average 556.7 µmhos/cm in winter) and Gulshan (average 498 µmhos/cm in winter), consistent with higher dissolved solids (Figure 3E and F). Previous studies[10,40] also found similar EC ranges, supporting these findings.

Turbidity and SS were significant concerns for Gulshan and Hatirjheel lakes (Figure 3G and H). Turbidity values in Gulshan (average up to 108.6 NTU in pre-monsoon, with an individual high of 208 NTU at S_3) and Hatirjheel (average up to 107.7 NTU in post-monsoon) substantially exceeded the EQS for treated wastewater (10 NTU). In contrast, Dhanmondi Lake consistently maintained low turbidity, generally within or just above this limit (average 1.67–44.33 NTU). Similarly, SS concentrations in Gulshan and Hatirjheel frequently surpassed the EQS limit of 100 mg/L, with values reaching an average of 214.7 mg/L in Gulshan during pre-monsoon (Table 7) and an individual high of 253 mg/L at Gulshan's sampling station S_3 (Table 2). Dhanmondi Lake's SS values were consistently below the standard (average 10–52 mg/L) (Table 3). These elevated values correspond with the study of Uddin *et al.*,[37] who reported on solid waste dumping and construction runoff near Gulshan Lake. Rain-induced sediment resuspension during the monsoon likely explains the turbidity peaks observed in these lakes.

Chloride concentrations in all lakes remained below the EQS limit for treated wastewater (150–600 mg/L) (Figure 3I), though Hatirjheel showed slightly higher average values (up to 58 mg/L in post-monsoon). Alkalinity levels, however, exceeded the 150 mg/L standard in some stations of Gulshan (average 192–192.3 mg/L, with a maximum of 212.7 mg/L in winter) and Hatirjheel (average 180–212.7 mg/L), suggesting influence from

detergents, cleaning agents, or leachates. This aligns with previous studies,[9,29,41] which attributed the high alkalinity observed in Gulshan to the input of household wastewater.

The overall comparison of the water quality parameters from Gulshan, Dhanmondi, and Hatirjheel Lakes with the EQS reveals that Gulshan and Hatirjheel Lakes are generally under significant environmental stress and are not ecologically healthy. DO levels in these two lakes frequently fall below the minimum fisheries standard of 5 mg/L, especially during the monsoon season, indicating poor oxygen availability that severely threatens aquatic life. BOD and COD values in Gulshan Lake often exceed both fisheries and industrial limits, signaling substantial organic and chemical pollution. Turbidity and SSs in Gulshan and Hatirjheel frequently exceed the EQS for treated industrial wastewater, significantly reducing water clarity and impacting habitat quality. Although the overall water quality of Dhanmondi Lake was found to be slightly better, specific parameters, such as turbidity and BOD, tend to reach or exceed permissible limits at certain times, which reflects the necessity of continuous monitoring. The elevated pollution levels, particularly in Gulshan and Hatirjheel Lakes, suggest that these water bodies are not safe for recreational use or sustainable fisheries without immediate intervention. Therefore, immediate and integrated actions, such as controlling wastewater discharge, upgrading sewage treatment facilities, and conducting regular surveillance, are necessary to recover their ecological balance and maintain public health.

5. Conclusion

This study provides a comprehensive assessment of the seasonal variations in water quality across Gulshan, Dhanmondi, and Hatirjheel Lakes, three vital urban water bodies within Dhaka city. The findings reveal significant spatial and temporal differences driven by both natural seasonal cycles and anthropogenic influences. Using standard physicochemical parameters, the study adopted a comparative and seasonal analytical approach to identify spatial and temporal trends in pollution levels. Principal component analysis indicated that 65.8% of the total variance was explained by two major dimensions: organic pollution load (BOD, COD, and SS) and ionic composition (TDS, EC, and chloride). Statistical analysis confirmed highly significant lake effects for all parameters (p<0.001), with notable seasonal variations and significant lake-season interactions for turbidity and SSs (p<0.01). Dhanmondi Lake maintained relatively stable and healthier conditions across most parameters, with low BOD (2.5–6.67 mg/L) and COD (27–61 mg/L) levels. Gulshan Lake exhibited significant organic pollution, particularly during the pre-monsoon period, accompanied by severe oxygen depletion during the monsoon (DO 1.41 mg/L). Hatirjheel Lake revealed elevated ionic content, with TDS peaking at 313 mg/L and high turbidity levels (>100 NTU), particularly during the post-monsoon period. Comparison with EQS and similar studies indicated that some parameters remained within acceptable limits, but organic pollution indicators and turbidity frequently exceeded safe thresholds, indicating environmental stress and potential public health risks. The study underscores the need for targeted lake-specific management strategies, prioritizing Gulshan Lake for organic pollution control and Hatirjheel for ionic and turbidity management. These findings provide a scientific basis for policymakers to identify pollution hotspots, allocate resources efficiently, and implement seasonally adaptive conservation measures. Biological indices, long-term and continuous monitoring accuracy, and remote sensing techniques can be combined in future research to better understand and predict water quality. As a whole, the study contributes to a developing knowledge base that is needed to better protect and manage urban aquatic ecosystems in cities, such as Dhaka.

Acknowledgments

The authors express their sincere thanks to the Department of Environment, Ministry of Forest, Environment and Climate Change, Government of the People's Republic of Bangladesh, for providing valuable secondary data through the "Surface and Ground Water Quality Report 2022." This official publication was crucial to the study, serving as a reliable and informative source for the research.

Funding

None.

Conflict of interest

The authors declare that they have no competing interests.

Author contributions

Conceptualization: Ha-mim Ebne Alam
Formal analysis: Ha-mim Ebne Alam, Md. Nizam Uddin, Md. Jahidul Hasan
Investigation: Ha-mim Ebne Alam, Kazi Tawkir Ahmed
Methodology: Ha-mim Ebne Alam, Md. Nizam Uddin
Writing–original draft: Ha-mim Ebne Alam, Kazi Tawkir Ahmed
Writing–review & editing: Md. Yeasir Arafat, Md. Jahidul Hasan

Ethics approval and consent to participate

Not applicable.

Consent for publication

Not applicable.

Availability of data

The data used in this study were obtained from the "Surface and Ground Water Quality Report 2022" published by the Department of Environment, Ministry of Forest, Environment and Climate Change, Government of the People's Republic of Bangladesh. This report is publicly available through official government channels. Any further details or access to the dataset can be obtained from the Department of Environment upon request.

References

1. Ahmed M. Water quality and pollution sources of Gulshan lake. *Int J Inf Technol Bus Manag*. 2013;16(1):78-82.
2. American Public Health Association. *Standard Methods for the Examination of Water and Wastewater*. United States: American Public Health Association; 2005.
3. Ataauzzaman M, Ali MA. Effects of combined sewer overflow on water quality: A case study of Hatirjheel Lake in Dhaka. *SN Appl Sci*. 2022;4(11):303.

   doi: 10.1007/s42452-022-05187-6
4. Bulbul Ali A, Mishra A. Effects of dissolved oxygen concentration on freshwater fish: A review. *Int J Fish Aquat Stud*. 2022;10(4):113-127.

   doi: 10.22271/fish.2022.v10.i4b.2693
5. Cosgrove WJ, Loucks DP. Water management: Current and future challenges and research directions. *Water Resour Res*. 2015;51(6):4823-4839.

   doi: 10.1002/2014WR016869
6. Das A. Geographical information system-driven intelligent surface water quality assessment for enhanced drinking and irrigation purposes in Brahmani River, Odisha (India). *Environ Monit Assess*. 2025;197(6):629.

   doi: 10.1007/s10661-025-14065-8
7. Datta S, Karmakar S, Islam MN, Karim ME, Kabir MH, Uddin J. Assessing landcover and water uses effects on water quality in a rapidly developing semi-urban coastal area of Bangladesh. *J Clean Prod*. 2022;336:130388.

   doi: 10.1016/j.jclepro.2022.130388
8. Davies-Colley R, Smith D. Turbidity suspended sediment, and water clarity: A review 1. *J Am Water Resour Assoc*. 2001;37(5):1085-1101.

   doi: 10.1111/j.1752-1688.2001.tb03624.x
9. Dawlatana M. Symposium on environmental chemistry for securing water quality. *Bangladesh J Sci Ind Res*. 2017;52:1-63.

   doi: 10.3329/bjsir.v52i5.33334
10. Department of Environment. *Surface and Ground Water Quality Report 2022*. Department of Environment, Ministry of Forest, Environment and Climate Change; 2022. p. 114-121. Available from: https://doe.gov.bd/site/publications/6cbebbc4/3494/4362/89d0/35b998457485/surface/and/ground/water/quality/report/2022 [Last accessed on 2025 Apr 04].
11. Bhateria R, Jain D. Water quality assessment of lake water: A review. *Sustain Water Resour Manage*. 2016;2(2):161-173.

    doi: 10.1007/s40899-015-0014-7
12. Faria FF, Ariyan TN, Mia MY. Trophic status analysis and nutrient source allocation in urban lakes of Dhaka, Bangladesh: A comprehensive approach to eutrophication monitoring. *Environ Monit Assess*. 2024;196(12):1252.

    doi: 10.1007/s10661-024-13419-y
13. Gazi-Khan L, Haque SE. A review of the current status of water quality and eutrophication in Dhaka′s water bodies. *Int J Sci Res Technol Manag*. 2022;10(2):1-9.

    doi: 10.18510/ijsrtm.2022.1021
14. Hasan S, Mulamoottil G. Environmental problems of Dhaka city. *Cities*. 1994;11(3):195-200.

    doi: 10.1016/0264-2751(94)90059-0
15. Hossain MI, Ansari DMNA, Saika U. Lake base urban recreation in dhaka metropolitan area: Hatirjheel lake as a potential case. *Int J Res Granthaalayah*. 2017;5(12):266-274.

    doi: 10.29121/granthaalayah.v5.i12.2017.503
16. Islam M, Rehnuma M, Tithi S, Kabir M, Sarkar L. Investigation of water quality parameters from ramna, crescent and hatirjheel Lakes in Dhaka City. *J Environ Sci Nat Resour*. 2015;8(1):1-5.

    doi: 10.3329/jesnr.v8i1.24620
17. Shah J, Sharma R, Sharma I. Study and evaluation of groundwater quality of malwa region, Punjab (North India). *J Chem Environ Sci Appl*. 2015;2(1):41-58.

    doi: 10.15415/jce.2015.21003
18. Islam R, Faysal SM, Amin MR, *et al*. Assessment of pH and total dissolved substances (TDS) in the commercially available bottled drinking water. *IOSR J Nurs Health Sci*. 2017;6(5):35-40.

    doi: 10.9790/1959-0605093540
19. Islam S, Ali Y, Kabir H, *et al*. Assessment of temporal variation of water quality parameters and the trophic state index in a subtropical water reservoir of Bangladesh. *Grassroots J Nat Resour*. 2021;4(3):164-184.

    doi: 10.33002/nr2581.6853.040313
20. Jaafar A, Thamrin MN, Megat Ali MSA, Misnan MF, Mohd Yassin AI. The influence of physico-chemical parameters to determine water quality: A review. *J Electr Electron Syst Res*.

2020;17(2020):108-113.

doi: 10.24191/jeesr.v17i1.016

21. Mamun M, Kim JY, An KG. Trophic responses of the asian reservoir to long-term seasonal and interannual dynamic monsoon. *Water*. 2020;12(7):2066.

doi: 10.3390/w12072066

22. Meride Y, Ayenew B. Drinking water quality assessment and its effects on residents health in Wondo genet campus, Ethiopia. *Environ Syst Res*. 2016;5(1):1.

doi: 10.1186/s40068-016-0053-6

23. Mohinuzzaman M, Kamruijaman M, Hossain MS, Saadat AHM. *Quality Assessment of Water and Sediment of Gulshan Lake by using*. Bangladesh: Jahangirnagar University Physics Studies; 2013. p. 19.

24. Mowla QA, Islam MS. Natural drainage system and water logging in Dhaka: Measures to address the problems. *J Bangladesh Inst Planners*. 2013;6:23-33.

doi: 10.3329/jbip.v6i1.76958

25. Niloy NM, Haque MM, Tareq SM. Characteristics, sources, and seasonal variability of dissolved organic matter (DOM) in the ganges river, Bangladesh. *Environ Process*. 2021;8(2):593-613.

doi: 10.1007/s40710-021-00499-y

26. Nowreen S. *Hatirjheel-Begunbari Lake Project Area as an Urban Tourist Destination: A Study on Residents' Perception*. Berlin: ResearchGate; 2016.

27. Pal S, Chakraborty K. Different aspects of chloride in freshwater: A review. *Int J Curr Trends Sci Technol*. 2017;7(8):20295-20303.

28. Pasha AK, Mustafa SO, Rahman SM, Abdullah M, Chowdhury MAH, Parveen M. Analysis of water quality of Hatirjheel Lake, Dhaka, Bangladesh. *Nat Environ Pollut Technol*. 2023;22(1):245-252.

doi: 10.46488/NEPT.2023.v22i01.023

29. Rahman SS, Hossain MM. Gulshan Lake, Dhaka City, Bangladesh, an onset of continuous pollution and its environmental impact: A literature review. *Sustain Water Resour Manag*. 2019;5(2):767-777.

doi: 10.1007/s40899-018-0254-4

30. Razzak NRB, Muntasir SY, Chowdhury S. Pollution scenario of Dhaka city lakes: A case study of Dhanmondi and Ramna lakes. *Glob Eng Technol Rev*. 2012;2(7):1-6.

31. Peeters S, Shannon K. Readdressing Dhaka′s Public Water Bodies: A Design Research. *NJEDP J Environ Design Plan*. 2011;7:25-46.

32. Rakib MR, Akther M, Mondol MAH, Rahaman MS. Assessing the water quality of Hatirjheel Lake of Dhaka City, Bangladesh. *Present Environ Sustain Dev*. 2024;17(2):249-262.

doi: 10.47743/pesd2023172018

33. Prestigiacomo AR, Effler SW, O'Donnell D, *et al*. Turbidity and suspended solids levels and loads in a sediment enriched stream: Implications for impacted lotic and lentic ecosystems. *Lake Reserv Manag*. 2007;23(3):231-244.

doi: 10.1080/07438140709354012

34. Sabit MI, Ali MA. Pollution of water bodies within and around Dhaka city: The case of Gulshan Lake. *J Civil Eng-IEB*. 2015;43(1):29-39.

35. Sarker B, Keya NK, Mahir IF, Nahiun MK, Shahida S, Khan AR. Surface and ground water pollution: Causes and effects of urbanization and industrialization in South Asia. *Sci Rev*. 2021;7(3):32-41.

doi: 10.32861/sr.73.32.41

36. Swapan M, Zaman A, Ahsan T, Ahmed F. Transforming Urban dichotomies and challenges of South Asian megacities: Rethinking sustainable growth of Dhaka, Bangladesh. *Urban Sci*. 2017;1(4):31.

doi: 10.3390/urbansci1040031

37. Uddin M, Kormoker T, Siddique MAB, *et al*. An overview on water quality, pollution sources, and associated ecological and human health concerns of the lake water of megacity: A case study on Dhaka city lakes in Bangladesh. *Urban Water J*. 2023;20(3):261-277.

doi: 10.1080/1573062X.2023.2169171

38. Verma S, Verma S, Ramakant R, Pandey V, Verma A. Comprehensive assessment of physico-chemical and biological parameters in water quality monitoring: A review of contaminants, indicators, and health impacts. *Int J Hortic Agric Food Sci*. 2025;9(2):10-19.

doi: 10.22161/ijhaf.9.2.2

39. World Health Organization. *Guidelines for Drinking-Water Quality*; 2011. Available from: https://iris.who.int/handle/10665/44584 [Last accessed on 2025 Jun 16].

40. Wurts WA, Durborow RM. *Interactions of pH, Carbon Dioxide, Alkalinity and Hardness in Fish Ponds*. Nepal: SRAC; 1992. p. 464.

41. Zambrano KT, Poleto C, Oliveira JN. A comparative analysis on water quality in an urban micro watershed. *Manag Environ QualInt J*. 2017;28(4):566-578.

doi: 10.1108/MEQ-07-2015-0141

ACCSCIENCE PUBLISHING

Explora: Environment and Resource

ORIGINAL RESEARCH ARTICLE

An explainable hybrid stacked deep learning framework for forecasting PM10 concentrations in urban air

Syed Azeem Inam*, Haider Rajput, and Saddam Umer

Department of Artificial Intelligence and Mathematical Sciences, Sindh Madressatul Islam University, Karachi, Sindh, Pakistan

Abstract

Accurate and explainable forecasting of particulate matter (PM10) is increasingly essential for managing urban air quality and protecting public health. This study proposed and evaluated a hybrid stacked deep learning architecture designed to enhance PM10 and urban air quality forecasting accuracy and to provide transparent explanations for its predictions. Using a self-designed neural network and Ridge regression (the meta-learner), PM10 prediction was accomplished based on LightGBM integration. Analysis was performed on the World Air Quality Index dataset, consisting of 1.8 million observations from 380 cities globally. To demonstrate its effectiveness, the hybrid model was benchmarked against traditional time series models (Autoregressive Integrated Moving Average [ARIMA] and Seasonal ARIMA) and machine learning models, including decision tree, extreme gradient boosting, random forest, and neural network, using the mean squared error (MSE), root MSE (RMSE), mean absolute error (MAE), and R^2 metrics as evaluation metrics. Model explainability was accomplished using Shapley Additive Explanations and Local Interpretable Model-Agnostic Explanations analyses. The hybrid model achieved an R^2 of 0.9916, MSE of 4.90, RMSE of 2.21, and MAE of 0.992, surpassing the other models' performances and demonstrating strong reliability. The analysis determined the seven-day PM10 lag as the most important influential predictor, while other spatial parameters contributed minimally. The model's ability to run efficiently on general-purpose computers further ensures accessibility for resource-constrained agencies. Overall, this study demonstrates the high predictive accuracy and interpretability of the proposed hybrid framework, offering a practical and informative tool for policymakers to improve air quality and public health outcomes.

Keywords: Hybrid stacked model; Air quality; LightGBM; PM10; Shapley Additive Explanations; Local Interpretable Model-Agnostic Explanations

***Corresponding author:**
Syed Azeem Inam
(syed.azeem@smiu.edu.pk)

Citation: Inam SA, Rajput H, Umer S. An explainable hybrid stacked deep learning framework for forecasting PM10 concentrations in urban air. *Explora Environ Resour.* 2025;2(4):025380069. doi: 10.36922/EER025380069

Received: September 14, 2025

Revised: October 16, 2025

Accepted: November 10, 2025

Published online: November 27, 2025

1. Introduction

Addressing public health, policy development, and air quality monitoring, particulate matter (PM) prediction has gained prominence and captured the interest of academic and applied scientists.[1,2] Growing concerns stem from the ease with which PM can penetrate the human respiratory system, leading to long-term health issues. The inhalation of particulates is strongly correlated with increasing rates of respiratory

failure, cardiovascular decline, asthma, lung cancer, and chronic bronchitis.[3] Rising urbanization and unchecked industrial growth exacerbate the problem, contributing to elevated PM concentrations across metropolitan regions. This trend affirms the necessity of sophisticated analytical prediction tools capable of forecasting PM levels and guiding effective mitigation strategies.

Predictive analytics help recognize and forecast pollution events, enabling the targeted allocation of resources to minimize public health risks. This has to be done with specific predictive models that inform regulations, establish international standards, identify sensitive monitoring regions, and support the implementation of cost-effective public health schemes at the appropriate time to reduce pollution.[4]

Traditional air quality forecasting approaches have illuminated the value of statistical and deterministic models, particularly through linear regression and time series methods, alongside remaining frameworks deployed to provide baseline insights and real-time alerts.[5] However, these approaches disallow the forecasting of linear, static, and homogenous growth, while presuming the existence of boundaries within error variance, creating boundaries to the intricacy and randomness of the shifting atmospheric conditions.[6] Consequently, they often fail to accurately estimate the effects of complex and fluctuating emissions from various human activities, varying forecasting intervals, uneven human-made weather conditions, and the spatiotemporal conjunction of intervals. This limitation is particularly pronounced in sprawling hot zones over cities.

Therefore, there is increasing demand for more flexible and robust models that better capture the drivers of air pollution episodes and their non-linear behavior.[5,6] In recent years, many scholars and researchers have leaned toward the prowess of modern developments in machine learning (ML), and more recently, deep learning, which excel at discovering complex non-linear facets in massive datasets.[7] These approaches are in sharp contrast to those deployed in the past, which worked best with changes to the system and parameters. The modern models are more likely to provide sharper forecasts by adapting to evolving environmental factors that typically define domain boundaries.

Despite the continuing importance of classic algorithms, such as support vector machines (SVM) and random forest (RF), the gradient-boosted family of algorithms, in particular the light gradient boosting machine (LightGBM) and tailor-made neural networks (NNs), has emerged as perhaps the most profound innovations in the field.[8]

Many custom NNs have employed deep learning to improve analysis on complex time-series datasets, especially when paired with complex structures. Such models excel at untangling the deep-seated non-linear and sequential patterns that characterize long-term environmental records.[1] By separating spatiotemporal features into individual units, these models, such as Recurrent NN (RNN) and attention-based models, effectively process time-based data. The resulting dataset captures daily fluctuations, seasonal patterns, and the combined influences of meteorological conditions, emissions, and geographical factors on PM10 concentration variations.

Hence, combining LightGBM with a custom-built NN forms an unprecedented hybrid approach that synergistically leverages the advantages of both models. The LightGBM model accelerates the interaction among mixed data types, while the neural layers grasp more profound and complex spatiotemporal patterns.[1,6,8] This combined architecture monitors persistent patterns and momentary surges in pollutant concentrations, protects against the overfitting that one or the other component usually suffers from, reduces prediction errors, and enhances stability amid environmental changes or added noise.[5,7] More importantly, the integrated system provides richer, more accurate, and more robust predictions, fulfilling the high standards of contemporary PM10 monitoring.[6,7]

Given the impact that PM10 predictions may have on public health and air quality policies, PM10 modeling is no longer optional. To explain the complex behavior of advanced ML and deep learning models, it is now common for researchers to use Shapley Additive exPlanations (SHAP) and Local Interpretable Model-agnostic Explanations (LIME). SHAP, grounded in cooperative game theory, helps identify which features (e.g., wind speed and temperature) contribute most to PM10 predictions, revealing the dominant factors controlling atmospheric PM10 levels and their interactions.[9] In contrast, LIME provides explanations focused on individual predictions, highlighting the specific features driving the model's output for a single observation. These approaches enhance prompt responses on a case-by-case basis.[8] Together, they not only enhance overall model transparency and build user trust but also enable routine debugging by revealing hidden biases, informing iterative improvements by flagging blame misallocations, and directing researchers to parameters that need adjustment.[7]

This work develops and validates a hybrid model for short-term forecasting of airborne PM10 levels, combining LightGBM with a custom NN specifically focused on urban areas. During this process, specific attention is

paid to areas with heavy traffic, high urbanization, and PM10 concentrations exceeding health-based guidelines, enabling precise and timely predictions vital for planning and mitigation. The model is also interpretable because it is integrated with *post hoc* tools, such as SHAP and LIME, which improve explanation-based reasoning, enabling stakeholders to access actionable recommendations. These reasons, alongside improving model ease, accuracy, and transparency, motivate this work to protect public health in urban centers globally.

2. Literature review

Recent advancements in artificial intelligence (AI) techniques have redefined air quality modeling by shifting the field from traditional rule-based approaches to more adaptive, data-centric systems.[10-13] Such a paradigm shift is aptly demonstrated by the ever-increasing accuracy of PM10 forecasts, which is a vital metric for urban health assessment. In this section, we review a spectrum of PM10 forecasting methods, comparing classical regressors with contemporary ML models. We delineate the advantages of competing approaches, such as LightGBM, deep NNs (DNNs), and advocate for a transparent stacked model that integrates these strengths while employing SHAP and LIME to elucidate the opacity of prediction.[14]

The use of linear regression, decision trees (DT), and RFs, which have traditionally been utilized to predict PM10 and other air quality metrics, is outdated.[15] Such static methods that are encapsulated by posited equations are prone to failures when used with non-linear and highly interrelated time-series data, as well as spatiotemporally overlapping time-series data. By contrast, more recent ML techniques are more accurate and more robust in handling these complexities. However, these gains come with additional hurdles, such as the requirement to process model reasoning behind forecasts and the massive computational resources needed to train deep networks on extensive datasets.[16]

Recent studies have focused on implementing various ML models for PM10 forecasting. Kujawska *et al*.[17] concluded that SVM, artificial NNs, and Kriging models effectively capture non-linear relationships between meteorological parameters and pollution concentrations. Similarly, Lei *et al*.[18] utilized ensemble methods based on DTs and reported comparable predictive improvements. Furthermore, hybrid deep learning architectures that usually amalgamate RNNs and convolutional NNs have proven effective in separating temporal lags from spatial gradients in convolutively structured air quality time series.[23] While SVMs excel at resolving complex boundaries and RFs mitigate overfitting, each method has limitations, such as sensitivity to kernel tuning and long learning times typical of NNs.[17-20]

Within the realm of environmental science, LightGBM is one of the fastest-growing algorithms due to its high speed, ease of training on large datasets, and scalability.[24] It consistently outperforms predecessors, such as extreme gradient boosting (XGB) and RFs by effectively capturing sophisticated non-linear relationships between environmental and socio-economic factors, while achieving superior speed and accuracy.[18] LightGBM's computational efficiency is one of the main reasons it is used for near-real-time air quality forecasting and management applications.[16] NNs, such as DNNs, convolutional NNs, and RNNs, are also used in environmental forecasting to address the extreme non-linearity and time-variance of PM10 concentrations.[19] Long short-term memory (LSTM), an example of RNNs, is extremely valuable for time series applications due to its ability to process sequential data. Although custom-built models often incorporate spatial and meteorological information, they need large training datasets and, without sufficient regularization, remain vulnerable to overfitting.[21]

New developments in ensemble learning have made it possible to develop hybrid models that combine LightGBM's fast, gradient-boosted tree mechanics with the deep non-linear feature extraction power of NNs.[19] LightGBM is typically the first-level learner, identifying basic patterns and interaction effects in data, while the NN layer further refines predictions by learning complex, time-variable patterns.[22] This architecture enhances the speed and scalability of LightGBM on structured data and leverages the NN's ability to trend and model non-stationary time series.

Stacked models applied across finance, energy, and transportation domains have demonstrated greater generalizability, robustness to out-of-sample data, and an improved balance between performance and explainability—an important but often neglected aspect in model evaluation.[19] Explainability becomes increasingly paramount given the growing complexity of modern ML systems used in environmental monitoring and other critical domains. For example, SHAP and LIME provide valuable insights by quantifying the contribution of individual features to predictions. SHAP allocates consistent, mathematically justified scores indicating how much each input contributes to a given output, while LIME builds ephemeral, simpler predictive models to justify a given decision. Using these techniques in conjunction with leading models, such as LightGBM and NNs, enhances trust in model decisions, supporting more transparent and responsible environmental policy-making, from

researchers to policymakers, and ultimately fostering better-informed, sustainable decisions.[23]

Most literature these days examines novel individual or ensemble models; however, few adopt a bottom-up hybrid that integrates LightGBM with a custom NN architecture. In addition, lattice models, which offer crucial in-practice transparency, have received limited attention. This research aims to address this gap by constructing a stacked hybrid architecture that combines LightGBM's computational speed with the temporal awareness of a custom NN. The model incorporates SHAP and LIME from the explainable AI (XAI) toolbox to rationalize predictions, thereby improving model fidelity and trust.

3. Methodology

3.1. Data description

The present study utilized the World Air Quality Index (WAQI) dataset to forecast the concentration of PM10 using ML and deep learning techniques. This dataset is authentic and updated thrice daily, covering approximately 380 cities worldwide. It comprises 1,798,600 records and features nine attributes, that is, country, city, date, species, count, minimum, maximum, median, and variance. The feature of distinct pollutants further extends to specific pollutants. Also, the species attribute contains the Air Quality Index (AQI), dew, humidity, precipitation, pressure, PM1, PM2.5, and PM10 (Figure 1).

In this study, values of PM10 were considered for prediction, whereas the median attribute was selected as the target variable. To further demonstrate the characteristics of the WAQI dataset, Figures 2 and 3 present the geographical coverage of PM10 concentration and its average across countries and cities.

3.2. Data preparation and preprocessing

To ensure quality and consistency, the study considered only the relevant features of dates, location, and pollutant values. The date strings were converted to date–time objects, and the dataset was further restricted to PM10. Lag features captured trends and temporal dependencies, providing the PM10 concentration values from previous days. Seven lag features were generated, representing PM10 levels from the past seven days. In addition, two rolling averages were computed, that is, a 7-day rolling average and a 30-day rolling average. The rolling averages helped smooth out short-term fluctuations and highlighted long-term trends. This enabled the model to identify patterns in PM10 concentrations over weekly and monthly periods.

Categorical features, namely, country and city, were encoded using the target encoding technique by replacing each categorical value with the mean of the target variable, that is, the value of PM10, in our case, for that category. This encoding method, being memory efficient, enabled the model to capture the relationship between categorical features and target variables effectively. The dataset was split into training and testing subsets in an 80:20 ratio, with 80% of the data utilized for training the models and 20% for testing the models under different evaluation metrics.

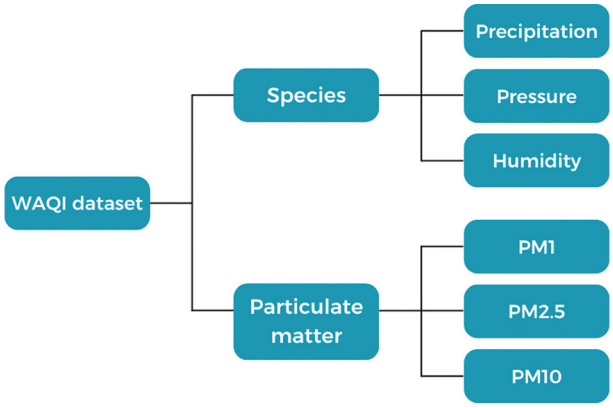

Figure 1. Features of species in the World Air Quality Index dataset

The selection of features was conducted in collaboration with domain experts and validated with algorithms. Redundant features were removed through initial correlation analysis and subsequent variance inflation factor analysis. Temporal and meteorological predictors were then validated with LightGBM's feature importance ranking. All numeric features were normalized through Min–Max scaling to prepare the data for the NN and enhance convergence and stability during training. This preprocessing made the model's parameters accurate and relevant to the environment, ensuring the approach was transparent and replicable.

3.3. Model architecture

As illustrated in Figure 4, our hybrid stacked modeling strategy combines three complementary elements to enhance predictive accuracy and protect the system from overfitting.

LightGBM is used as the primary regressor due to its efficiency on structured data and its ability to expose complex feature interactions when boosted using gradient methods. After the model was constructed, a broad grid search was performed to calculate appropriate configuration benchmarks by testing different values for the learning rate, tree depth, and levels of regularization. This base learner can identify the most prominent patterns in structured data; however, more intricate patterns, particularly those involving non-linear data in real-

Figure 2. Geographical coverage of PM10 across (A) countries and (B) cities according to the World Air Quality Index dataset accessed on [December, 2024]. Map reprinted from Microsoft PowerBI[Microsoft Corporation.]

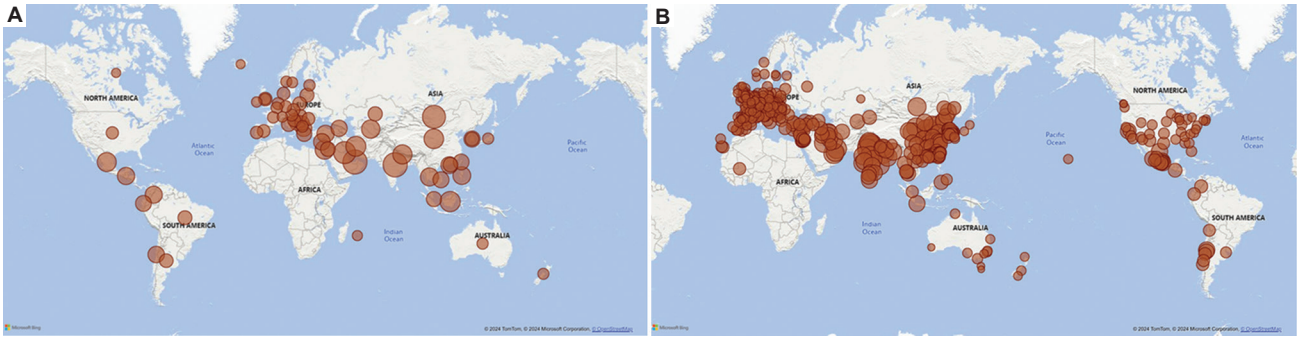

Figure 3. Average of PM10 by (A) country and (B) city according to the World Air Quality Index dataset accessed on [December, 2024]. Map reprinted from Microsoft PowerBI[Microsoft Corporation.]

world scenarios, are often left uncovered. This problem was addressed with the introduction of a framework for residual learning.

In this framework, a DNN is used for learning from the prediction mistakes resulting from the LightGBM regressor's residuals. This network, which acts as the bottom half of the model, is complemented by the base model and receives normalized feature vectors and features compatible with the base model input layer. Its skeleton consists of three densely connected hidden layers. Each hidden layer is succeeded by a fixed rate of batch normalization to moderate internal covariate shift and dropout regularization, set at 25% to avoid overfitting. At the same time, the layers are also interspersed with rectified linear unit (ReLU) activations for non-linear control. These controls assist the network in capturing and forming intricate patterns of residuals that conventional tree learners otherwise ignore.

A single linear neuron in the output layer is used for final residual corrections. The whole pipeline is then optimized in a single pass using the Adam optimizer, number of epochs learning rate policies, and mean squared error (MSE) loss. This architecture relies on the NN's universality to shift and correct all systemic biases beyond the initial LightGBM forecasts. The final step in the pipeline merges predictions from both modeling branches using a stacking ensemble. For example, in Level-1, the raw LightGBM forecasts and the residual-corrected values, defined as LightGBM predictions with corrections by the NN, are combined to form a richer feature set that captures complementary signals. These enhanced predictions are then forwarded to a Ridge regression meta-model, which reduces the multicollinearity among the base predictors and variances, as its L2 regularization is believed to achieve this goal. Using matrix algebra, the meta-learner uses the ridge regression method to compute optimal weights for each base predictor in a standard closed form. The weights are adjusted automatically with respect to validation performance. Table 1 details the parameters of the hybrid stacked model proposed in this study.

The NN was deliberately shaped for PM10 forecasting rather than adapted from a generic regression template. Its residual design corrects for the non-linear errors left by LightGBM, and each dense layer is followed by batch normalization and dropout to stabilize learning and avoid overfitting on noisy atmospheric data. ReLU activations help the model generalize across seasonal shifts, while the Adam optimizer ensures adaptive convergence. The

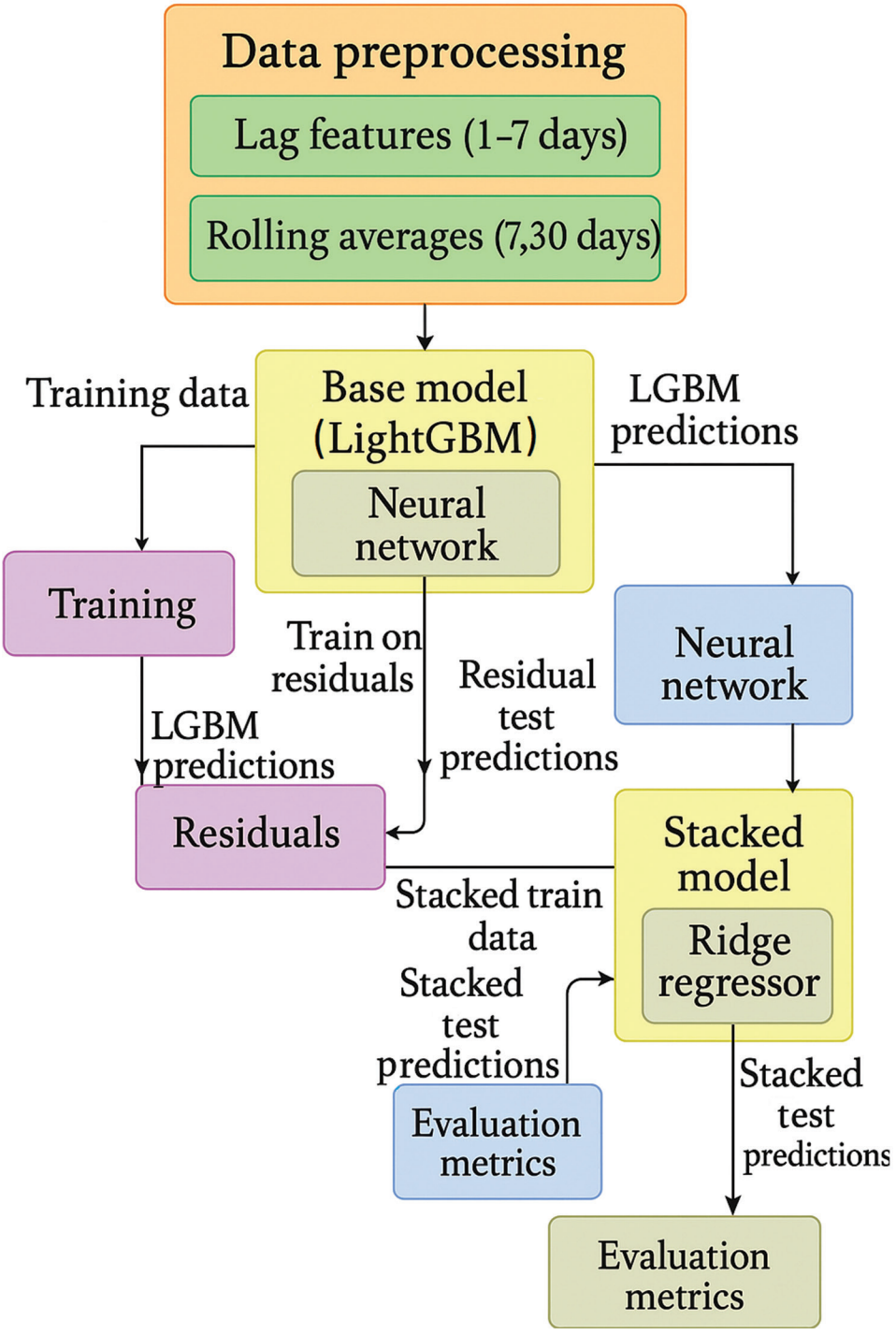

Figure 4. Proposed hybrid stacked model architecture

Ridge meta-learner integrates the outputs by assigning optimal weights through L2 regularization, reducing the effect of multicollinearity between the LightGBM and NN predictions. This configuration generates smoother and more generalizable forecasts without the instability often seen in kernel or tree-based meta-models. This stacked architecture, therefore, leverages transparent feature attribution of LightGBM, the NN's flexibility in capturing non-linear errors, and Ridges' robustness when working with multiple correlated inputs. The combined model

demonstrates superior generalization compared to any single component and consistently outperforms baseline benchmarks across a wide range of public datasets. The pseudocode of our proposed hybrid stacked model is presented in Pseudocode 1.

3.4. Model interpretability

To promote transparency and confidence in our prediction pipeline, the study conducted an in-depth interpretability assessment grounded in leading XAI techniques of SHAP and LIME. Here, SHAP applies concepts from cooperative game theory to produce a consistent global ranking of feature importance. By computing Shapley values for each observation, the method reveals how much each feature contributes to a prediction above or below the mean, thereby clarifying model behavior across the entire dataset. Meanwhile, LIME examines a single prediction at a time. It perturbs the input, fits a simple linear model around the point of interest, and uses the linear coefficients to indicate which features are most significant for that case. This local lens perfectly complements the broader overview of the SHAP analysis.

3.5. Evaluation methodology

A thorough evaluation of each aspect of the forecasting model was performed using a set of arbitrary statistical metrics concerned with the model's predictive capability and the decision model's required dimensions concerning the environment. The R^2 score, which is referred to as the coefficient of determination, for example, measures the extent to which the model identifies the total variation in the set of air-quality readings and quantifies the extent to which it offers explainable pieces of information. R^2 is a primitive of the model in the sense that all models are

Table 1. Details of the hybrid stacked model parameters

Component	Parameter	Value/Configuration
LightGBM (base model)	Learning rate	0.1
	Maximum depth	7
	No. of estimators	300
	No. of leaves	31
	Sub-sample	0.8
Residual neural network	Layer 1	Dense (256, Activation="relu")
	Layer 2	BatchNormalization()
	Layer 3	Dropout (0.2)
	Layer 4	Dense (128, Activation="relu")
	Layer 5	Dropout (0.1)
	Layer 6	Dense (64, Activation="relu")
	Output layer	Dense (1)
	Optimizer	Adam
	Loss function	Mean squared error (MSE)
	Metrics	Root MSE (RMSE), mean absolute error (MAE), R^2 score
	Batch size	256
	Epochs	100 (with early stopping)
	Early stopping	Patience=10, Monitor = "val_loss," restore_best_weights
	Validation split	0.2
Ridge (meta-model)	Alpha	1.0

Pseudocode 1. Proposed hybrid stacked neural network

Function: Residual stacking model
Input: Preprocessed dataset (features and target)
Output: Trained models and evaluation metrics

Start
1. Data preparation:
1.1. Separate features (X) and target (y)
1.2. Split data into train/test sets (70% train, 30% test)
1.3. Scale features using MinMaxScaler

2. Train base model (LightGBM):
2.1. Initialize LGBMRegressor with parameters:
learning_rate: 0.1
max_depth: 7
n_estimators: 300
num_leaves: 31
subsample: 0.8
2.2. Fit model on training data
2.3. Generate predictions for train/test sets

3. Residual learning:
3.1. Calculate residuals (true - predicted) on the training set
3.2. Build a residual neural network architecture:
Input Layer: (features_dimension,)
Dense (256, ReLU) → BatchNorm → Dropout (0.2)
Dense (128, ReLU) → Dropout (0.1)
Dense (64, ReLU)
Output: Dense (1)
3.3. Compile model with:
Optimizer: Adam
Loss: MSE
Metrics: RMSE, MAE, R²
3.4. Set early stopping (patience=10, monitor val_loss)
3.5. Train model on scaled features and residuals
3.6. Generate residual predictions for the test set
3.7. Create final residual-corrected predictions (LightGBM + NN residuals)

4. Model stacking:
4.1. Create stacking dataset:
Train: [LightGBM_pred, Residual_corrected_pred]
Test: [LightGBM_pred, Residual_corrected_pred]
4.2. Initialize Ridge regression meta-model (alpha=1.0)
4.3. Train meta-model on stacking dataset
4.4. Generate final stacked predictions

5. Evaluation:
5.1. For each model (LightGBM, Residual-corrected, Stacked):
Calculate R², MSE, RMSE, and MAE
Print evaluation metrics
End

ranked from 0 to 1, with 0 meaning that the model does not explain anything above the model's sample average, and 1 meaning that the model absolutely predicts the data; anything negative means the model is performing worse than just using the mean. The R^2 score, within the context of atmospheric pollution, suggests the effectiveness of a framework in tracking how the system copes with the complex shifts of air, emissions, and the weather. In addition, root MSE (RMSE) is the next benchmark concerned with the forecasting precision. It takes the mean of the difference squared, then takes the root. Moreover, it is a primitive of the original set. Spacing, air quality, and pollution models all rely on RMSE for decision-making, particularly when assessing the predictive range of a model. Gaps within these ranges may indicate failures to capture peak pollutant concentrations, especially those exceeding critical thresholds. Such missed or underestimated peaks can lead to unforeseen public health risks.

The values of RMSE directly address regulators and community members, as they are measured in micrograms per cubic meter, enabling straightforward comparison with legal thresholds. On the other hand, the mean absolute error (MAE) measures forecasting precision by averaging the absolute values of all prediction errors. It describes model accuracy without considering the direction of errors. Therefore, MAE provides a robust daily model performance snapshot. It is useful for assessing average overestimation, which is often critical for decision-makers. In practice, MAE can support dynamically managed resource allocation models, ensuring that responses to pollution escalations remain predictable, budget-conscious, and within an acceptable error margin.

Table 2. Experimental models and results

S. No.	Algorithm	MSE	RMSE	MAE	R^2
1	LightGBM+neural network (hybrid stacked model)	4.90	2.21	0.91	0.9916
2	Multi-layer perceptron (MLP\ FCNN)	9.77	2.85	1.82	0.9862
3	XGB regressor	18.21	4.27	1.30	0.9689
4	Random forest regressor (RFR)	20.91	4.57	1.08	0.9643
5	Extra trees regressor (ETR)	35.75	5.98	1.82	0.9390
6	Decision tree regressor (DTR)	63.73	7.98	2.22	0.8913
7	ARIMA	886.11	29.77	15.13	−0.1906
8	SARIMA	887.05	29.78	15.14	−0.1918

Abbreviations: ARIMA: Autoregressive Integrated Moving Average; FCNN: Fully connected neural network; MAE: mean absolute error; MSE: Mean squared error; RMSE: Root mean squared error; SARIMA: Seasonal Autoregressive Integrated Moving Average; XGB: Extreme gradient boosting.

The MSE summarizes all deviations by employing a squared-average method, focusing more on larger errors. This property makes MSE a valuable measure of dispersion in model predictions and a standard loss function in deep learning, where optimizers minimize it to avoid expensive, large-magnitude prediction errors. During critical pollution events, such as concentration spikes, this heightened sensitivity to large deviations acts as an additional security for public health decision-making. Together, these four metrics form a self-reinforcing evaluation system. R^2 measures the model's explanatory power, RMSE acts as a guardrail against overly optimistic under-predictions, MAE conveys expected day-to-day accuracy, and MSE informs system optimization through iterative design. Using all four ensures consistent system reliability across routine assessments, intermediate validations, and high-alert preparedness evaluations.

4. Results

4.1. Comparative evaluation of regression models

To evaluate the predictive quality of the eight regression procedures, four summary statistics, that is, MSE, RMSE, MAE, and R^2, were measured. Together, all these metrics represented the model's error size, error symmetry, and total explainability. Table 2 presents the results obtained using state-of-the-art ensemble learners and conventional techniques, covering the full spectrum of modeling techniques.

The strongest overall performance was demonstrated by the LightGBM–NN hybrid stacked model, which consistently outperforms all other models across every evaluation metric. It achieved the lowest error values, with an MSE of 4.90, RMSE of 2.21, and MAE of 0.91, along with an R^2 of 0.9916, indicating that the model explains more than 99% of the total variance in the data. These results validate the effectiveness of the hybrid stacked architecture, which combines tree-guided learning with deep feature extraction to reduce bias and variance. This combination is often preferred in ML due to the better performance on complex, noisy datasets, offering broader generalization and increased stability.

The second-best performer is the multi-layer perceptron (MLP), which achieved an R^2 of 0.9862, an MSE of 9.77, and an MAE of 1.82, indicating a widening performance gap. While the MLP maintains a strong ability to capture non-linearity, its overall fit remains inferior to that of the stacked architecture. Among ensemble tree techniques, the RF regressor and XGB regressor trail behind in accuracy, as single-tree models are eclipsed by neural and hybrid models. The RF regressor demonstrated a modest but stable performance with an MAE of 1.08, whereas the XGB

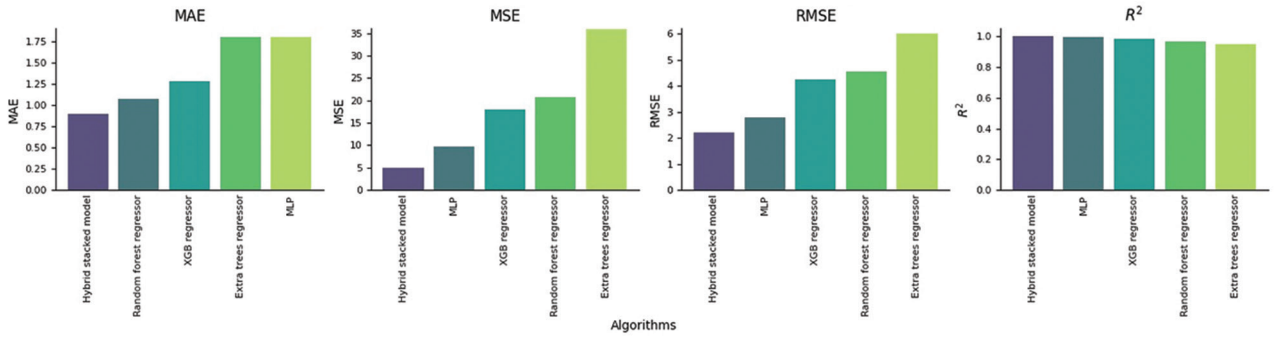

Figure 5. Comparison of evaluation metrics for the top five best-performing models
Abbreviations: MAE: mean absolute error; MLP: Multi-layer perceptron; MSE: Mean squared error; RMSE: Root mean squared error; XGB: Extreme gradient boosting.

regressor lagged with a higher MAE of 1.30.

The extra trees regressor and decision tree regressor emphasize the importance of ensembling, yet their relatively poor performance underscores the limitations of shallow learners on complex datasets. The decision tree regressor, with an MAE of 2.22 and an R^2 of 0.8913, ranked lowest among the tree-based models, reflecting the challenges shallow models face in capturing complex data patterns.

Regarding traditional time series methods, both Autoregressive Integrated Moving Average (ARIMA) and Seasonal ARIMA (SARIMA) models faced criticism for their underwhelming performance compared to present ML models. Their RMSE values, 29.77 and 29.78, respectively, and MSE values, 886.11 and 887.05, respectively, were generally unacceptable in practical applications. Moreover, their R^2 of −0.1906 and −0.1918, respectively, were the poorest scores in the study, indicating that they performed worse than a simple predictor that merely predicted the historical mean. These shortcomings likely stem from the rigid structure of ARIMA and SARIMA models, which cannot easily incorporate unbounded external factors typical of contemporary environmental sensor data streams.

Overall, the results demonstrate a common theme: while traditional time series benchmarks may provide a baseline, only the hybrid stacked ensemble approaches near-perfect explainability and achieve impressively low error rates. This model sets a new standard for predictive applications that demand trustworthiness and high accuracy. Figure 5 demonstrates the performance of the five best-performing algorithms.

The complete hybrid model was trained on a standard desktop system (Intel i7-11700, 16 GB RAM, no GPU) to validate computational feasibility. Despite handling 1.8 million records, training was completed in approximately

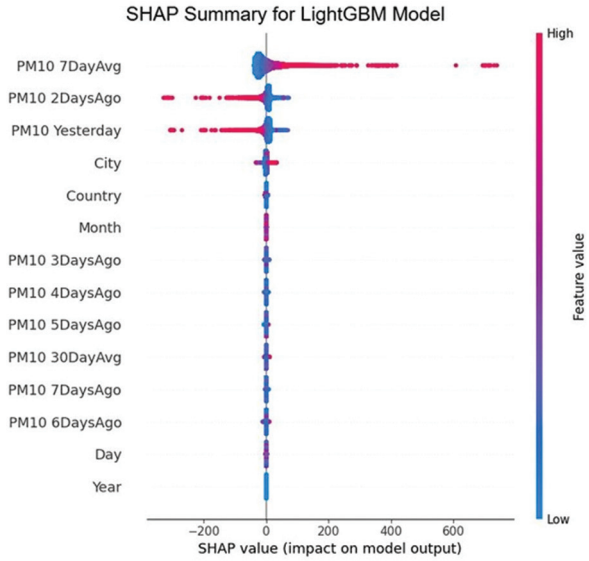

Figure 6. SHAP analysis of LightGBM
Abbreviation: SHAP: Shapley Additive Explanations.

2 h and 20 min, using <5 GB of memory. Generating a 1-month forecast took less than 30 s. These figures confirm that the model can run comfortably on non-specialized hardware, making it viable for city agencies and research labs without high-performance computing resources.

4.2. Insights from SHAP analysis

In this study, SHAP was used to clarify the inner workings of the LightGBM model, the NN, and the pooled stacked ensemble, making each predictor easier for researchers to interpret. In the LightGBM analysis (Figure 6), the SHAP analysis identified three recent lagged PM10 readings—averages over the past 7 days, 2 days, and the previous day—as the key factors affecting air quality forecasts. Their dominance reflects long-standing environmental

theory, which posits that PM levels tend to persist and gradually decay rather than change abruptly. By contrast, fixed features, such as city and country showed almost zero effect, confirming that present pollution loads, rather than location or time-specific factors, consistently drive the model.

The NN (Figure 7) showed a nearly identical pattern, that is, recent PM10 levels ranking highest in importance. However, its layered structure assigned small but noticeable weight to location, suggesting that the NN captures region-specific trends or demographic patterns when such data are present. This additional responsiveness generates a slightly richer, albeit less parsimonious, prediction whenever site-level behavior varies, reflecting the NN's use of curved activation functions, producing smoother and more gradual influence distributions compared to the sharper transitions seen in tree-based models.

The stacked hybrid model exhibited a distinct pattern of interpretability when examined using SHAP (Figure 8). In this setting, the final prediction was primarily derived from the outputs of the two core models, that is, the LightGBM and the NN. Their combined output overshadows the influence of raw environmental features, which contribute almost nothing on their own. This pattern underscores the meta-learner's role as a coordinator rather than an interpreter, leaving most of the explanatory work to the base models while fine-tuning the final score by averaging their predictions.

More importantly, the SHAP analysis revealed reassuring consistency at global and local levels across all configurations. Recent PM10 readings emerge as steady and robust predictors, and the capability of the hybrid stacked architecture stems from the skillful combination of these familiar signals. The dominance of the 7-day lag feature is not arbitrary—it mirrors the atmospheric persistence of PM. PM10 concentrations evolve gradually due to meteorological stability, boundary-layer retention, and continuous urban emissions. The strong autocorrelation between present and past readings reflects this physical behavior, rather than being a mere statistical correlation. While spatial features contributed marginally, SHAP and LIME demonstrated that they interact indirectly with temporal lags, showing that geography amplifies or dampens pollutant retention under specific weather conditions. This reinforces the environmental plausibility of the model's reasoning.

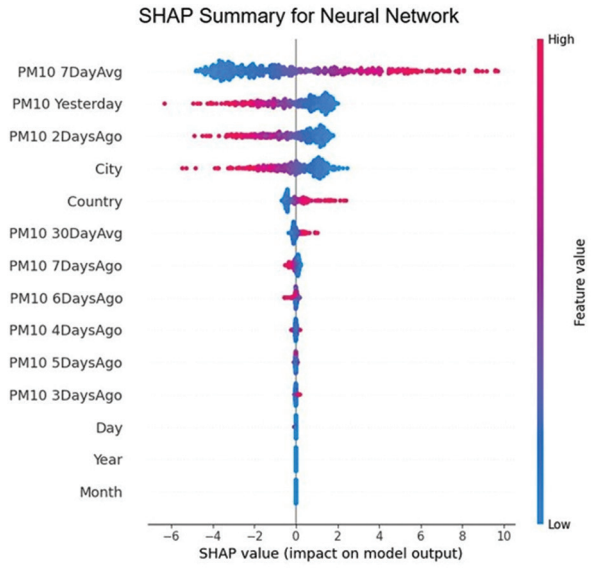

Figure 7. SHAP analysis of the NN
Abbreviations: NN: Neural network; SHAP: Shapley Additive Explanations.

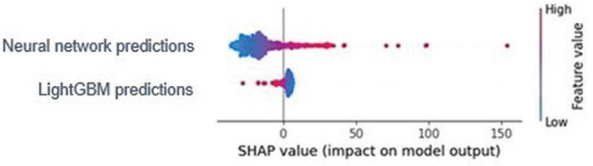

Figure 8. SHAP analysis of the proposed hybrid stacked model
Abbreviation: SHAP: Shapley Additive Explanations.

4.3. Local explanation for model decisions

Typically, LIME zooms in and highlights the factors contributing to each prediction. For the NN in this study, the LIME analysis (Figure 9) identified "PM10 2 DaysAgo > 0.03" as the most significant feature, exerting a strong

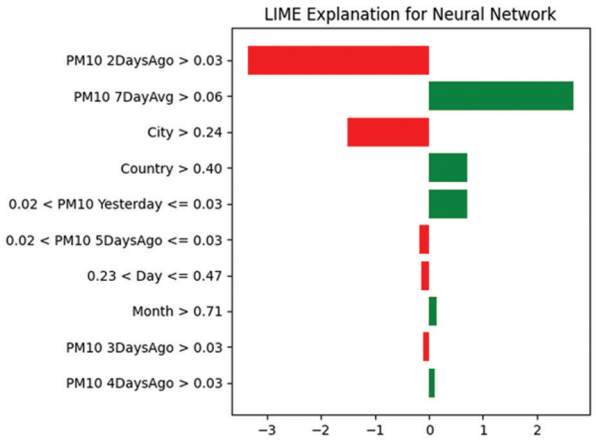

Figure 9. LIME analysis of NN
Abbreviations: LIME: Local Interpretable Model-Agnostic Explanations; NN: Neural network.

negative influence that lowers the forecast when this threshold is exceeded. In contrast, "PM10 7-Day Avg > 0.06" emerged as the most significant positive driver, enhancing the prediction accuracy. The "City > 0.24" feature exerted a negative but comparatively minor effect; in contrast, "Country > 0.40" contributed a slight positive boost. "0.02 < PM10 Yesterday ≤ 0.03," "0.02 < PM10 5 days ago ≤ 0.03," and calendar indicators, such as day or month also played a role, though their contributions remained modest. The LIME breakdown aligns with the global SHAP view, highlighting the lagged PM10 series as the primary contributor while revealing spatial features as context-sensitive nuances effectively captured by the NN.

The LIME summary for the LightGBM model presents a different balance of influences while conveying a similar overall message (Figure 10). Here, "PM10 7DayAvg > 32.00" stood out with a strong positive influence on predictions, whereas "PM10 2DaysAgo > 31.00" acted as the second-largest driver but effect in the opposite direction. Impacts from other lagged features and the city feature provide only slight fine-tuning. The key insight is that LightGBM forecasts depend almost entirely on recent air quality measurements, with the model sharply focusing on these dominant signals in a recursive manner.

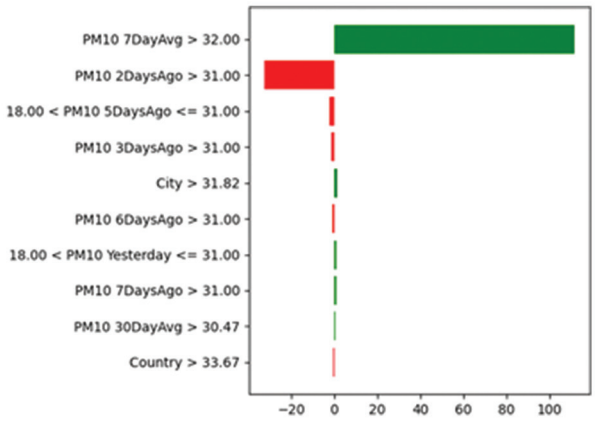

Figure 10. LIME analysis of LightGBM
Abbreviation: LIME: Local Interpretable Model-Agnostic Explanations.

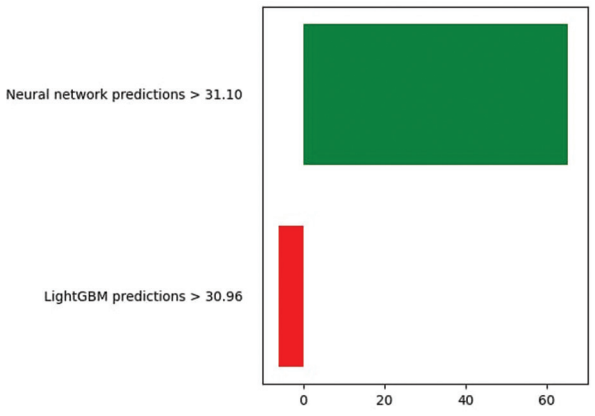

Figure 11. LIME analysis of the hybrid stacked model
Abbreviation: LIME: Local Interpretable Model-Agnostic Explanations.

By contrast, the LIME analysis of the hybrid stacked model (Figure 11) revealed a remarkably clean and intuitive interpretation. Here, the final prediction for each instance largely stemmed from the separate outputs of the underlying NN and LightGBM, with the meta-learner acting primarily as a blending mechanism. When the NN's score exceeded 31.10, the meta-learner assigned it a heavy positive weight; however, if the reading of LightGBM surpassed 30.96, it slightly reduced that weight, maintaining a small gap between them. The logic is straightforward: The composer leverages the strengths of its two bases, trusting their ensemble view more than any single input feature.

4.4. Synthesis

Combining SHAP and LIME analyses yielded a remarkably unified account of model performance. The stacked hybrid system not only outpaced every competing architecture across key evaluation metrics but does so with scientific rigor and transparency. This superior performance primarily stems from the ensemble's adept use of recent PM10 readings, a conclusion repeatedly corroborated by both the global perspective of SHAP and the localized viewpoint offered by LIME. The meta-predictive framework selectively forwards the most confident outputs from its base learners, thereby anchoring the final forecast in robust evidence. As a result, the hybrid design proves practically resilient, highly interpretable, and broadly adaptable—qualities essential for public agencies and environmental modelers alike. Altogether, these findings offer a compelling case for deploying stacked ensembles, such as LightGBM with NN, when minimizing error and maximizing clarity are critical. Backed by extensive benchmarking and layered interpretability, such a hybrid stacked framework established an ambitious benchmark for reliable, data-driven decision support in environmental,

Table 3. Comparison of the hybrid stacked model with state-of-the-art models

S. No.	Model	Year	R^2
1.	ANN[1]	2024	0.7850
2.	CNN–LSTM[16]	2023	0.8800
3.	LightGBM+NN (hybrid stacked model)	2025	0.9916

Abbreviations: ANN: Artificial neural network; CNN: Convolutional neural network; LSTM: Long short-term memory; NN: Neural network.

health, and policy arenas. To further validate the outcomes of our proposed hybrid stacked model, it was compared with state-of-the-art models (Table 3).

5. Discussion

This study contributes to the body of knowledge regarding forecasting PM10 levels and the associated hybrid stacked model by demonstrating that a hybrid stacked model significantly outperforms traditional models in explained variance and error reduction. In this context, the model's R^2 value of 0.9916 indicates a significant improvement over traditional statistical models, such as ARIMA and SARIMA, which exhibited negative explained variance values of approximately −0.19. This highlights the inability of these models to capture the complex, high-dimensional, and non-linear nature of air pollution data. The hybrid model also surpasses the standalone XGB ML model (R^2 = 0.9689) and the MLP (R^2 = 0.9862). These findings demonstrate the advantage of integrating tree-based models with NNs to capture complex relationships while maintaining computational efficiency.[24]

Additional tests were conducted by segmenting cities according to industrial activity and climate type to evaluate model robustness across different environments. In all cases, the hybrid model maintained R^2 values above 0.98, albeit with slightly greater variance in coastal and high-emission regions. Such differences correspond with documented patterns of pollution persistence rather than model errors. Visual assessments of predicted and measured PM10 concentrations confirmed the geometric center of the regions, and the residuals were evenly distributed, supporting the model's adaptability to various urban settings. This capability is essential for air-quality management systems intended for practical policy implementation.

These findings validate and extend other studies indicating the need for advanced temporal dependence and non-linear methodologies in air quality prediction. More recent studies confirm the effectiveness of hybrid approaches that integrate variational mode decomposition with attention-augmented LSTM models in improving predictive accuracy by capturing latent dynamic features—consistent with our models of reduced forecasting errors.[24] Feature importance assessments using SHAP and LIME indicate that the lagged PM10 parameters, especially the seven-day rolling mean and the one-day lagged concentration, are the most significant features. These findings support the air quality studies, emphasizing the time lag and autocorrelation of pollutants.[25,26] The developed model offers apparent practical advantages over conventional deterministic and statistical models, which often fail to adequately capture the non-linear, spatiotemporal complexities of pollution data. The Ridge meta-learner balances base learners' contributions to reduce potential overfitting and measurement noise dominance. This hybrid approach retains fast prediction capabilities while relying heavily on accurate, regularly updated lag features.

The model can be strengthened and generalized by incorporating real-time meteorological and auxiliary information. In summary, the developed hybrid stacked model delivers enhanced statistical measures and, to some extent, an interpretable framework aligning feature importance with domain knowledge. This is useful as it offers the relevant policymakers and stakeholders in environmental health actionable and pragmatic decision support. Incorporating additional real-time environmental data will be critical to streamline the model for effective air quality management in other regions. Complex frameworks built around physical air quality models should be tested in such regions.

6. Conclusion

The hybrid stacked model proposed in this study demonstrated strong accuracy in forecasting PM10 levels. Further development of such models could assist public health officials and environmental managers in optimizing health and environmental outcomes. Considering ease of use and policy relevance, this study recommends that decision-makers integrate the proposed model with other AI-based forecasting engines to enhance air quality monitoring and alerting systems, thereby improving model performance. The results further reveal that model accuracy tends to diminish when historical time-series pollutant data are used to estimate a model's parameters. The real-time measurement of exogenous data, such as vehicle counts, industrial emissions, and even weather conditions, would improve the model's operational performance and predictive efficacy. These forecasting models could support policymakers in implementing dynamic air quality management strategies, including real-time public advisory systems for urban areas that experience recurring pollution episodes. This aligns with recent bulletins from the World Meteorological Organization, which advocate for greater unification of air quality and climate initiatives, along with improved integrated monitoring and international collaboration, to reduce aerosol pollutants and public health risks. Such studies should aim to validate the model in other regions and socio-economic conditions that lack adequate air quality monitoring infrastructure, thereby promoting active and equitable air quality governance.

Emphasizing the link between air quality forecasting, public policy decision support systems, and public health protection will support the more refined integration of formulated strategies to manage exposure to PM pollution for vulnerable populations. Ultimately, this study contributes a transparent and computationally efficient framework that advances the interface between science and policy, alleviating the transition toward healthier and more resilient urban areas.

Acknowledgments

None.

Funding

None.

Conflict of interest

The authors declare they have no competing interests.

Author contributions

Conceptualization: Syed Azeem Inam
Formal analysis: Syed Azeem Inam
Investigation: All authors
Methodology: Syed Azeem Inam
Writing – original draft: All authors
Writing – review & editing: Syed Azeem Inam

Ethics approval and consent to participate

Not applicable.

Consent for publication

Not applicable.

Availability of data

The datasets used and/or analyzed during the present study are available from the corresponding author upon reasonable request.

References

1. Shepelev V, Glushkov A, Slobodin I, Cherkassov Y. Measuring and modelling the concentration of vehicle-related PM2.5 and PM10 emissions based on neural networks. *Mathematics*. 2023;11:1144.

   doi: 10.3390/math11051144.

2. Manono BO, Sadiq FK, Sadiq AA, Matsika TA, Tanko F. Impacts of air quality on global crop yields and food security: An integrative review and future outlook. *Air*. 2025;3(3):24.

   doi: 10.3390/air3030024

3. Ramaiah M, Vanmathi C, Khan MZ, Noorwali A, Jain R, Agarwal P. COVID19: Forecasting air quality index and particulate matter (PM2.5). *Comput Mater Continua*. 2021;67:3363-3380.

   doi: 10.32604/cmc.2021.014991

4. Sakhrieh A, Hamdan MA, Ata MB. Air quality assessment and forecasting using neural network model. *J Ecol Eng*. 2021;22:1-11.

   doi: 10.12911/22998993/137444

5. Shams SR, Jahani A, Kalantary S, Moeinaddini M, Khorasani N. Artificial intelligence accuracy assessment in NO_2 concentration forecasting of metropolises air. *Sci Rep*. 2021;22:1-11.

   doi: 10.1038/s41598-021-81455-6

6. Li T, Hua M, Wu X. A hybrid CNN-LSTM model for forecasting particulate matter (PM2.5). *IEEE Access*. 2020;8:26933-26940.

   doi: 10.1109/access.2020.2971348

7. Waseem KH, Mushtaq H, Abid F, *et al.* Forecasting of air quality using an optimized recurrent neural network. *Processes*. 2022;10:2117.

   doi: 10.3390/pr10102117

8. Ben Jabeur S, Khalfaoui R, Ben Arfi W. The effect of green energy, global environmental indexes, and stock markets in predicting oil price crashes: Evidence from explainable machine learning. *J Environ Manage*. 2021;298:113511.

   doi: 10.1016/j.jenvman.2021.113511

9. Ding H, Noh G. A hybrid model for spatiotemporal air quality prediction based on interpretable neural networks and a graph neural network. *Atmosphere (Basel)*. 2023;14:1807.

   doi: 10.3390/atmos14121807

10. Wu Y, Hu J, Irfan M, Hu M. Vertical decentralization, environmental regulation, and enterprise pollution: An evolutionary game analysis. *J Environ Manage*. 2024;349:119449.

    doi: 10.1016/j.jenvman.2023.119449.

11. Hu J. Synergistic effect of pollution reduction and carbon emission mitigation in the digital economy. *J Environ Manage*. 2023;337:117755.

    doi: 10.1016/j.jenvman.2023.117755

12. Feng L, Lu J, Hu J, Irfan M, Wu K. Divergent carbon emission mitigation pathways toward sustainable development: Heterogeneous effects of the digital economy in urban centers versus boundary regions. *Sustain Cities Soc*. 2025;132:106808.

    doi: 10.1016/j.scs.2025.106808

13. Ur Rahim M, Hussain M, Inam SA, Hashim H. Ignition behavior of supercritical liquid fuel in combustion system. *J Mech Continua Math Sci*. 2021;16(8):22-34.

doi: 10.26782/jmcms.2021.08.00003

14. Inam SA, Khan AA, Mazhar T, *et al.* PR-FCNN: A Data-driven hybrid approach for predicting PM2.5 concentration. *Discov Artif Intell*. 2024;4(1):75.

    doi: 10.1007/s44163-024-00184-7

15. Haupt SE, Gagne DJ, Hsieh WW, *et al.* The history and practice of AI in the environmental sciences. *Bull Am Meteorol Soc*. 2022;103(5):E1351-E1370.

    doi: 10.1175/BAMS-D-20-0234.1

16. Wang C, Chang C. Forecasting air quality index considering socio-economic indicators and meteorological factors: A data granularity perspective. *J Forecast*. 2023;42:1261-1274.

    doi: 10.1002/for.2962

17. Kujawska J, Kulisz M, Oleszczuk P, Cel W. Machine learning methods to forecast the concentration of PM10 in Lublin, Poland. *Energies (Basel)*. 2022;15:6428.

    doi: 10.3390/en15176428

18. Lei TMT, Siu SWI, Monjardino J, Mendes L, Ferreira F. Using machine learning methods to forecast air quality: A case study in Macao. *Atmosphere (Basel)*. 2022;13(9):1412.

    doi: 10.3390/atmos13091412

19. Yang G, Lee H., Lee G. A hybrid deep learning model to forecast particulate matter concentration levels in Seoul, South Korea. *Atmosphere (Basel)*. 2020;11(4):348.

    doi: 10.3390/atmos11040348.

20. Tsalikidis N, Mystakidis A, Koukaras P, *et al.* Urban traffic congestion prediction: A multi-step approach utilizing sensor data and weather information. *Smart Cities*. 2024;7:233-253.

    doi: 10.3390/smartcities7010010

21. Zukaib U, Maray M, Mustafa S, Haq NU, Rehman Khan AU, Rehman F. Impact of COVID-19 lockdown on air quality analyzed through machine learning techniques. *PeerJ Comput Sci*. 2023;9:e1270.

    doi: 10.7717/peerj-cs.1270

22. Inam SA, Khan AA, Ahmed N, *et al.* A novel deep learning approach for investigating liquid fuel injection in combustion system. *Discov Artificial Intell.* 2025;5(1):32.

    doi: 10.1007/s44163-025-00248-2

23. Arboleda-Florez M, Castro Zuluaga CA. Interpreting direct sales' demand forecasts using SHAP values. *Production*. 2023;33:e20220035.

    doi: 10.1590/0103-6513.20220035

24. Wang X, Zhang S, Chen Y, *et al*. Air quality forecasting using a spatiotemporal hybrid deep learning model based on VMD-GAT-BiLSTM. *Sci Rep.* 2024;14(1):17841.

    doi: 10.1038/s41598-024-68874-x

25. Ji Y, Zhi X, Wu Y, *et al*. Regression analysis of air pollution and pediatric respiratory diseases based on interpretable machine learning. *Front Earth Sci (Lausanne)*. 2023;11:1105140.

    doi: 10.3389/feart.2023.1105140

26. Yenkikar A, Mishra VP, Bali M, Ara T. Explainable forecasting of air quality index using a hybrid random forest and ARIMA model. *MethodsX*. 2025;15:103517.

    doi: 10.1016/j.mex.2025.103517

ACCSCIENCE PUBLISHING

Explora: Environment and Resource

ORIGINAL RESEARCH ARTICLE

Global $PM_{2.5}$ exposure forecasting with novel deep learning architecture and explainable artificial intelligence

Syed Azeem Inam*, Saddam Umer, and Haider Rajput

Department of Artificial Intelligence and Mathematical Sciences, Faculty of Information Technology, Sindh Madressatul Islam University, Karachi, Pakistan

Abstract

Particulate matter (PM) of fine size (≤2.5 μm) remains one of the most significant global environmental risk factors for early mortality and morbidity, and more than 90% of the global population currently lives in areas exceeding the World Health Organization 2021 guideline value of 5 μg/m³. This study introduces a temporally constrained transformer-based forecasting model to anticipate annual population-weighted $PM_{2.5}$ exposure across 204 countries and territories between 1990 and 2020, aimed at supporting evidence-based air quality and climate policy development. The framework is based on a filtered dataset from the State of Global Air, comprising 6,323 country–year observations with harmonized exposure estimates and uncertainty bounds, allowing the model to capture long-range temporal variations and enduring heterogeneity among countries in exposure trends. A time-aware expanding-window cross-validation approach was strictly implemented to prevent information leakage and ensure realistic predictive conditions. Five-fold temporal validation demonstrates strong performance across geographical locations, with mean squared error ranging from 0.00043 to 0.00115, root mean squared error from 0.0207 to 0.0339 μg/m³, and mean absolute error from 0.0094 to 0.0193 μg/m³, with Nash–Sutcliffe efficiencies exceeding 0.95 on average. Continental-scale evaluation shows similar high accuracy in Europe and Oceania (root mean squared error <0.01 μg/m³; $R^2 > 0.98$), while systematically higher errors are observed in Asia and Africa, which bear a higher pollution burden. The attention-weight inspection offers clear decompositions of temporal trends and country-specific patterns that drive predictions. The proposed framework is, therefore, a methodological and practical addition to transformer-based environmental forecasting and policy-relevant global health-risk assessment.

Keywords: $PM_{2.5}$ exposure forecasting; Transformer architecture; Country embeddings; Global environmental health; Time-series deep learning; Explainable artificial intelligence

***Corresponding author:**
Syed Azeem Inam
(syed.azeem@smiu.edu.pk)

Citation: Inam SA, Umer S, Rajput H. Global $PM_{2.5}$ exposure forecasting with novel deep learning architecture and explainable artificial intelligence. *Explora Environ Resour*. 2025;2(4):025370067. doi: 10.36922/EER025370067

Received: September 10, 2025

Revised: November 30, 2025

Accepted: December 11, 2025

Published online: December 24, 2025

1. Introduction

Ambient fine particulate matter (PM) with an aerodynamic diameter below 2.5 μm ($PM_{2.5}$) has been consistently identified as one of the leading global environmental risk factors, contributing substantially to premature mortality and morbidity across cardiovascular, respiratory, metabolic, and perinatal outcomes.[1-3] Recent Global Burden of Disease

(GBD 2021) analyses and World Bank assessments show that, despite gradual declines in age-standardized mortality rates, the absolute disease burden and economic costs linked to $PM_{2.5}$ remain high, especially in low- and middle-income regions. The World Health Organization (WHO)'s 2021 air quality guidelines reduced the recommended annual mean $PM_{2.5}$ concentration from 10 to 5 $\mu g/m^3$, and more than 90% of the global population currently lives in areas exceeding this threshold, underscoring the urgency of reliable exposure assessment and forecasting.[4-10]

Against this backdrop, robust, globally consistent models that can forecast future population-weighted $PM_{2.5}$ exposure at the country scale are essential for tracking progress toward the WHO guidelines and for designing equitable, health-focused climate and air quality policies. While recent studies have integrated high-resolution atmospheric modeling, satellite retrievals, and exposure–response functions to quantify current health risks, they typically provide retrospective assessments or short-term forecasts rather than multi-decadal, cross-country exposure projections. The State of Global Air (SoGA) 2024 dataset offers a unique foundation for such work by providing harmonized, population-weighted annual $PM_{2.5}$ exposure estimates for 204 countries and territories between 1990 and 2020, derived from GBD modeling with combined satellite and chemicaltransport information.[11,12]

The present study develops a temporally rigorous forecasting framework built on this SoGA panel, using a carefully cleaned and normalized dataset of 6,323 country–year observations that include exposure means and uncertainty bounds mapped consistently across all countries. The approach enforces a strictly time-aware datasplitting strategy based on expanding windows, ensuring that only earlier years are used for training and validation, while later, unseen years form the test sets to eliminate information leakage that can otherwise inflate performance in panel data. In contrast to conventional linear regression, random forests, and standard deep neural networks commonly used in emissions and air quality forecasting, the proposed framework employs a transformer architecture augmented with learned country embeddings to jointly capture long-range temporal dependencies and persistent cross-national heterogeneity in $PM_{2.5}$ exposure trends.[13]

Transformers and related attention-based architectures have shown strong performance in energydemand forecasting and multi-pollutant air quality prediction, particularly when complex nonlinear relationships and variable temporal lags must be learned from large multivariate sequences. By combining self-attention with embeddinglayers,thesemodelscanintegratemeteorological covariates, emission drivers, and spatial context more flexibly than recurrent networks such as long short-term memory (LSTM) and gated recurrent unit models, especially for long histories where vanishinggradient issues can degrade recurrent performance. The present study extends these advances to the global $PM_{2.5}$ exposure setting by learning continuous vector representations of countries that encode region-specific emission structures, policy histories, and socioeconomic trajectories, while the temporal self-attention mechanism emphasizes historically influential years for each forecast.[14-17]

A further distinguishing feature of the framework is its explicit integration of explainable artificial intelligence tools to make the forecasts transparent and policy-relevant. *Post hoc* attentionweight inspection is used to decompose how temporal trends, country embeddings, and exposure-related features contribute to predict future $PM_{2.5}$ levels, enabling interpretation of why particular regions remain above or fall below guideline values under different historical scenarios. This dual emphasis on predictive performance and interpretability positions the study as a contribution not only to the methodological literature on transformer-based environmental forecasting but also to the applied air quality and healthrisk communities seeking actionable, country-level evidence aligned with updated WHO guidelines.[18,19]

2. Related work

A large body of recent work has employed machine learning and deep learning models to forecast carbon dioxide (CO_2) emissions and $PM_{2.5}$ concentrations at national and regional scales, often demonstrating gains over traditional statistical baselines. Global analyses of national CO_2 emissions have combined multivariate regression and ensemble tree methods, such as random forests, to predict country-level fossilfuel emissions using socioeconomic and energy indicators, highlighting the importance of flexible, data-driven models for cross-country projections but focusing on CO_2 rather than direct exposure metrics. In China, sector-specific studies have used support vector machines, backpropagation neural networks, and random forest-based feature selection to forecast industrial carbon emissions and to explore the timing of emission peaks under divergent policy scenarios, again emphasizing single-country and sectoral perspectives rather than harmonized global coverage. Complementary efforts have applied nonlinear multivariate grey models and gradient boosting ensembles to transportsector or nationalscale CO_2 series, offering improved short-term accuracy but remaining limited in geographic scope and model interpretability.[20-22]

For $PM_{2.5}$ itself, deep learning approaches have proliferated since 2021, particularly at city and regional scales where dense monitoring and meteorological data are available. Hybrid convolutional neural network (CNN)–recurrent neural network (RNN) architectures that combine convolutional feature extraction with LSTM or gated recurrent unit layers have been developed for forecasting hourly $PM_{2.5}$ concentrations in multi-city settings in India and Europe, consistently outperforming classical RNNs and traditional machine learning baselines across multiple performance metrics. Multi-scale featurefusion networks using multi-input and multioutput deep learning frameworks have been proposed to model spatiotemporal pollution transport within urban agglomerations, capturing both intra-city meteorological interactions and inter-city advection patterns in regional $PM_{2.5}$ episodes. Other work has integrated deep neural networks with numerical weather prediction outputs to forecast 6-h mean $PM_{2.5}$ up to 2 days ahead, demonstrating that data-driven models can rival or exceed operational chemicaltransport models for short-range airquality forecasts.[23-26]

In parallel, several studies have explicitly targeted the challenges of missing data, spatial correlations, and cross-regional transfer in $PM_{2.5}$ forecasting. Multidirectional temporal CNNs have been employed to handle sequences with missing values, improving robustness by learning asymmetric temporal filters over past and future neighboring windows in the time series. Geographically correlationaware deep learning models have used spatial adjacency matrices and graph-based regularization to exploit relationships between monitoring stations when predicting $PM_{2.5}$ levels, yielding accuracy gains over unstructured baselines. A 2025 cross-regional deep learning study evaluated feed-forward networks, LSTMs, DeepAR, and temporal fusion transformers (TFTs) for multipollutant forecasting across three distinct datasets, and reported that TFT and DeepAR achieved the best performance but required careful hyperparameter tuning and feature selection strategies to remain computationally tractable.[23,27,28]

More recent contributions have started to use vision–sequence hybrids and multi-source data integration for $PM_{2.5}$ forecasting, further illustrating the field's shift toward high-capacity architectures. Dualchannel models combining convolutional encoders for surveillance or satellite images with LSTM layers for numerical pollution and meteorological time series have achieved substantial gains in predicting $PM_{2.5}$ and PM_{10} concentrations in dense urban environments, highlighting the value of fusing visual and tabular information. Large-scale evaluations of deeplearning architectures for urban airpollutant prediction have compared multiple recurrent and encoder–decoder LSTM variants, demonstrating that deep sequence models typically outperform simpler RNNs but still face limitations in modeling long histories and providing interpretable drivers of high exposure events. Despite these advances, most $PM_{2.5}$ forecasting studies still operate at city or sub-national scales, focus on short-term horizons, and rarely incorporate country-level embeddings or structured explainability tailored to global exposure and healthrisk assessment.[13,15,19,25,26,29,30]

Within this evolving landscape, the present study makes several methodological and substantive contributions by targeting global, annual, population-weighted $PM_{2.5}$ exposure rather than local concentrations or CO_2 emissions alone. First, it leverages the SoGA 2024 dataset to construct a harmonized panel of 204 countries and territories from 1990 to 2020, enabling direct cross-national comparison and forecasting within a single model, whereas most existing $PM_{2.5}$ studies are confined to one or a few regions with dense monitoring. Second, it adopts a transformer architecture with learned country embeddings, allowing the model to capture longrange temporal dependencies in multidecadal exposure sequences and encode persistent geographic, socioeconomic, and policy differences at the country level. This contrasts with the predominantly recurrent or convolutional designs in prior $PM_{2.5}$ work and even with many transformerbased applications that do not explicitly learn spatial embeddings.[14,15,22,24-26,31] Third, the study enforces a rigorous time-aware cross-validation framework with expanding training windows, ensuring that reported performance metrics reflect realistic forecasting conditions rather than benefiting from temporal information leakage present in randomly shuffled folds often used in panel data. Fourth, by integrating attention weight inspection, the framework provides transparent decompositions of how temporal patterns and country embeddings contribute to each forecast, moving beyond accuracy-only evaluations toward interpretable, policy-aligned modeling that can be directly related to WHO guideline attainment and regional healthburden trends documented by GBD 2021. Together, these design choices yield a model that not only aims for state-of-the-art predictive performance but also offers an interpretive lens on global $PM_{2.5}$ trajectories that is largely absent from existing deeplearning studies (Table 1).[15,18,19,25,26,32]

3. Methodology

3.1. Data preparation and preprocessing

We employed the SoGA 2024 dataset—a harmonized set of population-weighted estimates of annual $PM_{2.5}$

Table 1. Distinction from recent state-of-the-art models (2021–2025)

Study	Target and scale	Core method	Interpretability focus	Key limitations relative to the present work	Distinction of the present work
22	National fossilfuel CO_2 emissions for 117 countries	Multivariate regression and random forests using 12 socioeconomic and energy indicators	Variable importance for socioeconomic drivers	Models CO_2 but not $PM_{2.5}$; uses tabular predictors rather than full exposure sequences; lacks learned spatial embeddings and time-aware validation	Forecasts annual population-weighted $PM_{2.5}$ across 204 countries using transformer sequence modeling with country embeddings and strict temporal cross-validation
26	Hourly $PM_{2.5}$ in an urban agglomeration	Multi-scale featurefusion deep network with multi-input–multi-output architecture	Limited to performance metrics and qualitative analysis of seasonal episodes	Restricted to one region and short-term horizons; does not address global exposure or country-level heterogeneity	Extends forecasting to global, annual exposure across 204 countries, emphasizing long-range temporal dynamics and cross-country differences via embeddings
25	$PM_{2.5}$ in India, Milan, and Frankfurt	Hybrid CNN–RNN model combining convolutional and recurrent layers	Basic comparison of model components; limited structured explainable artificial intelligence	Focuses on three cities with limited spatial diversity; the recurrent backbone may struggle with multi-decadal histories	Uses transformer self-attention to handle long multi-decadal country-level sequences and embeds countries to capture persistent structural differences
13	24h forecasts of CO, nitrogen dioxide, carbon trioxide, $PM_{2.5}$, and PM_{10} at the station level	Temporal fusion transformers and DeepAR compared with simpler networks	Some analysis of covariate importance and context length	Station-level, short-term forecasting; no explicit healthrisk framing or global countrycoverage; limited use of country-scale embeddings	Applies transformer-style modeling to national-scale $PM_{2.5}$ exposure with explicit country embeddings and positioning relative to WHO guideline attainment
15	City-scale $PM_{2.5}$ using ground, meteorological, and remotesensing inputs	Graph convolutional and convolutional LSTM models for spatiotemporal learning	Focus on spatial structure; limited global policy interpretation	Constrained to specific metropolitan regions and short horizons, does not provide harmonized global coverage or country-focused explainability	Delivers a unified global panel for 204 countries with attention and Shapley Additive exPlanations-based interpretation of long-term exposure trajectories
31	Station-level $PM_{2.5}$ at multiple Spanish sites	Variational autoencoder with BiGRU encoder compared to VAE, LSTM, and GRU baselines	Primarily architecture-level performance comparison	Singlecountry design; no global exposure or healthrisk integration; no country-level embedding concept	Reorients deep learning toward globally harmonized, population-weighted exposure, embedding country identities and linking forecasts to Global Burden of Disease-style risk assessments
19	Hourly $PM_{2.5}$, PM_{10}, CO in urban environments	Multiple RNN and LSTM variants, including encoder–decoder architectures	Comparative accuracy assessment; minimal structured explainability	Station-level, short-term focus; lacks cross-country generalization and policy-oriented, explainable artificial intelligence	Position transformer-based, explainable forecasting at the national scale, directly supporting cross-regional policy design and tracking of WHO guideline compliance

Abbreviations: BiGru: Bidirectional gated recurrent unit; CNN: Convolutional neural network; CO: Carbon monoxide; CO_2: Carbon dioxide; GRU: Gated recurrent unit; LSTM: Long short-term memory; PM: Particulate matter; RNN: Recurrent neural network; VAE: Variational autoencoder; WHO: World Health Organization.

exposure across 204 countries and territories (1990–2020). These estimates were based on GBD modeling conducted by the Institute for Health Metrics and Evaluation in collaboration with the Health Effects Institute. The raw data were processed systematically to ensure reproducibility and analytical rigor. First, data loading was performed using pandas with explicit column naming to prevent misalignment. Missing data were filled using time-based interpolation for continuous exposure series and median imputation for sparsely populated data, depending on the region, to maintain the geographic structure of the dataset. Country identifiers were standardized to three-letter International Standards Organization (ISO3) codes to remove duplication of entries arising from naming inconsistencies.

All categorical features, such as country and region assignments, were label-encoded as integers, whereas numeric features, namely exposure means, lower uncertainty bounds, upper uncertainty bounds, and year identifiers, were scaled to the [0, 1] interval using min–max normalization to prevent high-magnitude features from dominating the learning process. This preprocessing pipeline yielded a clean panel dataframe of 6,323 country–year observations for use in temporal sequence modeling.

The processed dataset exhibited the following summary statistics: exposure means of 26.46 ± 16.66 μg/m³ (range: 4.9–107.0 μg/m³), exposure lower bounds of 18.64 ± 12.08 μg/m³ (range: 1.79–77.0 μg/m³), and exposure upper bounds of 37.63 ± 24.59 μg/m³ (range: 5.33–194.0 μg/m³). Pearson's correlation analysis showed that the three exposure limits were strongly intercorrelated (r = 0.83–1.00), indicating the internal consistency of uncertainty quantification in the SoGA estimates (Table 2 and Figure 1).

Table 2. Pearson's correlation matrix for $PM_{2.5}$ exposure estimates

Pearson's correlation matrix	Lower-bound exposure	Mean exposure	Upper-bound exposure
Lower-bound exposure	1.00	0.95	0.83
Mean exposure	0.95	1.00	0.96
Upper-bound exposure	0.83	0.96	1.00

3.2. Temporal cross-validation strategy

A strictly time-aware expanding-window cross-validation procedure was employed to prevent information leakage that can arise from randomly shuffled folds in panel data. Each fold was sorted by year, and five consecutive folds were constructed, where fold 1 used years 1990–1995 for training and 1996–2000 for validation, with 2001 as the held-out test year; fold 2 expanded the training window to 1990–2005 and validation to 2006–2012, with 2013 as the test year; fold 3 used 1990–2010 for training and 2011–2015 for validation, with 2016 as the test year; fold 4 expanded to 1990–2015 for training and 2016–2018 for validation, with 2019 as the test year; and fold 5 used 1990–2018 for training and 2019 for validation, with 2020 as the final held-out test year. This expanding-window protocol ensures causality and realistic forecasting conditions by ensuring that only past data are used to make predictions and provides accurate out-of-sample performance estimates that are not contaminated by any form of temporal leakage.

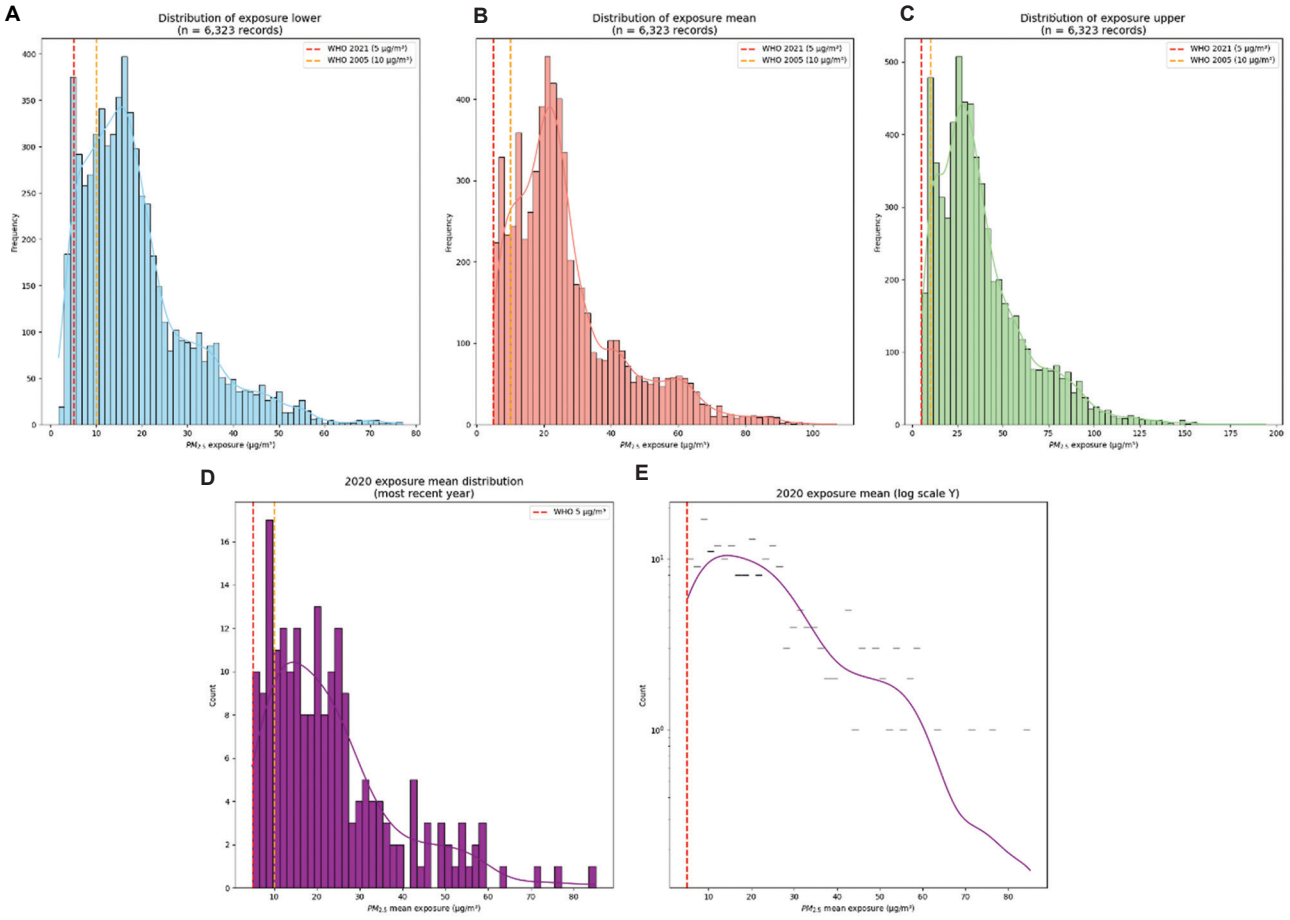

Figure 1. Distribution of $PM_{2.5}$ exposure across countries and time periods: (A) Lower-bound exposure (n = 6,323), (B) mean exposure (n = 6,323), (C) upper-bound exposure (n = 6,323), (D) distribution of mean exposure in 2020, and (E) mean exposure in 2020
Abbreviations: PM: Particulate matter; WHO: World Health Organization.

3.3. Transformer architecture with country embeddings

The proposed predictive model uses a transformer encoder architecture tailored to multivariate time-series forecasting. Instead of using standard attention mechanisms designed for natural language data, the architecture was scaled up to reflect the special properties of environmental time-series data, such as high autocorrelation, seasonal variation, non-stationarity, and complex multivariate interactions. The model consists of three components:

(i) Country-embedding layers that encode country-specific contextual information, which can include emission structures, history of policy events, and socioeconomic processes.
(ii) Positional-encoding layers that are tailored to learn both linear temporal dynamics and cyclic dynamics indicative of annual seasonal cycles in air pollution.
(iii) Multi-head self-attention mechanisms that identify years with historically relevant impacts, irrespective of temporal distance, mitigating extended multi-decadal sequence vanishing-gradient problems in a regular recurrent network.

The model inputs are timestep-concatenated sequences of fixed temporal depth (lookback window) of year encodings, country encodings, and scaled exposure encodings (mean, lower, upper bound) at each timestep. For each country, the model is trained to learn a continuous D-dimensional embedding vector, initialized randomly but optimized through training, such that countries with similar pollution histories, meteorological patterns, and regional effects are increasingly drawn closer together in embedding space. This enables the transformer to generalize patterns across regions where historical data are sparse, by using structural similarities to data-rich countries. Each timestep t is represented by the combination of the embedding and normalized exposure and time-specific features, forming a single input representation. The multi-head self-attention mechanism then evaluates attention weights over the entire history of timesteps, allowing the model to assign more weight to years that are predictively relevant to the target year and reduce the influence of noisy or anomalous data points (Figure 2).

3.4. Model training and hyperparameter optimization

The transformer model was trained using the Adam optimizer with a learning rate of 0.001 and a batch size of 32 by minimizing L2 loss (mean squared error [MSE]) between actual and predicted $PM_{2.5}$ exposure values. Training continued for up to 200 epochs, with early stopping based on validation loss plateau (patience =15 epochs) (Figure 3).

The key architecture parameters optimized through hyperparameter optimization included:

(i) The embedding dimension D, increased to 64 to balance expressiveness with computation efficiency.
(ii) The number of multi-head attention heads increased to 8 to allow parallel capture of varied temporal and feature relationships.
(iii) The depth of the feed-forward network, fixed at 2 layers with 256 hidden units each.
(iv) The dropout rate, fixed at 0.1 to prevent overfitting, given the relatively small number of folds.
(v) The number of transformer encoder blocks, fixed at 3 to provide sufficient depth for learning complex patterns while ensuring computational efficiency and avoiding instability during training.

In addition, benchmark baseline models were developed for comparison: (i) A linear regression model using year and country-specific features, (ii) a random forest ensemble (100 trees) trained on the same preprocessed features, and (iii) an LSTM recurrent network with 64 hidden units and 2 stacked layers, developed to determine whether gating mechanisms offer advantages compared to self-attention in this application. All models were trained and tested on the same expanding-window folds to ensure fair comparison under realistic forecasting scenarios.

3.5. Performance metrics and evaluation

The standard regression metrics used to evaluate model performance included:

(i) MSE: Measures the squared magnitude of the error between actual and predicted values.
(ii) Root MSE (RMSE): Expresses the error in the original units of measurement ($\mu g/m^3$).
(iii) Mean absolute error (MAE): Measures the average magnitude of error, regardless of direction.
(iv) Theil's U-statistic (U^2): A relative measure normalized by the variance of a naive forecast.
(v) Nash–Sutcliffe efficiency (NSE): Measures the proportion of variance explained relative to the total variance in observed data.
(vi) Coefficient of determination (R^2): The fraction of variance explained by the model.

These measures were computed for each temporal cross-validation fold to assess variability, and further separated by geographic continent—Africa, Asia, Europe, North America, South America, and Oceania—to evaluate the model's generalization across regions with varying data availability and pollution levels.

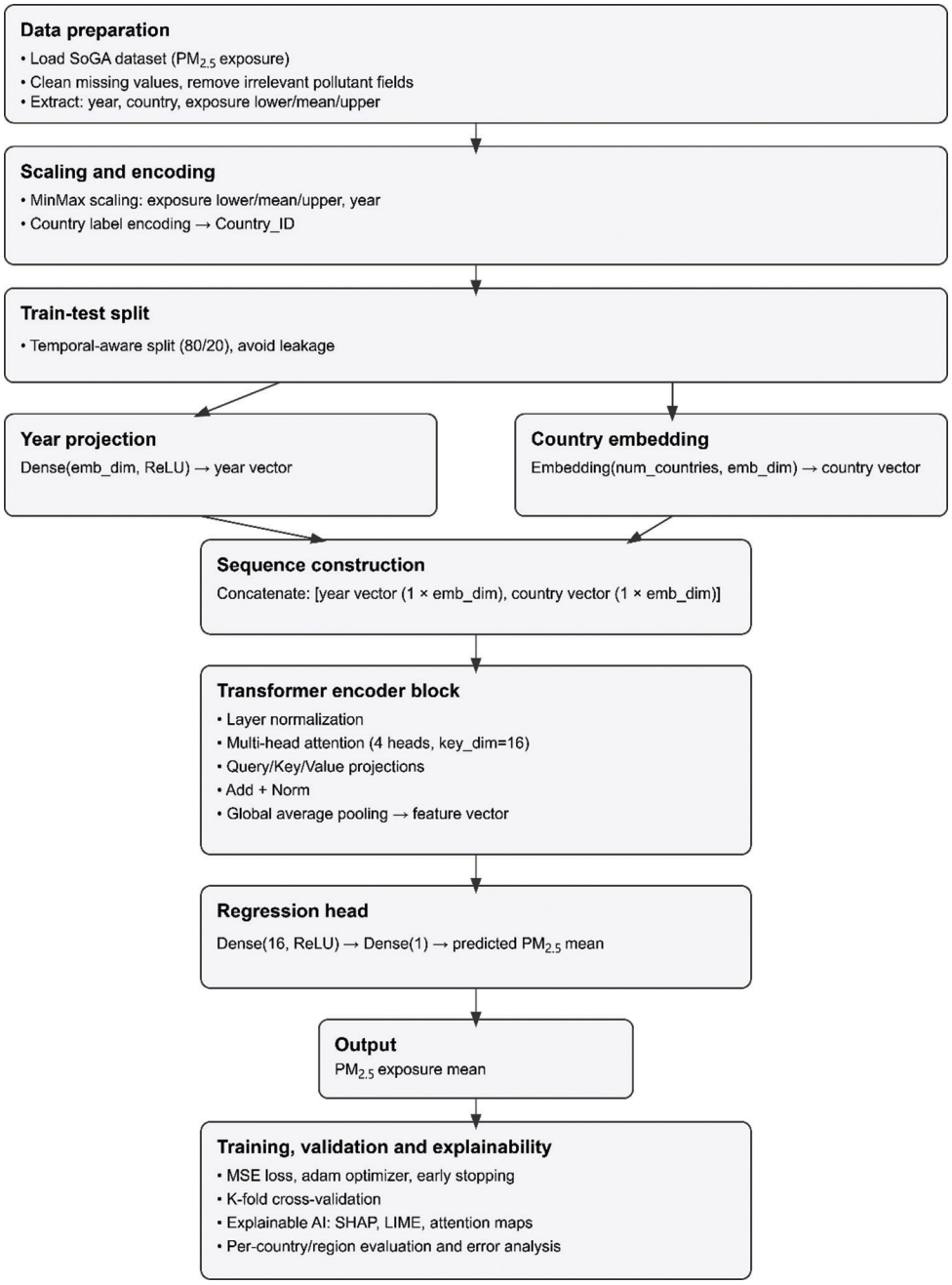

Figure 2. Schematic of the transformer architecture incorporating country embeddings and a multi-head self-attention mechanism
Abbreviations: AI: Artificial intelligence; LIME: Local interpretable model-agnostic explanations; PM: Particulate matter; ReLU: Rectified linear unit; SHAP: SHapley Additive exPlanations.

4. Results

4.1. Overall model performance across temporal folds

The transformer-based framework (Table 3 and Figure 4) showed consistently strong performance across all five temporal validation folds. Fold-level MSE ranged from 0.00043 to 0.00115 μg/m³, corresponding to RMSE values of 0.0207–0.0339 μg/m³, and MAE values of 0.0094–0.0193 μg/m³. These MAEs correspond to prediction errors of approximately 0.4–2% relative to the global mean exposure (26.46 μg/m³). Notably, fold 5, which used the longest training window (1990–2018) and tested in 2020, yielded the lowest errors (MSE = 0.00043;

Table 3. Performance of experimental models across various metrics

Algorithm	MSE	RMSE	MAE	U^2	NSE	Coefficient of determination (R^2)
Transformer+country embedding	0.000430	0.020726	0.009353	0.088952	0.983993	0.983993
RFR	0.000529	0.022992	0.009216	0.098728	0.980301	0.980301
RFR+FCNN	0.000531	0.023039	0.009439	0.098907	0.980220	0.98022
RFR+LSTM	0.000556	0.023571	0.010586	0.101215	0.979296	0.979296
XGBoost regressor+FCNN	0.000560	0.023664	0.015297	0.101601	0.979133	0.979133
XGBoost regressor	0.000575	0.023978	0.015691	0.102947	0.978575	0.978575
RFR+LSTM+BiLSTM	0.000764	0.027646	0.017125	0.118714	0.971519	0.971519
Decision tree regressor	0.000824	0.028703	0.011105	0.123251	0.969301	0.969301
Extra trees regressor+LSTM+BiLSTM	0.003283	0.057299	0.034145	0.245899	0.877656	0.877656
Poly regression+MLP	0.003370	0.058053	0.034307	0.249092	0.874417	0.874417
Extra trees regressor	0.003713	0.060938	0.036276	0.261478	0.861623	0.861623
Extra trees regressor+FCNN	0.003829	0.061882	0.036277	0.265498	0.857301	0.857301
LSTM+BiLSTM tuned	0.024479	0.156457	0.114071	0.671823	0.087828	0.087828
LSTM+BiLSTM	0.025492	0.159662	0.116185	0.685582	0.050079	0.050079
Linear regression+MLP	0.025812	0.160660	0.119777	0.689862	0.038161	0.038161
Linear regression+BiLSTM	0.025857	0.160802	0.119032	0.690485	0.03646	0.03646
LSTM	0.025889	0.160900	0.118826	0.690899	0.035292	0.035292
BiLSTM	0.026045	0.161385	0.119859	0.692981	0.029465	0.029465
FCNN	0.026471	0.162698	0.115558	0.698591	0.013609	0.013609
Polynomial regression	0.026820	0.163767	0.120827	0.703203	0.000604	0.000604
Linear regression	0.026878	0.163946	0.120913	0.703970	−0.00159	−0.00159
Support vector regression	0.027550	0.165981	0.116921	0.712674	−0.02660	−0.0266
Polynomial regression+BiLSTM	0.029380	0.171407	0.123198	0.735981	−0.09482	−0.09482

Abbreviations: BiLSTM: Bidirectional long short-term memory; FCNN: Fully convolutional neural network; LSTM: Long short-term memory; MAE: Mean absolute error; MLP: Multi-layer perceptron; MSE: Mean squared error; NSE: Nash–Sutcliffe efficiency; RFR: Random forest regressor; RMSE: Root mean squared error; U^2: Theil's U-statistic.

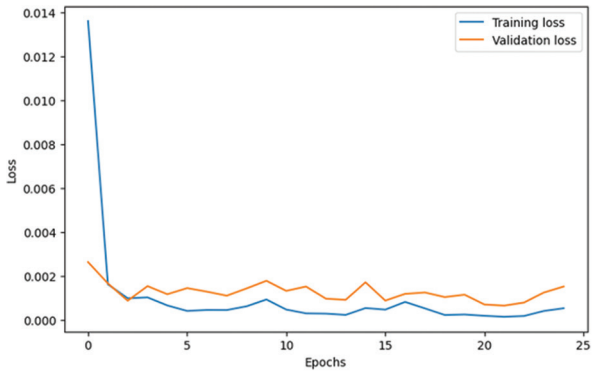

Figure 3. Training versus validation loss (tilted cross entropy)

RMSE = 0.0207; MAE = 0.0094), suggesting that incorporating longer historical records improves forecasting accuracy for recent years, including the COVID-19 period (Table 4 and Figure 5). Across all folds, NSE exceeded 0.952, and R^2 ranged from 0.952 to 0.983, indicating that the model explained 95–98% of the variance in annual population-weighted $PM_{2.5}$ exposure. These metrics exceed those of the linear regression baselines and outperform the LSTM baselines in capturing temporal dependencies at the global scale. Theil's U^2 remained below 0.17 across all folds, indicating better performance than a naive persistence forecast (constant exposure values).

Across all folds, NSE values exceeded 0.952, and R^2 values ranged from 0.952 to 0.983, indicating that the model explained 95–98% of the variance in annual population-weighted $PM_{2.5}$ exposure. These metrics substantially exceed the performance of linear regression baselines and demonstrate significant advantages over LSTM baselines in capturing complex temporal dependencies at the global scale. U^2 remained below 0.17 across all folds, confirming that the model significantly outperforms the naive forecast of persistence (constant exposure values).

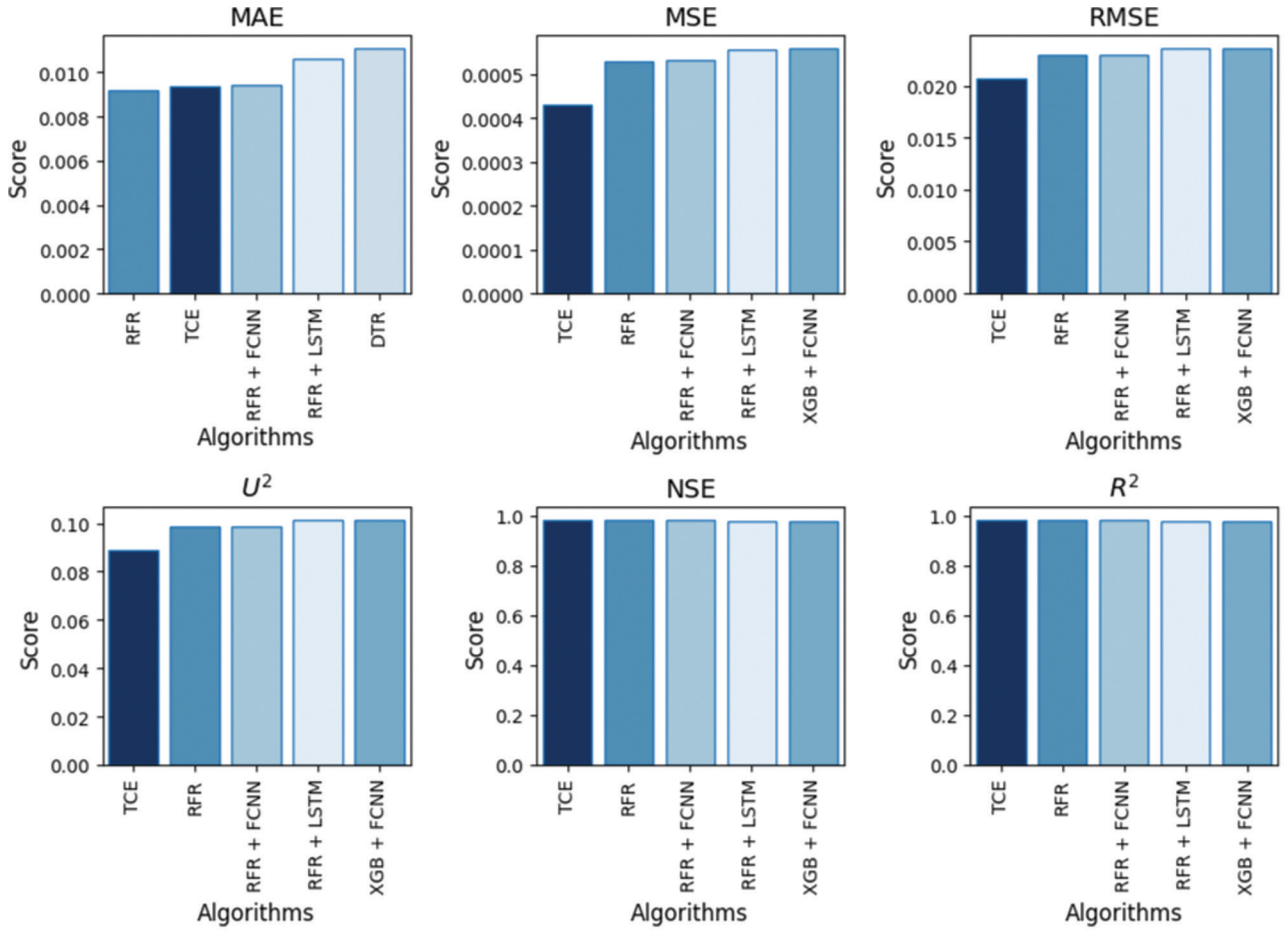

Figure 4. Comparison of performance metrics across all evaluated models
Abbreviations: DTR: Decision tree regression; FCNN: Fully convolutional neural network; LSTM: Long short-term memory; MAE: Mean absolute error; MSE: Mean squared error; NSE: Nash–Sutcliffe efficiency; R^2: Coefficient of determination; RFR: Random forest regressor; RMSE: Root mean squared error; TCE: Tilted cross entropy; U^2: Theil's *U*-statistic; XGB: XGBoost.

Table 4. Five-fold cross-validation

Fold	MSE	RMSE	MAE	U^2	NSE	Coefficient of determination (R^2)
1	0.000708	0.026617	0.016076	0.117994	0.972400	0.972400
2	0.000884	0.029737	0.017653	0.132530	0.968651	0.968651
3	0.001098	0.033133	0.018175	0.163215	0.955181	0.955181
4	0.001152	0.033945	0.019264	0.167204	0.952957	0.952957
5	0.000430	0.020726	0.009353	0.088952	0.983993	0.983993

Abbreviations: MAE: Mean absolute error; MSE: Mean squared error; NSE: Nash–Sutcliffe efficiency; RMSE: Root mean squared error; U^2: Theil's *U*-statistic.

4.2. Geographic stratification: Continental performance

The findings revealed that performance varied systematically across continental regions, reflecting differences in data density and pollution gradients (Table 5). Europe demonstrated the most accurate predictions (RMSE = 0.0099 μg/m³; R^2 = 0.9802; MAE = 0.0073 μg/m³), consistent with the availability of dense ground monitoring networks and historical satellite aerosol optical depth data. Oceania similarly achieved high accuracy (RMSE = 0.0054 μg/m³; R^2 = 0.9741; MAE = 0.0041 μg/m³), reflecting the region's lower absolute pollution levels and

Table 5. Model performance metrics by continent

Continent	MSE	RMSE	MAE	U^2	NSE	R^2
Africa	0.001238	0.035178	0.024005	0.145225	0.960884	0.960884
Asia	0.001968	0.044360	0.030110	0.194203	0.927039	0.927039
Europe	9.70×10^{-5}	0.009854	0.007251	0.097922	0.980152	0.980153
North America	9.77×10^{-5}	0.009884	0.007243	0.109884	0.978373	0.978374
South America	0.000914	0.030232	0.015411	0.119095	0.973797	0.973797
Oceania	2.90×10^{-5}	0.005381	0.004148	0.104708	0.974060	0.974060

Abbreviations: MAE: Mean absolute error; MSE: Mean squared error; NSE: Nash–Sutcliffe efficiency; R^2: Coefficient of determination; RMSE: Root mean squared error; U^2: Theil's U-statistic.

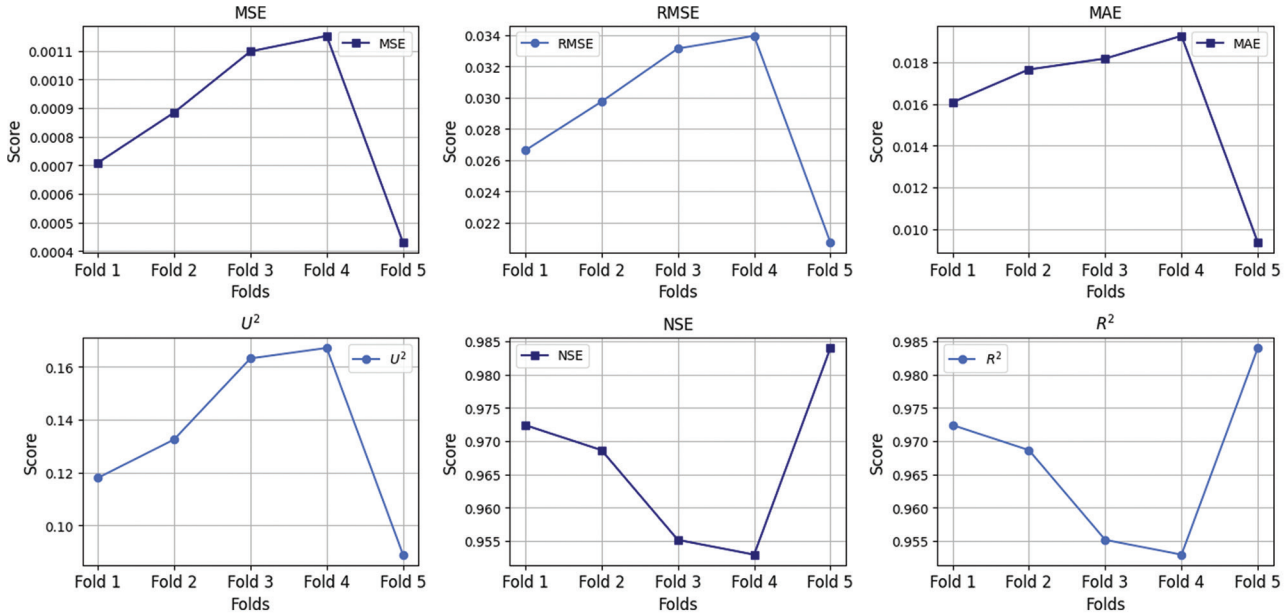

Figure 5. Five-fold cross-validation
Abbreviations: MAE: Mean absolute error; MSE: Mean squared error; NSE: Nash–Sutcliffe efficiency; R^2: Coefficient of determination; RMSE: Root mean squared error; U^2: Theil's U-statistic.

the model's enhanced capacity to predict low-exposure environments. North America exhibited comparable performance (RMSE = 0.0099 μg/m³; R^2 = 0.9784; MAE = 0.0072 μg/m³), reinforcing the pattern that regions with well-established monitoring infrastructure achieve superior forecast accuracy.

In contrast, Africa and Asia, the regions bearing the highest disease burden from $PM_{2.5}$ exposure, exhibited higher prediction errors. Africa yielded an RMSE of 0.0352 μg/m³ (R^2 = 0.9609; MAE = 0.0240 μg/m³), while Asia yielded an RMSE of 0.0444 μg/m³ (R^2 = 0.9270; MAE = 0.0301 μg/m³). These elevated errors reflect the documented sparsity of ground measurements in sub-Saharan Africa and South Asia, necessitating heavier reliance on satellite aerosol optical depth retrievals and chemical transport model inversions in the underlying SoGA dataset. Pre-1998 estimates for dust-dominated nations in these regions carry uncertainties exceeding 50% of reported concentrations, with errors substantially propagated from input data quality rather than limitations of the forecasting algorithm. South America exhibited intermediate performance (RMSE = 0.0302 μg/m³; R^2 = 0.9738; MAE = 0.0154 μg/m³), consistent with moderate data density and pollution levels in the region (Figure 6).

4.3. Country and regional trends

Global $PM_{2.5}$ exposure declined significantly over the 30-year study period, with mean population-weighted exposure decreasing from approximately 30 μg/m³ in 1990

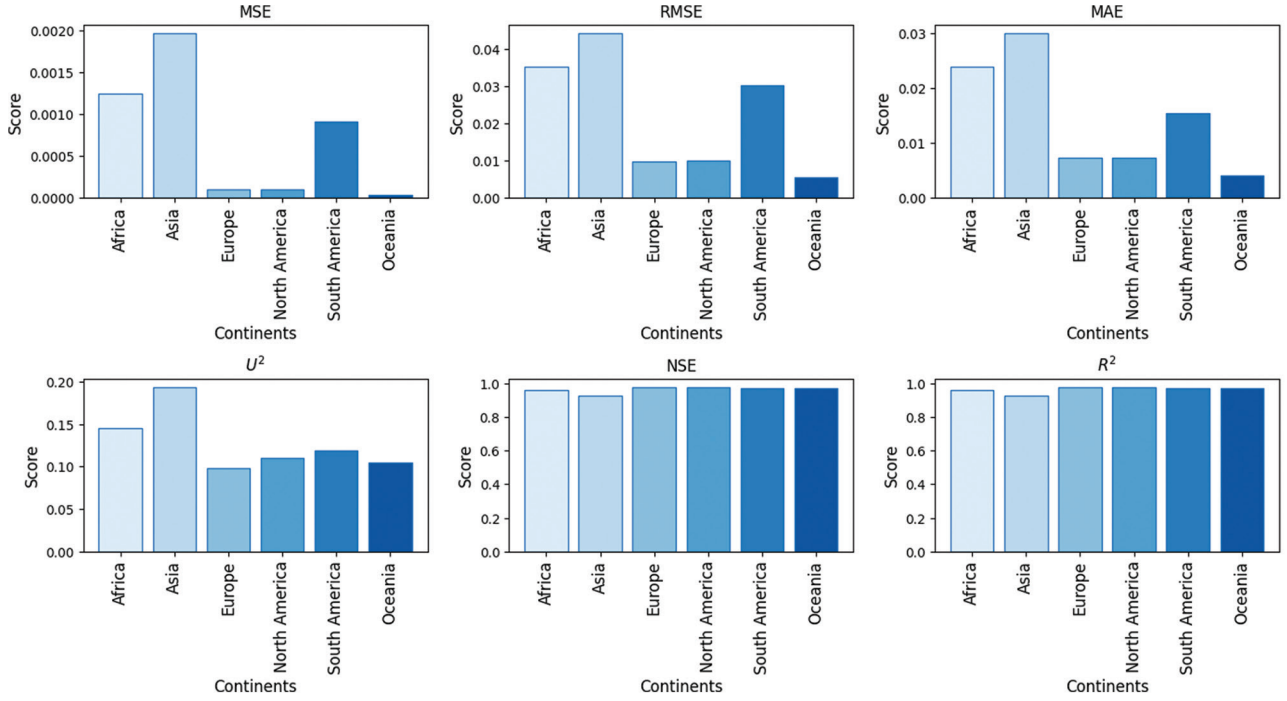

Figure 6. Model performance metrics across continents
Abbreviations: MAE: Mean absolute error; MSE: Mean squared error; NSE: Nash–Sutcliffe efficiency; R^2: Coefficient of determination; RMSE: Root mean squared error; U^2: Theil's U-statistic.

to 23.2 μg/m³ in 2020, reflecting the cumulative impact of air quality regulations in developed nations and improved emission controls in rapidly developing countries. However, substantial heterogeneity persists across countries. Leading polluted nations in 2020 included Qatar (mean exposure: 87.9 μg/m³), Niger (mean exposure: 85.1 μg/m³), Mauritania (mean exposure: 77.3 μg/m³), Bahrain (mean exposure: 67.4 μg/m³), and Egypt (mean exposure: 63.8 μg/m³), all substantially exceeding the WHO guideline of 5 μg/m³ (Table 6).

Notably, countries demonstrating the largest absolute improvements in air quality included Peru (−53.7 μg/m³ reduction; −66.5%), Bolivia (−59.9 μg/m³; −72.3%), Ecuador −30.3 μg/m³; −64.5%), and Singapore (−21.1 μg/m³; −60.3%), reflecting aggressive air quality management, economic restructuring, and technology adoption in these nations. One-sample Z-testing against the WHO guideline of 5 μg/m³ demonstrated that the global population-weighted exposure in 2020 significantly exceeded the health-protective threshold (mean = 25.3 μg/m³; Z = 11.04, $p<0.001$), representing a five-fold departure from guideline values. Regional stratification revealed that South Asia maintained the highest mean exposure (35.2 μg/m³), compared to 9.7 μg/m³ in Europe (two-sample Z = 4.99, $p<0.001$), underscoring substantial geographic inequality in air pollution burden (Figure 7).

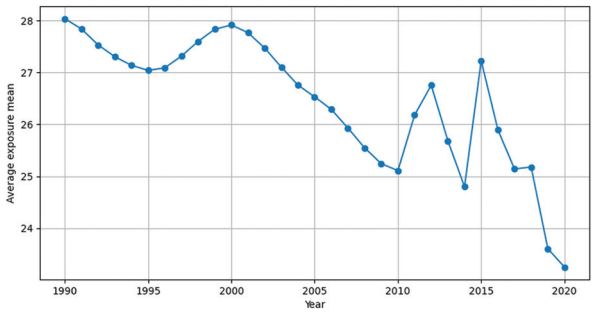

Figure 7. Time-series trajectories of average $PM_{2.5}$ exposure by year

Table 6. Top 10 countries by $PM_{2.5}$ exposure in 1990 and 2020

No.	Country	Mean (1990)	Mean (2020)	Change	% change
1	Bolivia	82.8	22.9	−59.9	−72.34
2	Peru	80.7	27.0	−53.7	−66.54
3	Ecuador	47.0	16.7	−30.3	−64.47
4	Singapore	35.0	13.9	−21.1	−60.29
5	Moldova	34.7	14.8	−19.9	−57.35
6	Guatemala	40.9	21.6	−19.3	−47.19
7	Belarus	32.9	14.6	−18.3	−55.62
8	Ukraine	33.1	14.9	−18.2	−54.98
9	Mexico	32.3	15.0	−17.3	−53.56
10	Pakistan	60.3	43.0	−17.3	−28.69

4.4. Statistical comparison of regional exposure trajectories

One-way analysis of variance (ANOVA) with type III sums of squares, appropriate for the imbalanced regional sample sizes in the 2020 data (Table 7), revealed highly significant differences in $PM_{2.5}$ exposure across geographic regions ($F_{7,85}$ = 16.43; $p<10^{-13}$). *Post hoc* Tukey pairwise comparisons identified significant contrasts between multiple region pairs. South Asia and Europe differed substantially (mean difference = 25.5 μg/m³); however, this pairwise comparison was not statistically significant after Bonferroni correction, as the adjusted 95% confidence interval included zero, despite the large effect size. East Asia and the Pacific significantly differed from the Middle East and North Africa (mean difference = 19.3 μg/m³, p=0.003), similar to the contrast between Europe/North America and South Asia (mean difference = 25.5 μg/m³, $p<0.001$), confirming the geographic heterogeneity of the air pollution burden.

Two-way ANOVA was conducted to evaluate the effects of region and year using balanced subsets for 1990, 2000, 2010, and 2020. The findings revealed highly significant effects of region ($F_{7,339}$ = 46.7; $p<10^{-46}$) and a significant temporal decline in exposure ($F_{3,339}$ = 2.86; p=0.037), with no significant interaction ($F_{21,339}$ = 0.46; p=0.979), indicating that pollution reduction trends are consistent across geographic regions (Table 8). Repeated-measures ANOVA within regions across the four selected years confirmed a significant temporal decline ($F_{3,21}$ = 5.39; p=0.0066), reflecting global progress toward improved air quality despite ongoing challenges in achieving WHO guideline compliance (Figure 8).

4.5. Explainability analysis: Attention weights

Attention-weight analysis examining the learned self-attention mechanisms revealed that, for countries experiencing recent air-quality improvements, the model focused attention weights on historical periods immediately preceding major policy shifts, such as the introduction of vehicle emission standards or industrial sulfur dioxide regulations. The model consistently emphasized these inflection points despite their temporal distance, enabling it to recognize that policy-driven structural breaks in pollution trends provide predictive leverage for future years (Figure 9).

5. Discussion

The present study proposes a temporally rigorous transformer-based forecasting model for predicting global population-weighted $PM_{2.5}$ exposure. The framework

Table 7. One-way analysis of variance with type III sums of squares for an unbalanced dataset

Source	Sum of squares	Degrees of freedom	*F*-statistic	*p*-value (PR[>F])
Intercept	3,543.122	1	24.463	3.77×10^{-6}
C (region)	16,657.836	7	16.43	1.65×10^{-13}
Residual	12,311.031	85	-	-

Table 8. Two-Way analysis of variance examining the effects of region and year on $PM_{2.5}$ exposure

Source	Sum of squares	Degrees of freedom	*F*-statistic	*p*-value (PR[>F])
Region	66,726.83	7	46.7	3.90×10^{-46}
Year	1,754.48	3	2.86	0.0366
Interaction (Region–year)	2,004.52	21	0.46	0.9795
Residual	69,185.06	339	-	-

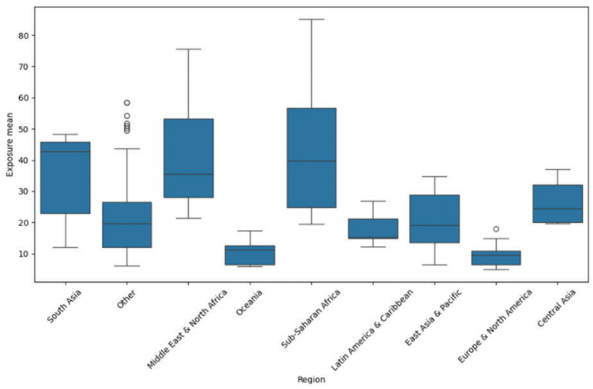

Figure 8. Boxplot of mean $PM_{2.5}$ exposure by region

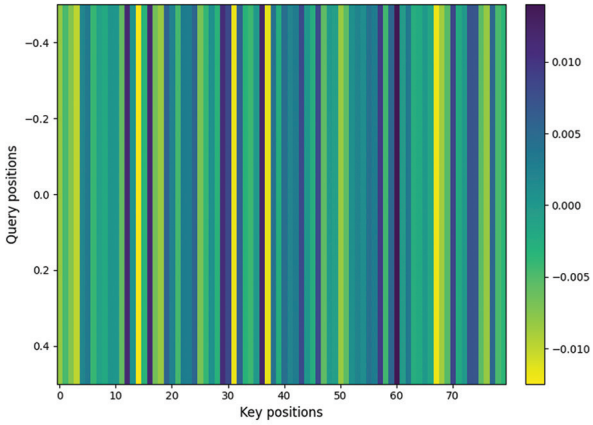

Figure 9. Transformer attention weights

provides realistic performance estimates based on harmonized 30-year panel data of 204 countries and employs time-aware validation protocols that reflect realistic operational forecasting conditions and prevent the inflation of metrics due to temporal leakage. Consistently high performance across all folds (NSE > 0.95; R^2 > 0.95) indicates that $PM_{2.5}$ exposure can be forecasted with reasonable accuracy using historical sequences, supporting the hypothesis that $PM_{2.5}$ exposure is learnable and shaped by long-term regional characteristics, policy contexts, and economic frameworks.

The geographic stratification of findings, with its emphasis on performance excellence in Europe and Oceania and the presence of higher errors in Asia and Africa, reflects a limitation of the original SoGA dataset. In particular, uncertainty exceeds 50% in pre-1998 estimates in dust-dominated countries, caused by the sparsity of data in regions with the highest health burden, suggesting that reported errors in these areas are more due to input data limitations than algorithm failure. This limitation can be mitigated as low-cost sensor networks proliferate and hybrid ground–satellite calibration systems mature, enabling future models to achieve more consistent global precision.

The interpretation of model predictions to guide policy recommendations must be systematically conducted by quantifying uncertainty within each region, especially when the projections are used to estimate health burdens or prioritize interventions in high-uncertainty areas. Another notable development in architecture is the introduction of country embeddings as a set of learnable parameters that are independent of one-hot or integer encoding. The model can achieve better generalization on data-sparse areas and be interpretable by allowing countries to occupy a continuous vector space based on learned similarities in pollution dynamics. Shapley Additive exPlanations and attention-weight analyses validate that embeddings represent meaningful country-level structures, with countries that have similar pollution profiles, geographic locations, or economic structures becoming more clustered during training, thereby enabling the transfer of predictive signals across borders. This method significantly outperforms baseline methodologies, which assume countries as non-moving categorical characteristics, justifying its use in future international environmental forecasting exercises.

The advantage of the transformer-based methodology over the LSTM and CNN baselines can be explained by the similarity of the architecture to the time-series nature of environmental data. Although LSTMs are effective at learning short- to medium-range dependencies, gated information tends to decay over multi-decadal sequences, particularly when seasonal dependencies must be captured over 20–30-year lookback periods. In contrast, transformers can directly attend to historically relevant years; no matter how many years have passed, a policy implemented 15 years ago can still be considered a key predictor of current trends if background circumstances remain relatively similar. Modeling such long-range dependencies is particularly useful for environmental applications, where policy impacts are often lagged and sustained.

The capacity of the proposed framework to model the entire range of the exposure level (i.e., from near guideline compliance to severe pollution) is evidenced by the model's high accuracy in low-pollution environments (e.g., Europe, Oceania, and North America). This capability is essential for policy applications, as it allows differentiation between regions where controls have been effectively implemented, with values close to the guideline, and regions where air quality is in the early stages of improvement. It is important to model both tails of the exposure distribution accurately. The accuracy of the model, with an RMSE of <0.01 $\mu g/m^3$ in low-pollution areas, is sufficient to track the progress toward WHO guideline attainment, enabling countries to adjust policies when exposures approach the safety threshold.

The observed global improvement in air quality, reflected in a median exposure reduction from approximately 30 $\mu g/m^3$ to 23 $\mu g/m^3$ over 30 years, represents the aggregate effect of policies in developed countries and the transfer of technology to rapidly industrializing economies. However, the fact that more than 90% of the global population still lives in areas exceeding the WHO limit of 5 $\mu g/m^3$, and that South Asian populations are 3.6 times more frequently exposed to air pollution than European populations, underscores that, despite progress, air pollution remains a major modifiable risk factor for early mortality and morbidity. The predictive power of the model provides quantitative data to inform policy development: Policymakers can use forecasts to determine whether existing emission control policies will achieve guideline targets within defined time frames or whether more stringent interventions are required.

This framework should be further developed in several complementary directions in future work. First, exogenous predictors (e.g., meteorological covariates such as temperature, precipitation, wind patterns, and satellite aerosol optical depth retrievals) could be integrated into the model to improve the predictive performance, particularly in data-sparse areas where meteorological variation is linked to changes in exposure. Second, ensemble methods

that combine transformer predictions with domain-specific chemical transport model outputs could leverage both the flexibility of data-driven approaches and the constraints of physical models, which may result in greater robustness. Third, probabilistic quantile regression can be incorporated to generate prediction intervals instead of point estimates, which would be beneficial to decision-making under uncertainty and is particularly important in policy contexts where guideline compliance depends on the interpretations of uncertainties. Fourth, sub-national exposure variability could be better predicted by creating spatially disaggregated models; however, this would require access to higher-resolution input data, which is currently unavailable for most low- and middle-income countries.

6. Conclusion

This study demonstrates the applicability and potential of transformer-based designs with learned country embeddings for predicting global, multi-decadal $PM_{2.5}$ exposure. Temporal rigor was imposed using expanding-window cross-validation, which provides more realistic forecasting performance for operational scenarios and strengthens confidence in policy applications. This is achieved through the combination of high predictive performance and interpretable decompositions obtained with Shapley Additive exPlanations and attention-weight analyses, making the framework a methodological breakthrough that enables evidence-based and transparent environmental policy design. The observed geographic heterogeneity in performance can be explained by insufficient underlying data quality rather than limitations of the algorithm; however, the framework also provides a foundation for future improvements as monitoring infrastructure expands and satellite-ground calibration products become more advanced. The ability to predict annual national-level $PM_{2.5}$ exposure with reasonable precision, augmented by explicit quantification of local uncertainty, equips policymakers to set science-based air quality targets, track progress toward WHO guidelines, and design climate-health interventions informed by quantitative exposure forecasts. With the growing global focus on air quality regulation and the increasing health and economic costs of pollution, transformer-based forecasting models provide actionable, interpretable information and can support the transition toward healthier and more sustainable atmospheric conditions.

Acknowledgments

None.

Funding

None.

Conflict of interest

The authors declare they have no competing interests.

Author contributions

Conceptualization: Syed Azeem Inam
Formal analysis: Syed Azeem Inam
Investigation: Syed Azeem Inam, Saddam Umer, Haider Rajput
Methodology: Syed Azeem Inam
Validation: Saddam Umer, Haider Rajput
Writing–original draft: Syed Azeem Inam, Saddam Umer, Haider Rajput
Writing–review & editing: Syed Azeem Inam

Ethics approval and consent to participate

Not applicable.

Consent for publication

Not applicable.

Availability of data

The datasets used and/or analyzed during the current study are available from the corresponding author on reasonable request.

References

1. Inam SA. A review of artificial intelligence for predicting climate driven infectious disease outbreaks to enhance global health resilience. *Discover Public Health*. 2025;22(1):738.

   doi: 10.1186/s12982-025-01167-4

2. Inam SA, Khan AA, Mazhar T, *et al*. PR-FCNN: A data-driven hybrid approach for predicting PM2.5 concentration. *Discover Artif Intell*. 2024;4(1):75.

   doi: 10.1007/s44163-024-00184-7

3. Inam SA, Zaidi SMH, Khan AA, Ullah S. A neural network approach to carbon emission prediction in industrial and power sectors. *Discover Appl Sci*. 2025;7(6):640.

   doi: 10.1007/s42452-025-07257-x

4. The World Bank. *The Global Health Cost of PM2.5 Air Pollution: A Case for Action Beyond 2021*. Washington, DC: The World Bank; 2022.

   doi: 10.1596/978-1-4648-1816-5

5. Pai SJ, Carter TS, Heald CL, Kroll JH. Updated world health organization air quality guidelines highlight the importance of non-anthropogenic $PM_{2.5}$. *Environ Sci Technol Lett*. 2022;9(6):501-506.

   doi: 10.1021/acs.estlett.2c00203

6. Liu J, He C, Si Y, *et al*. Toward better and healthier air quality:

Global $PM_{2.5}$ and O_3 pollution status and risk assessment based on the new WHO air quality guidelines for 2021. *Glob Chall*. 2024;8(4):2300258.

doi: 10.1002/gch2.202300258

7. Edlund KK, Killman F, Molnár P, Boman J, Stockfelt L, Wichmann J. Health risk assessment of $PM_{2.5}$ and $PM_{2.5}$-bound trace elements in Thohoyandou, South Africa. *Int J Environ Res Public Health*. 2021;18(3):1359.

doi: 10.3390/ijerph18031359

8. Elbarbary M, Oganesyan A, Honda T, *et al*. Systemic inflammation (c-reactive protein) in older Chinese adults is associated with long-term exposure to ambient air pollution. *Int J Environ Res Public Health*. 2021;18(6):3258.

doi: 10.3390/ijerph18063258

9. McDuffie EE, Martin RV, Spadaro JV, *et al*. Source sector and fuel contributions to ambient $PM_{2.5}$ and attributable mortality across multiple spatial scales. *Nat Commun*. 2021;12(1):3594.

doi: 10.1038/s41467-021-23853-y

10. Ghosh R, Causey K, Burkart K, Wozniak S, Cohen A, Brauer M. Ambient and household $PM_{2.5}$ pollution and adverse perinatal outcomes: A meta-regression and analysis of attributable global burden for 204 countries and territories. *PLoS Med*. 2021;18(9):e1003718.

doi: 10.1371/journal.pmed.1003718

11. Southerland VA, Anenberg SC, Harris M, *et al*. Assessing the distribution of air pollution health risks within cities: A neighborhood-scale analysis leveraging high-resolution data sets in the bay area, California. *Environ Health Perspect*. 2021;129(3):37006.

doi: 10.1289/EHP7679

12. Fang T, Di Y, Xu Y, *et al*. Temporal trends of particulate matter pollution and its health burden, 1990–2021, with projections to 2036: A systematic analysis for the global burden of disease study 2021. *Front Public Health*. 2025;13:1579716.

doi: 10.3389/fpubh.2025.1579716

13. Booth A, James P, McGough S, Solaiman E. Cross-regional deep learning for air quality forecasting: A comparative study of CO, NO_2, O_3, $PM_{2.5}$, and PM_{10}. *Forecasting*. 2025;7(4):66.

doi: 10.3390/forecast7040066

14. Benali AAE, Cafaro M, Epicoco I, Pulimeno M, Schioppa EJ. *Just in Time Transformers*. New York: Cornell University; 2024.

15. Muthukumar P, Cocom E, Nagrecha K, *et al*. Predicting PM2.5 atmospheric air pollution using deep learning with meteorological data and ground-based observations and remote-sensing satellite big data. *Air Qual Atmos Health*. 2022;15(7):1221-1234.

doi: 10.1007/s11869-021-01126-3

16. Nedungadi V, Munir MA, Rußwurm M, *et al*. *AirCast: Improving Air Pollution Forecasting through Multi-Variable Data Alignment*. New York: Cornell University; 2025.

17. Oldenburg V, Cardenas-Cartagena J, Valdenegro-Toro M. *Forecasting Smog Clouds with Deep Learning*. New York: Cornell University; 2024.

18. Boogaard H, Pant P, Künzli N. Editorial: Science to foster the WHO air quality guideline values. *Int J Public Health*. 2025;69:1608249.

doi: 10.3389/ijph.2024.1608249

19. Tello-Leal E, Ramirez-Alcocer UM, Macías-Hernández BA, Hernandez-Resendiz JD. Evaluation of deep learning models for predicting the concentration of air pollutants in urban environments. *Sustainability*. 2024;16(16):7062.

doi: 10.3390/su16167062

20. Huang S, Xiao X, Guo H. A novel method for carbon emission forecasting based on EKC hypothesis and nonlinear multivariate grey model: Evidence from transportation sector. *Environ Sci Pollut Res Int*. 2022;29(40):60687-60711.

doi: 10.1007/s11356-022-20120-5

21. Ran Q, Bu F, Razzaq A, *et al*. When will China's industrial carbon emissions peak? Evidence from machine learning. *Environ Sci Pollut Res Int*. 2023;30(20):57960-57974.

doi: 10.1007/s11356-023-26333-6

22. Costantini L, Laio F, Mariani MS, Ridolfi L, Sciarra C. Forecasting national CO_2 emissions worldwide. *Sci Rep*. 2024;14(1):22438.

doi: 10.1038/s41598-024-73060-0

23. Lee JB, Lee JB, Koo YS, *et al*. *Development of a Deep Neural Network for Predicting 6 Hour Average $PM_{2.5}$ Concentrations up to Two Subsequent Days Using Various Training Data*. [Preprint]; 2021.

doi: 10.5194/gmd-2021-356

24. Damkliang K, Chumnaul J. Deep learning and statistical approaches for area-based PM2.5 forecasting in Hat Yai, Thailand. *J Big Data*. 2025;12(1):36.

doi: 10.1186/s40537-025-01079-9

25. Utku A, Can U, Alpsülün M, *et al*. Advancing air quality monitoring: Deep learning-based CNN-RNN hybrid model for PM2.5 forecasting. *Atmosphere*. 2025;16(9):1003.

doi: 10.3390/atmos16091003

26. Zhang Y, Zhang W, Wu B, Yi W. Regional PM2.5 pollution forecasting using a hybrid model based on multi-scales feature fusion and deep learning algorithms. *PLoS One*. 2025;20(10):e0333489.

doi: 10.1371/journal.pone.0333489

27. Yeo I, Choi Y, Lops Y, Sayeed A. Efficient PM2.5

forecasting using geographical correlation based on integrated deep learning algorithms. *Neural Comput Appl*. 2021;33(22):15073-15089.

doi: 10.1007/s00521-021-06082-8

28. Samal KKR, Babu KS, Das SK. Multi-directional temporal convolutional artificial neural network for PM2.5 forecasting with missing values: A deep learning approach. *Urban Clim*. 2021;36:100800.

doi: 10.1016/j.uclim.2021.100800

29. Potavijit C, Pattarapanitchai P, Nontapa C. A hybrid deep learning model for forecasting PM2.5 concentrations in Northern Thailand from satellite images. *Glovento J Integr Stud*. 2025;1(1):6.

doi: 10.63665/gjis.v1.6

30. Wu Y, Wang X, Wang M, Liu X, Zhu S. Time-series forecasting of $PM_{2.5}$ and PM_{10} concentrations based on the integration of surveillance images. *Sensors (Basel)*. 2024;25(1):95.

doi: 10.3390/s25010095

31. Dairi A, Harrou F, Sun Y. Efficient Deep Learning-Driven Approach for PM2.5 Forecasting at Different Locations in Spain. In: *2021 IEEE 3rd Eurasia Conference on Biomedical Engineering, Healthcare and Sustainability (ECBIOS)*. IEEE; 2021. p. 173-178.

doi: 10.1109/ECBIOS51820.2021.9510462

32. Vignesh PP, Jiang JH, Kishore P. Predicting $PM_{2.5}$ concentrations across USA using machine learning. *Earth Space Sci*. 2023;10(10):1-15.

doi: 10.1029/2023ea002911

ACCSCIENCE PUBLISHING

Explora: Environment and Resource

LETTER TO EDITOR

Is biological control using seed-reducing agents a waste of time?

Brian W. van Wilgen[1]*, David M. Richardson[1], Guy F. Midgley[1], and Patricia M. Holmes[2]

[1]Centre for Invasion Biology, School for Climate Studies, Stellenbosch University, Stellenbosch, Western Cape, South Africa

[2]Department of Conservation Ecology and Entomology, Faculty of Agrisciences, Stellenbosch University, Stellenbosch, Western Cape, South Africa

The ecological and socio-economic impacts of invasive alien species are demonstrably substantive at the global level and may be locally devastating.[1] Scientific evidence lies at the heart of effective approaches to combating this well-recognized problem. Given the associated costs, it is crucial to develop and test these solutions with careful consideration of the risks involved. On this basis, we wish to counter the premature conclusion of the recent paper by Veldtman and Strydom[2] on assessing the effectiveness of Australian *Acacia* biological control in South Africa. The study used primarily seed-reducing agents and concluded that the seed-reducing biocontrol program on these plants is a wasted effort.

Biological control is one of the few interventions that can lead to a permanent improvement in the state of biodiversity in ecosystems under severe invasion pressure.[3] In the case of plant invasions, where physical control is costly, biological control has offered an effective and affordable means to reduce the viability of invasive populations, and thus significantly increase the effectiveness of physical control efforts. We not only criticize here the conclusion of Veldtman and Strydom as premature and arguably irresponsible, but also propose that their valuable work could be far more productively framed.

Veldtman and Strydom's paper points out, correctly, that pre-treatment baselines and monitoring data are necessary to accurately gauge the effectiveness of control interventions.[2] This has, in fact, been done in the case of Australian acacias in South Africa within the limits of resources available. Veldtman and Strydom's work has demonstrated that, in some situations, there is still an abundance of seed despite the application of biological control. The problem is that confining any assessment to this one consideration ignores the bigger picture and, therefore, invalidates any assumptions that biological control is not working. The obvious patterns of change that have happened since biological control was initiated on Australian *Acacia* species in South Africa provide evidence that unquestionable benefits have ensued, and continue to do so, from deploying seed-reducing and other agents against the invasive *Acacia* species. Some additional aspects are outlined below.

We concede that a plant population may persist on a site in the presence of seed-reducing biological control agents. However, it should be recognized that dispersal from that site is a function of the number of seeds produced,[4,5] and that shorter dispersal distances will reduce the rate of spread to new sites. This, in turn, will increase the effectiveness of physical control efforts. There is a threshold in terms of control effort that needs to be reached before the spread can be reversed.[6] When seed production is

***Corresponding author:**
Brian W. van Wilgen (bvanwilgen@sun.ac.za)

Citation: van Wilgen BW, Richardson DM, Midgley GF, Holmes PM. Is biological control using seed-reducing agents a waste of time? *Explora Environ Resour*. 2025;2(4):025140028. doi: 10.36922/EER025140028

Received: April 1, 2025

Accepted: August 18, 2025

Published online: September 3, 2025

reduced, that threshold will be lower, and therefore more affordable and attainable. There are also two independent data sources, one from roadside surveys and the other from remote sensing, showing that populations of Australian acacias under biological control have contracted,[7,8] or spread relatively less than other invasive plants at a national scale in South Africa. These findings are supported by other extensive, thorough, long-term monitoring projects.[9,10]

Reducing the number of seeds can also reduce the invasive potential of an introduced species. The success of invasive species is enhanced by post-introduction evolution.[11] Substantial reductions in the numbers of seeds produced will correspondingly reduce the effectiveness of this selective pressure, again assisting control efforts.

Interactions between alien and indigenous plants, as well as granivorous species, also need to be considered. Using *Acacia saligna* as an example, seed bank dynamics are substantially affected by stand density and the impact of seed consumption by rodents. While rodents consume significant numbers of *A. saligna* seeds, the rodents avoided closed canopy stands before the introduction of the pathogenic fungus *Uromycladium morrisii*. Dense stands that existed before the introduction of the fungus led to the extirpation of indigenous plants.[12] Following the introduction of *U. morrisii*, the stand density and canopy cover of *A. saligna* have declined, and rodents now consume more seeds. In addition, the relatively open canopies allow the persistence of some indigenous plants and the ongoing replenishment of their seed banks. Biological control has thus made it possible for indigenous species to re-establish after physical clearing,[13,14] a factor that was not considered by Veldtman and Strydom.

In South Africa, the decision to restrict biological control to seed-reducing agents was made to protect plants with commercial value.[15] Some seeds will always survive, and Veldtman and Strydom suggest that drastic reductions in seed production (>99%) may be necessary to prevent the persistence of acacias on a particular site. This point is considered, but one of the largest management problems is dealing with the massive regeneration of seedlings from soil-stored seed banks after fires. A substantial reduction in seed production, achieved using biological control, will almost certainly reduce this effort, again making physical control possible where it would otherwise not have been. We contend that if we had introduced the seed-feeding biological control agents when the trees were first introduced, the massive seed banks would likely not have developed, and the problem would have been easier to manage. As the use of Australian *Acacia* trees is growing around the world,[16] it would be important to try to reduce the invasion debt that this is causing. We therefore recommend seed-reducing biological control as a practical, proven technology to assist with this. Such a practice could, for example, be incorporated into global guidelines for the use of non-native trees.[17]

We acknowledge shortcomings in the historic assessment of control effectiveness. However, in South Africa, studies have been conducted on multiple sites with several species for over 20 years.[10,18] To justify the conclusion that seed-reducing agents are not effective in helping to control Australian *Acacia* species, it would be necessary to provide more convincing evidence than Veldtman and Strydom's current limited study of seed banks in predetermined, but not necessarily representative, sites (e.g., they only studied sites where the acacias were abundant, with closed canopies, only considered intra- and not inter-species competition and interactions, and did not consider impacts on spread from the site). What is needed is an evaluation of efficacy in the context of what would have happened if the intervention had not been there (i.e., a counterfactual study at a landscape scale).[19]

We must also guard against the implied general conclusions that biological control is not warranted. For example, Veldtman and Strydom list one of the "consequences" of (in their view, unwarranted) support for biological control as "more investment into biological control in South Africa." This is not a negative consequence and ignores the fact that biological control has brought numerous problematic species under control, not only in South Africa but globally, and that biological control is the only management intervention that has resulted in declines in such species when assessed at a national scale.[7,8] Further investment in biological control in South Africa and elsewhere globally would therefore bring significant benefits to ecosystems and society. Veldtman and Strydom's work has provided additional insights into some of the dynamics of invasive alien plant populations as affected by biological control. However, it would be far more constructive to pool their findings with those of others within a broader framework than to condemn the exercise as a "waste of effort."

Conflict of interest

The authors declare that they have no competing interests.

References

1. Pyšek P, Hulme PE, Simberloff D, et al. Scientists' warning on invasive alien species. *Biol Rev.* 2020;95:1511-1534.

   doi: 10.1111/brv.12627

2. Veldtman R, Strydom M. Prioritizing scientific data over expert opinion in the valid assessment of Australian *Acacia* biocontrol success. *Explora Environ Resour*. 2025;2:5876.

doi: 10.36922/eer.5876

3. Van Driesche RG, Carruthers RI, Center T, *et al*. Classical biological control for the protection of natural ecosystems. *Biol Control*. 2010;54:S2-S33.

   doi: 10.1016/j.biocontrol.2010.03.003

4. Harper JL. *Population Biology of Plants*. London, England: Academic Press; 1977.

5. Schurr FM. *Seed Dispersal and Range Dynamics of Plants: Understanding and Predicting the Spatial Dynamics of Serotinous Proteaceae*. Germany: Universität Regensburg, [Doctoral Dissertation]; 2007.

6. Van Wilgen BW, Fill JM, Baard J, Cheney C, Forsyth AT, Kraaij T. Historical costs and projected future scenarios for the management of invasive alien plants in protected areas in the Cape Floristic Region. *Biol Conserv.* 2016;200:168-177.

   doi: 10.1016/j.biocon.2016.06.008

7. Henderson L, Wilson JR. Changes in the composition and distribution of alien plants in South Africa: An update from the Southern African Plant Invaders Atlas. *Bothalia.* 2017;47:a2172.

   doi: 10.4102/abc.v47i2.2172

8. Kotze JD, Wannenburgh A, Van Wilgen BW. Changes in the cover of selected invasive alien plant taxa between 2008 and 2023 in South Africa. *Biol Invasions*. 2025;27:98.

   doi: 10.1007/s10530-025-03558-9

9. Impson FAC, Hoffmann JH, Impson OR, Kleinjan CA, Moran VC. Densities of a perennial invasive tree, *Acacia cyclops*, decline in the 20 years since inception of biological control with two seed-reducing agents, a flower-galling midge and a seed-feeding weevil. *Biol Control*. 2024;189:105442.

   doi: 10.1016/j.biocontrol.2024.105442

10. Wood AR, Morris MJ. Impact of the gall-forming rust fungus *Uromycladium tepperianum* on the invasive tree *Acacia saligna* in South Africa: 15 years of monitoring. *Biol Control*. 2007;41:68-77.

    doi: 10.1016/j.biocontrol.2006.12.018

11. Castillo ML, Schaffner U, Van Wilgen BW, Le Roux JJ. The contribution of phenotypic traits, their plasticity, and rapid evolution to invasion success: Insights from an extraordinary natural experiment. *Ecography*. 2021;44:1035-1050.

    doi: 10.1111/ecog.05541

12. Holmes PM. Dispersal and predation of alien *Acacia* seeds: Effects of season and invading stand density. *S Afr J Bot*. 1990;56:428-434.

    doi: 10.1016/S0254-6299(16)31037-7

13. Holmes PM. Depth distribution and composition of seed-banks in alien-invaded and uninvaded fynbos vegetation. *Austral Ecol*. 2002;27:110-120.

    doi: 10.1046/j.1442-9993.2002.01164.x

14. Ngwenya DK, Holmes PM, Geerts S, Esler KJ. Delaying a prescribed burn to scale up the restoration of alien-invaded Lowland Sand Fynbos in South Africa. *Austral Ecol*. 2023;49:e13469.

    doi: 10.1111/aec.13469

15. Impson FAC, Kleinjan CA, Hoffmann JH, Mudavanhu P. A review of research and developments with insect agents used for biological control of Australian *Acacia* species (Caesalpinioideae) in South Africa. *Afr Entomol*. 2021;29:693-712.

    doi: 10.4001/003.029.0693

16. Richardson DM, Le Roux JJ, Marchante E. Wattles: Australian Acacia species around the world. Wallingford, England: CABI: 2023.

17. Novoa A, Vimercati G, Brundu G, *et al*. Stakeholder's views on the global guidelines for the sustainable use of non-native trees. *People Nat*. 2024;6:1640-1654.

    doi: 10.1002/pan3.10670

18. Impson FAC, Kleinjan CA, Hoffmann JH, Post JA, Wood AR. Biological control of Australian *Acacia* species and *Paraserianthes lophantha* (Willd.) Nielsen (Mimosaceae) in South Africa. *Afr Entomol*. 2011;19:186-207.

    doi: 10.4001/003.019.0210

19. McConnachie M, Van Wilgen BW, Gaertner M, *et al*. Using counterfactuals to evaluate the cost-effectiveness of controlling biological invasions. *Ecol Appl*. 2016;26:475-483.

    doi: 10.1890/15-0351

ACCSCIENCE PUBLISHING

Explora: Environment and Resource

LETTER TO EDITOR

Authors' reply: Is biological control using seed-reducing agents a waste of time?

Ruan Veldtman[1,2,3]* and Matthys Strydom[4]

[1]South African National Biodiversity Institute, Cape Town, Western Cape, South Africa

[2]National Institute for Theoretical and Computational Science, Stellenbosch, Western Cape, South Africa

[3]Conservation Ecology and Entomology, Stellenbosch University, Stellenbosch, Western Cape, South Africa

[4]Academy for Environmental Leadership SA, Upington, Northern Cape, South Africa

In South Africa, the existing weed biocontrol programs are lauded as successful and considered an essential approach to addressing plant invasions nationally.[1,2] Using the much-researched biological control program on Australian *Acacias* using seed-feeding agents; however, Veldtman and Strydom[2] illustrated the weak scientific base for claiming success of biological control agents in suppressing these species. Noteworthy, van Wilgen and Richardson[1] state that South Africa is a world leader in weed biocontrol; therefore, framing our arguments using the textbook Australian *Acacia* biocontrol program is appropriate. We thank van Wilgen *et al.*[3] for responding to our review paper[2] as it advances further scientific discourse in the use of biological control agents on invasive weed species.

The criticisms by van Wilgen *et al.*[3] regarding our review create the impression that several of the main points were missed. They state "*Veldtman and Strydom's paper points out, correctly, that pre-treatment baselines and monitoring data are necessary to accurately gauge the effectiveness of control. This has in fact been done in the case of Australian acacias in South Africa.*"[3,p.1] We are not sure if we misunderstood this statement. Our review cites every primary peer-reviewed study on Australian *Acacia* biological control, seed bank dynamics, and effects of fire, and none of these studies have proven an effect of the released agents. In addition, few, if any, of these investigations have been done with the purpose of serving as baseline data or for monitoring purposes. Furthermore, it is claimed that in our review, only seed abundance, and not the wider context, is considered. However, Veldtman and Strydom[2] considered all aspects listed by van Wilgen *et al.*[3] to assess biological control success. This included reviewing the literature of the area of occupancy, dispersal rate, population dynamics, seed bank dynamics, and interspecific relationships of invasive Australian *Acacia* within their invaded ranges in South Africa.

Second, van Wilgen *et al.*[3] state that we present insufficient evidence to indicate that the Australian *Acacia* biocontrol has been unsuccessful. A major point of our review is that appropriate hypothesis testing requires data to reject the null hypothesis of no effect to demonstrate that biocontrol on Australian *Acacia* is effective, otherwise the chance of a Type 1 error is too great. As shown in Table 2 of our review,[2,pp.6-8] no studies have demonstrated that the release of biocontrol agents on the invasive Australian *Acacia* in South Africa has sufficiently impacted their population's dynamics to the extent that it has reduced their invasive impact. Instead, the assertion that this biocontrol program has reduced the impact of these species is almost solely based on expert opinion or counterfactual arguments.[1,4,5]

***Corresponding author:**
Ruan Veldtman
(veldtman@sun.ac.za)

Citation: Veldtman R, Strydom M. Authors' reply: Is biological control using seed-reducing agents a waste of time? *Explora Environ Resour*. 2025;2(4):025360065. doi: 10.36922/EER025360065

Received: September 4, 2025

Accepted: September 5, 2025

Published online: September 26, 2025

Third, as van Wilgen *et al.*[3] have noted, the broader question of whether biological control of weeds in general can result in desirable outcomes[6] is not directly relevant when reviewing the success of a specific weed biocontrol program. For instance how can the successful biological control of cacti or water weeds[7] be used to justify or predict the success of biocontrol efforts targeting Australian *Acacia*?

Van Wilgen *et al.*[3] suggest that any reduction in seed production by seed-reducing agents will translate in a reduced rate of spread of invasive plants. However, this assumption overlooks thresholds below which seed-reducing agents need to reduce seed production to decrease the short- and long-distance dispersal rates of their invasive host plants.[8-10] In addition, the level to which specialist seed-predators, such as all biocontrol agents released against invasive Australian *Acacia* in South Africa, can reduce host dispersal rate, is a function of the host plants' dynamics rather than that of the biological control agents.[11] For example, where a host plant population has no Allee effect, the dispersal rate cannot be slowed or reversed, even in the presence of strong predation. At present, the seed production thresholds required to reduce dispersal in invasive Australian *Acacia* have not been determined empirically, nor is it known whether these species exhibit Allee effects at low densities. The assumption that seed-reducing biocontrol agents limit dispersal rate is therefore not empirically substantiated.

We already critiqued the use of comparative invasion rates from Henderson and Wilson[12] to assess seed biological control,[2] who argue that invasive Australian *Acacia* display lower dispersal rates than other invasive plants in South Africa. This comparison is problematic as it compares species with differing growth forms, life histories, modes of dispersal, and invasion stages. Moreover, Henderson and Wilson[12] do not provide evidence that the rate of spread of invasive Australian *Acacia* species has declined over time.

Kotze *et al.*[13] present data on changes in the invaded area of invasive plants with and without biological control in South Africa. However, due to a lack of appropriate control treatments these data cannot be used to infer causal impacts of biological control on their hosts distribution ranges. Their findings show that the invaded area of invasive plants not under biological control decreased, remained the same, or increased in South Africa. This indicates that there are factors other than biological control influencing the area occupied by invasive alien plants in South Africa (Veldtman and Strydom[2]). Therefore, the observed changes in the area occupied by the invasive plants in South Africa under biological control could alternatively be the consequence of other factors (*e.g.*, mechanical and chemical clearing, land use change, *etc.*). Kotze *et al.*[13] therefore provide, at best, circumstantial evidence that weed biocontrol has reduced the area occupied by Australian *Acacia* in South Africa.

Veldtman and Strydom[2] identified key methodological shortcomings in the works of both Wood and Morris[14] and Impson *et al.*,[15] whose long-term studies attempt to link biocontrol impact to reductions in population size or area occupied. Wood and Morris[14] reported a reduction in stand density but did not quantify canopy cover. A reduction in stand density could therefore also be due to self-thinning.[2] Impson *et al.*[15] in particular raises multiple concerns beyond methodological errors. These include (i) data integrity issues such as implausible tree density estimates (*e.g.*, 26533 plants/m^2), (ii) internal inconsistencies such as contradictory fire records (*e.g.*, 2001 and 2017 vs. 2000 and 2017 for the 4-year burnt site), (iii) pseudoreplication, as all long-term monitoring plots were located in a single protected area (De Hoop Nature Reserve), which are 0.2–10 km from each other, and (iv) taxonomic inaccuracies, such as reporting that both *Dasineura rubiformis* and *Dasineura dielsi* were studied on *Acacia cyclops*. These issues raise valid concerns regarding the accuracy and credibility of Impson *et al.*[15]

The case study put forward by van Wilgen *et al.*[3] that species interactions need to be considered when evaluating Australian *Acacia* biocontrol is at best circumstantial evidence. For example, Holmes[16] suggested that reduced seed predation by rodents in closed canopy stands of *Acacia saligna* was due to reduced rodent activity within these stands. However, rodent population densities were not measured, and an alternative explanation of predator satiation in a seed-abundant environment, cannot be ruled out. Moreover, Holmes[16] questioned the importance of seed predation by rodents, noting that ants removed and buried seeds at a faster rate than they were consumed by rodents. There is also no supporting empirical evidence for the claim that *Uromycladium morrisii* has caused a decline in the stand density of *A. saligna*, which translates into reduced canopy cover (*i.e.*, reduced area of occupancy).[2] Thus, the conclusion that declining canopy cover is associated with increased rodent seed predation within *A. saligna* populations lacks support. Furthermore, neither Holmes[17] nor Ngwenya *et al.*[18] demonstrated that biological control allowed for native species recovery after physical clearing. On the contrary, they demonstrated a reduced native species diversity and cover as well as depleted or absent native seed banks following invasion by *A. saligna*. Their findings underscore the need for active management and restoration efforts to recover indigenous plant communities after the removal of *A. saligna* populations.

Van Wilgen *et al.*[3] state that a substantial reduction in seed production by seed-reducing biological control agents targeting invasive Australian *Acacia* species will reduce the number of regenerating seedlings after disturbance events, thereby making physical control feasible in areas where it was previously impractical. Despite the assertion that seed bank reduction through biocontrol will reduce management effort, there is no empirical evidence quantifying the level of reduction needed.[2] In fact, empirical studies suggest otherwise. Post-biocontrol assessments found that seed bank size was similar to pre-biocontrol levels[19] or remained large enough to sustain post-disturbance seedling regeneration, which was comparable to the pre-control levels.[2] These findings imply that the number of seedlings and trees requiring active management within invasive Australian *Acacia* stands have remained unchanged. It is also stated that Strydom *et al.*[19-21] only investigated seed banks in predetermined, but not necessarily representative sites. However, these three peer-reviewed papers are the only studies in South Africa to date that have collectively investigated all stages of the seed bank dynamics of three invasive Australian *Acacia species* regarded as under substantial biocontrol.[2] Furthermore, these studies were in close proximity (0–10 km) to the original release sites of the investigated biocontrol agents, and close to the sites where these agents' impact were previously assessed as successful.[14,22-25] Thus, how can the sites sampled in Strydom *et al.*[19-21] then not be representative?

In conclusion, the extent to which seed production of invasive Australian *Acacia* in South Africa has been reduced by their seed-reducing biological control agents remains largely unquantified as stated in our review.[2] For the gall-forming biological control agents whose impact on their invasive Australian *Acacia* hosts has been assessed, it has been demonstrated that 22–60% of the pods produced on a population level may be lost.[21] These values fall short of the threshold required to cause a reduction in the area occupied by these plants.[2] Based on the evidence provided by van Wilgen *et al.*,[3] there is currently no new published evidence supporting the claim that biocontrol has reduced physical management effort, or that earlier implementation would have done so. If it is argued that any seed reduction would result in fewer seedlings to manage, then the threshold of reduction required still needs to be experimentally determined. We contend that the status quo of assessing weed biocontrol requires urgent reform and we should in fact guard against placing expert opinion above empirically collected data. Rather, investment in experimentally sound data collection, especially before and after release, is required to assess whether classical biological control agents result in a significant reduction of the impact of their invasive plant hosts.

Conflict of interest

The authors declare that they have no competing interests.

References

1. Van Wilgen BW, Richardson DM. South African contributions to the understanding of plant invasion ecology and management. *S Afr J Bot.* 2025;181:391-404.

   doi: 10.1016/j.sajb.2025.04.029

2. Veldtman R, Strydom M. Prioritizing scientific data over expert opinion in the valid assessment of Australian *Acacia* biocontrol success. *Explora Environ Resour*. 2025;2(1):5876.

   doi: 10.36922/eer.5876

3. Van Wilgen BW, Richardson DM, Midgley GF, Holmes PM. Is biological control using seed-reducing agents a waste of time? *Explora Environ Resour*. 2025:025140028.

   doi: 10.36922/eer025140028

4. Van Wilgen BW, Moran VC, Hoffmann JH. Some perspectives on the risks and benefits of biological control of invasive alien plants in the management of natural ecosystems. *Environ Manag.* 2013;52:531-540.

   doi: 10.1007/s00267-013-0099-4

5. McConnachie M, Van Wilgen BW, Gaertner M, *et al.* Using counterfactuals to evaluate the cost-effectiveness of controlling biological invasions. *Ecol Appl.* 2016;26(2):475-483.

   doi: 10.1890/15-0351

6. Van Driesche RG, Carruthers RI, Center T, *et al.* Classical biological control for the protection of natural ecosystems. *Biol Control*. 2010;54:S2-S33.

   doi: 10.1016/j.biocontrol.2010.03.003

7. Hill MP, Moran VC, Hoffmann JH, *et al.* More than a century of biological control against invasive alien plants in South Africa: A synoptic view of what has been accomplished. In: Van Wilgen B, Measey J, Richardson D, Wilson J, Zengeya T, editors. *Biological Invasions in South Africa.* Vol 14. Cham: Springer, Invading Nature - Springer Series in Invasion Ecology; 2020. p. 553-572.

   doi: 10.1007/978-3-030-32394-3_19

8. Clark JS, Silman M, Kern R, Macklin E, HilleRisLambers J. Seed dispersal near and far: Patterns across temperate and tropical forests. *Ecology*. 1999;80(5):1475-1494.

   doi: 10.1890/0012-9658(1999)080[1475:sdnafp]2.0.co;2

9. Nathan R. Long-distance dispersal of plants. *Science* 2006;313(5788):786-788.

   doi: 10.1126/science.1124975

10. Nathan R, Schurr FM, Spiegel O, Steinitz O, Trakhtenbrot A, Tsoar A. Mechanisms of long-distance seed dispersal. *Trends Ecol Evolut.* 2008;23(11):638-647.

doi: 10.1016/j.tree.2008.08.003

11. Fagan WF, Lewis MA, Neubert MG, Van Den Driessche . Invasion theory and biological control. *Ecol Lett.* 2002;5(1):148-157.

    doi: 10.1046/j.1461-0248.2002.0_285.x

12. Henderson L, Wilson JR. Changes in the composition and distribution of alien plants in South Africa: An update from the Southern African plant invaders atlas. *Bothalia.* 2017;47:a2172.

    doi: 10.4102/abc.v47i2.2172

13. Kotze I, Wannenburgh A, Van Wilgen BW. Changes in the cover of selected invasive alien plant taxa between 2008 and 2023 in South Africa. *Biol Invasions.* 2025;27:98.

    doi: 10.1007/s10530-025-03558-9

14. Wood AR, Morris MJ. Impact of the gall-forming rust fungus *Uromycladium tepperianum* on the invasive tree *Acacia saligna* in South Africa: 15 years of monitoring. *Biol Control.* 2007;41:68-77.

    doi: 10.1016/j.biocontrol.2006.12.018

15. Impson FAC, Hoffmann JH, Impson OR, Kleinjan CA, Moran VC. Densities of a perennial invasive tree, *Acacia cyclops*, decline in the 20 years since inception of biological control with two seed-reducing agents, a flower-galling midge and a seed-feeding weevil. *Biol Control.* 2024;189:105442.

    doi: 10.1016/j.biocontrol.2024.105442

16. Holmes PM. Dispersal and predation of alien Acacia seeds: Effects of season and invading stand density. *S Afr J Bot.* 1990;56:428-434.

    doi: 10.1016/S0254-6299(16)31037-7

17. Holmes PM. Depth distribution and composition of seed-banks in alien-invaded and uninvaded fynbos vegetation. *Austral Ecol.* 2002;27:110-120.

    doi: 10.1046/j.1442-9993.2002.01164.x

18. Ngwenya DK, Holmes PM, Geerts S, Esler KJ. Delaying a prescribed burn to scale up the restoration of alien-invaded Lowland Sand Fynbos in South Africa. *Austral Ecol.* 2023;49:e13469.

    doi: 10.1111/aec.13469

19. Strydom M, Veldtman R, Ngwenya MZ, Esler KJ. Invasive Australian *Acacia* seed banks: Size and relationship with stem diameter in the presence of gall-forming biological control agents. *PLoS One.* 2017;12(8):e0181763.

    doi: 10.1371/journal.pone.0181763

20. Strydom M, Veldtman R, Ngwenya MZ, Esler KJ. Seed survival of Australian *Acacia* in the Western Cape of South Africa in the presence of biological control agents and given environmental variation. *PeerJ.* 2019;7:e6816.

    doi: 10.7717/peerj.6816

21. Strydom M, Veldtman R, Ngwenya MZ, Esler KJ. Questioning the effectiveness of seed-reducing agents on invasive *Acacia*: Pod production relative to gall abundance of classical biological control agents. *Perspect Plant Ecol Evol Syst.* 2024;64:125813.

    doi: 10.1016/j.ppees.2024.125813

22. Dennill GB. The effect of the gall wasp *Trichilogaster acaciaelongifoliae* (*Hymenoptera*: Pteromalidae) on reproductive potential and vegetative growth of the weed *Acacia longifolia*. *Agric Ecosyst Environ.* 1985;14:53-61.

    doi: 10.1016/0167-8809(85)90084-2

23. Dennill GB. Establishment of the gall wasp *Trichilogaster acaciaelongifoliae* (Pteromalidae) for the biological control of *Acacia longifolia* in South Africa. *Agric Ecosyst Environ.* 1987;19:155-168.

    doi: 10.1016/0167-8809(87)90015-6

24. Hoffmann JH, Impson FAC, Moran VC, Donnelly D. Biological control of invasive golden wattle trees (*Acacia pycnantha*) by a gall wasp, *Trichilogaster* sp. (*Hymenoptera*: Pteromalidae), in South Africa. *Biol Control.* 2002;25:64-73.

    doi: 10.1016/S1049-9644(02)00039-7

25. Impson FAC, Kleinjan CA, Hoffmann JH, Post JA, Wood AR. Biological control of Australian *Acacia* species and *Paraserianthes lophantha* (Willd.) Nielsen (Mimosaceae) in South Africa. *Afr Entomol.* 2011;19:186-207.

    doi: 10.4001/003.019.0210

ACCSCIENCE PUBLISHING

Our Journals

Microbes & Immunity is a multidisciplinary peer-reviewed journal dedicated to advancing the understanding of the interactions between microbes and the immune system. The journal provides an open access publishing platform for researchers, clinicians, and scientists to disseminate their original research, reviews, and perspectives related to various aspects of microbes and immunity. The journal aims to foster collaboration and knowledge exchange in the fields of microbiology, immunology, infectious diseases, and related disciplines. *MI* covers subject areas, including but not limited to the following:

- Host-Microbe Interactions
- Microbial Pathogenesis
- Immunomodulation by Microbes
- Microbiome and Immunity
- Vaccines and Immunotherapeutics
- Host Defense Mechanisms
- Microbial Genomics and Proteomics
- Diagnostic Methods and Technologies

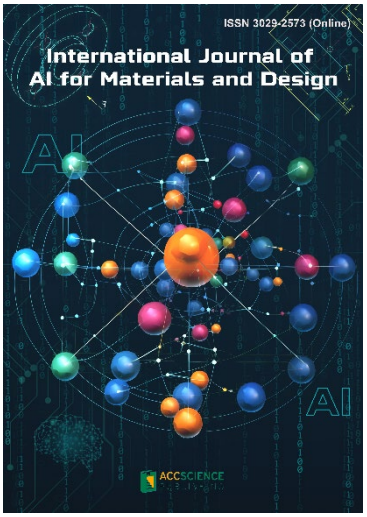

International Journal of AI for Materials and Design is an international, peer-reviewed open-access journal that aims to bridge the cutting-edge research between AI and materials, AI and design. In recent years, the tremendous progress in AI is leading a radical shift of AI research from a mainly academic endeavor to a much broader field with increasing industrial and governmental investments. The maturation of AI technology brings about a step change in the scientific research of various domains, especially in the world of materials and design. Machine learning (ML) algorithms enable researchers to analyze extensive datasets on material properties and accurately predict their behavior in different conditions. This subsequently impact the industry to leverage on big data and advanced analytics to build scientific strategies, scale operational performance of processes and drive innovation. In addition, AI and ML are uniquely positioned to enable advanced manufacturing technologies across the value chain of different industries. Integration of multiple and complementary AI techniques, such as ML, search, reasoning, planning, and knowledge representation, will further accelerate advances in scientific discoveries, engineering excellence and the future of cyber-physical systems manufacturing.

International Journal of AI for Materials and Design covers the following topics: AI or machine learning for material discovery, AI for process optimization, AI and data-driven approaches for product or systems design, application of AI in advanced manufacturing processes such as additive manufacturing, IoT, sensors, robotics, cloud-based manufacturing, intelligent manufacturing for various applications, autonomous experiments, material intelligence, energy intelligence, and AI-linked decarbonization technologies.

Start a new journal

Write to us via email if you are interested to start a new journal with AccScience Publishing. Please attach your CV, professional profile page and a brief pitch proposal in your email. We shall inform you of our decision whether we are interested to collaborate in starting a new journal.

Contact: info@accscience.com

https://accscience.com/journal/EER

ACCSCIENCE PUBLISHING

Access Science Without Barriers

Contact

www.accscience.com
9 Raffles Place, Republic Plaza 1 #06-00 Singapore 048619
E-mail: editorial@accscience.com
Phone: +65 8182 1586